Inamuddin
Mohd Imran Ahamed
Abdullah M. Asiri *Editors*

Applications of Ion Exchange Materials in the Environment

Springer

Applications of Ion Exchange Materials in the Environment

Inamuddin · Mohd Imran Ahamed ·
Abdullah M. Asiri
Editors

Applications of Ion Exchange Materials in the Environment

Springer

Editors
Inamuddin
Department of Chemistry
Faculty of Science
King Abdulaziz University
Jeddah, Saudi Arabia

Abdullah M. Asiri
Department of Chemistry
Faculty of Science
King Abdulaziz University
Jeddah, Saudi Arabia

Mohd Imran Ahamed
Department of Chemistry
Faculty of Science
Aligarh Muslim University
Aligarh, India

ISBN 978-3-030-10429-0 ISBN 978-3-030-10430-6 (eBook)
https://doi.org/10.1007/978-3-030-10430-6

Library of Congress Control Number: 2018965907

This Springer imprint is published by the registered company Springer Nature Switzerland AG
The registered company address is: Gewerbestrasse 11, 6330 Cham, Switzerland

Preface

The chemical species present in water streams have turned into a noteworthy worry for the innovative scientific world since their harmful impacts have officially settled on human well-being, aquatic vegetation and animals.

The range of chemical species found in water sources including heavy metals, pesticides, dyes and uncharged species is increasing exponentially owing to industrialization, urbanization and uncontrolled use of chemicals without proper legislation. To safeguard the natural environment such as water, soil and land, it is desirable to find a solution to the unregulated discharge of chemicals into these environmental entities. The government bodies may frame strict guidelines and take stern actions against individuals not complying with the guidelines; however, at the same time, the discharge should be regulated and treated to remove the harmful chemicals to protect people and the environment. An assortment of methodologies is documented in the literature for removal of unsafe contaminants from water such as ion exchange, chemical precipitation, adsorption, membrane filtration, electrochemical treatment technologies and thermal treatment. Among these strategies, ion exchange is one of the more efficient and cheaper techniques for the removal of toxic species from water streams. This book provides an overview of the use of this technique for the treatment of wastewater containing harmful impurities.

Applications of Ion Exchange Materials in the Environment will cover applications of ion exchange materials in the area of environmental analysis and treatment. The book presents the applications of organic, inorganic and composite ion exchange materials in various fields including chemical and biochemical separations, water purification and removal of harmful impurities such as dyes and cationic and anionic complexes.

It provides an in-depth knowledge of ion exchange materials and their applications suitable for postgraduate students and researchers as well as industrial research and development specialists working in environmental science, chemistry and chemical and biochemical technology. Additionally, this book presents an overview of ion exchange columns and operation suitable for engineers and industrialists. This book is divided into the following ten chapters.

Chapter 1 discusses the microbial removal of organic dyes and metal pollutants along with the mechanisms involved. Innovations to enhance the removal of dyes and metal ions are also presented.

Chapter 2 introduces heavy metals like chromium, nickel, copper, zinc, cadmium, mercury and lead. The physical and chemical methods of heavy metal treatment are summarized. Finally, challenges and future perspectives of wastewater treatment by ion exchange membranes are highlighted.

Chapter 3 provides a systematic and comparative presentation of the available information on the separation of heavy metals and dyes, vitamins, haemoglobin owing to their application in various fields of biotechnology.

Chapter 4 aims to present the developments in the field of geopolymers used for the removal of alkali and alkaline earth metals, ammonium ion and heavy metals from wastewater.

Chapter 5 presents the study for the microwave-assisted hydrothermal synthesis of zirconium phosphate which is further used for the removal of Cs^{+} and Sr^{2+} ions from aqueous solutions.

Chapter 6 discusses the ion exchange capabilities of metal hexacyanoferrates in areas such as potentiometric ion sensors and recovery of metal ions. The electrochemically diffusion-driven processes with meaningful examples, ranging from ESIX-based depletion of ions to battery systems, are discussed.

Chapter 7 highlights the low-cost methods with different degrees of effectiveness for heavy metal ions removal using agro-based biosorbents and biopolymers based on cellulose, chitosan and alginate. Factors influencing the efficiency of nanofibre membranes and packed bed adsorbers are discussed. Different types of composite ion exchangers used for water treatment are also discussed.

Chapter 8 introduces the characteristics, occurrence, properties, applications, production and consumption of rare earth elements. It explores the methods used for the rare earth elements recovery from nickel metal hydride batteries and permanent magnets using ion exchange materials. A detailed overview of the separation of high purity rare earth elements using cation exchangers is discussed.

Chapter 9 demonstrates various materials (inorganic to nanocomposite) recently developed for the removal of heavy metals from wastewater. Their mechanisms and treatment performance are also mentioned.

Chapter 10 discusses the applications of organic ion exchange resins in water treatment. The emphasis is given for the removal of heavy metals, organics, salinity, boron, anions and cations.

Jeddah, Saudi Arabia — Inamuddin
Aligarh, India — Mohd Imran Ahamed
Jeddah, Saudi Arabia — Abdullah M. Asiri

Contents

Chapter 1
Green Approach: Microbes for Removal of Dyes and Metals via Ion Binding

Adeline Su Yien Ting

Abstract Metal ions and organic dyes are common pollutants in the environment. These are toxic to living organisms and the environment. Removal strategies using biological agents have been attempted, with many of these successfully performed by a variety of micro-organisms. The use of micro-organisms is aligned to the green approach, as micro-organisms are capable of biosorbing, bioaccumulating and/or biodegrading the pollutants. This approach is environmentally friendly and sustainable, as readily available biological resources are utilized to convert harmful pollutants into less hazardous forms. In this chapter, the microbes for removal of organic dyes and metal pollutants are discussed, along with their mechanisms involved. Innovations to enhance the removal of dyes and metal ions are also presented.

1.1 Introduction

Pollution in the environment due to metal ions and organic dyes is mainly attributed to rampant, anthropogenic factors. Through industrialization (mining, electroplating and wielding) and urbanization, metals such as aluminium (Al^{3+}), copper (Cu^{2+}), lead (Pb^{2+}), zinc (Zn^{2+}) and cadmium (Cd^{2+}); and dyes (azo, triphenylmethane and anthraquinone dyes) are released into the environment [129]. Metals typically contaminate wastewaters from fertilizer and pesticide manufacturing. Metals are potent with carcinogenic and mutagenic potentials [12, 74]. The prolonged accumulation of toxic metals in the environment may lead to biomagnification, impacting living organisms via biomagnification of toxic metals in the food chain [1, 8]. For dyes, they typically originate from residual dyes in wastewaters from the various industries. There are over 10,000 different synthetic dyes available in the market, with the collective production of 700,000–1,000,000 ton annually [29].

A. S. Y. Ting (✉)
School of Science, Monash University Malaysia, Jalan Lagoon Selatan, 46150 Bandar Sunway, Selangor Darul Ehsan, Malaysia
e-mail: adeline.ting@monash.edu

Inamuddin et al. (eds.), *Applications of Ion Exchange Materials in the Environment*,
https://doi.org/10.1007/978-3-030-10430-6_1

Common dyes found in the environment include azo, triphenylmethane and anthraquinone, used in various industries: in the dyeing of textiles and paper; manufacturing of printing ink, plastic, cosmetic; pharmaceuticals and food production [48]. Dyes are toxic to many living organisms with similar potency to metal toxicity. Low concentrations (<1 ppm) of synthetic dyes also impart colour to water bodies, affecting aesthetic value, impeding photosynthesis and disrupting aquatic organisms [43].

Removal of pollutants is therefore pertinent to ensure the biosafety of the environment. The typical methods employed are the conventional physicochemical (bioremediation), which include ion exchange, reverse osmosis and chemical precipitation. Nevertheless, these conventional approaches are limited by the formation of toxic by-products (sludge) and the high cost involved in their disposal [24, 91, 127]. This led to the development of bioremediation as a greener and more environmentally friendly alternative for the removal of pollutants. Bioremediation adopts the use of biological origins such as plants and micro-organisms (bacteria, fungi and algae) to remove pollutants from the environment. Of these, micro-organisms are the most useful as they have been shown to tolerate these pollutants, withstand adverse environmental conditions, are amenable to innovations and upscaling. The microbes have also been found useful for a broader range of application [16–18, 30, 41, 66, 103].

In this chapter, the role, potential and importance of microbes for removal of dyes and metallic species are discussed. The type of microbes, their mechanisms of removal and innovations to further improve their efficacy are presented. Attempts are made to highlight the emerging role of microbes as a green approach in mitigating dye and metal pollution in the environment.

1.2 Pollutants in the Environment

Pollutants in the environment are broadly categorized as the organic and inorganic pollutants. The organic pollutants comprise primarily of compounds such as synthetic dyes, pharmaceutical products, pesticides and phenol-based compounds, while metals are the main inorganic pollutants found in the environment [56]. This chapter is devoted to emphasizing the role of dyes and metal ions in the environment, which include an array of triphenylmethane (TPM) dyes (crystal violet, methyl violet, cotton blue, malachite green) and metal cations (Pb^{2+}, Al^{3+}, Zn^{2+}, Cu^{2+} and Cd^{2+}). Both TPM dyes and metal cations are often found in excess in wastewaters of the food, pharmaceutical, fertilizer and electroplating industries [23, 54]. These pollutants in the environment present a serious health threat to living organisms. Exposure (absorbing, inhaling or ingesting) to high concentrations of these pollutants typically result in poisoning, irritation and/or damages to the vital organs and body systems [13, 110].

1.2.1 Toxic Metals

Metals in the environment are classified into three main groups; toxic metals (Cu^{2+}, Pb^{2+} and Zn^{2+}), valuable elements (Pt^{2+} or Pt^{4+}, Ag^{+} or Ag^{2+} and Au^{+} or Au^{3+}) and radionuclides (U, Ra) [128]. These are often discharged into the environment through natural occurrences (weathering, erosion, volcanic activities) and anthropogenic activities, with the latter overwhelming the former (Table 1.1). Metals have been found in waterlogged areas such as lakes, estuaries and peat swamps, where residual metal accumulates from effluent discharged into the water environment [27, 28]. In the environment, metals are typically found in various oxidative forms [77]. The various oxidative forms give rise to either +1 and +2 (example for Cu) or +3 and +6 (example for Cr), each conferring different degrees of toxicity. For example, the hexavalent chromium (Cr^{6+}) has been revealed to be more toxic than the trivalent state (Cr^{3+}) [80]. The oxidative forms of metals are relatively water-soluble. In water-soluble forms, metals are easily transported in the wastewaters and enter the water and food cycles easily. Of the various types of metals, some are not required by living organisms (Al^{3+}, Pb^{2+} and Cd^{2+}), but some are essential metals (Cu^{2+}, Zn^{2+}, Fe^{3+} and Mn^{2+}) which are critical to support physiological and enzymatic activities in living organisms. Essential metals are required in trace amounts, but high concentrations lead to toxicity and other health threats (Table 1.1). The World Health Organization (WHO) (2011) has proposed threshold levels for specific metals as a guideline on the permissible levels of common metals in drinking water (Table 1.1). This guideline serves as a reference to various water management practices.

Table 1.1 Summary of common metals in the environment

Metal ion	Toxicity	Concentrations in drinking water (mg/L)	Threshold concentrations (mg/L)	Pollution source	Health risk
$^{e}Cu^{2+}$	Average	$\leq$ 0.005 to > 30	2.0	Metal finishing and plating	Damage to brain, liver and gastrointestine
$^{e}Zn^{2+}$	Average	<0.1	3.0	Metal finishing and plating	Affects the nerve systems
$^{ne}Pb^{2+}$	High	<0.005	0.01	Mining, welding, plumbing; petrol discharge	Affects cardiovascular, nerve, immunity and reproductive systems
$^{ne}Cd^{2+}$	High	<0.001	0.003	Steel industries, batteries	Carcinogenic affects renal function, destroys red blood cells

e Essential metals; *ne* Non-essential metals

Source Cheremisinoff [21], Davis et al. [31], Järup [58], Thakur [120] and World Health Organization [131]

1.2.2 Triphenylmethane Dyes

Triphenylmethane (TPM) dyes are common dyes used as colourants in many industries. TPM dyes are relatively cheaper than other dyes and have intense colours and high tinctorial strength. The TPM dyes consist of hydrocarbon (triphenylmethane), tertiary alcohol (triphenylcarbinol) and the quinonoid and amino/hydroxyl groups to give rise to the chromophore and auxochromes, respectively [47]. TPM dyes are considered basic dyes with cationic properties (positively charged) and can easily react with materials that are negatively charged. TPM dyes are variable, with colours ranging from shades of violet, blue, green and red. These shades are identified by the following names: crystal violet, ethyl violet, methyl violet, bromophenol blue, brilliant blue FCF, Coomassie brilliant blue, methyl blue, patent blue V, brilliant green, malachite green, methyl green and cresol red [16, 70, 73, 81, 89, 138]. TPM dyes are typically water-soluble, hence are easy to use but also persistent in water environments. Of available TPM dyes, this chapter is aimed to focus on the following four TPM dyes: crystal violet, methyl violet, methyl blue and malachite green. These are the main dyes used for the dyeing of textile items (e.g. wool, silk, cotton, leather, nylon and polyacrylonitrile), paper, plastic, printing inks, food, cosmetic, and for manufacturing of drugs and therapeutic agents (Table 1.2). The persistence of dyes or their metabolites (e.g. leucomalachite green, leucocrystal violet) in the environment is toxic to living organisms: animals, plants and human [6, 11, 43, 100]. Common symptoms include irritation and sensitization of the eyes, skin, respiratory and the gastrointestinal tract [81, 84, 125] (Table 1.2). Aggravated symptoms in the cells and organs may occur as a result of prolonged exposure to the dyes, including carcinogenic and mutagenic effects [73].

Table 1.2 Summary of the four selected triphenylmethane dyes, their applications in various industries and health hazards

TPM dye	Other names	Industrial applications	Health hazards	References
Crystal violet	Basic violet 3, gentian violet and methyl violet 10b	Textile industry; printing; biological stain; pharmaceutical (antimicrobial, skin disinfectant)	Irritant (to the eyes, skin and digestive tract); can cause respiratory and kidney failures	[44, 84]
Methyl violet	Methyl violet 2b	Textile industry; printing; dyeing of leather and rubber; pH indicator and cell viability assay	Irritant (to the eyes, skin, respiratory and gastrointestinal systems)	[78]
Malachite green	Basic green 4, aniline green and diamond green B	Textile industry; pharmaceutical (antifungal and antiparasitic)	Irritant (to the eyes); failure of the reproductive system	[68, 125]
Methyl blue	Acid blue 93 and cotton blue	Textile industry; biological stain and dyeing of leather	Irritant (to the eyes, skin, respiratory and gastrointestinal systems)	[4]

1.3 Bioremediation Approaches in Removing Pollutants

The bioremediation approach to removing pollutants is achieved through the use of organisms, utilizing live or dead cells. The live cells include a variety of micro-organisms and plants [44, 100, 103, 111]. Micro-organisms are primarily studied for their potential in removing pollutants, as these are the natural decomposers in the environment. A variety of bacteria, fungi, yeast and actinomycetes have been explored, and some have demonstrated potential to degrade recalcitrant pollutant molecules such as synthetic dyes, toxic metals, polycyclic aromatic hydrocarbons, pesticides, crude oil and petroleum-based products [37, 59, 134]. The dead organisms (i.e. organic in nature) may also aid bioremediation. This includes dead microbial cells and plant tissues (agricultural waste). Both dead and live cells perform biosorption as their first uptake mechanism. This process binds metal or dye ions to the negatively charged surfaces of the biomass. In live cells, this ionic binding of pollutant ions to the functional groups of the cells precedes the bioaccumulation or biodegradation processes. Biosorption also occurs more rapidly, with uptake often occurring within hours rather than days compared to bioaccumulation [96]. While both live and dead cells can be used for pollutant removal, the living organisms are potentially more effective to remove pollutants by biodegrading or biotransforming the pollutants into simpler, less toxic molecules. With biodegradation, it is possible to achieve complete mineralization of pollutants into carbon dioxide and water [29]. This is a desirable pathway to achieve complete removal of the toxic pollutants. The dead cells typically remove pollutants as such, without biotransformation or biodegradation.

The living and dead cells remove pollutants via two main mechanisms: biosorption and/or biodegradation [86, 109]. Biosorption involves the binding of pollutants onto surfaces of the cells used. On the contrary, biodegradation relies on not just the binding of pollutants to cells, but the bioaccumulation of pollutants into the cells or biodegradation via extracellular molecules produced. Biosorption capitalizes on the cell wall of cells, which are rich in various functional groups. These groups (carboxyl, hydroxyl, amine and phosphoryl) are negatively charged, therefore binds strongly to the positively charged pollutants (dyes, metal cations) [69]. Hence, the primary mode of removal of pollutants is via the ionic binding to the live or dead cells.

1.3.1 Non-microbial Strategies

The non-microbial strategies involve the use of sorbents of non-microbial origin. The most common sorbents used are agricultural wastes, which include the activated charcoal. Activated charcoal is popularly produced commercially in granular or powder forms, and has high sorption capacity, attributed to their microporous nature and large surface area (500–1500 m^2/g) [42, 51, 63]. Activated charcoal has

been found to remove TPM dyes and metals successfully. Commercial activated charcoal could adsorb as much as 151.52 and 200 mg/g of crystal violet and basic green 4 (malachite green), respectively [68, 94]. Toxic metals adsorbed on activated charcoal include Cd^{2+}, Cr^{6+}, Cu^{2+}, Ni^{2+}, Pb^{2+} and Zn^{2+} [42, 50, 51, 63, 98]. The sorption capacity of activated charcoal is evident, but their application is challenged by the demands in producing activated charcoal (high-cost, energy-consuming processes). Activated charcoal also has poor reusability due to poor amenability to sorption–desorption processes [50].

Other agricultural wastes used include leaves, bagasse, fruit peels, among others. These are effective biosorbents to remove various pollutants (e.g. synthetic dyes, toxic metals, phenolic compounds and radionuclides) [97, 122, 123]. Adsorption of ionic pollutants to these wastes depends on the cell wall composition of the biosorbents, which consists primarily of cellulose, hemicellulose and lignin [75]. These lignocellulosic materials are rich in functional groups, particularly the negatively charged hydroxyl groups that are able to attract and bind the cationic metals and other pollutants, especially when present in low concentrations [68, 86]. Several types of the wastes have been found to remove TPM dyes successfully. This includes raw forms of sugarcane bagasse [86], biochar of *Miscanthus sacchariflorus* (grass) [65], cones of *Pinus brutia* (Calabrian pine) [89], walnut shells [118], leaves of *Artocarpus odoratissimus* (tarap) [78], leaves of *Ananas comosus* (pineapple) [97], leaves of *Psidium guajava* (Guava) [104], rice husk [75], spent tea leaves [3], spent ground coffee [61], olive pomace [68], orange peel [107], oak charcoal [53] and stems and leaves of potatoes [52]. Modified (via esterification, etherification and oxidizing agents) or converted (into activated carbon) forms of the agricultural wastes have also been found suitable to remove pollutants successfully [3, 123]. Modifications via chemical processes resulted in additional functional groups on the sorbents, such as carboxylic groups, which increased their biosorption capacity [86]. Despite the efficacy of agricultural wastes as sorbents, their large-scale application is, however, limited by the resulting toxic sludge generated and potential clogging problems in bioreactors.

1.3.2 Microbial-Based Strategies

Micro-organisms have also been explored for their potential in removing toxic pollutant ions. Bacteria, fungi and algae are increasingly popular as environmentally friendly alternatives to conventional sorbents. Out of these, bacteria are the most commonly studied. Their ability to rapidly grow and increase in biomass and amenability to upscaling are attractive traits for use as biosorbents. Bacteria are also adaptable to harsh conditions, whilst demonstrating the efficient removal of dyes and metals [79, 119, 137]. Bacteria that are well known as efficient removers of toxic pollutants include species of *Bacillus*, *Pseudomonas, Burkholderia*, *Klebsiella*, *Shewanella* and *Sphingomonas* [4, 6, 79, 96, 132, 135–137]. Species of *Escherichia*, *Proteus*, *Bacillus* and *Salmonella* have also shown dye-degrading

potential [32, 57]. Bacteria are capable of removing pollutants via biosorption or/and biodegradation [36, 96]. The biosorption process in bacteria is dependent on the negatively charged carboxyl, amine, hydroxyl and phosphonate groups [4, 11]. The degradation of dyes by bacteria is regulated by a variety of enzymes such as laccase, lignin peroxidase, manganese peroxidase and NADH-DCIP reductase [15, 37]. Removal of metals by bacteria involves both active and passive removal mechanisms, which includes precipitation, as well as intracellular and extracellular accumulation of metals [67].

Fungi are also capable of removing toxic pollutants, which include various metals, synthetic dyes, polycyclic aromatic hydrocarbons, pesticides and hydrocarbon [2, 56, 72]. These pollutants bind to the anionic surfaces of fungi. Common fungal species known to remove metals and dyes include species of *Phanerochaete*, *Coriolopsis*, *Irpex*, *Trichoderma*, *Aspergillus*, *Penicillium, Rhizopus, Pleurotus ostreatus*, *Polyporus picipes*, *Gloephyllum odoratum*, *Colletotrichum gloeosporioides* and *Diaporthe* sp. [16, 17, 19, 22, 45, 56, 100, 103, 108, 121]. Fungi produce non-specific, extracellular enzymes to catalyse the breakdown of pollutants [17, 103]. These enzymes could also actively exclude, adsorb, compartmentalize or sequester metals as means to detoxify metals [105]. These are typically achieved in live fungal cells. For dead fungal cells, pollutants are removed via biosorption, aided by the ionic binding to functional groups on the surface of the biomass [22].

According to the literature, the single-celled fungi, yeasts, have also been studied. Yeasts for the treatment of pollutants were typically sourced from industrial waste where they were available in abundance especially from fermentation, brewing and distillation processes [117, 134, 138]. Metal cations (Cd^{2+}, Cr^{3+}, Cu^{2+}, Hg^{2+} and Pb^{2+}) bind easily to the negative charges found on the surface of a variety of yeast species, which include *Candida tropicalis*, *Saccharomyces cerevisiae, Pichia acacia*, *Kluyveromyces lactis*, *Cyberlindnera fabianii*, *Wickerhamomyces anomalus* and *Cryptococcus* sp. [7, 55, 71, 76, 134]. The potential of yeast in removing dyes, however, has not been extensively studied. To date, only *S. cerevisiae* and *Yarrowia lipolytica* have been reported as positive for decolourization of malachite green, brilliant green, methyl violet, aniline blue and crystal violet [5, 48, 106, 117]. The extensive use of yeasts as bioagents for metal or dye removal is, however, limited due to their poor reusability and the generation of toxic sludge [134].

Algae have also demonstrated potential for removing pollutants. Algae are photosynthetic and range from single-celled microscopic algae to as large as kelps [20]. In most cases, the effective metal removal has been documented for brown, green and red algae [14, 24]. These include *Aphanocapsa roseana* de Bary [95], *Chlamydomonas* sp., *Euglena* sp., *Cystoseira compressa* [10], *Durvillaea antarctica* [24], *Chlorella vulgaris* [20], *Gracilaria edulis* [60], *Cosmarium* sp. [29], *Scenedesmus quadricauda* [69], *Pterocladia capillacea* [39], *Kappaphycus alvarezii* [39] and *Sargassum muticum* [14]. Algae are present as an attractive alternative, as they are abundant in nature, fast-growing, have a large surface area-to-volume ratio and known to have a high tolerance and uptake capacities for pollutants [24, 29]. The efficient removal of pollutants by algae is attributed to the functional

groups (primarily carboxylic) found in the alginate polymers of algae, which perform the ionic bonding with metal and dye ions [69]. In addition, algae are fast-growing, able to achieve sufficient biomass for application within a short period of time; hence, this process is extremely cost-effective. Nevertheless, further studies are required to better understand the response of algae to pollutants and environmental parameters, particularly pertaining to the removal of TPM dyes [60, 69].

1.4 Mechanisms for Removal of Pollutant Ions

Micro-organisms typically remove metal and dye pollutants via biosorption and/or bioaccumulation. The biosorption process involves the binding of the pollutant ions to the surface of the cell. This is usually the result of chemical and/or physical interactions between the pollutant ions with the functional groups found on the surface of the microbial cells. Biosorption is performed by both live and dead cells, through the binding of ions to the cells as the primary process. This takes place even when the cells are no longer viable (dead cells). On the contrary, bioaccumulation only occurs in live cells. In live cells, bioaccumulation is an extended process where upon binding of ionic pollutants to the cell surface, the pollutant ions may be further transported across the cell membrane into the cells and compartmentalized or immobilized within the cells. For some pollutants such as dyes, the dye molecules may be further degraded enzymatically by live cells. In both bioaccumulation and biodegradation processes, biosorption has to take place and the ionic bonding here is important to ensure the effectiveness of the processes.

1.4.1 Mechanisms for Removal of Metal Ions

The metal ions are typically adsorbed to microbial cells via the physical and/or chemical interactions between the metal cations and the negatively charged functional groups in the cell walls and cell membranes [64]. The successful binding of metal cations to these functional groups has been confirmed through changes in peaks of the functional groups, detected via Fourier transform infrared spectroscopy (FTIR). The functional groups in the cell walls are critical for metal binding. In bacteria, these functional groups are found in the peptidoglycan of their cell wall, rich with *N*-acetylglucosamine (NAG) and *N*-acetylmuramic acid (NAM) [30]. Bacteria cells also bind metals through the numerous functional groups found in the capsule or slime layer produced [33, 90]. The slime and capsules also contribute to the metal complexation process [38]. A wide variety of fungal species have been documented to adsorb metals, and these include *Penicillium lilacinum, Microsphaeropsis* sp. and *Trichoderma asperellum* [40, 113, 133]. *T. asperellum* showed preference for removal of Zn^{2+} (18 mg/g), Cu^{2+} (17.26 mg/g), Pb^{2+} (19.24 mg/g), Cd^{2+} (19.78 mg/g) and Cr^{3+} (16.75 mg/g) [113]. For

Microsphaeropsis sp. LSE10, the isolate was capable to adsorb significantly higher amount of Cd^{2+} at 247.5 mg/g [133]. The isolate *P. lilacinum* reportedly removed Cu^{2+} (85.4%) and Cd^{2+} (31.43%) [40].

Bioaccumulation of metals also occurs in some microbial species. This involves the movement of metal cations across cellular structures (cell membrane) of the live cells, to be further compartmentalized or detoxified. The movement of metal cations across the cell membrane demands energy from the cells and is therefore exclusive to only live cells. The energy is also required for cells to perform metal precipitation, redox reactions, crystallization and/or covalent bonding with cellular structures [83, 130]. The bioaccumulation process occurs at a slower rate than biosorption, presumably due to the adaptive stage required by live cells in response to metal toxicity [19]. Nevertheless, bioaccumulation often results in the higher removal of metals than biosorption. The superiority of live cells in removing metals was observed in *Lasiodiplodia* sp. MXSF31, capable of bioaccumulating Pb^{2+} (5.6×10^5 mg kg^{-1}), Cd^{2+} (4.6×10^4 mg kg^{-1}) and Zn^{2+} (7.0×10^4 mg kg^{-1}) [35]; and *Mucor* sp. for Cd^{2+} removal (173 mg g^{-1}) [34].

The removal mechanism of metal ions can be enhanced by optimizing several factors: pH, temperature, adsorbent dosage/amount and initial metal concentrations. Of these, the initial pH of the metal solution is critical as it influences metal precipitation, availability of functional groups, and the interaction between metal cations and hydrogen protons with the functional groups [9]. At low pH (acidic), more hydrogen ions are available to compete with metal cations for binding onto the functional groups [62]. As hydrogen ions bind to the functional groups, less binding sites are available for metal cations. This leads to poorer metal removal activities under low pH conditions. Typically, the pH range of 4 to 8 is the optimum for metal biosorption [26, 128]. The other factors, particularly adsorbent dosage and initial metal concentrations, vary depending on the type of microbial cells used [18].

1.4.2 Mechanisms for Removal of Dyes

Removal of dyes by microbial cells involves two mechanisms: the biosorption or/and biodegradation [100, 121]. While the former occurs most commonly, the latter is a more effective mechanism as it often leads to the breakdown of toxic dye molecules into less hazardous molecules. The dead and live cells can both perform biosorption, but the biodegradation process is exclusive to live cells [46, 100, 102, 109, 121]. In biosorption, dye ions bind to the functional groups present in the cell wall (i.e. carboxyl, hydroxyl, amino and phosphate groups), specifically the lipid, chitin, glucan and chitosan components of the cell wall [99]. Dye biosorption is detected visually, (a) when microbial biomass is stained with the dye (dyes binding to the cells), (b) with shifts detected in spectra peaks via FTIR and (c) decolourization of the dye solution [85, 100, 121].

However, the biodegradation of dyes only occurs in live cells. This process is dependent on the enzymatic breakdown of the dye molecules. Biodegradation of dyes is most effectively performed by lignolytic enzymes, as these enzymes are responsible for the catalytic breakdown of dyes, particularly their chromophoric centres, into less harmful compounds [100]. Live cells typically bind dye ions onto their cell wall, subsequently secreting extracellular enzymes to catalyse the degradation of the dye molecules [85, 109, 121]. In some microbial cells, the dye molecules are transported across the membrane into the cells, and further degraded by the intracellular enzymes. The lignolytic enzymes are well known for their ability to degrade dye molecules. This includes the enzymes laccase (Lac), manganese peroxidase (MnP), lignin peroxidase (LiP), tyrosinase and the reductase enzymes [99, 116, 124]. Among the enzymes, laccase (EC 1.10.3.2) is the most studied enzyme for its role in biodegradation of dyes. This enzyme is found in most micro-organisms [111]. The oxidative activity takes place in the presence of oxygen, and the oxidation of dye molecules by Lac releases free radicals for further dye degradation. Laccase production in several isolates has demonstrated effective decolourization of aniline blue, methylene blue, malachite green and Bismarck brown [109, 112].

The biodegradation of dyes often results in less toxic compounds, which are validated by toxicity assays of treated dye samples via microbial or seed germination assays [59, 80, 100]. In a study by Chen and Ting [16], the mere presence of dyes was found to induce production of dye-degrading enzymes. Isolate *Coriolopsis* sp. (1c3) produced more LiP and NADH-DCIP reductase in dye solutions, compared to controls (absence of dyes). It was assumed that the enzymes produced and their roles in biodegradation could perhaps be species specific. For *Coriolopsis* sp. (1c3), biodegradation potential was most evidently attributed to LiP and NADH-DCIP. The enzyme laccase was not involved in this process at all, although these three enzymes are typically known to be crucial in degrading TPM dyes. *Coriolopsis* sp. may rely more on LiP and NADH-DCIP reductase for dye biodegradation. The enzymatic breakdown of dyes results in notable changes to dye intensity (reduced intensity) (Fig. 1.1). The biodegradation takes place after ionic bonding, where enzymes secreted aids during the breakdown of dye molecules into simpler fragments or less hazardous molecules. The breakdown of dyes would eventually lead to reducing the toxicity level of the dyes. This can be established via phytotoxicity tests, where treated dye solutions are used to treat seeds, leading to seedling germination (Fig. 1.2).

The dye removal was more efficient when optimized conditions were provided, especially initial dye concentration and incubation conditions (agitation, aeration) [100, 101]. These factors played an important role as dye binding is an ionic process, following monolayer sorption kinetics [18]. Initial dye concentrations are important as high initial dye concentrations often lead to decreased decolourization efficiency. However, the high initial dye concentrations are toxic to living cells and may kill the cells or inhibit production of enzymes crucial for dye degradation [16]. This has been observed in cases of many fungi, including *Phanerochaete chrysosporium*, which has been typically used in degradation studies of most dyes.

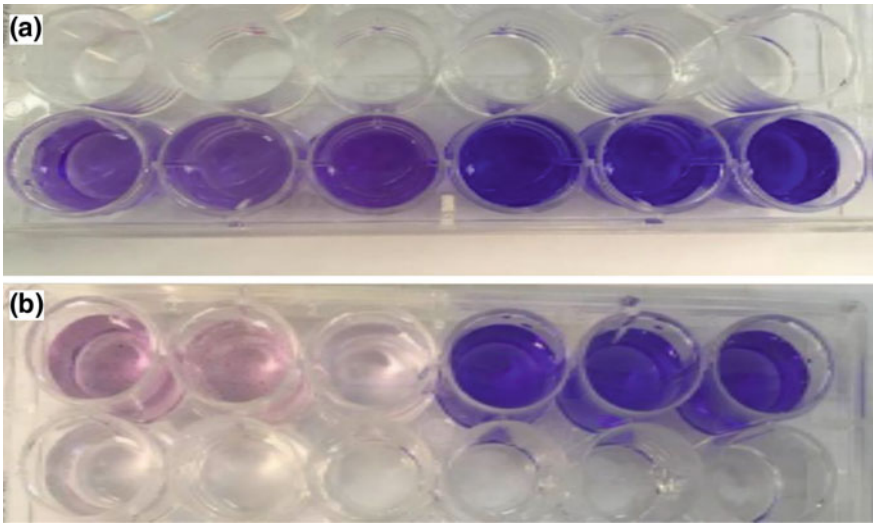

Fig. 1.1 Decolourization of crystal violet (three wells from the left) due to enzymatic biodegradation by **a** free-cell and **b** pseudo-biofilm forms of *Coriolopsis* sp. Three wells from the right are controls (without treatment of *Coriolopsis* sp.)

Fig. 1.2 Seedling germination and growth for mung beans applied with cotton blue dye solution treated with *Penicillium simplicissimum*

With an initial dye concentration of 0.05 g/L, *P. chrysosporium* decolourized methyl violet at 90%. On the contrary, when the initial dye concentration was increased to 0.4 g/L, decolourization efficiency decreased to 30% [103]. Similar observations were noted for decolourization of crystal violet, methyl violet and malachite green by *Penicillium simplicissimum* and *Coriolopsis* sp. [16, 17].

Another important factor is the incubation condition, i.e. agitation and aeration. Agitation is crucial to allow oxygenation in the removal process. It also promotes better contact of biomass with dye molecules. Studies have demonstrated that decolourization rate and efficiency were enhanced when incubated with agitation [100]. This has been noted for *P. ostreatus* (BWPH and MB strains), *P. picipes* (RWP17) and *G. odoratum* (DCA) for the degradation of brilliant green, with 73.81–95.00% achieved with agitation, as compared to static incubation (56.74–79.30%). The superiority of decolourization under agitated conditions was also evident for *Absidia spinosa* M15 in which degradation of cresol red was 97.1% under 120 rpm agitation, compared to only 44.5% under static conditions [70]. Agitation at 150 rpm was also useful in enhancing degradation (96%) of malachite green by *Aspergillus ochraceus*, compared to without agitation (72%) [108]. This efficiency was attributed to enhance contact between cells and dye compounds for oxidative metabolism. Nevertheless, the rate of agitation, i.e. at 120 or 150 rpm, was dependent on fungal species. Higher decolourization efficiencies for brilliant green were observed for *P. ostreatus* (BWPH and MB strains), *P. picipes* (RWP17) and *G. odoratum* (DCA) when agitated (73.81–95.00%) as compared to static incubation (56.74–79.30%).

1.5 Innovations in the Removal of Pollutant Ions

Removal of pollutant ions can be improved by introducing new approaches or modifications to the microbes or to the techniques. The microbial cells can be modified by physical and chemical pre-treatments, grafting, immobilization or genetic engineering, to enhance sorption capacity. All these strategies are based on the enhancement of ionic binding of dye or metal ions to the cells. In addition, the use of microbial consortium, solid-state fermentation (SSF), and testing in single- and multi-metal solutions can also be explored as strategies to improve removal of pollutants. Pre-treatments include both physical and chemical treatments that when applied to increase the binding of ions to the cells. Physical pre-treatments include treatment with heat via boiling or autoclaving, while chemical pre-treatments involve the use of acids, alkalis or detergents. Both physical and chemical pre-treatments liberate functional groups of cell walls so that more binding sites are available for ionic binding of metals or dyes [126]. Of the reagents used, pre-treatment with acids (hydrochloric acid, nitric acid) or alkalis (sodium carbonate) has demonstrated good removal efficacy, especially for metal ions. Treatment with 0.5 M sodium carbonate for fungal isolate STRI: ICBG-Panama: TK1285 enhanced Cr^{3+} removal to 91.2% from 27% compared against non-treated cells [64]. Yang et al. (2013) reported the similar effects of citric-acid treated *Fusarium* sp., with enhanced thorium(IV) removal (75.47 mg/g) compared to non-treated cells (11.35 mg/g). Therefore, pre-treatments are beneficial as these generally enhance the performance of biosorbents in removing pollutant ions.

Grafting is the other innovation that enhances the removal of pollutants [82]. This technique involves the polymerization and layer-by-layer grafting of functional groups to the microbial biomass to increase ionic binding. This is achieved by simple cross-linking formations and adding functional groups to the surface, modifying the surface and enhancing surface area for biosorption activities. One common approach is the grafting of poly(allylamine hydrochloride) (PAA) layers onto the bacterial surface using glutaraldehyde as the cross-linking agent [82]. This has resulted in metal removal that was tenfold higher than the non-modified bacteria. In addition to grafting, the surface area and functional groups can be enhanced via immobilization as well. Immobilization is performed using a polymer matrix (e.g. alginate, polyacrylamide and polyurethane) to encapsulate or entrap microbial cells within [88]. The polymer matrix contributed to enhancing biosorption, by providing superior surface binding or functional groups for efficient biosorption of metal ions [22]. The amount of metals adsorbed is significantly increased by immobilization compared to free-cell forms (Fig. 1.3). Improvement in metal removal (i.e. Cr^{3+}) using alginate-immobilized isolate STRI: ICBG-Panama: TK1285 could be as high as 98.5% compared to 27% by free-cell forms [64]. In addition, immobilized microbial cells also have lesser issues with respect to blockage and separation of biosorbents from wastewaters. Application of immobilized forms also allowed for high biomass loading with standardized preferred sizes, reusability and is relatively less expensive [22].

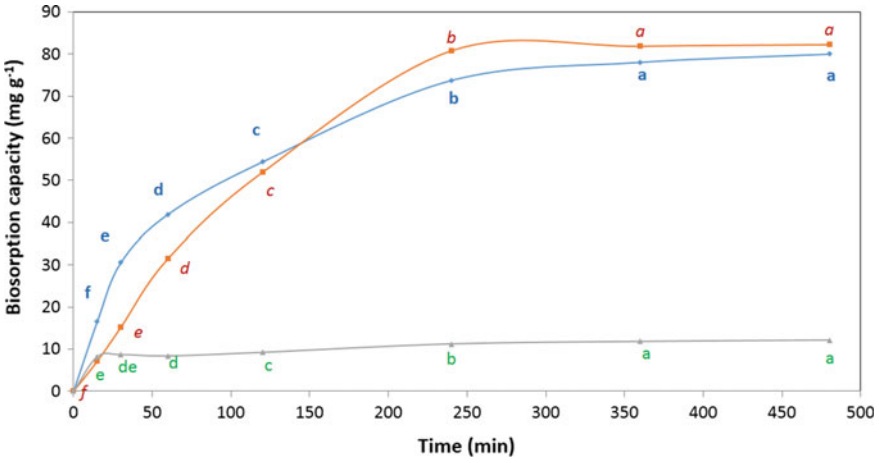

Fig. 1.3 Biosorption of Pb (II) by free-cells of *Diaporthe* sp. (filled triangle) and alginate-immobilized *Diaporthe* sp. (filled box) as compared to control (plain alginate beads) (filled diamond) at various time intervals. Means with the same letters within the same treatment are not significantly different according to Tukey's comparisons ($HSD_{(0.05)}$). Biosorption conditions–initial concentration of metal ion: 100 mg/L; pH 5.0 ± 0.2, temperature: 30 ± 2 °C, agitation rate: 200 rpm

The other alternative to improving microbial innovation is via the genetic engineering approach. This method explores the recombinant approach of introducing dye-degrading enzymes and the over-expression of these enzymes in hosts such as bacteria [111]. As a result, mass production of the stable enzymes (at relatively low costs) is possible. In recent years, the laccase gene (Lac4) from *Pantoea ananatis* Sd-1 was successfully cloned and expressed in *Escherichia coli* by Shi et al. [111]. This recombinant enzyme laccase was stable under various conditions: acidic (pH 1–3), high temperature (30–70 °C) and the presence of metal ions (Fe^{2+} and Cu^{2+}). The enzyme is valuable for the biodegradation of aniline blue (47%) as well as the azo dyes Remazol brilliant blue R (35%) and Congo red (89%).

New strategies to examine the efficacy of biosorbents can be adopted. One such strategy is the innovative approach of applying microbial consortium. The use of multiple strains of microbes in a consortium may contribute to better removal rate as various species responsible for the breakdown of different molecules of the pollutants are present to synergistically co-metabolize the pollutants [25]. Sim and Ting [114] adopted the mixed consortia approach and tested the mixed consortia on both single- and multi-metal systems. Results revealed the improved removal of Cu^{2+}, Pb^{2+}, Zn^{2+} and Cd^{2+} by microbial consortia than the use of a single fungal isolate. Similarly, Mastretta et al. [87] reported the enhanced Cd^{2+} accumulation (by three-folds) by bacteria consortium (mixtures of *Pseudomonas* sp., *Sanguibacter* sp., *Stenotrophomonas* sp., *Enterobacter* sp.), compared to single isolates.

The other strategy is to investigate the efficacy of the biosorbents in both single- and multi- or binary-systems. This can be achieved by performing assessments on these solution systems, as the multi- and binary-systems closely mimic the environment. This helps to validate the efficacy of the microbial cells as their interactions with multiple pollutant ions in the environment have been tested [49, 114, 115]. According to these studies, removal of metal ions in multi-metal systems is generally inferior compared to single-metal solutions (Fig. 1.4). This is closely linked to pollutants binding to biosorbents via ionic binding and may be limited by the surface available for binding of metals, and the general competitiveness among metals for binding. In multi-metal solutions, the biosorption of pollutant ions was the rate-limiting chemisorption process, with cationic metals competing for limited binding sites [114, 115].

Other innovations such as the use of solid-state fermentation (SSF) were also found to enhance removal of pollutants. In SSF culture conditions, secretion of enzymes is induced, typically in large quantities, due to the presence of the substrate as support for mycelial growth. With SSF, production of enzymes such as laccase can be increased and subsequently immobilized in 3% sodium alginate to facilitate decolourization of textile dyes [93]. The enzymes can be purified and applied for dye degradation applications. This concept of SSF has been adopted and modified to induce pseudo-biofilm formation in fungi, which improved the degradation of crystal violet and cotton blue [92].

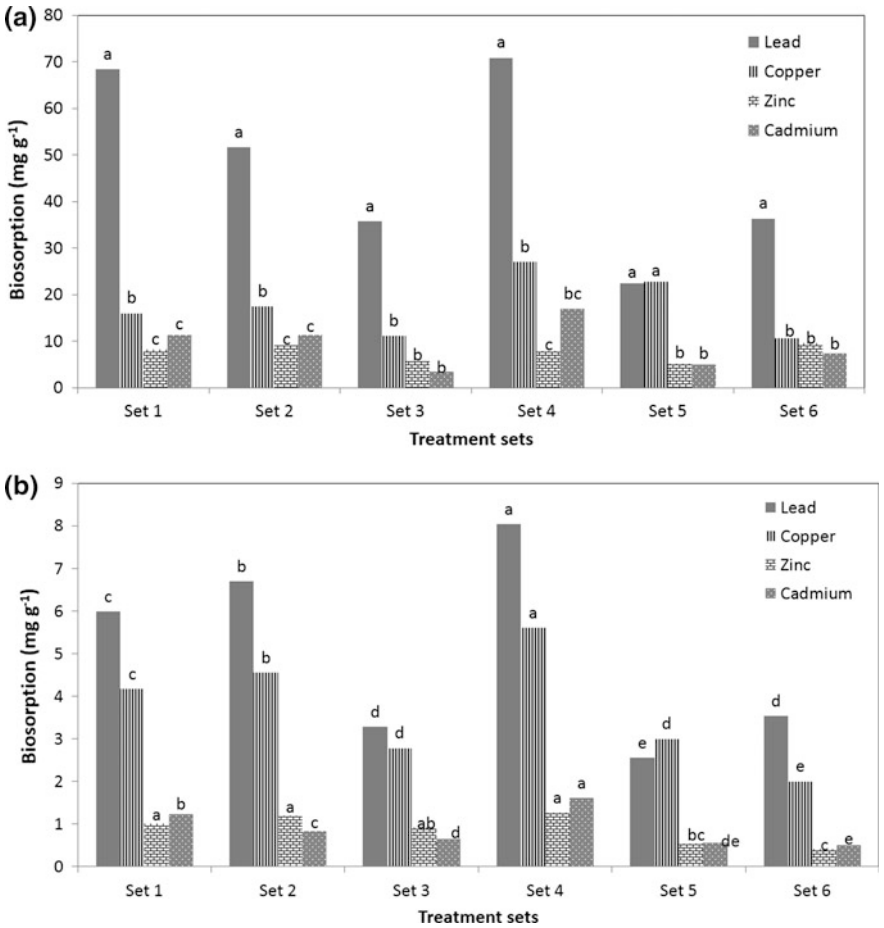

Fig. 1.4 Biosorption by biosorbents (Set 1—Sm + Sb; Set 2—Sm + Ta; Set 3—Sb + Ta; Set 4—Sm; Set 5—Sb and Set 6—Ta) for the removal of Pb^{2+}, Cu^{2+}, Zn^{2+} and Cd^{2+} in **a** single-metal and **b** multi-metal solutions. Means with the same letters within the biosorbent sets are not significantly different ($HSD_{(0.05)}$). *Note* Sm—*Stenotrophomonas maltophilia*, Sb—*Saccharicola bicolour*, Ta—*Trichoderma asperellum*

1.6 Conclusions and Future Prospects

The use of microbial cells, or their derivatives (e.g. enzymes), is the green approach in mitigating pollutants in the environment. Microbial cells are non-toxic and produce biomolecules such as enzymes to remove the metal and dye ions. Removal of metal and dye ions can be improved via several innovations, which include grafting, genetic engineering, using microbial consortia and others. These innovations have significantly enhanced the removal of pollutants by improving biosorption of pollutant ions (e.g. grafting of functional groups) or by

bioaccumulation or biodegradation (e.g. production of laccase enzymes). The alternative of using microbial cells for pollutant removal is good but requires further optimization studies and explorations to further increase the feasibility of the use. Future studies are to include considerations of their applications to a wider range of toxic pollutants, the reuse of the microbial cells and the economic impact of the microbial-based approach.

Acknowledgements The author is thankful for the research funding provided by the Malaysian Ministry of Higher Education under the FRGS grant scheme (FRGS/2/2013/STWN01/MUSM/02/2) and to Monash University Malaysia for the funds and research facility, also to her team of research students and collaborators for their equally passionate endeavour into studies related to microbial-based strategies for pollutant removal.

References

1. Abdel-Baki AS, Dkhil MA, Al-Quraishy S (2011) African bioaccumulation of some heavy metals in tilapia fish relevant to their concentration in water and sediment of Wadi Hanifah. J Biotechnol 10:2541–2547
2. Adekunle A, Oluyode T (2005) Biodegradation of crude petroleum and petroleum products by fungi isolated from two oil seeds (melon and soybean). J Environ Biol 26:37–42
3. Akar E, Altinişik A, Seki Y (2013) Using of activated carbon produced from spent tea leaves for the removal of malachite green from aqueous solution. Ecol Eng 52:19–27. https://doi.org/10.1016/j.ecoleng.2012.12.032
4. Arunarani A, Chandran P, Ranganathan BV, Vasanthi NS, Sudheer Khan S (2013) Bioremoval of basic violet 3 and acid blue 93 by *Pseudomonas putida* and its adsorption isotherms and kinetics. Colloids Surf B Biointerfaces 102:379–384. https://doi.org/10.1016/j.colsurfb.2012.08.049
5. Asfaram A, Ghaedi M, Ghezelbash GR, Dil EA, Tyagi I, Agarwal S, Gupta VK (2016) Biosorption of malachite green by novel biosorbent *Yarrowia lipolytica* isf7: application of response surface methodology. J Mol Liq 214:249–258. https://doi.org/10.1016/j.molliq.2015.12.075
6. Ayed L, Chaieb K, Cheref A, Bakhrouf A (2008) Biodegradation of triphenylmethane dye Malachite Green by *Sphingomonas paucimobilis*. World J Microbiol Biotechnol 25:705–711. https://doi.org/10.1007/s11274-008-9941-x
7. Bahafid W, Joutey NT, Sayel H, Iraqui-Houssaini M, El Ghachtouli N (2013) Chromium adsorption by three yeast strains isolated from sediments in Morocco. Geomicrobiol J 30:422–429. https://doi.org/10.1080/01490451.2012.705228
8. Barakat MA (2011) New trends in removing heavy metals from industrial wastewater. Arab J Chem 4:361–337
9. Bayramoglu G, Denizli A, Bektas S, Arica MY (2002) Entrapment of *Lentinus sajorcaju* into Ca-alginate gel beads for removal of Cd (II) ions from aqueous solution: preparation and biosorption kinetics analysis. Microchem J 72:63–76
10. Benfares R, Seridi H, Belkacem Y, Inal A (2015) Heavy metal bioaccumulation in brown algae *Cystoseira compressa* in Algerian coasts, Mediterranean sea. Environ Process 2:429–439. https://doi.org/10.1007/s40710-015-0075-5
11. Bera S, Sharma VP, Dutta S, Dutta D (2016) Biological decolorization and detoxification of malachite green from aqueous solution by *Dietzia maris* NIT-D. J Taiwan Inst Chem Eng 67:271–284. https://doi.org/10.1016/j.jtice.2016.07.028
12. Bilal M, Shah JA, Ashfaq T, Gardazi SMH, Tahir AA, Pervez A, Haroon H, Mahmood Q (2013) Waste biomass adsorbents for copper removal from industrial wastewater—a review. J Hazard Mater 263:322–333

13. Bravo L (1998) Polyphenols: chemistry, dietary sources, metabolism, and nutritional significance. Nutr Rev 56:317–333
14. Carro L, Barriada JL, Herrero R, Sastre de Vicente ME (2015) Interaction of heavy metals with Ca-pretreated *Sargassum muticum* algal biomass: characterization as a cation exchange process. Chem Eng J 264:181–187. https://doi.org/10.1016/j.cej.2014.11.079
15. Chaturvedi V, Bhange K, Bhatt R, Verma P (2013) Biodetoxification of high amounts of malachite green by a multifunctional strain of *Pseudomonas mendocina* and its ability to metabolize dye adsorbed chicken feathers. J Environ Chem Eng 1:1205–1213. https://doi.org/10.1016/j.jece.2013.09.009
16. Chen SH, Ting ASY (2015) Biodecolorization and biodegradation potential of recalcitrant triphenylmethane dyes by *Coriolopsis* sp. isolated from compost. J Environ Manage 150:274–280. https://doi.org/10.1016/j.jenvman.2014.09.014
17. Chen SH, Ting ASY (2015) Biosorption and biodegradation potential of triphenylmethane dyes by newly discovered *Penicillium simplicissimum* isolated from indoor wastewater sample. Int Biodeterior Biodegradation 103:1–7. https://doi.org/10.1016/j.ibiod.2015.04.004
18. Chen SH, Ting ASY (2017). Microfungi for the removal of toxic triphenylmethane dyes. In: Kalia VC, Shouche Y, Purohit HJ, Rahi P (eds) Mining for microbial wealth and metagenomics. Springer, Singapore, pp 405–429. ISBN 978-981-10-5708-3
19. Chen SH, Ng SL, Cheow YL, Ting ASY (2017) A novel study based on adaptive metal tolerance behavior in fungi and SEM-EDX analysis. J Hazard Mater 334:132–141
20. Cheng J, Qiu H, Chang Z, Jiang Z, Yin W (2016) The effect of cadmium on the growth and antioxidant response for freshwater algae *Chlorella vulgaris*. Springerplus 5:1290. https://doi.org/10.1186/s40064-016-2963-1
21. Cheremisinoff PN (1995) Handbook of water and wastewater treatment technology. Marcel Dekker Incorporation, New York
22. Chew SY, Ting ASY (2015) Common filamentous *Trichoderma asperellum* for effective removal of triphenylmethane dyes. Desalin Water Treat 57:13534–13539. https://doi.org/10.1080/19443994.2015.1060173
23. Chinalia FA, Reghali-Seleghin MH, Correa EM (2007) 2,4-D toxicity, cause, effect and control. Terr Aquat Environ Toxicol 1:24–33
24. Cid H, Ortiz C, Pizarro J, Barros D, Castillo X, Giraldo L, Moreno-Piraján JC (2015) Characterization of copper (II) biosorption by brown algae *Durvillaea antarctica* dead biomass. Adsorption 21:645–658. https://doi.org/10.1007/s10450-015-9715-3
25. Collins JS, Stotzky G (1989) Factors affecting the toxicity of heavy metals to microbes. In: Beveridge TJ, Doyle RJ (eds) Metal ions and bacteria. Wiley, Toronto, p 31
26. Congeevaram S, Dhanarani S, Park J, Dexilin M, Thamaraiselvi K (2007) Biosorption of chromium and nickel by heavy metal resistant fungal and bacterial isolates. J Hazard Mater 146:270–277
27. Cozma D, Tanase C, Tunsu C, Olariu R, Ionas A, Pui A (2010) Statistical study of heavy metal distribution in the specific mushrooms from the sterile dumps Calimani area. Environ Eng Manag J 9:659–665
28. Cvijovic M, Djurdjevic P, Cvetkovic S, Cretescu I (2010) A case study of industrial water polluted with chromium (VI) and its impact to river recipient in western Serbia. Environ Eng Manag J 9:45–49
29. Daneshvar N, Khataee AR, Rasoulifard MH, Pourhassan M (2007) Biodegradation of dye solution containing Malachite Green: optimization of effective parameters using Taguchi method. J Hazard Mater 143:214–219. https://doi.org/10.1016/j.jhazmat.2006.09.016
30. Das N, Vimala R, Karthika P (2008) Biosorption of heavy metals—a review. Indian J Biotechnol 7:159–169
31. Davis TA, Volesky B, Mucci A (2000) A review of the biochemistry of heavy metal biosorption by brown algae. Water Resour 37:4311–4330
32. Deng D, Guo J, Zeng G, Sun G (2008) Decolorization of anthraquinone, triphenylmethane and azo dyes by a new isolated *Bacillus cereus* strain DC11. Int Biodeterior Biodegrad 62:263–269. https://doi.org/10.1016/j.ibiod.2008.01.017

33. Deng X, Wang P (2012) Isolation of marine bacteria highly resistant to mercury and their bioaccumulation process. Bioresour Technol 121:342–347
34. Deng Z, Cao L, Huang H, Jiang X, Wang W, Shi Y, Zhang R (2011) Characterization of Cd- and Pb-resistant fungal endophyte *Mucor* sp. CBRF59 isolated from rapes (*Brassica chinensis*) in a metal-contaminated soil. J Hazard Mater 185:717–724
35. Deng Z, Zhang R, Shi Y, Hu L, Tan H, Cao L (2014) Characterization of Cd-, Pb-, Zn-resistant endophytic *Lasiodiplodia* sp. MXSF31 from metal accumulating *Portulaca oleracea* and its potential in promoting the growth of rape in metal-contaminated soils. Environ Sci Pollut Res 31:2346–2357
36. Du LN, Wang S, Li G, Wang B, Jia XM, Zhao YH, Chen YL (2011) Biodegradation of malachite green by *Pseudomonas* sp. strain DY1 under aerobic condition: characteristics, degradation products, enzyme analysis and phytotoxicity. Ecotoxicology 20:438–446. https://doi.org/10.1007/s10646-011-0595-3
37. Du L-N, Zhao M, Li G, Xu F-C, Chen W-H, Zhao Y-H (2013) Biodegradation of malachite green by *Micrococcus* sp. strain BD15: biodegradation pathway and enzyme analysis. Int Biodeterior Biodegradation 78:108–116. https://doi.org/10.1016/j.ibiod.2012.12.011
38. Dursun AY, Uslu G, Tepe O, Cuci Y, Ekiz HI (2003) A comparative investigation on the bioaccumulation of heavy metal ions by growing *Rhizopus arrhizus* and *Aspergillus niger*. Biochem Eng J 15:87–92
39. El Nemr A, El-Sikaily A, Khaled A, Abdelwahab O (2015) Removal of toxic chromium from aqueous solution, wastewater and saline water by marine red alga *Pterocladia capillacea* and its activated carbon. Arab J Chem 8:105–117. https://doi.org/10.1016/j.arabjc.2011.01.016
40. El-Gendy MMA, Hassanein NM, El-Hay IHA, El-Baky ADH (2011) Evaluation of some fungal endophytes of plant potentiality as low-cost adsorbents for heavy metals uptake from aqueous solution. Aust J Basic Appl Sci 5:466–473
41. Eman ZG (2012) Production and characteristics of a heavy metals removing bioflocculant produced by *Pseudomonas aeruginosa*. Polish J Microbiol 61:281–289
42. Erto A, Giraldo L, Lancia A, Moreno-Piraján JC (2013) A comparison between a low-cost sorbent and an activated carbon for the adsorption of heavy metals from water. Water Air Soil Pollut 224. https://doi.org/10.1007/s11270-013-1531-3
43. Fallah AA, Barani A (2014) Determination of malachite green residues in farmed rainbow trout in Iran. Food Control 40:100–105. https://doi.org/10.1016/j.foodcont.2013.11.045
44. Fu X-Y, Zhao W, Xiong A-S, Tian Y-S, Zhu B, Peng R-H, Yao Q-H (2013) Phytoremediation of triphenylmethane dyes by overexpressing a *Citrobacter* sp. triphenylmethane reductase in transgenic *Arabidopsis*. Appld Microbiol Biotechnol 97:1799–1806. https://doi.org/10.1007/s00253-012-4106-0
45. Gangadevi V, Muthumary J (2014) Isolation of *Colletotrichum gloeosporioides*, a novel endophytic taxol-producing fungus from the leaves of a medicinal plant, *Justicia gendarussa*. IJSER 5:1087–1094
46. Gayathri S, Saravanan D, Radhakrishnan M, Balagurunathan R, Kathiresan K (2010) Bioprospecting potential of fast growing endophytic bacteria from leaves of mangrove and salt-marsh plant species. Indian J Biotechnol 9:397–402
47. Geethakrishnan T, Sakthivel P, Palanisamy PK (2015) Triphenylmethane dye-doped gelatin films for low-power optical phase-conjugation. Opt Commun 335:218–223. https://doi.org/10.1016/j.optcom.2014.09.033
48. Ghaedi M, Hajati S, Barazesh B, Karimi F, Ghezelbash G (2013) *Saccharomyces cerevisiae* for the biosorption of basic dyes from binary component systems and the high order derivative spectrophotometric method for simultaneous analysis of Brilliant green and Methylene blue. J Ind Eng Chem 19:227–233. https://doi.org/10.1016/j.jiec.2012.08.006
49. Göksungur Y, Dagbagli S, Ucan A, Guvenc U (2005) Optimization of pullulan production from synthetic medium by *Aureobasidium pullulans* in a stirred tank reactor by response surface methodology. J Chem Technol Biotechnol 80:819–827

50. Gomez LM, Colpas-Castillo F, Fernandez-Maestre R (2014) Cation exchange for mercury and cadmium of xanthated, sulfonated, activated and non-treated subbituminous coal, commercial activated carbon and commercial synthetic resin: effect of pre-oxidation on xanthation of subbituminous coal. Int J Coal Sci Technol 1:235–240. https://doi.org/10.1007/s40789-014-0033-2
51. Gorzin F, Ghoreyshi AA (2013) Synthesis of a new low-cost activated carbon from activated sludge for the removal of Cr (VI) from aqueous solution: equilibrium, kinetics, thermodynamics and desorption studies. Korean J Chem Eng 30:1594–1602. https://doi.org/10.1007/s11814-013-0079-7
52. Gupta N, Kushwaha AK, Chattopadhyaya MC (2016) Application of potato (*Solanum tuberosum*) plant wastes for the removal of methylene blue and malachite green dye from aqueous solution. Arab J Chem 9:S707–S716. https://doi.org/10.1016/j.arabjc.2011.07.021
53. Hamad H, Ezzeddine Z, Kanaan S, Lakis F, Hijazi A, Moussawi M-A (2016) A novel modification and selective route for the adsorption of Pb^{2+} by oak charcoal functionalized with glutaraldehyde. Adv Powder Technol 27:631–637. https://doi.org/10.1016/j.apt.2016.02.019
54. Hamid AA, Aiyelaagbe OO, Balogun GA (2011) Herbicides and its application. Adv Nat Appl Sci 5:201–213
55. Honfi K, Tálos K, Kőnig-Péter A, Kilár F, Pernyeszi T (2016) Copper(II) and Phenol adsorption by cell surface treated *Candida tropicalis* cells in aqueous suspension. Water Air Soil Pollut 227. https://doi.org/10.1007/s11270-016-2751-0
56. Iram S, Shabbir R, Zafar H, Javaid M (2015) Biosorption and bioaccumulation of copper and lead by heavy metal-resistant fungal isolates. Arab J Sci Eng 40:1867–1873. https://doi.org/10.1007/s13369-015-1702-1
57. Işik M, Sponza DT (2003) Effect of oxygen on decolorization of azo dyes by *Escherichia coli* and *Pseudomonas* sp. and fate of aromatic amines. Process Biochem 38:1183–1192. https://doi.org/10.1016/S0032-9592(02)00282-0
58. Järup L (2003) Hazards of heavy metal contamination. Br Med Bull 68:167–182
59. Jasińska A, Paraszkiewicz K, Sip A, Długoński J (2015) Malachite green decolorization by the filamentous fungus *Myrothecium roridum*—Mechanistic study and process optimization. Bioresour Technol 194:43–48. https://doi.org/10.1016/j.biortech.2015.07.008
60. Jegan J, Vijayaraghavan J, Bhagavathi Pushpa T, Sardhar Basha SJ (2016) Application of seaweeds for the removal of cationic dye from aqueous solution. Desalin Water Treat 57:25812–25821. https://doi.org/10.1080/19443994.2016.1151835
61. Jutakridsada P, Prajaksud C, Kuboonya-Aruk L, Theerakulpisut S, Kamwilaisak K (2015) Adsorption characteristics of activated carbon prepared from spent ground coffee. Clean Technol Environ Policy 18:639–645. https://doi.org/10.1007/s10098-015-1083-x
62. Kalyani S, Rao PS, Krishnaiah A (2004) Removal of nickel (II) from aqueous solutions using marine macroalgae as the sorbing biomass. Chemosphere 57:1225–1229
63. Kavand M, Kaghazchi T, Soleimani M (2014) Optimization of parameters for competitive adsorption of heavy metal ions (Pb^{+2}, Ni^{+2}, Cd^{+2}) onto activated carbon. Korean J Chem Eng 31:692–700. https://doi.org/10.1007/s11814-013-0280-8
64. Khalil MMH, Abou-Shanab RAI, Salem ANM, Omer AM, Aboelazm TA (2016) Biosorption of trivalent chromium using Ca-alginate immobilized and alkali-treated biomass. J Chem Sci Technol. https://doi.org/10.5963/jcst0501001
65. Kim WK, Shim T, Kim YS, Hyun S, Ryu C, Park YK, Jung J (2013) Characterization of cadmium removal from aqueous solution by biochar produced from a giant *Miscanthus* at different pyrolytic temperatures. Bioresour Technol 138:266–270. https://doi.org/10.1016/j.biortech.2013.03.186
66. Kinoshita KF, Bolleman J, Campbell MP, Kawano S, Kim J, Lutteke T, Matsubara M, Okuda S, Ranzinger R, Sawaki H, Shikanai T, Shinmachi D, Suzuki Y, V. Toukach V, Yamada I, Packer NH, Narimatsu H (2013) Introducing glycomics data into the Semantic Web. J Biomed Semant 3:39–43

67. Kiran MG, Pakshirajan K, Das G (2017) Heavy metal removal from multicomponent system by sulfate reducing bacteria: Mechanism and cell surface characterization. J Hazard Mater 324:62–70. https://doi.org/10.1016/j.jhazmat.2015.12.042
68. Koçer O, Acemioğlu B (2015) Adsorption of basic green 4 from aqueous solution by olive pomace and commercial activated carbon: process design, isotherm, kinetic and thermodynamic studies. Desalin Water Treat 57:16653–16669. https://doi.org/10.1080/19443994.2015.1080194
69. Kousha M, Farhadian O, Dorafshan S, Soofiani NM, Bhatnagar A (2013) Optimization of malachite green biosorption by green microalgae—*Scenedesmus quadricauda* and *Chlorella vulgaris*: application of response surface methodology. J Taiwan Inst Chem Eng 44:291–294. https://doi.org/10.1016/j.jtice.2012.10.009
70. Kristanti RA, Fikri Ahmad Zubir MM, Hadibarata T (2016) Biotransformation studies of cresol red by *Absidia spinosa* M15. J Environ Manage 172:107–111. https://doi.org/10.1016/j.jenvman.2015.11.017
71. Kuang X, Fang Z, Wang S, Shi P, Huang Z (2015) Effects of cadmium on intracellular cation homoeostasis in the yeast *Saccharomyces cerevisiae*. Toxicol Environ Chem 97:922–930. https://doi.org/10.1080/02772248.2015.1074689
72. Kück U, Pöggeler S, Nowrousian M, Nolting N, Engh I (2009) *Sordaria macrospora*, a model system for fungal development. In: Anke T, Weber D (eds) Physiology and genetics: selected basic and applied aspects. Springer, Berlin, Heidelberg, pp 17–39. https://doi.org/10.1007/978-3-642-00286-1_2
73. Kus E, Eroglu H (2015) Genotoxic and cytotoxic effects of sunset yellow and brilliant blue, colorant food additives, on human blood lymphocytes. Pak J Pharm Sci 28:227–230
74. Lee JC, Son YO, Pratheeshkumar P, Shi X (2012) Oxidative stress and metal carcinogenesis. Free Radic Bil Med 53:742–757
75. Leng L, Yuan X, Zeng G, Shao J, Chen X, Wu Z, Wang H, Peng X (2015) Surface characterization of rice husk bio-char produced by liquefaction and application for cationic dye (Malachite green) adsorption. Fuel 155:77–85. https://doi.org/10.1016/j.fuel.2015.04.019
76. Liang X, Csetenyi L, Gadd GM (2016) Lead bioprecipitation by yeasts utilizing organic phosphorus substrates. Geomicrobiol J 33:294–307. https://doi.org/10.1080/01490451.2015.1051639
77. Lim KT, Shukor MY, Wasoh H (2014) Physical, chemical, and biological methods for the removal of arsenic compounds. Biomed Res Int. https://doi.org/10.1155/2014/503784
78. Lim LBL, Priyantha N, Mohamad Zaidi NAH (2016) A superb modified new adsorbent, *Artocarpus odoratissimus* leaves, for removal of cationic methyl violet 2B dye. Environ Earth Sci 75. https://doi.org/10.1007/s12665-016-5969-7
79. Limcharoensuk T, Sooksawat N, Sumarnrote A, Awutpet T, Kruatrachue M, Pokethitiyook P, Auesukaree C (2015) Bioaccumulation and biosorption of Cd(2 +) and Zn(2 +) by bacteria isolated from a zinc mine in Thailand. Ecotoxicol Environ Saf 122:322–330. https://doi.org/10.1016/j.ecoenv.2015.08.013
80. Lopez-Luna J, Gonzalez-Chavez MC, Esparza-Garcia FJ, Rodriguez-Vazquez R (2009) Toxicity assessment of soil amended with tannery sludge, trivalent chromium and hexavalent chromium, using wheat, oat and sorghum plants. J Hazard Mater 163:829–834. https://doi.org/10.1016/j.jhazmat.2008.07.034
81. Lucova M, Hojerova J, Pazourekova S, Klimova Z (2013) Absorption of triphenylmethane dyes brilliant blue and patent blue through intact skin, shaven skin and lingual mucosa from daily life products. Food Chem Toxicol 52:19–27. https://doi.org/10.1016/j.fct.2012.10.027
82. Luo S, Li X, Chen L, Chen J, Wan Y, Liu C (2014) Layer-by-layer strategy for adsorption capacity fattening of endophytic bacterial biomass for highly effective removal of heavy metals. Chem Eng J 239:312–321
83. Malekzadeh F, Latifi AM, Shahamat M, Levin M, Colwell RR (2002) Effects of selected physical and chemical parameters on uranium uptake by the bacterium *Chryseomonas* MGF-48. World J Microbiol Biotechnol 18:599–602

84. Mani S, Bharagava RN (2016) Exposure to crystal violet, its toxic, genotoxic and carcinogenic effects on environment and its degradation and detoxification for environmental safety. In: de Voogt WP (ed) Reviews of environmental contamination and toxicology, vol 237. Springer International Publishing, Cham, pp 71–104. https://doi.org/10.1007/978-3-319-23573-8_4
85. Marcharchand S, Ting ASY (2017) *Trichoderma asperellum* cultured in reduced concentrations of synthetic medium retained dye decolourization efficacy. J Environ Manage 203:542–549
86. Martins LR, Rodrigues JAV, Adarme OFH, Melo TMS, Gurgel LVA, Gil LF (2017) Optimization of cellulose and sugarcane bagasse oxidation: application for adsorptive removal of crystal violet and auramine-O from aqueous solution. J Colloid Interface Sci 494:223–241. https://doi.org/10.1016/j.jcis.2017.01.085
87. Mastretta C, Taghavi S, van der Lelie D, Mengoni A, Galardi F, Gonnelli C, Barac T, Boulet J, Weyens N, Vangronsveld J (2009) Endophytic bacteria from seeds of *Nicotiana tabacum* can reduce cadmium phytotoxicity. Int J Phytoremediation 11:251–267
88. Mehta SK, Gaur JP (2005) Use of algae for removing heavy metal ions from wastewater: progress and prospects. Crit Rev Biotechnol 25:113–152
89. Mekhalif T, Guediri K, Reffas A, Chebli D, Bouguettoucha A, Amrane A (2016) Effect of acid and alkali treatments of a forest waste, *Pinus brutia* cones, on adsorption efficiency of methyl green. J Dispersion Sci Technol 38:463–471. https://doi.org/10.1080/01932691.2016.1178585
90. Moat AG, Foster JW, Spector MP (2003) Microbial physiology. Wiley, Canada
91. Mohee R, Mudhoo A (eds) (2012) Bioremediation and sustainability: research and applications. Wiley, Canada
92. Munck C, Thierry E, Gräßle S, Chen SH, Ting ASY (2018) Biofilm formation of filamentous fungi *Coriolopsis* sp. on simple muslin cloth to enhance removal of triphenylmethane dyes. J Environ Manage 214:261–266
93. Muthezhilan R, Vinoth S, Gopi K, Jaffar Hussain A (2014) Dye degrading potential of immobilized laccase from endophytic fungi of coastal sand dune plants. Int J ChemTech Res 6:4154–4160
94. Nagda G, Ghole V (2008) Utilization of lignocellulosic waste from Bidi industry for removal of dye from aqueous solution. Int J Environ Res Publ Health 2:385–390
95. Nandi R, Laskar S, Saha B (2016) Surfactant-promoted enhancement in bioremediation of hexavalent chromium to trivalent chromium by naturally occurring wall algae. Res Chem Intermed. https://doi.org/10.1007/s11164-016-2719-0
96. Nath J, Ray L (2015) Biosorption of malachite green from aqueous solution by dry cells of *Bacillus cereus* M116 (MTCC 5521). J Environ Chem Eng 3:386–394. https://doi.org/10.1016/j.jece.2014.12.022
97. Neupane S, Ramesh ST, Gandhimathi R, Nidheesh PV (2014) Pineapple leaf (*Ananas comosus*) powder as a biosorbent for the removal of crystal violet from aqueous solution. Desalin Water Treat 54:2041–2054. https://doi.org/10.1080/19443994.2014.903867
98. Owamah HI (2013) Biosorptive removal of Pb(II) and Cu(II) from wastewater using activated carbon from cassava peels. J Mater Cycles Waste 16:347–358. https://doi.org/10.1007/s10163-013-0192-z
99. Patil SM, Chandanshive VV, Rane NR, Khandare RV, Watharkar AD, Govindwar SP (2016) Bioreactor with *Ipomoea hederifolia* adventitious roots and its endophyte *Cladosporium cladosporioides* for textile dye degradation. Environ Res 146:340–349. https://doi.org/10.1016/j.envres.2016.01.019
100. Przystas W, Zablocka-Godlewska E, Grabinska-Sota E (2012) Biological Removal of azo and triphenylmethane dyes and toxicity of process by-products. Water Air Soil Pollut 223:1581–1592. https://doi.org/10.1007/s11270-011-0966-7
101. Przystas W, Zablocka-Godlewska E, Grabinska-Sota E (2015) Efficacy of fungal decolorization of a mixture of dyes belonging to different classes. Braz J Microbiol 46:415–424. https://doi.org/10.1590/S1517-838246246220140167

102. Pundir R, Rana S, Kaur A, Kashyap N, Jain P (2014) Bioprospecting potential of endophytic bacteria isolated from indigenous plants of Ambala (Haryana, India). Int J Pharma Sci Res 5. https://doi.org/10.13040/ijpsr.0975-8232.5(6).2309-19
103. Radha KV, Regupathi I, Arunagiri A, Murugesan T (2005) Decolorization studies of synthetic dyes using *Phanerochaete chrysosporium* and their kinetics. Process Biochem 40:3337–3345. https://doi.org/10.1016/j.procbio.2005.03.033
104. Rehman R, Mahmud T, Irum M (2015) Brilliant green dye elimination from water using *Psidium guajava* leaves and *Solanum tuberosum* peels as adsorbents in environmentally benign way. J Chem 2015:1–8. https://doi.org/10.1155/2015/126036
105. Rhee YJ, Hillier S, Gadd GM (2016) A new lead hydroxycarbonate produced during transformation of lead metal by the soil fungus *Paecilomyces javanicus*. Geomicrobiol J 33:250–260. https://doi.org/10.1080/01490451.2015.1076544
106. Safarikova M, Ptackova L, Kibrikova I, Safarik I (2005) Biosorption of water-soluble dyes on magnetically modified *Saccharomyces cerevisiae* subsp. *uvarum* cells. Chemosphere 59:831–835. https://doi.org/10.1016/j.chemosphere.2004.10.062
107. Santos CM, Dweck J, Viotto RS, Rosa AH, de Morais LC (2015) Application of orange peel waste in the production of solid biofuels and biosorbents. Bioresour Technol 196:469–479. https://doi.org/10.1016/j.biortech.2015.07.114
108. Saratale G, Kalme S, Govindwar S (2006) Decolorisation of textile dyes by *Aspergillus ochraceus* (NCIM-1146). Indian J Biotechnol 5:407–410
109. Sathish L, Pavithra N, Ananda K (2012) Antimicrobial activity and biodegrading enzymes of endophytic fungi from *Eucalyptus*. Int J Pharma Sci Res 3:2574–2583
110. Seth PK, Jaffery FN, Khanna VK (2000) Toxicology. Indian J Pharmacol 32:134–151
111. Shi X, Liu Q, Ma J, Liao H, Xiong X, Zhang K, Wang T, Liu X, Xu T, Yuan S, Zhang X, Zhu Y (2015) An acid-stable bacterial laccase identified from the endophyte *Pantoea ananatis* Sd-1 genome exhibiting lignin degradation and dye decolorization abilities. Biotechnol Lett 37:2279–2288. https://doi.org/10.1007/s10529-015-1914-1
112. Sidhu A, Agrawal S, Sable V, Patil S, Gaikwad V (2014) Isolation of *Colletotrichum gloeosporioides* gr., a novel endophytic laccase producing fungus from the leaves of a medicinal plant, *Piper betle*. Int J Sci Eng Res 5:1087–1096
113. Sim CSF, Tan WS, Ting ASY (2016) Endophytes from *Phragmites* for metal removal: evaluating their metal tolerance, adaptive tolerance behaviour and biosorption efficacy. Desalin Water Treat 57:6959–6966. https://doi.org/10.1080/19443994.2015.1013507
114. Sim CSF, Ting ASY (2017a) Metal biosorption in single- and multi-metal solutions by biosorbents: indicators of efficacy in natural wastewater. CLEAN-Soil, Air, Water. https://doi.org/10.1002/clen.201600049
115. Sim CSF, Ting ASY (2017b) FTIR and kinetic modelling of fungal biosorbent *Trichoderma asperellum* for the removal of Pb(II), Cu(II), Zn(II) and Cd(II) from multi-metal solutions. Desalin Water Treat 63:167–171
116. Sing NN, Husaini A, Zulkharnain A, Roslan HA (2017) Decolourisation capabilities of ligninolytic enzymes produced by *Marasmius cladophyllus* UMAS MS8 on Remazol Brilliant Blue R and other azo dyes. Biomed Res Int 2017:1325754. https://doi.org/10.1155/2017/1325754
117. Singh A, Manju Rani S, Bishnoi NR (2012) Malachite green dye decolorization on immobilized dead yeast cells employing sequential design of experiments. Ecol Eng 47:291–296. https://doi.org/10.1016/j.ecoleng.2012.07.001
118. Song Y, Fang H, Xu H, Tan X, Chen S (2016) Treatment of wastewater containing crystal violet using walnut shell. J Residuals Sci Technol 13:243–249. https://doi.org/10.12783/issn.1544-8053/13/4/1
119. Sun J, Zheng M, Lu Z, Lu F, Zhang C (2017) Heterologous production of a temperature and pH-stable laccase from *Bacillus vallismortis* fmb-103 in *Escherichia coli* and its application. Process Biochem. https://doi.org/10.1016/j.procbio.2017.01.030
120. Thakur IS (2011) Environmental biotechnology: basic concepts and applications. I.K. International, India

121. Ting ASY, Lee MVJ, Chow YY, Cheong SL (2016) Novel exploration of endophytic *Diaporthe* sp. for the biosorption and biodegradation of triphenylmethane dyes. Water Air Soil Pollut 227:109. https://doi.org/10.1007/s11270-016-2810-6
122. Tseng R-L, Wu P-H, Wu F-C, Juang R-S (2011) Half-life and half-capacity concentration approach for the adsorption of 2,4-dichlorophenol and methylene blue from water on activated carbons. J Taiwan Instit Chem Eng 42:312–319. https://doi.org/10.1016/j.jtice.2010.07.002
123. Uçar G, Bakircioglu D, Kurtulus YB (2014) Determination of metal ions in water and tea samples by flame-AAS after preconcentration using sorghum in nature form and chemically activated. J Anal Chem 69:420–425. https://doi.org/10.1134/s1061934814050098
124. Urairuj C, Khanongnuch C, Lumyong S (2003) Ligninolytic enzymes from tropical endophytic *Xylariaceae*. Fungal Divers 13:209–219
125. Velpandian T, Saha K, Ravi AK, Kumari SS, Biswas NR, Ghose S (2007) Ocular hazards of the colors used during the festival-of-colors (Holi) in India–malachite green toxicity. J Hazard Mater 139:204–208. https://doi.org/10.1016/j.jhazmat.2006.06.046
126. Vieira RHSF, Volesky B (2000) Biosorption: a solution to pollution? Int Microbiol 3:17–24
127. Volesky B (2001) Detoxification of metal-bearing effluents: biosorption for the next century. Hydrometall 59:203–216
128. Wang JL, Chen C (2006) Biosorption of heavy metals by *Saccharomyces cerevisiae*: a review. Biotechnol Adv 24:427–451
129. Wang J, Chen C (2009) Biosorbents for heavy metals removal and their future. Biotechnol Adv 27:195–226
130. Wilde EW, Benemann JP (1993) Bioremoval of heavy metals by the use of microalgae. Biotechnol Adv 11:781–812
131. World Health Organization (2011) Guidelines for drinking-water quality. http://www.who.int/water_sanitation_health/publications/2011/dwq_guidelines/en/. Accessed 9 Feb 2017
132. Wu Y, Xiao X, Xu C, Cao D, Du D (2013) Decolorization and detoxification of a sulfonated triphenylmethane dye aniline blue by *Shewanella oneidensis* MR-1 under anaerobic conditions. Appl Microbiol Biotechnol 97:7439–7446. https://doi.org/10.1007/s00253-012-4476-3
133. Xiao X, Luo S, Zeng G, Wei W, Wan Y, Chen L, Guo H, Cao Z, Yang L, Chen J, Xi Q (2010) Biosorption of cadmium by endophytic fungus (EF) *Microsphaeropsis* sp. LSE10 isolated from cadmium hyperaccumulator *Solanum nigrum* L. Bioresour Technol 101:1668–1674
134. Xin S, Zeng Z, Zhou X, Luo W, Shi X, Wang Q, Deng H, Du Y (2017) Recyclable *Saccharomyces cerevisiae* loaded nanofibrous mats with sandwich structure constructing via bio-electrospraying for heavy metal removal. J Hazard Mater 324:365–372. https://doi.org/10.1016/j.jhazmat.2016.10.070
135. Yang J, Pan X, Zhao C, Mou S, Achal V, Al-Misned FA, Mortuza MG, Gadd GM (2016) Bioimmobilization of heavy metals in acidic copper mine tailings soil. Geomicrobiol J 33:261–266. https://doi.org/10.1080/01490451.2015.1068889
136. Zablocka-Godlewska E, Przystas W, Grabinska-Sota E (2015) Dye decolourisation using two *Klebsiella* strains. Water Air Soil Pollut 226:2249. https://doi.org/10.1007/s11270-014-2249-6
137. Zhou F, Cheng Y, Gan L, Chen Z, Megharaj M, Naidu R (2014) *Burkholderia vietnamiensis* C09 V as the functional biomaterial used to remove crystal violet and Cu(II). Ecotoxicol Environ Saf 105:1–6. https://doi.org/10.1016/j.ecoenv.2014.03.028
138. Zhuo R, He F, Zhang X, Yang Y (2015) Characterization of a yeast recombinant laccase rLAC-EN3-1 and its application in decolorizing synthetic dye with the coexistence of metal ions and organic solvents. Biochem Eng J 93:63–72. https://doi.org/10.1016/j.bej.2014.09.004

Chapter 2
Removal of Heavy Metal from Wastewater Using Ion Exchange Membranes

Z. F. Pan and L. An

Abstract Clean water supplies are vital for industry, agriculture, and energy production. However, the water pollution issue is becoming more serious due to ever-increasing wastewater discharges from the industries into the environment. As the freshwater resource is limited, it is extremely crucial to reuse the wastewater after it has been treated to remove the heavy metal ions and other organic pollutants, which is believed to be the only way to find the new water resource. In view of the significance of treatment of wastewater contaminants, various remediation technologies are proposed and developed for efficient removal of heavy metal ions, including ultrafiltration, nanofiltration, reverse osmosis, forward osmosis, adsorption, electrodialysis method, and fuel cell method. This chapter starts with a brief introduction of heavy metals, which are chromium, nickel, copper, zinc, cadmium, mercury, and lead. Then both physical treatment and chemical treatment are summarized. Finally, the remaining challenges and future perspectives are highlighted.

Abbreviations

AAEM	Alkaline anion exchange membrane
AC	Ativated carbon
AFM	Atomic force microscope
AMAH	2-acrylamido-2-methylpropane sulfonic acid based hydrogel
APTES	Aminopropyltriethoxysilane
BET	Brunauer–Emmett–Teller
BSA	Bovine serum albumin
CdS	Cadmium sulfide
CEM	Cation exchange membrane
CPANM	Chitosan/poly(ethylene oxide)/activated carbon (AC) nanofibrous membrane

Z. F. Pan · L. An (✉)
Department of Mechanical Engineering, The Hong Kong Polytechnic University, Hung Hom, Kowloon, Hong Kong SAR, China
e-mail: liang.an@polyu.edu.hk

Inamuddin et al. (eds.), *Applications of Ion Exchange Materials in the Environment*,
https://doi.org/10.1007/978-3-030-10430-6_2

CPF	Chitosan/PEO fiber
EDA	Ethylenediamine
FTIR	Fourier transform infrared
GO	Graphene oxide
HFO	Hydrous ferric oxide
HMO	Hydrous manganese dioxide
HNT	Halloysite nanotube
HPEI	Hyperbranched polyethylenimine
IEM	Ion exchange membrane
MMM	Mixed matrix membrane
MOF	Metal–organic framework
NP	Nanoparticle
PA	Polyamide
PANI	Polyaniline
PDA	Polydopamine
PEO	Poly(ethylene oxide)
PES	Polyethersulfone
PPy	Polypyrrole
PSf	Polysulfone
PVA	Polyvinyl alcohol
PVC	Polyvinyl chloride
PVDF	Polyvinylidene fluoride
SEM	Scanning electron microscope
TEM	Transmission electron microscope
TFC	Thin-film composite
UCrFC	Urine/Cr(VI) fuel cell
XRD	X-ray diffractor

2.1 Introduction

Water is one of the primitive requirements for humans' living and society development, suggesting that water is basically necessary for a variety of fields [1]. On the one hand, the freshwater that human can use directly is limited, resulting in that more than a billion people currently live in water-scarce regions, and as many as 3.5 billion could experience water scarcity by 2025 [2]. On the other hand, the water pollution problem has been ever increasingly serious due to the rapid development of industries, including fertilizer industries, metal plating facilities, tanneries, batteries, paper industries, mining operations, and pesticides [3]. Both the two issues lead to a severe water shortage. Since the exploitation of new freshwater is not easy and expensive, treatment of wastewater that is polluted is acceptable to remove the containments such as heavy metal ions, dyes, biodegradable waste, nitrates and phosphates, sediment, fluoride, hazardous and toxic chemicals, radioactive

pollutants, and pharmaceuticals for obtaining the freshwater [4]. Among the various pollutants, rejection of heavy metal ions is essential and challenging due to the fact that heavy metal ions are not biodegradable and tend to accumulate in living organisms [3]. In addition, excessive inhalation of heavy metal ions may cause serious toxic effects to humans. In general, the heavy metals are defined as the elements with atomic weights between 63.5 and 200.6 as well as a specific gravity greater than 5.0 [5]. In order to dispose of the pollutants in wastewater, both physical and chemical treatments have been adopted, which include ion exchange, supercritical fluid extraction, adsorption [6], filtration, electrodialysis, precipitation [7], and the electrochemical process [8]. Particularly, each treatment has its specific advantages and disadvantages. The advantage of ion exchange is the high transformation of components, but operational cost is high and only limited metal ions can be rejected. The advantages of adsorption are easy operation, less sludge production, and utilization of low-cost adsorbents, but the desorption still needs to be addressed so that the adsorbents can be reused. The advantages of filtration are lower space requirement and high removal of heavy metals, but it is expensive and complex as well as suffers from membrane fouling. The advantage of electrodialysis is the high rejection rate, but it requires high energy input and membrane clogging may occur. The advantages of precipitation are the low-cost and high dewatering qualities, but it uses plenty of chemicals and the precipitate generation rate is not satisfactory. The advantages of the electrochemical process are low chemical usage and efficient removal, but it needs high energy input. Typically, ion exchange membrane (IEM) plays an important role in these treatments, which is made up of specific porous material [1]. This chapter gives an introduction of common heavy metal ions, which are chromium (Cr), nickel (Ni), copper (Cu), zinc (Zn), cadmium (Cd), mercury (Hg), and lead (Pb) followed by both physical and chemical treatments. Finally, the remaining challenges and future perspectives are highlighted.

2.2 Heavy Metal

2.2.1 Chromium

The general information of Cr, which is the most available seventh element in the earth, can be concluded as follows: CAS number is #7440-47-3, atomic weight is 52, atomic number is 24, density is 7.2 g cm^{-3}, melting point is 1857 °C, boiling point is 2672 °C, and oxidation states are +2, +3, and +6. In nature, Cr occurs primarily as ferric chromite, which is the most stable state of oxidation. In spite of the stable state, it also occurs in divalent and hexavalent forms [9]. In general, the principal industrial consumers of Cr are metallurgical, refractory, and chemical industries. Hexavalent Cr(VI) and trivalent Cr(III) forms are produced during these industrial processes. In addition, Cr(VI) is more harmful than the Cr(III) for plants,

animals, and organisms [10, 11]. Particularly, vomiting, liver and kidney damage, skin inflammation, the creation of ulcer, and pulmonary congestion may be caused by excessive inhalation of chromium [12, 13]. Considering the harmful effects, the industrial wastewater must be treated to remove the Cr(VI) or to change the Cr(VI) into less toxic one before it is released to the environment.

2.2.2 Nickel

The general information of Ni can be concluded as follows: CAS number is #7440-02-0, atomic weight is 58.71, atomic number is 28, density is 8.9 g cm^{-3}, the melting point is 1453 °C, the boiling point is 2732 °C, and oxidation states are +1, +2, and +3. In nature, Ni exists primarily in sulfide or oxide ores as an earth element, which is the twenty-fourth most abundant element on earth. The procedures of extraction of Ni are flotation, magnetic separation, roasting, and melting [9]. Ni plays an important role in both industrial use and un-industrial use. The former includes steel and alloy production, nickel–cadmium battery production, electroplating, chemical catalysis, and manufacture of electronic components. The latter is associated with coins, jewelery, watches, and eyeglass frames [9]. A dry cough, chest pain, creates breathing problem, nausea, diarrhea, skin eruption, pulmonary fibrosis, gastrointestinal ache, renal edema may be caused by excessive inhalation of nickel [11, 14–16]. Therefore, to avoid the human health risks, adequate treatment technology is required to recover the copper from the wastewater.

2.2.3 Copper

The general information of Cu, which is an essential trace element, can be concluded as follows: CAS number is #7440-50-8, atomic weight is 63.54, atomic number is 29, density is 8.94 g cm^{-3}, the melting point is 1083 °C, the boiling point is 2595 °C, and oxidation states are +1 and +2. In nature, Cu occurs primarily as sulfidic copper ores (approximately 90%), oxidic copper ores (9%), and metallic copper ores (<1%). The processes of copper production are different based on the type of ores. Both sulfidic copper ores and oxidic copper ores involve extensive and concentration procedures subjected to roasting, converting, and electrolytic refining [9]. The most essential utilization of Cu is the transmission of electricity in wires and cables. Besides, Cu compounds are widely used in wood preservatives, fungicides, as pigments and antifouling agents in paints, as nutritional additives to livestock, and additive to fertilizers [9]. Comparing to Cu(I), Cu(II) is believed to be more toxic in the environment [17]. Hair loss, anemia, kidney damage, and headache may be caused by excessive inhalation of copper [18]. In order to remove the Cu from wastewater, it is urgent to develop an attractive treatment methodology to recover the Cu.

2.2.4 Zinc

The general information of Zn, which is an essential trace element, can be encapsulated as follows: CAS number is #7440-66-6, atomic weight is 65.38, atomic number is 30, density is 7.13 g cm^{-3}, the melting point is 419.5 °C, the boiling point is 908 °C, and oxidation state is +2. In nature, sphalerite is the most important Zn ore, and zinc oxide is the most common compound in the industry [9]. Zinc can act as a protective coating for other metals, preventing the corrosion of metals. It is also used in dye casting, construction industry, and noncorrosive alloys. Although it is required necessary for the humans in trace level, pain, vomiting, skin inflammation, fever, vomiting, and anemia may be caused by excessive inhalation of zinc [19]. As a result, the removal of zinc from the industrial effluent has recently gained a lot of attention.

2.2.5 Cadmium

The general information of Cd, which is silver-white malleable metal, can be summarized as follows: CAS number is #7440-43-9, atomic weight is 112.4, atomic number is 48, density is 8.6 g cm^{-3}, the melting point is 320.9 °C, the boiling point is 765 °C, and oxidation state is +2. Cd is a common impurity in zinc and lead ores; thus, it is principally obtained during the refining of zinc and lead as a by-product [9]. Cd has been used in a number of industrial applications. As it is capable to protect iron from rusting, Cd is used to coat iron products via electroplating [9]. In addition, Cd can be used in alloy synthesis, which contributes to improving the mechanical resistance at increased temperature, including copper–cadmium alloy and nickel–cadmium alloy [9]. Cd is also able to serve as an electrode component in a nickel–cadmium battery, which is the most important application of Cd currently [1]. Cadmium sulfide (CdS) and cadmium sulfoselenide are used as color pigments in various plastics and paints [9]. It is worth mentioning that CdS has been introduced into the photocatalysts for ultraviolet light response functioning as quantum dots in photoelectrochemical cells, which expands the absorption spectrum from ultraviolet light to visible light and facilitates the electron–hole pairs separation [20]. Cadmium oxide is used in black and white television phosphors and in the blue and green phosphors of color television cathode ray tubes [21]. However, it is regarded as most toxic heavy metal found in the industrial effluent as well. Both acute poisoning and chronic poisoning may be exerted on human health due to the excessive inhalation of cadmium. Generally, the former one was rare, while the latter has received ever-increasing attention. Lung cancer, hepatic toxicity, and harm to the kidney, liver, respiratory system, and reproductive organs may be caused by excessive inhalation of cadmium [11, 22]. Because of the negative effects, Cd from the wastewater is required to be removed via economically reliable and efficient treatment.

2.2.6 Mercury

The general information of Hg, which is the only liquid metallic element at standard conditions for temperature and pressure, can be concluded as follows: CAS number is #7439-97-6, atomic weight is 200.6, atomic number is 80, density is 13.6 g cm^{-3}, melting point is −38.9 °C, boiling point is 356.6 °C, and oxidation states are +1 and +2. In nature, up to 70%, Hg is contained in cinnabar, which is a red mercury sulfide and is the main component of mercury ores. In general, half of the Hg is consumed in chlorine–caustic soda manufacture, and half of the Hg is used in dental amalgams, mercury electronic switches, fluorescent lamps, and electronic devices [9]. Since the Hg metal ions, including Hg(I) and Hg(II), can transport in aqueous solution, it can accumulate in ecosystems, which is harmful to human health and the environment. Metallic Hg is rather volatile and the Hg vapor is toxic to human as well [23–25]. The Minamata happened in Japan in 1956 has raised worldwide awareness of the mercury pollution [26]. Kidney, brain, reproductive, and respiratory systems may be damaged due to excessive inhalation of mercury. Hence, it is urgent to develop an efficient methodology for the removal of mercury from the wastewater.

2.2.7 Lead

The general information of Pb, which is a relatively unreactive post-transition metal, can be concluded as follows: CAS number is #7439-92-1, atomic weight is 207.19, atomic number is 82, density is 11.3 g cm^{-3}, melting point is 327.5 °C, boiling point is 1740 °C, and oxidation states are +2 and +4 [9]. In nature, Pb exists in the form of sulfide, cerussite ($PbCl_2$), and galena [27]. Currently, 71% of Pb was used in batteries mainly for vehicles, which plays a dominant role. Others are used in pigment (12%), ammunition (6%), and cable sheeting (3%) [9]. Kidney and nervous system damage, mental retardation, and cancer may be caused by excessive inhalation of Pb [28, 29]. In view of the risks to the plants and animals, development of a treatment technology for removal of Pb has attracted ever-increasing attention.

In summary, the mentioned heavy metal ions can accumulate in humans and environment, which leads to various negative effects on humans as well as environmental problems based on their toxicity. The toxic effects are concluded in Table 2.1. As clean water is one of the most important elements for all living organisms, the heavy metal ions occurred in water resources should be removed efficiently and cost-effectively.

Table 2.1 Toxic effects of heavy metals

Heavy metal	Toxic effects
Cr	Vomiting, liver and kidney damage, skin inflammation, the creation of ulcer, and pulmonary congestion
Ni	A dry cough, chest pain, creates breathing problem, nausea, diarrhea, skin eruption, pulmonary fibrosis, gastrointestinal ache, renal edema
Cu	Hair loss, anemia, kidney damage, and headache
Zn	Pain, vomiting, skin inflammation, fever, vomiting, and anemia
Cd	Lung cancer, hepatic toxicity, and harm to the kidney, liver, respiratory system, and reproductive organs
Hg	Kidney, brain, reproductive, and respiratory systems
Pb	Kidney and nervous system damage, mental retardation, and cancer

2.3 Physical Treatment Methods

2.3.1 Ultrafiltration

Ultrafiltration is a separation technique, in which pressure gradient or concentration gradient as a driven force leads to a separation, requiring low energy for the wastewater treatment [30]. This process is capable to remove the particles with the size range of 10–100 nm [1]. Daraei et al. [31] prepared nanocomposite polymeric membrane from polyethersulfone (PES) and polyaniline/iron(II, III) oxide (PANI/Fe_3O_4) nanoparticles (NPs) by phase inversion method for Cu(II) removal. It was indicated that the most possible removal mechanism by this membrane was sorption. The results showed that the membrane with 0.1 wt% NPs exhibited the highest ion rejection, which was 85 and 75% for high concentration aqueous solution (20 mg L^{-1} $Cu(NO_3)_2$) and low concentration aqueous solution (5 mg L^{-1} $Cu(NO_3)_2$), respectively. Similarly, Gohari et al. [32] synthesized PES/hydrous manganese dioxide (HMO) ultrafiltration mixed matrix membranes (MMMs) for removal of Pb(II). The effect of weight ratio of HMO:PES on the membrane pure water flux, hydrophilicity, porosity, and Pb(II) adsorption capacity was investigated. It was demonstrated that a higher ratio resulted in a decreased pore size. In addition, a higher HMO loading resulted in a higher water flux, which was ascribed to the lower contact angle value, increased porosity, and greater surface roughness. The results from Pb(II) adsorption experiments showed that a remarkable uptake capacity of 204.1 mg g^{-1} was achieved at pH between 6 and 8, suggesting that the membrane with weight ratio of 2.0 was capable to treat natural water directly. The original adsorption capacity was 97.5% maintained after a simple recovery process, indicating its potential to be applied in industrial applications. Ghaemi et al. [33, 34] prepared the polypyrrole (PPy)-coated alumina (Al_2O_3) NPs via an oxidative polymerization reaction. Afterward, the PPy@Al_2O_3 NPs were added into pristine PES membrane for removal of Cu(II). It was found that the composite membrane

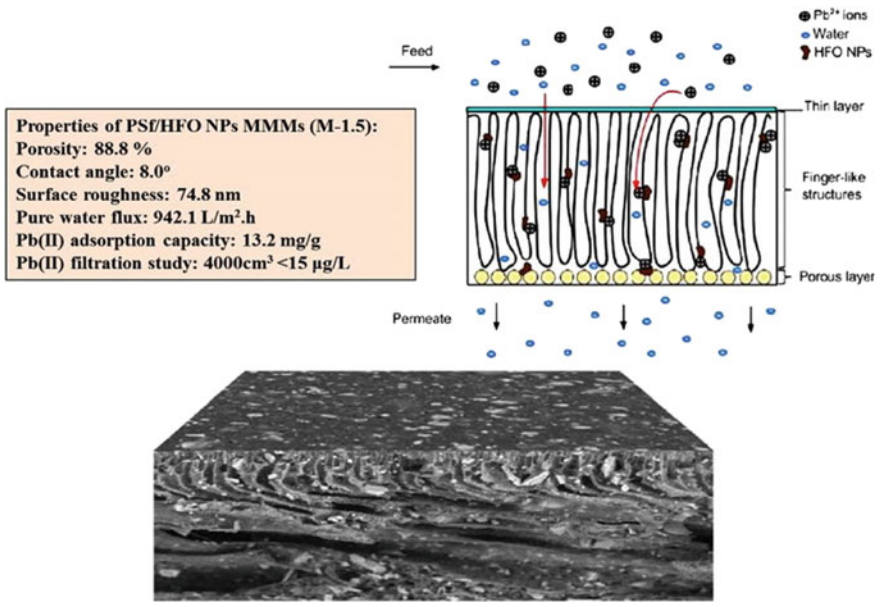

Fig. 2.1 Schematic of the PSf/HFO NPs ultrafiltration membrane [36]. Reproduced with the permission from Elsevier

with 1.0 wt% PPy@Al_2O_3 NPs yielded the highest Cu rejection (80%) comparing to other doping amount. Mukherjee et al. [35] integrated graphene oxide (GO) with mixed matrix membranes (MMM) via non-solvent induced phase inversion method. After GO was added into MMM, the membrane became highly permeable, hydrophilic, and charged. It was demonstrated that the optimal amount of GO addition was 0.2 wt%, which was ascribed to adsorption, diffusion, and convection. The results from the rejection tests showed that the adsorption capacities of Pb(II) (pH = 6.7), Cu(II) (pH = 6.5), Cd(II) (pH = 6.4), and Cr(VI) (pH = 3.5) were 79, 75, 68, and 154 mg g^{-1}, respectively. Abdullah et al. [36] proposed a polysulfone (PSf)/hydrous ferric oxide nanoparticles (HFO NPs) ultrafiltration MMMs for removal of Pb(II) from aqueous solution as shown in Fig. 2.1. The physiochemical properties of this membrane were characterized via transmission electron microscope (TEM), Brunauer–Emmett–Teller (BET), X-ray diffractor (XRD), Fourier transform infrared (FTIR), scanning electron microscope (SEM), atomic force microscope (AFM), pure water flux analysis, contact angle measurement, and membrane porosity analysis. The results showed that the specific surface area of the HFO NPs was 233.49 m^2 g^{-1} and a higher weight ratio of HFO NPs in membrane led to a significant increase in membrane pure water flux from 229.5 L m^{-2} h^{-1} to 942.1 L m^{-2} h^{-1}, which was because of the enhanced hydrophilicity and greater surface roughness. It was confirmed that the optimal weight ratio of HFO NPs:PSf was 1.5 and the optimum pH was 6.5–7.0, which resulted in the highest adsorption capacity of Pb(II) of 13.2 mg g^{-1}. The pore size of the membrane may be larger

than the size of metal ions, and hence, chemical or polymeric agents are added into the membrane for better removal performance. Moreover, it will be ideal that a universal membrane can be synthesized by removing the majority of heavy metal ions, which should attract more attention in the future.

2.3.2 Nanofiltration

Nanofiltration is also a membrane filtration-based method, and the mechanism is similar to ultrafiltration. While comparing to ultrafiltration, nanofiltration membranes have smaller pore sizes (1–10 nm). It is believed that nanofiltration is an intermediate technique between ultrafiltration and reverse osmosis [37]. Zhang et al. [38] synthesized nanometric graphene oxide framework nanofiltration membranes for removal of heavy metal ions. Initially, the GO framework was constructed by the cross-linking of ethylenediamine (EDA). Afterward, the GO framework was modified by hyperbranched polyethyleneimine (HPEI), introducing numerous amine functional groups. It was illustrated that the EDA cross-linking not only provided enhanced structural stability but also enlarged the nanochannels, resulting in promoted water permeability. HPEI 60 K could enhance the surface charge and reduce the transport resistance. The rejections of Pb(II), Ni(II), Zn(II), and Cd(II) were 95.7, 96.0, 97.4, and 90.5%, respectively. Ghaemi et al. [39] modified Fe_3O_4 nanoparticles with silica, metformine, and amine coating, which were employed for fabrication of polyethersulfone (PES) mixed matrix membranes. The optimal adding of modified Fe_3O_4 nanoparticles was 0.1 wt%, showing a copper removal as high as 92%. This remarkable removal ability was attributed to the improved hydrophilicity and the presence of nucleophilic functional groups on nanoparticles. Bolisetty et al. [40] developed amyloid–carbon hybrid membranes for universal water purification for removal of heavy metal ions, metal cyanides, and nuclear waste. The amount of heavy metal ions dropped three to five orders of magnitude per passage after filtration, and this membrane was able to reuse for numerous times. The rejected valuable heavy metal contaminants could be recycled easily via a simple thermal reduction process. Zeng et al. [41] synthesized halloysite nanotubes (HNTs) functionalized with 3-aminopropyltriethoxysilane (APTES), and polyvinylidene fluoride (PVDF) nanofiltration membranes for removal of Cu(II), Cd(II), and Cr(VI). The introduction of A-HNTs nanoparticles significantly improved the hydrophilicity of membranes due to the presence of abundant hydrophilic functional groups including hydroxyl and amino, resulting in a higher pure water flux. Particularly, the rejection of Cu(II) reached almost 100% with the pH > 9. Habiba et al. [42] synthesized chitosan/polyvinyl alcohol (PVA)/zeolite nanofibrous composite membrane via electrospinning for removal of Cr(VI), Fe (III), and Ni(II). This membrane showed remarkable stability in neutral, acidic, and basic media for 20 days as well as after five recycling runs. It was indicated that the

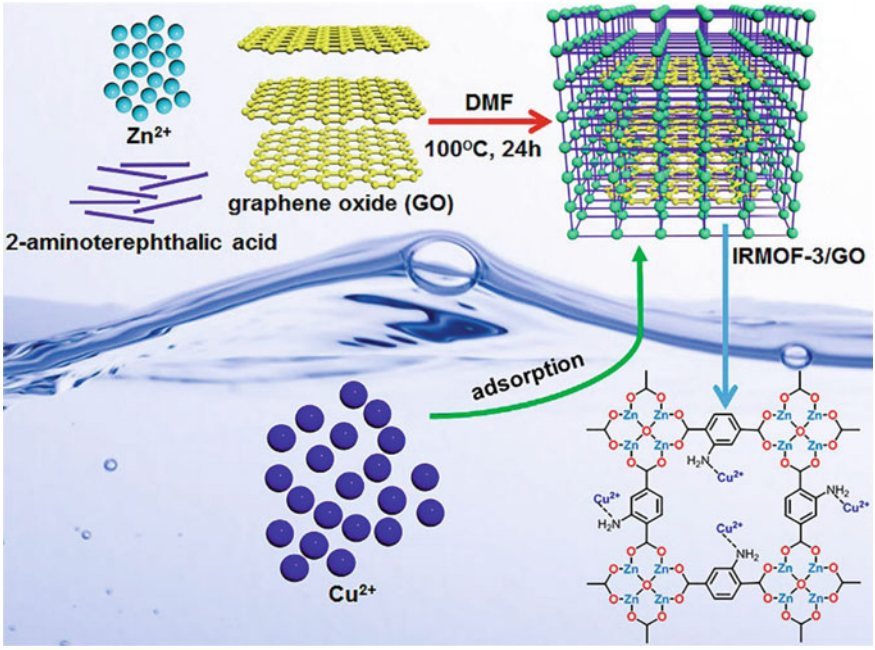

Fig. 2.2 Schematic diagram of the preparation of IRMOF-3/GO and the adsorption of Cu(II) on IRMOF-3/GO [43]. Reproduced with the permission from the American Chemical Society

Cr(VI) adsorption can be well described by the pseudo-second-order kinetic model. In addition, the adsorption of Fe(III) and Ni(II) was well described by Lagergren first-order model. However, the adsorption capacity at high concentration was not satisfactory. Rao et al. [43] prepared metal–organic framework/graphene oxide composite (IRMOF-3/GO) decorated polydopamine (PDA)-coated PSf membrane for Cu(II) removal as shown in Fig. 2.2. It was reported that this membrane exhibited a rejection of Cu(II) as high as 90% with a high flux of 31 L m^{-2} h^{-1}, which was attributed to the adsorption effect of IRMOF-3/GO and the enhancement of membrane surface potential. Meschke et al. [44] found that the dominant parameter of divalent cation removal was the size, while the pH exhibited negligible effect on the rejection. For monovalent cations, as the hydrated radius was smaller, the size exclusion is less dominating. They also reported that in acid media, the separation during concentrating was difficult to realize [45]. This was because of the shearing forces and the build-up concentration as well as the electric field gradient forced the permeation of the solutes. Nanofiltration is an effective method for heavy metal removal, which is easily operative and energy saving. Similarly, developing a universal membrane for removing the majority of heavy metal ions can be one of the future research directions.

2.3.3 *Reverse Osmosis*

Reverse osmosis is a water purification technology that employs semi-permeable membranes for removal of contaminants and only allows the water to pass through the membrane [37]. The pore size of the reverse osmosis membranes is in the range of 0.1–1.0 nm. Particularly, to overcome osmotic pressure, an applied pressure is essential in reverse osmosis; thus, the operation requires high energy [1]. Li et al. [46] theoretically evaluated the rejection performance of heavy metal ions utilizing nanoporous graphene surfaces as reverse osmosis membranes with functionalized groups (boron, nitrogen, and hydroxyl groups) as shown in Fig. 2.3. It was demonstrated that water permeability is 2–5 orders of magnitude higher than that of commercial membranes, which was attributed to the lower free energy barrier than ions when passing through graphene pores. The barrier for ion transport was ascribed to the combining contributions from the ion dehydration effect and the surface electrostatic interaction. This characteristic of the membrane showed the possibility that this membrane could be applied for the rejection of heavy metal ions. Petrinic et al. [47] proposed a combination of ultrafiltration and reverse

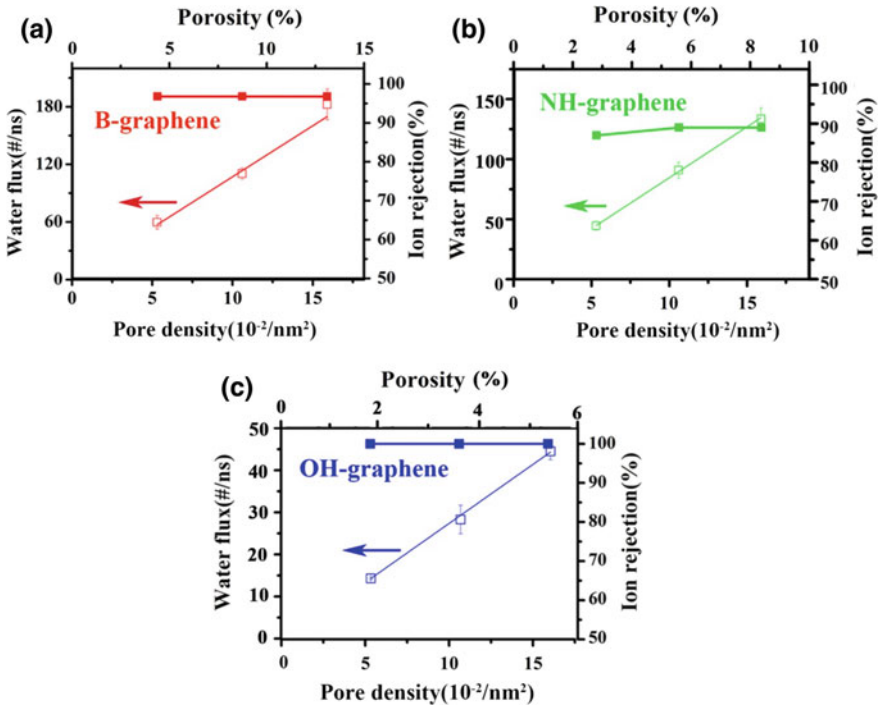

Fig. 2.3 Effect of pore density (or porosity) on water flux and ion rejection at an applied pressure of 200 MPa: **a** B-graphene, **b** NH-graphene, and **c** OH-graphene membranes [46]. Reproduced with the permission from Elsevier

osmosis for heavy metal removal. In view of the membrane fouling and clogging problem, the ultrafiltration serves as a pre-treatment to remove the contaminants, whose sizes were larger than 0.4 μm, before a final reverse osmosis process. It was demonstrated that almost 90% of suspended solids were first rejected by the ultrafiltration process, and 91.3–99.8% of metal elements and organic/inorganic compounds were removed by the reverse osmosis. It is widely agreed that the major shortcoming of reverse osmosis is the high power consumption and the restoration of the membranes [3]. Therefore, it is favorable to combine reverse osmosis with other wastewater treatment to compensate the high cost.

2.3.4 *Forward Osmosis*

Forward osmosis is an emerging technology for removal of heavy metals. Although it is similar to reverse osmosis, the major difference lies in the driven force. As the driven force of forward osmosis is the osmotic pressure gradient, this process possesses several advantages in terms of efficient water recovery, low energy consumption, less membrane fouling, and easy fouling removal [48]. Cui et al. [49] developed a forward osmosis using a thin-film composite (TFC) made from interfacial polymerization on a macrovoid-free polyimide support as the forward osmosis membrane and a novel bulky hydroacid complex $Na_4[Co(C_6H_4O_7)_2]\cdot 2H_2O$ (Na–Co–CA) as the draw solute. It was reported that the process exhibited a heavy metal rejection as high as 99.5% with water fluxes fixed at around 11 L m^{-2} h^{-1}, draw solution fixed at 1 M, and heavy metal salts concentration fixed at 2000 ppm, which was higher than most of nanofiltration processes. The rejection could be further increased by increasing the concentrations of draw solutions and heavy metal ions, or raising the temperature. Zhao et al. [50] synthesized forward osmosis membrane with the glass nanofiber supporting layer and the bovine serum albumin (BSA)-embedded polyamide (PA) swellable active layer as shown in Fig. 2.4.

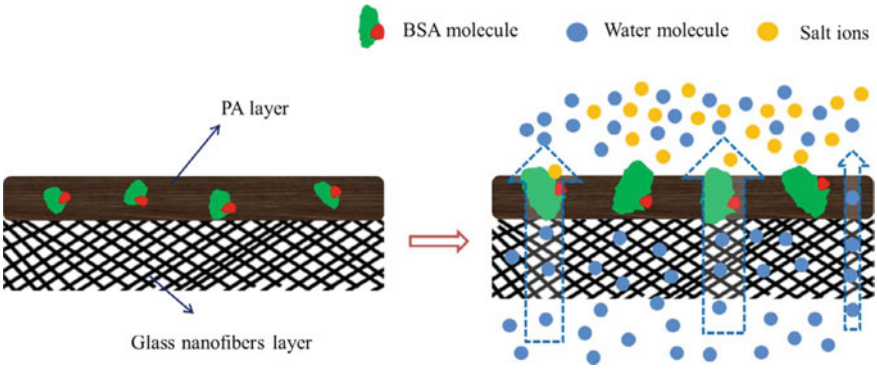

Fig. 2.4 Schematic diagram of the separation mechanism of the prepared FO membranes [50]. Reproduced with the permission from Elsevier

The glass nanofiber supporting layer provided transport channels for flow process, and active layer bi-functioned as water channels and reinforced barrier. The results showed that all the recovery ratios of Cu(II), Pb(II), and Cd(II) were exceeding 99.4%. The impressive performance was attributed to the double-layer structure, which was beneficial for enhancing the dissolution-diffusion-flow separation process as well as stabilizing the separation selectivity. Several issues associated with forward osmosis still need to be addressed to realize the commercialization. These include (1) the low-performance forward osmosis membranes; (2) the ineffective draw solutes; and (3) high cost in draw solute regeneration.

2.3.5 Adsorption

Adsorption is an efficient and admirable process to remove heavy metal ions. In principle, the advantages of this method are low operating cost, simple and flexible design, low fouling problems, and negligible toxic pollutant production [51]. In addition, adsorbents can be recreated by the desorption process after the adsorption process, which means that it is reversible technique. Li et al. [52] synthesized chitosan/sulfhydryl-functionalized graphene oxide composite (CS/GO-SH) via covalent modification and electrostatic self-assembly. This membrane was characterized by FTIR, Raman spectroscopy, SEM, XRD, and thermogravimetric examination. The results showed that this membrane possessed abundant multifunctional groups, including –OH, –COOH, –SH, and $–NH_2$. In unitary metal ion system, the adsorption capacities of Cu(II) and Pb(II) are similar, while the adsorption capacity of Cd(II) is lower. For ternary metal ion system, the order of adsorption capacity is Cd(II) > Cu(II) > Pb(II). Chen et al. [53] prepared 4-aminothiophenol and 3-aminopropyltriethoxysilane functioned GO via graft modification for Cu(II) removal from aqueous solution. It was illustrated that sulfhydryl (-SH) and amino groups ($-NH_2$) were associated with 4-aminothiophenol modified GO (GO-SH) and 3-aminopropyltriethoxysilane modified GO (GO-N). The maximum adsorption capacities of GO-SH and GO-N were 99.17 and 103.28 mg g^{-1}, which were much higher than the pristine GO (32.91 mg g^{-1}). The reason for this enhancement was the increase in sorption sites as well as the chelation with heavy metals. Henriques et al. [54] reported that combination of oxygen and nitrogen functional groups effectively improved the adsorption capacity of GO toward Hg(II). This improvement was attributed to shifting of the equilibrium of the reaction derived from the fact that the nitrogen and oxygen functional groups possessed different acidic properties. It was indicated that a small dose of this material (10 mg L^{-1}) showed a high removal rate of 95% after 24 h and a maximum sorption capacity of 35 mg g^{-1}. Wan et al. [55] proposed a GO-based sorbent for Pb(II) removal. Aiming at improving the adsorption selectivity and ability in solid–liquid separation of GO, nanosized hydrated manganese oxide (HMO) (10.8 ± 4.1 nm) was in situ grown on GO. The HMO@GO exhibited splendid adsorption selectivity and capacity toward Pb(II), reaching 500 mg g^{-1} in the presence of Ca(II). The outstanding performance

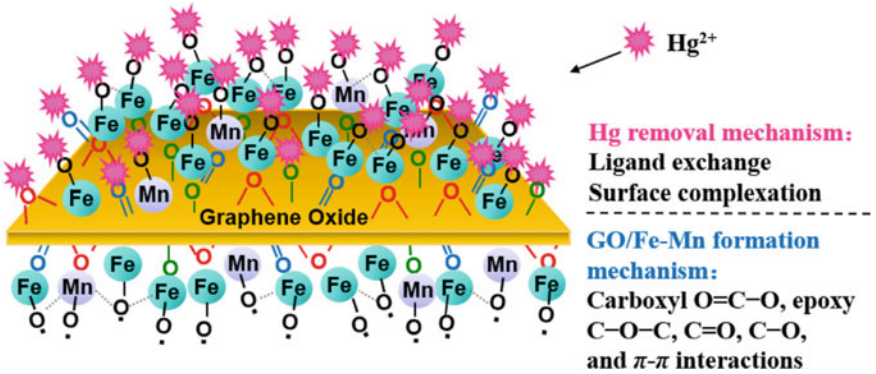

Fig. 2.5 Schematic of the separation mechanism of GO/Fe–Mn composite [56]. Reproduced with the permission from Elsevier

was mainly ascribed to the abundant oxygen-containing groups on GO that preferably sequestrated Pb(II) through specific interaction, and the host GO offering the pre-concentration of Pb(II) for enhanced sequestration through the Donnan membrane effect. Similarly, Tang et al. [56] fabricated GO/Fe–Mn composite with molar ratio of Fe/Mn = 3/1 and mass ratio of Fe/GO = 1/7.5 for Hg(II) removal as shown in Fig. 2.5. The separation of Hg(II) was dominated by ligand exchange and surface complexation. The adsorption capacity was 32.9 mg g^{-1}. It was worth mentioning that the bioavailability of mercury also could be reduced, thus promoting the seedling growth. Shariful et al. [57] prepared chitosan/poly(ethylene oxide) (PEO) nanofibrous membrane via electrospinning process. The beadless fibers possessed average diameter, maximum tensile strength, and the specific surface area as 115 ± 31 nm, 1.58 MPa, and 218 m^2 g^{-1}, respectively. Moreover, higher specific surface area and hydrophilicity also contributed to maximum adsorption capability. Shariful et al. [58] synthesized chitosan/poly(ethylene oxide)/activated carbon (AC) nanofibrous membrane (CPANM) via electrospinning process. The membrane showed that the highest adsorption capacities for Pb(II), Zn(II), Cu(II), Fe (III), and Cr(VI) were 176.9, 186.2, 195.3, 217.4, and 261.1 mg g^{-1}, respectively. It was explained that not only the $–NH_2$ in chitosan/PEO fiber (CPF) acted as active group, but also the –COOH in the fiber surface, which was introduced by the AC, contributed to superior adsorption. The adsorption process has become the leading technique in the heavy metal removal due to its superiorities, including low operating cost, simple and flexible design, low fouling problems, and negligible toxic pollutant production. The rejection performance was mainly dominated by the surface area, functional groups, pore size distribution, and the polarity of the adsorbent.

2.4 Chemical Treatment Methods

2.4.1 Electrodialysis Method

Electrodialysis is used to transport ions from one solution through IEMs to another solution under the control of an applied electric field [59]. The advantages of this separation process are as follows: (1) high water recovery; (2) easily scale up; (3) low usage of chemicals; and (4) easy combination with other technologies [60]. Babilas et al. [61] used electrodialysis to selectively recover zinc from simulated electroplating industry wastes, which was enhanced with complex formation method. It was demonstrated that the Zn recovery and current efficiency were 86.6 and 84.95%, respectively. Nemati et al. [60] prepared a heterogeneous cation exchange membrane (CEM) consisting of polyvinyl chloride (PVC) and 2-acrylamido-2-methylpropane sulfonic acid-based hydrogel (AMAH). It was indicated that this membrane showed promising dimensional stability, higher water content, more hydrophilic surface, and more porous structure. The results from rejection experiment showed that the outstanding rejection capacities of Pb(II) and Ni(II) were about 99.9%, suggesting that the membrane possessed the desirable potential for scaling practical applications. Ge et al. [62] used homemade nanofiltration membrane in electrodialysis to replace the conventional CEM so as to separate the multivalent ions and monovalent ions. It was reported that the porous structure of nanofiltration membrane could decrease the transfer resistance of ions, enhance the limiting current density, and improve the ion flux. The separation was feasible because the divalent cations rather than monovalent cations could be rejected effectively due to the presence of the dense layer of nanofiltration membrane. Since the anode releases electrons, where oxidation reactions take place, thus the anode side will be of acidic mature. Therefore, more attention should be paid into the corrosion problem. On the cathode, the electrons are received and reduction reactions take place, and thus cathode side will be alkaline. Hence, the scaling issue should be addressed for long-term durability.

2.4.2 Fuel Cell Method

Fuel cells are generally considered as an emerging energy conversion technology [63–65]. In principle, there is a reduction reaction at fuel cell cathode, which is basically identical to converting Cr(VI) to Cr(III) [66]. Therefore, Zhang et al. [67–69] proposed the strategy using fuel cell to deal with the Cr(VI)-containing wastewater with cogeneration of electricity. Zhang et al. [67] developed an alkaline fuel cell with ethanol-fed into the anode as fuel and Cr(VI) containing solution fed into the cathode as oxidant to operate the Cr(VI) reduction. The removal efficiency was found to improve with increasing Cr(VI) feeding concentration. The removal efficiency increased from 89.1 to 96.0% as the Cr(VI) concentration increased from

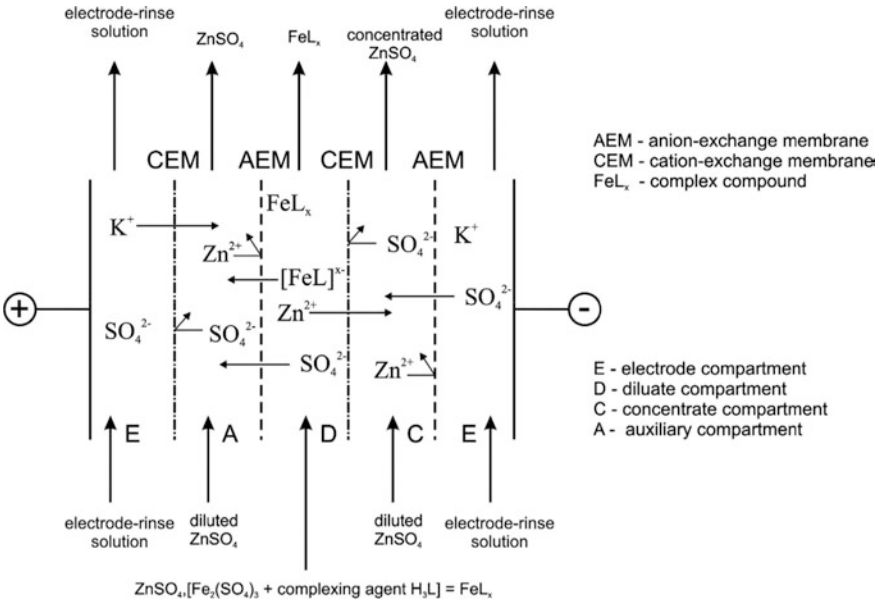

Fig. 2.6 Schematic representation of electrodialysis setup [61]. Reproduced with the permission from Elsevier

0.55 to 3.94 mM. When the H^+ concentration increased from 0.1 to 1.0 M, the removal efficiency increased from 64.6 to 83.3% as well. The cathodic efficiency was promoted from 24.86 to 63.15% as the Cr(VI) concentration increased from 0.5 to 3.94 mM. It should mention that the cathodic efficiency was always lower than 100%, which was attributed to the presence of oxygen that occupied the electrons for Cr(VI) reduction (Fig. 2.6). Xu et al. [68] developed a urine/Cr(VI) fuel cell (UCrFC) for reducing Cr(VI) and generating electricity simultaneously as shown in Fig. 2.7. It could be seen that the configuration of the UCrFC, which was composed of a Ni-based anode, an alkaline anion exchange membrane (AAEM), a CEM, and a cathode made of carbon cloth. It was observed that the removal efficiency of Cr(VI) was 93% after operating for 71 h. Afterward, Zhang et al. [69] proposed that a phenol-Cr(VI) coupled redox fuel cell was able to remove the phenol and Cr(VI) efficiently without energy supply. Phenol was oxidized on Ni/C anode to release electrons, and Cr(VI) was reduced to Cr(III) by receiving the electrons transported through the external circuit. It was indicated that the removal efficiency of phenol was 98.6% within 132 h, and removal efficiency of Cr(VI) was 99.8% within 60 h. Qian et al. [70] studied the dependency of migration and reduction of mixed $Cr_2O_7^{2-}$, Cu(II), and Cd(II) on electric field, ion exchange membranes (IEMs) and metal concentration in microbial fuel cells. Circuit current directed reduction of more metals on the cathodes with less migration across the IEMs, compared to the more metal transport in the absence of circuit current. A higher metal concentration led to more transport of net metal ions through the IEMs. In summary, employing a

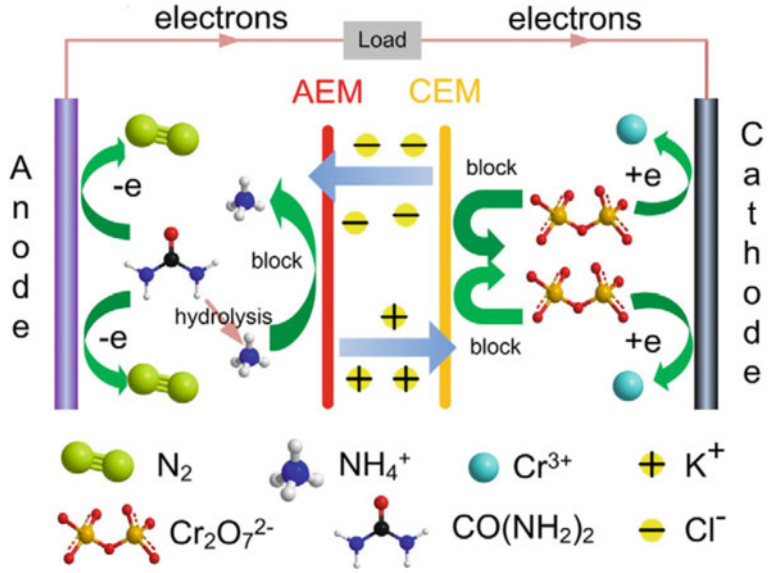

Fig. 2.7 Schematic of urine/Cr(VI) fuel cell (UCrFC) configuration [68]. Reproduced with the permission from Elsevier

fuel cell to reduce harmful heavy metal ions is a novel strategy in dealing with industrial wastewater. Though the removal efficiency is relatively high, the required operating time is long and the power output is negligible. Hence, future research direction should be focused on shorting the operating time as well as improving the peak power density of this type of reactor.

2.5 Remaining Challenges and Perspectives

Nowadays, the heavy metal removal from the wastewater is becoming more serious because several threats are arising to human health and the environment. Although several treatments that use ion exchange membranes have been proposed and improved, challenges are still existing in terms of the above-mentioned treatment technologies. Membrane filtration technology is capable to remove heavy metal ions efficiently, but it suffers from high cost, process complexity, membrane fouling, and low permeate flux. The use of osmosis processes such as reverse osmosis and forward osmosis has been restricted in terms of the high cost for large-scale applications. Adsorption is believed to be an effective method to treat low concentration wastewater. However, since the adsorbent is the most important component in adsorption process, cost-effectiveness and availability are two major concerns in finding the most probable adsorbent for heavy metal removal in wastewater. Electrochemical treatment is considered as an alternative choice for

heavy metal removal, which is rapid and well-controlled as well as requires fewer chemicals and provides promising yields. However, the high initial capital investment and expensive electricity supply still need to be taken into consideration. Especially in fuel cell mode, the power output demands a substantial improvement. More importantly, in the pace of expanding the breakthrough in laboratory scale into pilot scale and industrial scale, we need to take more aspects into consideration so as to select the optimal treatment.

2.6 Conclusion

In terms of the various negative effects of heavy metal accumulation on humans as well as environment, the removal of heavy metal ions from industrial wastewater is an essential part of most of the current research in the environmental field. In this chapter, both physical methods (ultrafiltration, nanofiltration, reverse osmosis, forward osmosis, and adsorption) and chemical methods (electrodialysis method and fuel cell method) are discussed. Particularly, in order to select the most suitable method among these methods, some parameters should be taken into consideration, including main target heavy metal ions, initial concentration of the target ions, economic parameter, environmental impact, pH values, and the overall performance. In addition, the advantages and limitations of each method have been introduced. Because the ion exchange membrane is the most critical component in all the processes, more research attention has been paid into this field. There are five directions associated with membranes that can be concluded as follows: (1) the preparation method of membranes should be simplified and easily controlled; (2) it is quite necessary to investigate the effects of coexisting ions in the solution on the removal of target ions; (3) it is desirable to fabricate a universal membrane for removing the majority of heavy metal ions; (4) it is crucial to develop novel and facile methods of regenerating membranes that have been fouled; and (5) special attention should be paid to modeling and simulation of transport phenomena, which can improve our understanding of mechanisms involved in removal of heavy metal ions.

Acknowledgements This work was fully supported by a grant from the Research Grants Council of the Hong Kong Special Administrative Region, China (Project No. 25211817).

References

1. Carolin CF, Kumar PS, Saravanan A, Joshiba GJ, Naushad M (2017) Efficient techniques for the removal of toxic heavy metals from aquatic environment: a review. J Environ Chem Eng 5(3):2782–2799
2. http://www.wri.org/our-work/topics/water
3. Fu F, Wang Q (2011) Removal of heavy metal ions from wastewaters: a review. J Environ Manage 92(3):407–418

4. Reddy DHK, Lee SM (2013) Application of magnetic chitosan composites for the removal of toxic metal and dyes from aqueous solutions. Adv Coll Interface Sci 201:68–93
5. Srivastava N, Majumder C (2008) Novel biofiltration methods for the treatment of heavy metals from industrial wastewater. J Hazard Mater 151(1):1–8
6. Lesmana SO, Febriana N, Soetaredjo FE, Sunarso J, Ismadji S (2009) Studies on potential applications of biomass for the separation of heavy metals from water and wastewater. Biochem Eng J 44(1):19–41
7. Boamah PO, Huang Y, Hua M, Zhang Q, Wu J, Onumah J, Sam-Amoah LK, Boamah PO (2015) Sorption of heavy metal ions onto carboxylate chitosan derivatives—a mini-review. Ecotoxicol Environ Saf 116:113–120
8. Ahmed MJK, Ahmaruzzaman M (2016) A review on potential usage of industrial waste materials for binding heavy metal ions from aqueous solutions. J Water Process Eng 10:39–47
9. Nordberg G, Fowler B, Nordberg M, Friberg L (2007) Handbook of the toxicology of metals, 3rd edn. Academic, London
10. Ali H, Khan E, Sajad MA (2013) Phytoremediation of heavy metals—concepts and applications. Chemosphere 91(7):869–881
11. Demim S, Drouiche N, Aouabed A, Benayad, T, Dendene-Badache, O, Semsari S (2013) Cadmium and nickel: assessment of the physiological effects and heavy metal removal using a response surface approach by L. gibba. Ecol Eng, 61:426–435
12. Miretzky P, Cirelli AF (2010) Cr (VI) and Cr (III) removal from aqueous solution by raw and modified lignocellulosic materials: a review. J Hazard Mater 180(1–3):1–19
13. Hu J, Chen C, Zhu X, Wang X (2009) Removal of chromium from aqueous solution by using oxidized multiwalled carbon nanotubes. J Hazard Mater 162(2–3):1542–1550
14. Yang S, Li J, Shao D, Hu J, Wang X (2009) Adsorption of Ni(II) on oxidized multi-walled carbon nanotubes: effect of contact time, pH, foreign ions and PAA. J Hazard Mater 166(1): 109–116
15. Mobasherpour I, Salahi E, Ebrahimi M (2012) Removal of divalent nickel cations from aqueous solution by multi-walled carbon nano tubes: equilibrium and kinetic processes. Res Chem Intermed 38(9):2205–2222
16. Malamis S, Katsou E (2013) A review on zinc and nickel adsorption on natural and modified zeolite, bentonite and vermiculite: examination of process parameters, kinetics and isotherms. J Hazard Mater 252:428–461
17. Awual MR, Ismael M, Khaleque MA, Yaita T (2014) Ultra-trace copper (II) detection and removal from wastewater using novel meso-adsorbent. J Ind Eng Chem 20(4):2332–2340
18. Tang WW, Zeng GM, Gong JL, Liang J, Xu P, Zhang C, Huang BB (2014) Impact of humic/fulvic acid on the removal of heavy metals from aqueous solutions using nanomaterials: a review. Sci Total Environ 468:1014–1027
19. Cristian P, Violeta P, Anita-Laura R, Raluca I, Alexandrescu E, Andrei S, Daniela IE, Raluca MA, Cristina M, Ioana CA (2015) Removal of zinc ions from model wastewater system using bicopolymer membranes with fumed silica. J Water Process Eng 8:1–10
20. Chen M, Chen R, Zhu X, Liao Q, An L, Ye D, Zhou Y, He X, Zhang W (2017) A membrane electrode assembled photoelectrochemical cell with a solar-responsive cadmium sulfide-zinc sulfide-titanium dioxide/mesoporous silica photoanode. J Power Sources 371:96–105
21. Lee CH, Hsi CS (2002) Recycling of scrap cathode ray tubes. Environ Sci Technol 36(1): 69–75
22. Filipič M (2012) Mechanisms of cadmium induced genomic instability. Mutat Res/Fundam Mol Mech Mutagen 733(1):69–77
23. Kumari S, Chauhan GS (2014) New cellulose–lysine schiff-base-based sensor–adsorbent for mercury ions. ACS Appl Mater Interfaces 6(8):5908–5917
24. Windham-Myers L, Fleck JA, Ackerman JT, Marvin-DiPasquale M, Stricker CA, Heim WA, Bachand PA, Eagles-Smith CA, Gill G, Stephenson M (2014) Mercury cycling in agricultural and managed wetlands: a synthesis of methylmercury production, hydrologic export, and bioaccumulation from an integrated field study. Sci Total Environ 484:221–231

25. Malar S, Sahi SV, Favas PJ, Venkatachalam P. (2015) Mercury heavy-metal-induced physiochemical changes and genotoxic alterations in water hyacinths [Eichhornia crassipes (Mart.)]. Environ Sci Poll Res 22(6):4597–4608
26. Li P, Feng X, Qiu G, Shang L, Li Z (2009) Mercury pollution in Asia: a review of the contaminated sites. J Hazard Mater 168(2–3):591–601
27. Acharya J, Sahu J, Mohanty C, Meikap B (2009) Removal of lead (II) from wastewater by activated carbon developed from Tamarind wood by zinc chloride activation. Chem Eng J 149(1–3):249–262
28. Qu X, Alvarez PJ, Li Q (2013) Applications of nanotechnology in water and wastewater treatment. Water Res 47(12):3931–3946
29. Cechinel MAP, de Souza AAU (2014) Study of lead(II) adsorption onto activated carbon originating from cow bone. J Clean Prod 65:342–349
30. Sun J, Hu C, Tong T, Zhao K, Qu J, Liu H, Elimelech M (2017) Performance and mechanisms of ultrafiltration membrane fouling mitigation by coupling coagulation and applied electric field in a novel electrocoagulation membrane reactor. Environ Sci Technol 51 (15):8544–8551
31. Daraei P, Madaeni SS, Ghaemi N, Salehi E, Khadivi MA, Moradian R, Astinchap B (2012) Novel polyethersulfone nanocomposite membrane prepared by PANI/Fe_3O_4 nanoparticles with enhanced performance for Cu(II) removal from water. J Membr Sci 415–416:250–259
32. Gohari RJ, Lau WJ, Matsuura T, Halakoo E, Ismail AF (2013) Adsorptive removal of Pb(II) from aqueous solution by novel PES/HMO ultrafiltration mixed matrix membrane. Sep Purif Technol 120:59–68
33. Ghaemi N, Daraei P (2016) Enhancement in copper ion removal by PPy@Al_2O_3 polymeric nanocomposite membrane. J Ind Eng Chem 40:26–33
34. Ghaemi N (2016) A new approach to copper ion removal from water by polymeric nanocomposite membrane embedded with γ-alumina nanoparticles. Appl Surf Sci 364: 221–228
35. Mukherjee R, Bhunia P, De S (2016) Impact of graphene oxide on removal of heavy metals using mixed matrix membrane. Chem Eng J 292:284–297
36. Abdullah N, Gohari RJ, Yusof N, Ismail AF, Juhana J, Lau WJ, Matsuura T (2016) Polysulfone/hydrous ferric oxide ultrafiltration mixed matrix membrane: preparation, characterization and its adsorptive removal of lead (II) from aqueous solution. Chem Eng J 289:28–37
37. Bilal M, Shah JA, Ashfaq T, Gardazi SMH, Tahir AA, Pervez A, Haroon H, Mahmood Q (2013) Waste biomass adsorbents for copper removal from industrial wastewater—a review. J Hazard Mater 263:322–333
38. Zhang Y, Zhang S, Chung TS (2015) Nanometric graphene oxide framework membranes with enhanced heavy metal removal via nanofiltration. Environ Sci Technol 49(16):10235–10242
39. Ghaemi N, Madaeni SS, Daraei P, Rajabi H, Zinadini S, Alizadeh A, Heydari R, Beygzadeh M, Ghouzivand S (2015) Polyethersulfone membrane enhanced with iron oxide nanoparticles for copper removal from water: application of new functionalized Fe_3O_4 nanoparticles. Chem Eng J 263:101–112
40. Bolisetty S, Mezzenga R (2016) Amyloid-carbon hybrid membranes for universal water purification. Nat Nanotechnol 11(4):365–371
41. Zeng G, He Y, Zhan Y, Zhang L, Pan Y, Zhang C, Yu Z (2016) Novel polyvinylidene fluoride nanofiltration membrane blended with functionalized halloysite nanotubes for dye and heavy metal ions removal. J Hazard Mater 317:60–72
42. Habiba U, Afifi AM, Salleh A, Ang BC (2017) Chitosan/(polyvinyl alcohol)/zeolite electrospun composite nanofibrous membrane for adsorption of Cr(6+), Fe(3+) and Ni(2+). J Hazard Materi 322(Part A):182–194

43. Rao Z, Feng K, Tang B, Wu P (2017) Surface decoration of amino-functionalized metal-organic framework/graphene oxide composite onto polydopamine-coated membrane substrate for highly efficient heavy metal removal. ACS Appl Mater Interfaces 9(3):2594–2605
44. Meschke K, Hansen N, Hofmann R, Haseneder R, Repke JU (2018) Characterization and performance evaluation of polymeric nanofiltration membranes for the separation of strategic elements from aqueous solutions. J Membr Sci 546:246–257
45. Meschke K, Daus B, Haseneder R, Repke JU (2017) Strategic elements from leaching solutions by nanofiltration–Influence of pH on separation performance. Sep Purif Technol 184:264–274
46. Li Y, Xu Z, Liu S, Zhang J, Yang X (2017) Molecular simulation of reverse osmosis for heavy metal ions using functionalized nanoporous graphenes. Comput Mater Sci 139:65–74
47. Petrinic I, Korenak J, Povodnik D, Hélix-Nielsen C (2015) A feasibility study of ultrafiltration/reverse osmosis (UF/RO)-based wastewater treatment and reuse in the metal finishing industry. J Clean Prod 101:292–300
48. You S, Lu J, Tang CY, Wang X (2017) Rejection of heavy metals in acidic wastewater by a novel thin-film inorganic forward osmosis membrane. Chem Eng J 320:532–538
49. Cui Y, Ge Q, Liu XY, Chung TS (2014) Novel forward osmosis process to effectively remove heavy metal ions. J Membr Sci 467:188–194
50. Zhao X, Liu C (2018) Efficient removal of heavy metal ions based on the optimized dissolution-diffusion-flow forward osmosis process. Chem Eng J 334:1128–1134
51. Demirbas A (2008) Heavy metal adsorption onto agro-based waste materials: a review. J Hazard Mater 157(2–3):220–229
52. Li X, Zhou H, Wu W, Wei S, Xu Y, Kuang Y (2015) Studies of heavy metal ion adsorption on chitosan/sulfydryl-functionalized graphene oxide composites. J Colloid Interface Sci 448:389–397
53. Chen D, Zhang H, Yang K, Wang H (2016) Functionalization of 4-aminothiophenol and 3-aminopropyltriethoxysilane with graphene oxide for potential dye and copper removal. J Hazard Mater 310:179–187
54. Henriques B, Goncalves G, Emami N, Pereira E, Vila M, Marques PA (2016) Optimized graphene oxide foam with enhanced performance and high selectivity for mercury removal from water. J Hazard Mater 301:453–461
55. Wan S, He F, Wu J, Wan W, Gu Y, Gao B (2016) Rapid and highly selective removal of lead from water using graphene oxide-hydrated manganese oxide nanocomposites. J Hazard Mater 314:32–40
56. Tang J, Huang Y, Gong Y, Lyu H, Wang Q, Ma J (2016) Preparation of a novel graphene oxide/Fe-Mn composite and its application for aqueous Hg(II) removal. J Hazard Mater 316:151–158
57. Shariful MI, Sharif SB, Lee JJL, Habiba U, Ang BC, Amalina MA (2017) Adsorption of divalent heavy metal ion by mesoporous-high surface area chitosan/poly (ethylene oxide) nanofibrous membrane. Carbohyd Polym 157:57–64
58. Shariful MI, Sepehr T, Mehrali M, Ang BC, Amalina MA (2018) Adsorption capability of heavy metals by chitosan/poly(ethylene oxide)/activated carbon electrospun nanofibrous membrane. J Appl Polym Sci 135(7):45851–45864
59. Porada S, Egmond W, Post J, Saakes M, Hamelers H (2018) Tailoring ion exchange membranes to enable low osmotic water transport and energy efficient electrodialysis. J Membr Sci 552:22–30
60. Nemati M, Hosseini S, Shabanian M (2017) Novel electrodialysis cation exchange membrane prepared by 2-acrylamido-2-methylpropane sulfonic acid; heavy metal ions removal. J Hazard Mater 337:90–104
61. Babilas D, Dydo P (2018) Selective zinc recovery from electroplating wastewaters by electrodialysis enhanced with complex formation. Sep Purif Technol 192:419–428

62. Ge L, Wu B, Li Q, Wang Y, Yu D, Wu L, Pan J, Miao J, Xu T (2016) Electrodialysis with nanofiltration membrane (EDNF) for high-efficiency cations fractionation. J Membr Sci 498:192–200
63. Wu QX, Pan ZF, An L (2018) Recent advances in alkali-doped polybenzimidazole membranes for fuel cell applications. Renew Sustain Energy Rev 89:168–183
64. Pan ZF, An L, Zhao TS, Tang ZK (2018) Advances and challenges in alkaline anion exchange membrane fuel cells. Prog Energy Combust Sci 66:141–175
65. An L, Zhao TS (2018) Anion exchange membrane fuel cells: principles, materials and systems. Springer International Publishing, Cham, Switzerland
66. Pan ZF, Chen R, An L, Li YS (2017) Alkaline anion exchange membrane fuel cells for cogeneration of electricity and valuable chemicals. J Power Sources 365:430–445
67. Zhang H, Xu W, Wu Z, Zhou M, Jin T (2013) Removal of Cr (VI) with cogeneration of electricity by an alkaline fuel cell reactor. The J Phys Chem C 117(28):14479–14484
68. Xu W, Zhang H, Li G, Wu Z (2016) A urine/Cr (VI) fuel cell—electrical power from processing heavy metal and human urine. J Electroanal Chem 764:38–44
69. Zhang HM, Xu W, Fan Z, Liu X, Wu ZC, Zhou MH (2017) Simultaneous removal of phenol and dichromate from aqueous solution through a phenol-Cr (VI) coupled redox fuel cell reactor. Sep Purif Technol 172:152–157
70. Qian Y, Huang L, Pan Y, Quan X, Lian H, Yang J (2018) Dependency of migration and reduction of mixed $Cr_2O_7^{2-}$, Cu^{2+} and Cd^{2+} on electric field, ion exchange membrane and metal concentration in microbial fuel cells. Sep Purif Technol 192:78–87

Chapter 3
Separation and Purification of Uncharged Molecules

Abhijit Mondal, Ria Majumdar, Nibedita Mahata and Biswanath Bhunia

Abstract The purification and separation of uncharged complexes is a challenging issue in the field of biotechnology. The most common metals required for our biological system are iron and cobalt, which play an important role in all living systems as these coordinate with haemoglobin and vitamin $B_{12,}$ respectively. Therefore, careful measurement of vitamin B_{12} and haemoglobin is a prerequisite for early detection of several diseases. Since detection of these compounds usually carried out in blood samples, therefore, purification of these compounds is utmost important before their measurement. Furthermore, the separation of uncharged dyes from wastewater sources is important to protect human health through preservation of supply of water which will protect the spread of various life-threatening diseases. Although there are several unit operations applied for the separation of uncharged complexes, however, all operations have their own drawbacks. The aim of this book chapter is the systematic and comparative presentation of the available information on the separation of these compounds owing to their application in various fields of biotechnology.

A. Mondal
Department of Chemical Engineering, National Institute of Technology Agartala, Barjala, Jirania 799046, Tripura (West), India
e-mail: abhijitju17@gmail.com

R. Majumdar
Department of Civil Engineering, National Institute of Technology Agartala, Barjala, Jirania 799046, Tripura (West), India
e-mail: majumdarria439@gmail.com

N. Mahata
Department of BioTechnology, National Institute of Technology Durgapur, Mahatma Gandhi Avenue, Durgapur 713209, India
e-mail: nibedita.mahata@gmail.com

B. Bhunia (✉)
Department of Bio Engineering, National Institute of Technology Agartala, Barjala, Jirania 799046, Tripura (West), India
e-mail: bbhunia@gmail.com; bhuniab2017@gmail.com

Inamuddin et al. (eds.), *Applications of Ion Exchange Materials in the Environment*,
https://doi.org/10.1007/978-3-030-10430-6_3

3.1 Introduction

A complex is defined as a molecular entity which is formed by the weak association of two or more component molecular entities, or the corresponding chemical species. It is obvious that the bonding energy between the components is normally lesser than a covalent bond. The complex indicates an association of the molecular entity where a metal atom or ion will be in the centre and surrounded by ligands. Ligands are usually considered as electron donors; therefore, these are attracted to the metal at the centre of the complex. Additionally, metals are considered as electron acceptors. They are usually transition metals (d-block metals) such as titanium, cobalt, vanadium, manganese, chromium, iron, cobalt, copper, gold, nickel, platinum and palladium. Other metals, such as magnesium, aluminium, calcium and tin also form complexes with suitable ligands. Moreover, the number of electrons on the central metal is crucial for complex formation. Since central metals can exist in different oxidation states—i.e. with different numbers of d electrons; therefore, complexes are either positively charged, uncharged or negatively charged. The various properties of the complex such as stereochemistry, stability, spectroscopic, magnetic and reactivity can be changed by oxidizing or reducing the metal in the centre of a complex with the similar number or type of ligands.

One of the distinguishing features of life is that cells are made of matter which is any substance that occupies space with a certain mass. Elements are unique forms of matter with specific chemical and physical properties that cannot be broken down into smaller substances by ordinary chemical reactions. The iron and cobalt are considered as the most common metals which play an important role for all living organisms. For example, iron complexes are used in the transportation of oxygen in the blood and tissues and cobalt acts as a coordinator for the formation of vitamin B_{12}. The haemoglobin content varies, depending upon on age and sex with the average range for an adult male is in the range of 14–18 g/L. However, haemoglobin content in the adult female is in the range from 12 to 16 g/L. The deficiency of haemoglobin level is considered as anaemia which is due to the interference of other molecules with haemoglobin which represents the number of red blood cells present in the body. There are several factors such as huge blood loss, disorder of bone marrow function, nutritional deficiency and inadequate intake of iron responsible for low haemoglobin content in the blood. Vitamin B_{12} maintains the routine function of the brain as well as in the nervous system. It also helps for red blood cells formation and to create and regulate DNA. The human body produces millions of red blood cells every minute to maintain the normal function of the biological system. Vitamin B_{12} helps to multiple of RBC properly in our body. The reduction of red blood cells occurs when vitamin B_{12} levels are low in our body. Therefore, careful measurements of Vitamin B_{12} and haemoglobin are required for detection of several diseases.

In the developed countries, the fastest growing industries have originated complexity and variability in their wastewater over the last decades and there are fresh and complex charges present in it. A huge variety of dyes are used in

cosmetics ingredients and hair colour products and the mixture of trichromatic is carried out for production of various shades. The wastewater generated from the fabric dyeing industry or the textile industries is a considerable source of environmental contamination. High levels of chemicals and residual coloured materials are present in these wastewater containing dyes. These dyes are important to be analysed for the quality control. According to some effluent regulations, the industries such as textile, pharmaceutical or even food-processing industries should lower the colour content from their wastewater. It is difficult to treat the wastewater coming from industries using dyes as the chemicals presents are recalcitrant molecules which posses resistant to the aerobic digestion [1]. Dye (colour) separation from the industrial effluents is one of the most recent and serious environmental concerns [2]. Every industry has to build up some efficient and economic techniques to do the same. Adsorption is one of the important processes of dye removal. It is a very cost-effective method of colour removal where activated carbon is the most commonly and extensively used adsorbent [3]. Moreover, reusability of these adsorbed dyes using various desorption processes could be an alternative route for sustainable economic uplift and positive drive with regard to economic concern. Recently, several desorption processes used for separation of adsorbed dyes are mass spectrometry using liquid secondary ion (LSI), fast atom bombardment (FAB) and plasma desorption (PD) mass spectrometry etc. These techniques have facilitated the characterization of various compounds. Thin layer chromatography (TLC) has been widely used for the analysis of volatile organic dyes [4, 5].

Recent advances of analytical chemistry depend on the progress towards the usability of more powerful tools of separation, as well as instrumental methods of determination. The chemical analysis of desired constituents is characterized through their separation followed by analysis. To this point, this book chapter has dealt principally with solutions of separation and purification of uncharged molecules. The aim of this chapter is to examine the characteristics of vitamin B_{12}, haemoglobin and several dyes which are uncharged macromolecules and their possible separation and purification.

3.2 Separation and Purification of Vitamin B_{12}

With regard to food and medicine, vitamin B_{12} has an important role in living systems. It is a naturally gifted uncharged complex biomolecule where a carbon bonded with metal. Vitamin B_{12} was invented in the 1920s and lots of research was made since then. Various applications with regard to anaemia and other diseases have come into the picture where vitamin B_{12} had a pivotal role [6]. A real breakthrough came in 1956 when the structure of vitamin B_{12} was recognized. Since then the application of X-ray crystallographic technique was immensely increased in the field of vitamin B_{12} research [7].The hydroxylcobalamin (OH-Cbl) and 5- deoxyadenosylcobalamin (Ado-Cbl), methylcobalamin (Me-Cbl) are the

natural forms of vitamin B_{12}. However, commercially name of vitamin B_{12} is cyanocobalamin (CN-Cbl) which is the stable form of vitamin B_{12}, produced by several microorganisms.

It is also noted that the nervous system is deeply affected if the supply of vitamin B_{12} is less in a biological system as myelin sheath surrounded in nerve cells in humans required vitamin B_{12} for maintenance [8]. Additionally, vitamin B_{12} assists in growth and development of the cell. Furthermore, vitamin B_{12} helps for metabolism of fat and carbohydrate as well as DNA replication. Additionally, it also helps in the maturation of red blood cell (RBC) in bone marrow [9]. It is also reported that several enzymes such as methionine synthase required vitamin B_{12} as a cofactor to maintain the integrity of function. Methyl malonyl coenzyme A (CoA) mutase requires vitamin B_{12} as a cofactor for maintaining 3D structure of this enzyme. The deficiency of vitamin B_{12} is the cause of megaloblasts which leads to associated with tiredness, listlessness and breathlessness. It is also reported that infection is also the cause of vitamin B_{12} deficiency. Deficiency of vitamin B_{12} for longer time damage the nervous system and nerve could not regenerate. The poor content of it also causes nutritional imbalance, malabsorption associated with gastrointestinal problems [10]. The daily requirement of vitamin B_{12} is comparatively low in the range of 1–2 μg in comparison with other vitamins [11, 12]. Since the amount of requirement is very low, therefore, deficiency may be as low in the range of nanogram to picogram level. Therefore, purification and separation along with the measurement of vitamin B_{12} are challenging problems for chemists. It is to be noted that no specific reproducible method exists for detection of vitamin B_{12}. Therefore, it is utmost important for all researchers to review existing methods and design the ultrasensitive and specific methods. Furthermore, existing methods used for the determination of vitamin B_{12} have their own advantages. In addition, time-consuming, laborious, non-specific and expensive are the main drawbacks.

L. leichmannii having ATCC 7830 is normally used for the microbial assay. Therefore, it is also considered as a test organism for the determination of vitamin B_{12} [26]. The other method used for determination is isotopic-mediated assay [27] where isotope is labelled. Furthermore, liquid chromatography, i.e. HPLC [28] has been widely used for the measurement of vitamin B_{12} in the various samples. In the HPLC system, the sample is injected and quantitative and qualitative measurements could be possible through the proper selection of liquid and solid phases. The other two methods such as chemiluminescence (CL) assay [22] and fluorimetric assay [17] were used for measurement of vitamin B_{12} level at lower concentration. In CL, after chemical reaction, emission of light is measured. However, the intensity of fluorescence is measured through fluorimetric assay. The capillary electrophoresis (CE) [21] and MALDI are the latest tools used for the determination of vitamin B_{12} in various samples. The components in the mixture are separated according to their molecular masses. These methods are quite expensive for the determination of vitamin B_{12}. Moreover, TOFMS [29] and AAS [30] have also been the widely used techniques for the determination of vitamin B_{12}. Recently, the application of biosensor has tremendously increased for detection purpose as it has several advantages. It is normally used for the detection of vitamin B_{12} which is present in

Table 3.1 Advantages and disadvantages of different methods applied for measurement of vitamin B_{12}

S. no.	Analysis	Limit of detection	Sample used	References
1	Assay using microbes	0.30 μg of vitamin B_{12} per g of cells	*A. flos-aquae*	[13]
2	Assay using isotopic	5 ng per mL of blood	Blood	[14]
3	UV–Vis technique	35 μg per mL of solution	Parenteral formulation containing vitamin B_{12}	[15]
4	High-pressure liquid chromatography	40 ng per mL of solution	Formulation containing vitamin B_{12}	[16]
5	High-pressure liquid chromatography with fluorescence detector	0.1 ng per mL of solution	A formulation containing vitamin B_{12} and fermentation media	[17]
6	High-pressure liquid chromatography with electrospray ionization	2 ng per g of formulation	A formulation containing vitamin B_{12}	[18]
7	Atomic absorption spectroscopy	42 μg per mL of solution	A formulation containing various vitamin	[19]
8	Intensity of fluorescence	0.1 ng per mL of solution	A formulation containing vitamin B_{12}	[17]
9	Capillary electrophoresis	20 μg per mL of solution	vitamin B_{12} in fermentation media	[20]
10	Capillary electrophoresis with mass spectrometry	50 ng per mL of solution	A formulation containing various vitamins	[21]
11	Luminescence	50 pg per mL of solution	A formulation containing various vitamins	[22]
12	Luminescence	5 pg per mL of solution	A formulation containing various vitamins	[23]
13	ELISA	0.09 μg per 100 g of product	Various products containing vitamin B_{12}	[24]
14	Assay using biosensor	2 μg per 100 g of product	A formulation containing various vitamins	[25]

liquid [25] and is considered as a best economic method with regard to reproducibility. The sensitivity of various methods for the determination of vitamin B_{12} is reported in Table 3.1.

The cobalamin group is normally present in the structure of vitamin B_{12}. Figure 3.1 illustrates the complex configuration of it. The four rings, namely pyrrole rings are present in the structure of vitamin B_{12}. In corrin, the ring contains two pyrrole rings named as A and B which are partially hydrogenated. These complex rings are differentiated with respect to the availability of the type of side chains. The cobalt is a metal which is present in cobalt (III) oxidation state in the ring.

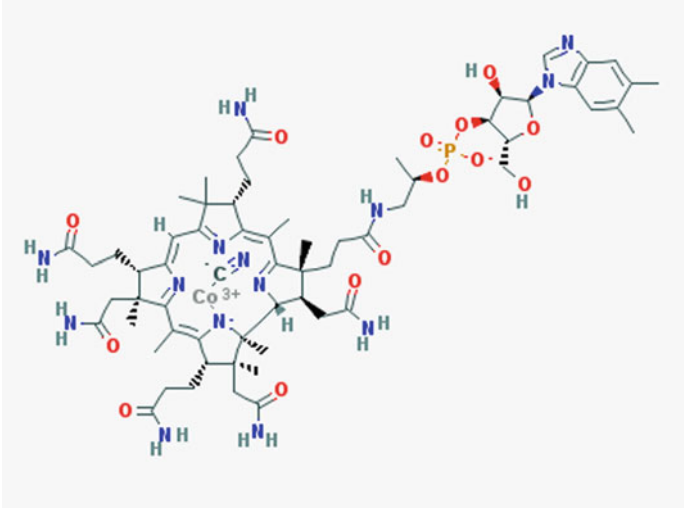

Fig. 3.1 Chemical structure of vitamin B_{12} molecule

This metal creates a complex with four available nitrogen atoms inside the rings. The cobalt (III) generates a coordination sphere which is maintained by the N7 atom of DMB. The phosphate group of DMB assists to join between DMB and ring D by a covalent bond with propionic acid side chains. The CN-Cbl, OH-Cbl, Me-Cbl and Adl-Cbl are considered as an isoform of vitamin B_{12}. These are differentiated on the basis of their ligand attached in cobalt atom.

It has been reported that the most of vitamin B_{12} analogue are light-sensitive as these are inactive in the presence of light. Therefore, it is utmost important to transform this analogue to CN-Cbl through the incorporation of cyanide. CN-Cbl is considered as a most stable form of vitamin B_{12}. Although several analogues are present in nature, however, these are not easily bioavailable in the human system as they cannot bind protein intrinsic factor (IF). Analogues of vitamin B_{12} are structurally similar but could not bind to IF. Since IF is present in gastrointestinal (the GI) tract, and therefore IF helps to the active transportation of vitamin B_{12}. Interestingly, CN-Cbl has high affinity to bind with IF as it can easily pocket in the grooves of this transporter. Hence, CN-Cbl is only available as IF helps for the absorption of vitamin B_{12} [31]. Figures 3.1 and 3.2 illustrate the various analogues of vitamin B_{12}. It is evident from the figures that analogues are similar in structure, however, they are different in respect of side chain. The Cobinamide is an analogue of vitamin B_{12} where carboxyl group of the D-ring is replaced by D-1-amino-propanol-2 when compared with cobalamin molecule. Cobalamin containing 5′-deoxyadenosyl group is considered as complete vitamin B_{12}.

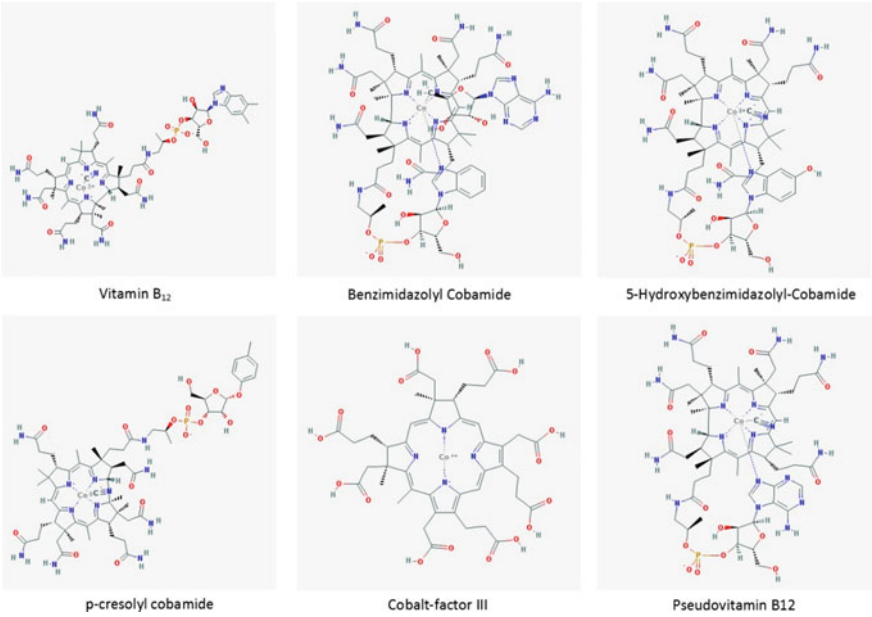

Fig. 3.2 Structure of various corrinoids

3.2.1 Downstream Processing of Vitamin B_{12} for Measurement

The vitamin B_{12} mostly exists in coenzyme form where several cellular proteins create a complex. During separation of vitamin B_{12} from the sample, most of the vitamin B_{12} gets denatured. Therefore, the exact measurement of vitamin B_{12} in the sample is not possible through any analytical measurement. It has been reported that the complex containing protein and CN-Cbl does not denature quickly in the presence of high-intensity light and extreme environmental conditions; therefore, it is utmost important to stabilize the vitamin B_{12} before quantification. It has been found that CN-Cbl is most stable analogue compared to naturally existing vitamin B_{12}. It is already reported that CN-Cbl can be prepared by chemical transformation through reaction with cyanide solutions and other analogues of vitamin B_{12}. The boiling of animal tissue is prerequisite for the extraction of vitamin B_{12} from the cell. It is also considered as a cost-effective process. However, homogenization of tissue at various pH values in the range 4–5 may be an alternative method for the extraction of vitamin B_{12} from animal tissue [32]. Additionally, another analogue, namely hydroxyl cobalamin is not stable in the presence of heat; therefore, boiling method is not appropriate for the extraction of OH-Cbl [33]. It has been recommended by several researchers that the addition of 0.01% (W/V) KCN was required to add before extraction is carried out [18]. Since water is responsible for the

instability of vitamin B_{12}, therefore several water immiscible liquids were tested for extraction purpose. The organic solvent, namely benzyl alcohol and chloroform were widely used as an organic solvent for the extraction of vitamin B_{12} from fermentation broth with complex matrix [34].

It has been found that the extraction of vitamin B_{12} from food materials using organic solvents augments the denaturation of vitamin B_{12}. According to the literature, vitamin B_{12} can be extracted through liquid chromatography for separation from food sample. However, immune affinity technique is more appropriate prior liquid chromatography to achieve exact quantification of vitamin B_{12} [28]. However, hot ethanol is used for the separation of vitamin B_{12} from plasma and bile. The above extraction is carried out for the precipitation of protein, and it avoids non-specific binding of the protein with OH-Cbl. It has been reported that thiol or histidine residues of proteins usually participate for such type of bonding. Most of the cases, 2 h pre-incubation with calcium acetate was required at room temperature for the precipitation of protein [35]. Additionally, a dark room is preferred to avoid degradation of vitamin B_{12} by illuminated light. Recently, biosensor-mediated measurement of vitamin B_{12} has been found suitable for the detection of vitamin B_{12} in food samples of infants. It has been reported that 0.2% sodium cyanide was initially mixed with phosphate-citrate buffer (pH 4.5). Additionally, autoclaving was carried out for 25 min to denature the binding protein which is, utmost, before quantification of vitamin B_{12} [25]. Affinity chromatography may be the alternative method to be adopted for the separation of vitamin B_{12} through column chromatography using Sepharose–IF resin [36].

3.3 Separation and Purification of Haemoglobin

Haemoglobin consists of four protein subunits including two alpha and two beta identical subunits. These subunits form a tetrahedral quaternary structure. The alpha helix is usually stabilized by hydrogen bond in protein structure. An internal hydrophobic pocket is present in all subunits of protein structure. These pockets are tightly associated with a heme group (Fig. 3.3) where a ferrous ion coordinates itself with four nitrogen atoms of four cyclically linked pyrrole groups. This is also known as a porphyrin ring. A non-covalent bond is formed to link heme group to each globular subunit. This bond creates with a ferrous ion of heme group to imidazole ring of F8 histidine. The last, unoccupied binding site to the iron ion is considered as the binding site of oxygen. As oxygen bound to deoxy haemoglobin, the iron is temporarily oxidized from ferric to ferrous state and moves into the plane of the porphyrin ring. Since each haemoglobin molecule has four haemo groups, therefore, a maximum of four oxygen atoms can bind to the molecule at once. Once oxygen binds to one subunit, conformational changes of haemoglobin take place in the other binding sites which leads to increase the affinity for oxygen.

Recent researches are focusing to develop suitable blood substitute by utilizing haemoglobin as the base material. However, the artificially prepared haemoglobin

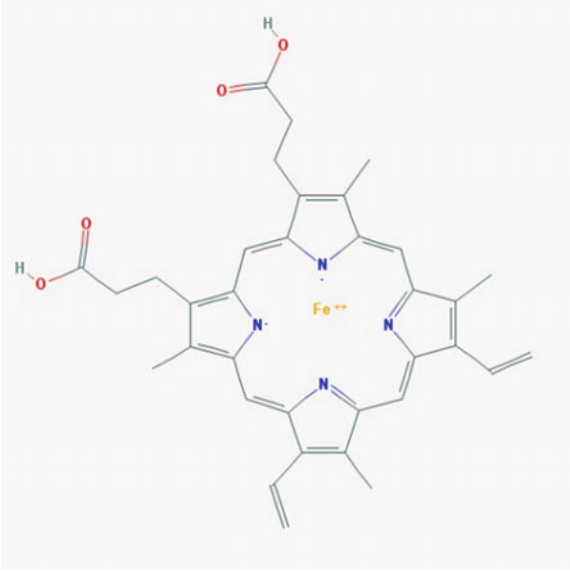

Fig. 3.3 Heme group

has not found capable to provide the same level of functionality as the naturally occurring haemoglobin. It has been, therefore, recommended by several researchers that human haemoglobin is processed with oxygen-carrying RBC before extraction from human blood. Initially, the haemoglobin needs to process through a series of separation steps to remove protein contaminants and stroma (containing phospholipids) which are considered as a stimulant for the human body and to cause undesirable side effects. Although, there are several methods adopted for haemoglobin purification for the development of blood substitute, however, high-speed centrifugation and ultrafiltration were the most widely used techniques applied in early stages. These unit operations have been helpful for physical separation. However, many other contaminants still exist in the haemoglobin solution after the treatment of this unit operation.

Rabiner et al. [37] separated haemoglobin from the outdated human whole blood. The human blood was initially centrifuged and then washed with saline. RBC was homogenized by using distilled water or organic solvents with low osmotic pressure. After homogenization, haemoglobin was released in solution. The solution was centrifuged under 35,000 g to precipitate and remove cell membrane stroma. It was further filtered through 0.1-μm filter membrane to obtain purified haemoglobin. This method was only able to remove the stromal particles which are relatively large. It failed to remove other proteins in the red blood cell and smaller cell membrane particles [37]. De Venuto et al. [38] developed crystallization methods for haemoglobin purification, including separating plasma followed by washing blood cells. The red blood cells were further haemolysed for releasing of haemoglobin due to haemolysis of RBC. The larger stromal particulate matter was separated when hemolysate was centrifuged under relatively low-speed

centrifugation of 4000 g. Haemoglobin was further salted out by using high concentration phosphate buffer salt. During salting out, the crystal growth of haemoglobin was observed which indicated the high purity of haemoglobin. As the crystallization process is time-consuming, therefore, mass production utilizing this technique is difficult, and it is not practical to use this process to obtain a large amount of high-purity haemoglobin [38].

Cheung et al. [39] developed a chromatography technique for haemoglobin purification using diethylaminoethyl (DEAE) cellulose which was used to adsorb negatively charged proteins. Initially, basic pH of 7.5 was maintained; therefore, proteins having isoelectric point (pI) less than 7.5 were adsorbed on the cellulose. However, haemoglobin was not be adsorbed by the cellulose as pI of haemoglobin is about 7 with slightly negatively charged. Therefore, purified haemoglobin can be obtained by mixing and adsorption followed by a series of filtration steps. As cellulose resins are relatively expensive in nature, therefore, this process is not economical for practical applications. However, it may be useful if the cellulose resins can be reused [39]. DeLoach et al. [40] reported that a combination of dialysis and ultrafiltration can be used for complete removal of phospholipids as it causes a strong immune reaction or side effects after blood transfusion. It has been reported controlled dialysis gradually changed the osmotic pressure of RBC and therefore prevented the osmotic shock to red blood cells for swelling. However, this procedure allowed to release of haemoglobin from red blood cell membranes permeable without rupturing the cell membrane. Further, RBC solution was filtered through a 0.1-μm pore to remove red blood cell membrane and phospholipid-free haemoglobin solution was obtained. However, other protein contaminants were not removed completely [40].

Christensen et al. [41] used anion-exchanger cellulose, such as DEAE, or cation-exchanger cellulose, such as carboxymethyl cellulose (CMC) for chromatographic separation of haemoglobin. The pH of the solution was adjusted in a controlled manner, to elute the proteins. This advanced technique showed significant improvement in the purification of haemoglobin, but it is quite expensive [41]. Přistoupil et al. [42] used chloroform to extract haemoglobin. Red blood cells were initially separated through centrifugation and sodium phosphate buffer (pH 7.5) and chloroform were added to a separation phase of RBC. The red blood cells were haemolysed which leads to the release of haemoglobin. The haemoglobin was further dissolved into the aqueous phase containing the phosphate buffer. The chloroform helped to precipitate the hydrophobic stroma and other non-heme proteins. Initially, charcoal was used as adsorbent and after adsorption, filtration was carried out through a 0.22-μm membrane to purify the haemoglobin. Since the small residual of chloroform is toxic to the human body, therefore, it is always a concern using this extraction technique [42]. Lee and Kan [43] developed a novel two-step dual-aqueous-phase extraction technique to separate the haemoglobin from red cell membrane stroma and other protein contaminants [43].

Paleari et al. [44] evaluated the performance of HPLC system for the quantification of HbA(2) and Hb F in blood. It was reported that results were found to correlate well with the previously established methods [44]. Lippi et al. [45]

investigated the feasibility of HPLC for quick screening of haemoglobin (Hb) from several variants. This technique was more reproducible and economical as compared with classic electrophoretic techniques. However, retention times for all variants were found to be similar. [45].

Elmer et al. [46] developed two analytical protocols for the separation of haemoglobin (Hb) from RBCs. The purification efficiency was compared with affinity chromatography. They used two processes where a single 50-nm tangential flow filtration (TFF) filter was used to retentate the lysate for affinity chromatography in the first step. In the second step, a three-stage TFF process was designed and used for concentration of samples prior to affinity chromatography. They also compared the purity level as the equilibrium constant of oxygen binding kinetics with Hb. In the first method, the clarification of RBCs was carried out with a filter with 50 nm tangential flow. Thereafter, affinity chromatography was used for separation of haemoglobin. In the second method, various tangential flow filters with the size of 50 nm, 500 kDa and 50-100 kDa were used for RBC lysate. Thereafter, haemoglobin was purified with affinity chromatography (AC). It was reported that filtration with a 50-nm tangential flow is a most efficient method for the purification of Hb, however, followed by AC might be adopted [46].

3.4 Separation and Purification of Uncharged Dyes

Dye molecules are categorized based on their charge, namely anionic, cationic and non-ionic [47]. Different types of dyes are used in foods for various purposes worldwide, and Sudan dyes are one of them which are most toxic. Food dyes are synthetic chemicals and are classified into four categories: xanthenes, indigoid, triphenylmethane and azo (Fig. 3.4). Sudan food dyes are chemicals which are synthetically prepared dyes. These are aromatic in nature, classified as Sudan I, II, III and IV and red in colour (Fig. 3.5). Except food colouring, there are various applications of Sudan II and III in cosmetics and drugs, whereas Sudan IV (also known as scarlet red) can be used in human medicine as dressings for stimulating wound healing and in veterinary. These dyes are specially used for the purpose of food colouring and in petrol, waxes, oils and floor polishes, etc. These dyes are considered harmful to the human health due to their teratogenicity, genotoxicity and carcinogenicity. The sensitive, selective and accurate method needs to be developed for the analysis of these dyes. A UV–vis spectrophotometry and an LC–ESI–tandem mass spectrometry (MS/MS) have been used for the quantification of Sudan dyes.

3.4.1 Purification and Separation of Dyes

Flocculating agents used are either in organic or polymeric in nature [48]. Polymeric flocculants containing functional groups are water-soluble. Functional

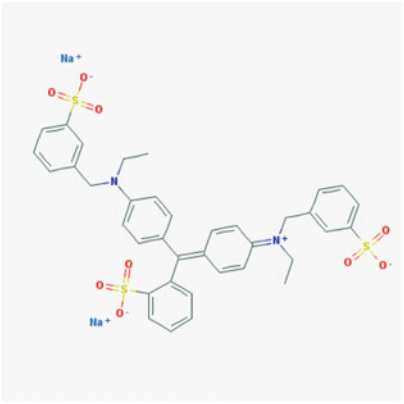

Brilliant Blue FCF

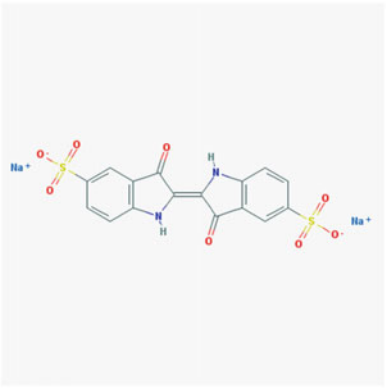

Indigo Carmine

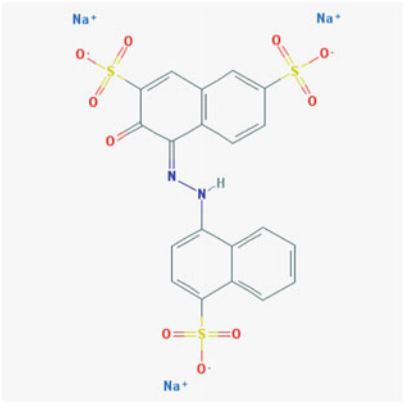

Amaranth

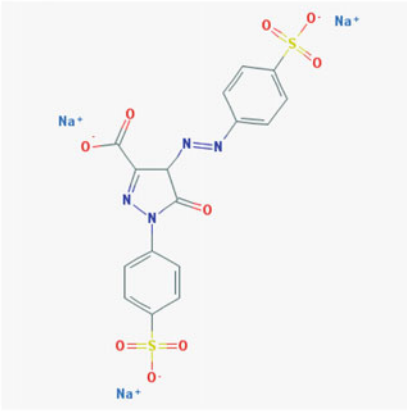

Tartrazine

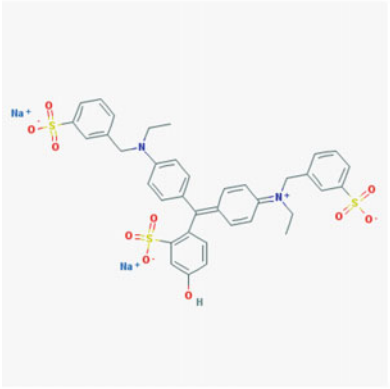

Fast Green FCF

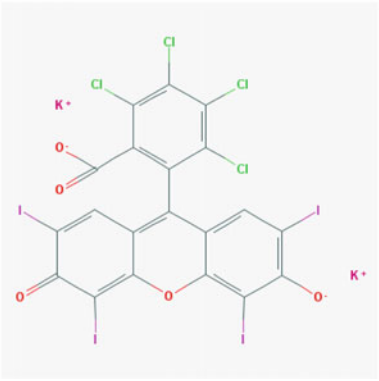

Rose Bengale

Fig. 3.4 Different types of food dyes

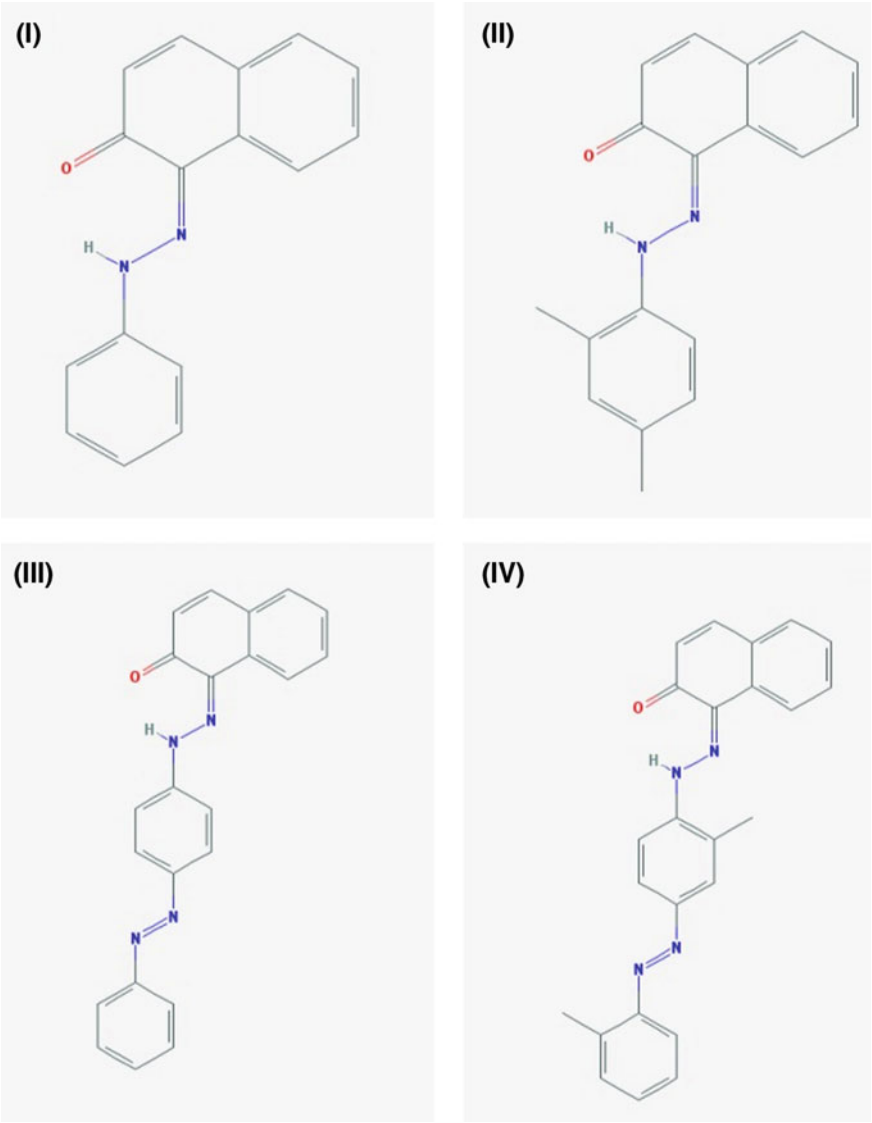

Fig. 3.5 Structure of Sudan dyes

groups are either quaternary amines or carboxyl group with repeating units. The inorganic coagulants have limited use for the precipitation of dyes from wastewater as a high amount of sludge is generated from the high volume of coagulants. However, a suitable use of polymeric flocculants (e.g. polyamines) helps to remove the suspended particles from wastewater. In industry, polyamines are used widely for the precipitation of dyes. Flocculation and precipitation of uncharged complexes

have been proved efficient removal techniques for the growing industries and mainly used for the decolourization of effluents. Flocculation and coagulation are used as pre-treatment steps for the decolourization of dye wastewater. Dye wastewater is a serious problem, and various treatment methods are used for the removal or decolourization of industrial dye-containing wastewater. Most of the colouring matters and suspended materials present in wastewater are removed during coagulation and flocculation processes [49].

HPLC methods have been used for the analysis of the basic dyes in hair-colouring products and textile products. Capillary electrophoresis has been proved to be the best technique for the analysis of ionic compounds in complex samples [50, 51]. Capillary electrophoresis is extensively used for acidic dyes. Zhang et al. employed central composite design (CCD) for the quick separation of Sudan dyes by reverse phase HPLC. The basic purpose of this study is to perform this analysis in relatively optimum conditions; so that, it would give the best separation output. The experimental conditions such as the variables (types of column, the composition of mobile phase, pH of the mobile phase, etc.) must be determined during the experiment which may influence the separation time and efficiency removal of these Sudan dyes. In addition, the resolution, retention time also need to be determined for the better resolution through minimum trail experiments [4]. A range of 200–800 nm wavelength was chosen as the detection wavelength of Sudan dyes and found a wavelength of 476 nm as the best suitable adsorption spectrum for detection. Harada et al. demonstrated the use of thin layer chromatography (TLC) and liquid secondary ion (LSI) mass chromatography using various matrices for the identification and rapid separation of the food dyes. In the separation process, two different solvents were used, namely methanol–methyl ethyl ketone and methanol–acetonitrile for xanthene dyes and for rest of the dyes reverse-phased thin-layer chromatographic plate was prepared. In this study, the established thin-layer chromatography/LSI method was used for the identification of an unknown dye from candy [5].

3.5 Conclusion

Precise purification and separation of vitamin B_{12} and haemoglobin from humans blood are still of intense research areas. Established separation techniques are currently approaching their limits in terms of reproducibility, selectivity and speed. Therefore, measurement of these compounds remains a time-consuming and costly process. With recent advances in technology and our understanding, some of the separation techniques may develop into a field of liquid–liquid extraction along with chromatography for efficient separation and purification of vitamin B_{12} and haemoglobin from human blood. Since organic dyes are conjugated chromophores, the extent of their reduction depends upon the reduction potential and influenced by the selection of matrices, therefore, thin-layer chromatography does not give suitable separation result for highly concentrated dye wastewater. Because of the faster

diffusion rate, thioglycerol has been proved most suitable matrix for the separation of dyes. HPLC method gives the rapid separation of Sudan dyes and quick detection result. Rapid, reliable and reproducible separation techniques of these uncharged complexes will augment our understanding for their applicability in various fields of biotechnology.

References

1. Robinson T, McMullan G, Marchant R, Nigam P (2001) Remediation of dyes in textile effluent: a critical review on current treatment technologies with a proposed alternative. Bioresour Technol 77:247–255
2. Dos Santos AB, Cervantes FJ, van Lier JB (2007) Review paper on current technologies for decolourisation of textile wastewaters: perspectives for anaerobic biotechnology. Bioresour Technol 98:2369–2385
3. Blackburn RS (2004) Natural polysaccharides and their interactions with dye molecules: applications in effluent treatment. Environ Sci Technol 38:4905–4909
4. Zhang YP, Zhang YJ, Gong WJ, Gopalan AI, Lee K-P (2005) Rapid separation of Sudan dyes by reverse-phase high performance liquid chromatography through statistically designed experiments. J Chromatogr A 1098:183–187
5. Harada KI, Masuda K, Suzuki M, Oka H (1991) Separation and identification of food dyes by thin-layer chromatography/liquid secondary ion mass spectrometry. Biol Mass Spectrom 20:522–528
6. Minot G (1901) The development of liver therapy in pernicious anemia: extract from Nobel Prize Lecture. Nobel Prize Win Med Physiol 1950:175–177
7. Hodgkin DC, Kamper J, Mackay M, Pickworth J, Trueblood KN, White JG (1956) Structure of vitamin B_{12}. Nature 178:64–66
8. Ament ME (1990) Enteral and parenteral nutrition. In: Brown ML (ed) Present knowledge in nutrition, 6th edn. International Life Sciences Institute, Nutrition Foundation, Washington, pp 444–450
9. Banerjee R (1999) Chemistry and biochemistry of B_{12}. Wiley
10. Oh R, Brown DL (2003) Vitamin B_{12} deficiency. Am Fam Physician 67:979–986
11. Herbert V (1987) Recommended dietary intakes (RDI) of vitamin B-12 in humans. The Am J Clin Nutr 45:671–678
12. Gopalan C, Sastri BR, Balasubramanian S (1980) Nutritive value of Indian foods. National Institute of Nutrition, Indian Council of Medical Research
13. Miyamoto E, Tanioka Y, Nakao T, Barla F, Inui H, Fujita T, Watanabe F, Nakano Y (2006) Purification and characterization of a corrinoid-compound in an edible cyanobacterium Aphanizomenon flos-aquae as a nutritional supplementary food. J Agric Food Chem 54:9604–9607
14. Sahni MK, Spanos S, Wahrman MZ, Sharma GM (2001) Marine corrinoid-binding proteins for the direct determination of vitamin B_{12} by radioassay. Anal Biochem 289:68–76
15. Morelli B (1995) Determination of a quaternary mixture of vitamins B6, B1, and B_{12} and uridine 5′-triphosphate, by derivative spectrophotometry. J Pharm Sci 84:34–37
16. Moreno P, Salvado V (2000) Determination of eight water-and fat-soluble vitamins in multi-vitamin pharmaceutical formulations by high-performance liquid chromatography. J Chromatogr A 870:207–215
17. Li H-B, Chen F, Jiang Y (2000) Determination of vitamin B_{12} in multivitamin tablets and fermentation medium by high-performance liquid chromatography with fluorescence detection. J Chromatogr A 891:243–247

18. Volcani B, Toohey J, Barker H (1961) Detection of cobamide coenzymes in microorganisms by the ionophoretic-bioautographic method. Arch Biochem Biophys 92:381–391
19. Vinas P, Campillo N, Garcia IL, Córdoba MH (1996) Speciation of vitamin B_{12} analogues by liquid chromatography with flame atomic absorption spectrometric detection. Anal Chim Acta 318:319–325
20. Lambert D, Adjalla C, Felden F, Benhayoun S, Nicolas J, Gueant J (1992) Identification of vitamin B_{12} and analogues by high-performance capillary electrophoresis and comparison with high-performance liquid chromatography. J Chromatogr A 608:311–315
21. Baker S, Miller-Ihli N (2000) Determination of cobalamins using capillary electrophoresis inductively coupled plasma mass spectrometry. Spectrochim Acta Part B: At Spectrosc 55:1823–1832
22. Song Z, Hou S (2003) Sub-picogram determination of Vitamin B_{12} in pharmaceuticals and human serum using flow injection with chemiluminescence detection. Anal Chim Acta 488:71–79
23. Kumar SS, Chouhan RS, Thakur MS (2009) Enhancement of chemiluminescence for vitamin B_{12} analysis. Anal Biochem 388:312–316
24. Alcock SC, Finglas PM, Morgan MR (1992) Production and purification of an R-protein-enzyme conjugate for use in a microtitration plate protein-binding assay for vitamin B_{12} in fortified food. Food Chem 45:199–203
25. Gao Y, Guo F, Gokavi S, Chow A, Sheng Q, Guo M (2008) Quantification of water-soluble vitamins in milk-based infant formulae using biosensor-based assays. Food Chem 110:769–776
26. Kelleher B, Scott J, O'Broin S (1990) Cryo-preservation of Lactobacillus leichmannii for vitamin B_{12} microbiological assay. Med Lab Sci 47:90–96
27. Muhammad K, Briggs D, Jones G (1993) Comparison of a competitive binding assay with Lactobacillus leichmannii ATCC 7830 assay for the determination of vitamin B_{12} in foods. Food Chem 48:431–434
28. Heudi O, Kilinc T, Fontannaz P, Marley E (2006) Determination of vitamin B_{12} in food products and in premixes by reversed-phase high performance liquid chromatography and immunoaffinity extraction. J Chromatogr A 1101:63–68
29. Fei X, Wei G, Murray KK (1996) Aerosol MALDI with a reflectron time-of-flight mass spectrometer. Anal Chem 68:1143–1147
30. Akatsuka K, Atsuya I (1989) Determination of vitamin B_{12} as cobalt by electrothermal atomic absorption spectrometry using the solid sampling techniqueBestimmung von Vitamin B_{12} als Cobalt mit Hilfe der elektrothermischen Feststoff-AAS. Fresenius' Zeitschrift für analytische Chemie 335:200–204
31. Stupperich E, Nexø E (1991) Effect of the cobalt-N coordination on the cobamide recognition by the human vitamin B_{12} binding proteins intrinsic factor, transcobalamin and haptocorrin. The FEBS J 199:299–303
32. Frenkel EP, Prough R, Kitchens RL (1980) [6] Measurement of tissue vitamin B_{12} by radioisotopic competitive inhibition assay and quantitation of tissue cobalamin fractions, in: Methods Enzymol., Elsevier, pp 31–40
33. Soars MH, Hendlin D (1951) The use of potassium cyanide in the Lactobacillus leichmannii assay for vitamin B_{12}. J Bacteriol 62:15
34. Rudkin G, Taylor R (1952) Chemical method for determining vitamin B_{12}. Anal Chem 24:1155–1156
35. Gimsing P, Beck W (1989) Cobalamin analogues in plasma. An in vitro phenomenon? Scand J Clin Lab Investig Supplementum 194:37–40
36. Shum H-Y, O'Neill BJ, Streeter AM (1971) Effect of pH changes on the binding of vitamin B_{12} by intrinsic factor. J Clin Pathol 24:239–243
37. Rabiner SF, Helbert JR, Lopas H, Friedman LH (1967) Evaluation of a stroma-free hemoglobin solution for use as a plasma expander. J Exp Med 126:1127–1142
38. De Venuto F, Zuck T, Zegna A, Moores W (1977) Characteristics of stroma-free hemoglobin prepared by crystallization. The J Lab Clin Med 89:509–516

39. Cheung L, Storm C, Gabriel B, Anderson W (1984) The preparation of stroma-free hemoglobin by selective DEAE-cellulose absorption. Anal Biochem 137:481–484
40. DeLoach JR, Sheffield CL, Spates GE (1986) A continuous-flow high-yield process for preparation of lipid-free hemoglobin. Anal Biochem 157:191–198
41. Christensen S, Medina F, Winslow R, Snell S, Zegna A, Marini M (1988) Preparation of human hemoglobin Ao for possible use as a blood substitute. J Biochem Biophys Methods 17:143–154
42. Přistoupil T, Mařík T, Suttnar J, Štěrbíková J, Tomsova Z (1990) Stroma-free hemoglobin solutions purified by chloroform and pasteurization. Int J Artif Organs 13:383–387
43. Lee C-J, Kan P (1995) Google Patents
44. Paleari R, Cannata M, Leto F, Maggio A, Demartis FR, Desogus MF, Galanello R, Mosca A (2005) Analytical evaluation of the Tosoh HLC-723 G7 automated HPLC analyzer for hemoglobin A2 and F determination. Clin Biochem 38:159–165
45. Lippi G, Carta M, Salvagno G, Bellorio F, Montagnana M, Soffiati G, Guidi G (2008) Separation of haemoglobin HbE and HbA2 by the fully automated, high-pressure liquid chromatography Tosoh HLC-723 G7 analyzer. Int J Lab Hematol 30:432–436
46. Elmer J, Harris D, Palmer AF (2011) Purification of hemoglobin from red blood cells using tangential flow filtration and immobilized metal ion affinity chromatography. J Chromatogr B 879:131–138
47. Kyzas GZ, Bikiaris DN, Lazaridis NK (2009) Selective separation of basic and reactive dyes by molecularly imprinted polymers (MIPs). Chem Eng J 149:263–272
48. Choi J-H, Shin WS, Lee S-H, Joo D-J, Lee J-D, Choi SJ, Park LS (2001) Application of synthetic polyamine flocculants for dye wastewater treatment. Sep Sci Technol 36:2945–2958
49. Nacheva PM, Bustillos LT, Camperos ER, Armenta SL, Vigueros LC (1996) Characterization and coagulation-flocculation treatability of Mexico City wastewater applying ferric chloride and polymers. Water Sci Technol 34:235–247
50. Jorgenson JW, Lukacs K (1981) Free-zone electrophoresis in glass capillaries. Clin Chem 27:1551–1553
51. Markuszewski MJ, Otsuka K, Terabe S, Matsuda K, Nishioka T (2003) Analysis of carboxylic acid metabolites from the tricarboxylic acid cycle in Bacillus subtilis cell extract by capillary electrophoresis using an indirect photometric detection method. J Chromatogr A 1010:113–121

Chapter 4
Aluminosilicate Inorganic Polymers (Geopolymers): Emerging Ion Exchangers for Removal of Metal Ions

Bassam I. El-Eswed

Abstract Geopolymers (GPs), also known as alkali-activated aluminosilicates or inorganic polymers, are synthesized from an aluminosilicate source (fly ash, metakaolin, or blast furnace slag) and very alkaline sodium hydroxide and/or silicate. Due to their high compressive strength, acid and fire resistance, GPs are used as construction and coating materials. However, since the structure of GP contains negatively charged Al(III) tetrahedra (balanced by alkali cations), they are feasible ion exchangers. The present chapter is aimed to encapsulate the developments in the field of using GPs for the removal of alkali metals (Li^+, K^+, Cs^+), alkaline earth metals (Mg^{2+}, Ca^{2+}, Sr^{2+}, and Ba^{2+}), ammonium ion, and heavy metals (Pb^{2+}, Cu^{2+}, Cd^{2+}, Zn^{2+}, Ni^{2+}, Cr^{3+}) from water. GPs are the first cementing materials that have remarkable ion exchange capacity. GPs have higher ion exchange/adsorption capacity, but a lower rate of adsorption than their precursors (fly ash, metakaolin,…). Thus, geopolymerization increases the adsorption sites on one hand but imposes kinetics limitations that render GPs slow adsorption. GPs resemble zeolites in respect of cation exchange capacity, high surface area, and thermal stability. However, the synthesis of GPs is easier and inexpensive with lower energy and water demand than zeolite synthesis. The prepared GP could be directly formulated as high compressive strength granules at a low temperature. Since GPs are more acid resistant, they are accessible for regeneration than zeolites, but this issue requires further work.

Abbreviations

BET	Brunauer–Emmett–Teller (BET) theory
BFS	Blast furnace slag from iron manufacturing
CEC	Cation exchange capacity (meq/mol)
EDS	Energy-dispersive X-ray spectroscopy
FA	Fly ash from electricity plant employing coal (low calcium, type F)
GP	Geopolymer

B. I. El-Eswed (✉)
Zarqa College, Al-Balqa Applied University, P.O. Box 313, Zarqa 13110, Jordan
e-mail: bassameswed@bau.edu.jo

Inamuddin et al. (eds.), *Applications of Ion Exchange Materials in the Environment*,
https://doi.org/10.1007/978-3-030-10430-6_4

k_2 Pseudo-second-order rate constant (g mg^{-1} min^{-1})
K_L Langmuir affinity constant (L mg^{-1})
MK Metakaolin
Q_m Adsorption capacity (mg g^{-1})
SEM Scanning electron micrographs
XRD X-ray diffraction

4.1 Introduction

The term geopolymer (GP) was first used by Joseph Davidovits in 1978 [1]. GPs, which are also known as alkali-activated materials [2], are synthetic aluminosilicate inorganic polymers which are prepared by reacting a low-calcium solid aluminosilicate with highly basic sodium or potassium hydroxides and silicates at a temperature ranges from 40 to 80 °C [3, 4]. The GPs are used as construction and coating materials [5]. These applications arise from the GPs characteristics which include rapid hardening, compressive strength, low thermal conductivity, stability in acids and fireproof [3, 5–7].

The structure of GP can be represented by a three-dimensional structure of tetrahedral Si(IV) and Al(III) atoms connected covalently by oxygen atoms (Fig. 4.1). Alkali cations (most commonly Na^+ and K^+) are complementary to the GP structure to balance the negative charges of Al(III) tetrahedra [6]. Thus, the structure of GP imposes strongly the property of ion exchange, considering that this property depends to some extent on the porosity of GP [2].

Any aluminosilicate source is suitable, in principle for the preparation of GP. Thus, industrial wastes like fly ash (FA) and blast furnace slag (BFS) obtained from coal electricity plants and metallurgical industries, respectively, could be used

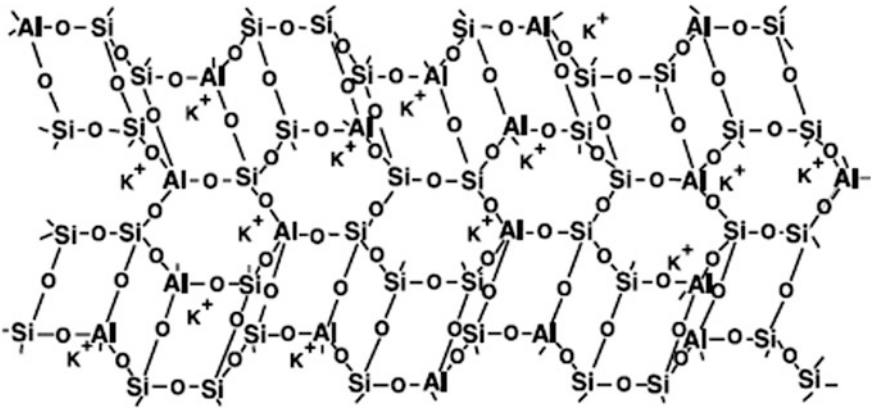

Fig. 4.1 Proposed structure of geopolymer or aluminosilicate inorganic polymer

as source material for GPs. Furthermore, natural aluminosilicates like kaolin and its dehydroxylated product (metakaolin, MK) are suitable for this purpose as well [6]. FA may be the most favored aluminosilicate source for the synthesis of GPs due to the high compressive strength of the GP product and the low water demand [3, 8]. Regarding sustainability, GPs are superior to ordinary Portland cement (OPC) since GPs are produced from inexhaustible sources of wastes using relatively low energy with low CO_2 emissions [6]. The typical stoichiometries for materials used in GP preparation are (in molar ratios): Na/Al = 1, Si/Al = 2, and H_2O/Na $\approx$ 7 [9].

There are two main lines of research for application of GPs in the field of treatment of heavy metals or hazardous wastes. The first is ion exchange/adsorption of heavy metals from an aqueous solution which is the topic of the present chapter. The second is stabilization/solidification/immobilization or encapsulation of heavy metal wastes in GP which involves incorporation of heavy metal waste during the preparation of GP and before hardening of GP paste [10–14]. Stabilization/solidification is a method for waste treatment in which the waste (including heavy metals and water) is encapsulated (as a whole) in the GP cementing material before being finally disposed of in a landfill. Since this immobilization process was assumed to occur via reactions involving precipitation of heavy metals, physical encapsulation, or chemical reactions, it will not be considered in the present chapter except in the cases relevant to ion exchange process.

According to Davidovits, GPs particulates are like those of rock-forming minerals. The OH groups are absent inside the GP network, providing long-term stability and corrosion resistance [15]. GPs are mainly amorphous, even though crystalline zeolitic phases could be embedded in the GP amorphous paste [8].

The aim of the present chapter is to shed some light on the available up-to-date literature in the research area of using GPs in ion exchange/adsorption of alkali, alkaline, and heavy metal ions, as well as ammonium and cationic dyes. These relatively new emerging ion exchangers will be reviewed regarding efficiency in removal of metal ions, kinetics, and mechanism. A comparison of GPs with traditional inorganic ion exchangers like zeolites will be established.

4.2 Methodology and Calculations

4.2.1 Terminology: Ion Exchange or Adsorption

Usually, the occurrence of an ion exchange/adsorption of metal ions on the GP is judged depending on the reduction of the concentration of metal ion in solution. A strict differentiation between ion exchange and adsorption is impossible. Thus, in the present work, the terminology (ion exchange or adsorption) used by the authors of original articles was adopted in the discussion of their works.

4.2.2 Evidence for Ion Exchange

The works which use ion exchange terminology were distinguished in considering not only the ions that are removed from the solutions but also those released from the solid phase (GPs) to achieve electroneutrality. Thus, the differentiation of ion exchange from adsorption processes is guided by the quantification of counterions released during the ion exchange process (Na^+ or K^+ balancing the Al tetrahedra in GPs). Furthermore, in some works, the occurrence of ion exchange was judged by XRF and EDS analyses of the GP after ion exchange where the attachment and release of ions can be evidenced.

4.2.3 Modeling of Adsorption of Metal Ions on Geopolymers

The adsorption experiment is usually carried out by preparing a standard solution of metal solution (C_i) and agitating specific volume (V in L) of this solution with an amount of GP (m, in grams) for a time sufficient to reach equilibrium. The equilibrium time is the time needed to reach a constant concentration of metal in solution (C_e). Then the amount of metal adsorbed (Q_e, mg g^{-1}) is calculated using (4.1).

$$Q_e = \frac{C_i - C_e}{m} V \tag{4.1}$$

Langmuir model (4.2) was used to evaluate the adsorption isotherms published in the articles reviewed:

$$Q_e = \frac{Q_m K_L C_e}{1 + (K_L C_e)} \tag{4.2}$$

where Q_m (mg g^{-1}) represents the efficiency of the GP in removing metal ions from solution, and K_L (L mg^{-1}) is the equilibrium constant used to estimate the affinity of metal toward the surface of GP [16].

Pseudo-second-order rate adsorption constant (k_2, g mg^{-1} min^{-1}) was used to evaluate and compare the kinetics data of articles being reviewed. The pseudo-second-order model is given in (4.3):

$$\frac{dQ_t}{dt} = k_2 (Q_e - Q_t)^2 \tag{4.3}$$

where Q_t and Q_e are the quantities of metal adsorbed at time t and equilibrium time, respectively [17].

4.2.4 Geopolymer Preparation

The preparation conditions of GPs were included in the description of works reviewed. The aluminosilicate source material used in preparation of GP (FA, BFS and MK, kaolin or zeolite) was indicated to give the reader some insight about the effect of variation of source material on the ion exchange behavior of GP. The alkali activator (sodium hydroxide or silicate, potassium hydroxide or silicate), as well as the molar ratios of Si/Al, Na or K/Al, and H_2O/Na, was also given because these are important in estimating the amount of negatively charged Al tetrahedra and the amount of Na^+ or K^+ balancing these negative charges in the GP framework.

4.2.5 Washing of the Geopolymeric Adsorbent

Unless otherwise specified, washing of the prepared GP with distilled or deionized water was carried out before using GP as an ion exchanger/adsorbent. This washing was necessary to avoid overestimation of adsorption capacity that resulted from precipitation of heavy metal ions by reaction of heavy metal ions with unreacted alkali in the GP matrix. Precipitation could not occur in the case of ion exchange or adsorption of alkali metals and ammonium ion on GPs, but washing was also conducted to remove unreacted alkali from the GP. Bortnovsky et al. suggested equilibration of the GPs with NH_4^+ to remove unreacted alkali that is usually hosted in the pores of GP before conduction ion exchange by metal ions [18].

However, Skorina pointed out the fact that over-washing, by analogy with zeolites, must be avoided in order not to replace the easily exchangeable ions like Na^+ or K^+ in the GP with strongly attached H_3O^+ [19]. This replacement may underestimate the ion exchange capacity of GPs. This effect was not taken into consideration in most of the works reviewed below where the GPs adsorbents were washed extensively with distilled water to reach a pH value of 7.

It is worth to mention that the pH increase of synthetic aqueous solutions of heavy metals after contact with GP is pronounced due to the lack of pH buffering capacity in these solutions. However, in the case of well-buffered real wastewater effluents, as well as with acidic industrial wastes, the pH increase is less significant. So there is no need to wash the GP adsorbents before being applied to real wastewater [20].

4.2.6 Comparison Between Geopolymers and Zeolites

In order to understand the feasibility of GPs as ion exchangers, the GPs were compared with traditional inorganic ion exchangers like zeolites regarding the

following properties: synthesis conditions, crystallinity, surface area, porosity, cation exchange capacity, selectivity for metal ions, stability in acidic solutions, thermal stability, mechanical strength, and possibility of regeneration.

4.2.7 Geopolymers as Ion Exchangers

4.2.7.1 Geopolymers as Ion Exchangers for Alkali Metal Ions

Cesium ion (Cs^+) is often found in nuclear waste streams. If the radioisotopes of cesium (^{137}Cs and ^{134}Cs) spread over a wide area, these will continue to radiate for a long time [21]. The immobilization of Cs^+ is challenging due to its high solubility in both alkaline and acidic media [22]. Thus, Cs^+ received special attention in the works devoted to using GPs as ion exchangers for alkali metal ions.

As mentioned in the above introduction, GPs contain negatively charged Al tetrahedra which are balanced by Na^+. The ion exchange of Na^+ ions in the metakaolin (MK)-based GP by Cs^+ was first studied by Bortnovsky et al. to test the accessibility of Na^+ ions in the GP pores. The GP was prepared from MK precursor (43.5% Al_2O_3 and 53.7% SiO_2) and sodium hydroxide and silicate activators with initial molar ratios of Si/Al and Na/Al equal to 1.6 and 1.1, respectively. The prepared GP was first equilibrated with NH_4^+ to remove unreacted alkalis before ion exchange with Cs^+. The EDS analysis indicated that the Na/Al molar ratio changed from 1.1 in the case of Na-GP to 0 upon ion exchange with Cs^+ (1.0 g GP per 100 mL of 0.05 M $CsNO_3$), and the resultant Cs/Al molar ratio was 0.56 [18].

Skorina studied ion exchange of Cs^+ on MK-based GP that was prepared using potassium hydroxide as an alkali activator with initial molar ratios of Si/Al = 2.8, K/Al = 3, and H_2O/Al = 10. The GP was repeatedly washed with deionized water to reach pH 7 (usually 5–7 cycles) before being used in ion exchange. Proton-induced X-ray emission (PIXE) analysis indicated that the K/Al molar ratio changed from 1.02 in the case of K^+-GP to 0 upon exchange with Na^+ and Cs^+, and the resultant Na/Al and Cs/Al molar ratios were 0.77 and 0.61, respectively [19]. The potential use of GPs as ion exchangers for Cs^+ was further confirmed by the study of López et al. which indicated that MK-based GP has higher adsorption selectivity for Cs^+ than heavy metal ions like, Cu^{2+}, Ni^{2+}, Cd^{2+}, Zn^{2+}, and Pb^{2+}. The adsorption capacity (Q_m) of Cs^+ on the GP (initial Si/Al = 2, Na/Al = 0.7) was 43 mg/g and was independent on the increase of ionic strength, indicating that the adsorption occurs via nonelectrostatic mechanism [23].

Lee et al. studied the adsorption of Cs^+ on FA/BFS-based GP. The GP, which was prepared from FA and BFS (4:1 mass ratio) and sodium silicate and sodium hydroxide, was found to contain zeolites (Na-P1, sodalite, faujasite, chabazite) as indicated by XRD pattern. The results indicated that the adsorption capacity of Cs^+ on the GP was small (15.2 mg/g) and the adsorption process was slow as the equilibration time was 24 h. This reflects that large size Cs^+ ion has strong

limitations to diffuse through the pores of the GP [24]. Nevertheless, this equilibration time could be reduced to 30 min by using pulverized samples of the GP.

Despite the ion exchange of Cs^+ on GP, stabilization/solidification was suggested as an alternative strategy for immobilization of Cs^+ in the GP matrix. This was achieved by synthesis of Cs^+ bearing zeolites inside the amorphous GP matrix. Haddad et al. studied the immobilization of Cs^+ in GP prepared from MK, sodium hydroxide, and CsOH keeping $(Na + Cs)/Al_2O_3$ molar ratio equal to 1 and $SiO_2/Al_2O_3 \leq 2$. The type of zeolite found in the GP was dependent on the % Cs in the GP: zeolites A and X in the case of 1% Cs and zeolite F ($CsAlSiO_4 \cdot H_2O$) in the case of 50% Cs. Leaching tests indicated strong binding of Na^+ to zeolites X and A and strong binding of Cs^+ to zeolite F [22]. Similarly, Yuan et al. prepared a ceramic product that contains stabilized Cs^+ in the form of pollucite ($CsAlSi_2O_6$) by reacting MK with a mixture of sodium and cesium hydroxide, with initial molar ratios of $SiO_2/Al_2O_3 = 4$ and $(Na + Cs)/Al_2O_3 = 1$, at 1300 °C [21].

Few studies were reported regarding ion exchange of K^+ and Li^+ on Na^+-GP. Complete exchange of Na^+ in MK-based GP (initial molar ratios $SiO_2/Al_2O_3 = 2.89$, $Na_2O/Al_2O_3 = 0.83$) by K^+ was achieved by agitating the GP (after grinding and without washing) with 0.1 M solution of K^+ as revealed by EDS analysis. A lower exchange capacity was obtained in the case of Li^+ (82%). The XRD patterns of the K^+ and Li^+ exchanged GP products, which were heated to 1100 °C, showed crystalline phases of leucite ($KAlSi_2O_6$) and spodumene ($LiAlSi_2O_6$), compared to nepheline ($NaAlSiO_4$) in the case of original Na^+-GP. This gave strong evidence for the ability of K^+ and Li^+ to replace the Na^+ in the GP matrix [25].

4.2.7.2 Geopolymers as Ion Exchangers for Ammonium Ion

Ammonium removal from municipal wastewater is a great challenge. The commonly used biological nitrification–denitrification process is frequently ineffective and difficult to be controlled, especially at low temperature [20]. The main advantage of using GP for the removal of NH_4^+ is the insignificant dependence on temperature [26]. Complete exchange of the Na^+ in MK-based GP ($SiO_2/Al_2O_3 = 2.89$ and $Na_2O/Al_2O_3 = 0.84$) by NH_4^+ was achieved by agitating the GP (without any treatment other than grinding) with 0.1 M NH_4^+ solution as indicated by EDS analysis [25].

Belchinskaya et al. studied the effect of treatment of an aluminosilicate adsorbent (montmorillonite/zeolite 56.56% SiO_2 and 14.32% Al_2O_3) with NaOH on its ion exchange capacity for NH_4^+. The ion exchange capacity of the alkali (NaOH)-treated aluminosilicate was 74.7 mg NH_4^+/g which is higher than that of untreated and acid (HCl)-activated product. The total number of displaced ions (Na^+, K^+, Ca^{2+}, Mg^{2+}) released from the GP was almost equal to the amount of adsorbed NH_4^+, confirming the ion exchange mechanism [27].

Luukkonen et al. studied the adsorption of NH_4^+ on a granulated GP prepared from MK, sodium hydroxide, and silicate. The granulated GP has a good

compressive strength where the force needed to break the granules was 63.85 N. The GP was found to be effective for removing 90% of NH_4^+ from municipal wastewater when the initial NH_4^+ concentration was 32–40 mg/L at 4 g/L dose of GP and 60 min contact time. Furthermore, the results of a field study demonstrated that a limit of 4 mg/L NH_4^+ could be readily reached after treatment of influent municipal wastewater (initial concentration 15–20 mg/L NH_4^+, 0.2 L/min flow rate, and 2 kg GP granules) [20]. Consequently, the same group of research tried to optimize GP preparation conditions for maximized NH_4^+ adsorption capacity (19.8 mg NH_4^+/g). This optimization was obtained using molar ratios of SiO_2/Al_2O_3 = 2.87, Na_2O/Al_2O_3 = 0.78, H_2O/Na_2O = 22.42. Interestingly, GPs prepared from sodium alkali activators were found to have 27-48% higher NH_4^+ adsorption capacity than those prepared from potassium activators [26].

4.2.7.3 Geopolymers as Ion Exchangers for Alkaline Earth Metals

The first important study on this issue was reported by Uehara et al. in 2009. The authors claimed that a cementitious material exhibited ion exchange. The GP was prepared by mixing fly ash (FA), NaOH or KOH, silica powder, and water (initial Si/Al molar ratio of 1.7). The maximum ions' exchange capacity of Ba^{2+} and Sr^{2+} on Na^+ and K^+-GP was found to increase from 2.5 to 3.0 mmol/g (up to 260 mg Sr^{2+}/L and 410 mg Ba^{2+}/L) with the increase of Na/Al or K/Al molar ratio from 0.4 to 0.8. The amount of Sr^{2+} and Ba^{2+} bound to the surface of GP was approximately equal to the released quantity of Na^+ and K^+ [28]. Furthermore, the Na^+ in MK-based GP (SiO_2/Al_2O_3 = 2.89, Na_2O/Al_2O_3 = 0.84) can be exchanged with Mg^{2+} by agitating the GP (without any treatment other than grinding) with 0.1 M solution of Mg^{2+} as revealed by EDS analysis. The % of Na^+ exchange by Mg^{2+} was 57%, which was lower than that of Pb^{2+}, Cd^{2+}, NH_4^+, K^+, Li^+ [25].

4.2.7.4 Geopolymers as Ion Exchangers for Heavy Metals

Metakaolin-Based Geopolymers

By employing a variety of spectroscopic techniques (UV–Vis–NIR diffuse reflectance and ^{27}Al-NMR spectroscopy), Bortnovsky et al. provided strong evidence for the exchange of Na^+ in MK-based GP by paramagnetic Co(II). Furthermore, EDS analysis indicated that the Na/Al molar ratio changed from 1.1 in the case of Na^+-GP to 0 upon ion exchange with Co(II) and the resultant Co/Al molar ratio was 0.59 [18]. Similarly, O'Connor et al. examined ion exchange of Na^+ in MK-based GP (SiO_2/Al_2O_3 = 2.89, Na_2O/Al_2O_3 = 0.84) by Pb(II), Cd (II), and Ag(I). The EDS analysis revealed that the % exchange was 100% in the case of Ag^+ and Pb^{2+} and 78% in the case of Cd^{2+} [25].

Some results for the adsorption of heavy metals on MK-based GP are shown in Table 4.1. Cheng et al. investigated the adsorption of Pb(II), Cd(II), Cu(II), and Cr

Table 4.1 Langmuir adsorption capacity (Q_m, mg/g), the affinity constant (K_L, L/mg), and pseudo-second-order rate constant (k_2, g mg^{-1} min^{-1}) parameters for adsorption of heavy metal on MK-based GP

Adsorbent	Adsorption conditions	Parameter	Pb(II)	Cu(II)	Cr(III)	Cd(II)	Ni(II)	Zn(II)	References
MK-GP	Ci: 50–300 mg/L, pH 4, Solid/liquid = 1.5 g/L	Q_m	147.1	48.78	19.94	67.57			[29]
		K_L	0.1135	0.025	0.158	0.449			
		k_2	1.8×10^{-5}	2.3×10^{-5}	1.8×10^{-3}	8.3×10^{-5}			
MK-GP	Ci: 50–500 mg/L, pH 5, Solid/liquid = 1.25 g/L	Q_m	63.40	59.22					[23]
		K_L	0.0181	0.0117					
Porous MK-GP	Ci: 100 mg/L, pH 5, Solid/liquid = 1.5 g/L	Q_m	45.1	34.5					[31]
		K_L							
		k_2		3.8×10^{-5}					
Porous MK-GP	Ci: 50 mg/L, pH 5, Solid/liquid = 1.5 g/L	Q_m		52.63					[32]
		K_L		0.1359					
		k_2		2.9×10^{-3}					
MK-GP	Ci: 25–600 mg/L, pH 6.4–7.3, Solid/liquid = 3.2 g/L	Q_m					42.61	74.54	[30]
		K_L					19.6	346	
		k_2					8.4×10^{-3}	3.8×10^{-3}	

MK—Metakaolin, *FA*—Fly ash, *BFS*—Blast furnace slag

(III), on MK-based GP. Depending on the obtained values of Q_m in mg metal/g GP, the following selectivity sequence was determined by the authors:

Pb(II) (147.06) > Cd(II) (67.57) > Cu(II) (48.78) > Cr(III) (19.94). This sequence reflects that ions with a large hydrated ionic radius like Cr(III) have a strong tendency to remain in solution and thus adsorbed weakly on the surface of GP [29]. It is worth to mention that the correct sequence for Q_m values should be in mmol metal/g GP:

Cu(II) (0.768) > Pb(II) (0.710) > Cd(II) (0.6011) > Cr(III) (0.383).

The ionic strength effect on the adsorption of heavy metals on MK-based GP was also studied [23, 30]. Lopez et al. observed that changing the ionic strength does not affect the adsorption of Pb(II) on MK-based GP, which suggests a non-electrostatic mechanism [23]. On the contrary, Kara et al. observed that the removal efficiency of MK-GP decreased from 90.69 to 61.68% for Zn(II) and from 87.65 to 73.90% for Ni(II) as the ionic strength changed from 0.02 to 0.2 M. This behavior was ascribed to the increased competition between electrolyte cations and the heavy metal ions by the increase of ionic strength. This reduction in adsorption removal efficiency of Zn(II) and Ni(II) by increasing ionic strength indicates that the adsorption of these ions on the GP involves electrostatic or outer-sphere surface reactions [30]. Furthermore, for the removal of heavy metal ions from water by MK-based GP, the ion exchange mechanism (outer sphere) seems to be more plausible than specific chemical adsorption (inner sphere) because the adsorption of heavy metals onto MK-based GP was also found to be endothermic [29].

Attempts to increase the adsorption performance (reducing the equilibrium time and increasing the Q_m value) of GPs by increasing the porosity of GP were without success. The porous MK-based GPs were prepared by employing sodium dodecyl sulfate or H_2O_2 foaming agents in the GP mixing design (Si/Al and Na/Al molar ratios equal to 1.6 and 1, respectively). Despite the significant increase in the porosity of GP by this technique, slow adsorption was observed by Tang et al. since the equilibrium time for adsorption of Cu(II) on the porous GP was about 50 h [31]. A similar observation was made by Ge et al. where equilibrium time for the adsorption of Cu(II) on the porous GP was 36 h [32]. The Q_m values of porous GP in the case of Pb(II) and Cu(II) (45.1 and 34.5 mg/g, respectively) were less than that classical MK-based GP (63.4 and 59.2 mg/g, respectively) [31].

As(III) and Sb (III) are found in aqueous solutions in the forms of oxyanionic arsenite/arsenate and antimonite/antimonate, respectively. The study of adsorption of these anions onto MK-based GP was carried out by Luukkonen et al. The obtained Q_m values (0.078 and 0.058 mg/g, respectively) were much lower than those obtained for metal cations (Table 4.1). This confirms that these anions are not amenable for being exchange with the Na^+ or K^+ in the GP [33]. Similarly, Medpeli et al. reported a very low adsorption capacity of 0.950 mg/g for adsorption of $HAsO_4^{2-}$ on MK-based GPs [34].

Fly Ash-Based Geopolymers

Some of the parameters (Q_m, K_L and k_2) obtained for adsorption of heavy metals on fly ash (FA)-based GPs [35–39] are summarized in Table 4.2. It is clear that FA-based GPs are good adsorbents for the removal of heavy metals ions. The adsorption capacity (Q_m) of Cu(II) on GP was much higher than that on the FA precursor, which indicates that geopolymerization process creates new adsorption sites [35]. As calculated from values in Table 4.2, the average adsorption capacity of Cu(II) and the affinity constant K_L are 93 ± 8 and 0.08 ± 0.03 L mg^{-1}, respectively, which indicate that the diversity in FA origin and variability in adsorption experiments hardly affect the values of Q_m and K_L. On the other hand, the kinetics parameters reflect different behavior. The adsorption rate constants (k_2, g mg^{-1} min^{-1}) were of much variability as shown in Table 4.2 [37–39]. Furthermore, the reported equilibrium times for adsorption of heavy metals on FA-based GPs vary from 15 min to 30 h [35–37], which indicate the dependence of the kinetics behavior on the degree of compactness of GPs.

An important study for ion exchange of Pb^{2+} on FA-based GP was reported by Uehara et al. The GP was prepared from FA with Si/Al molar ratio of 1.7. The

Table 4.2 Langmuir adsorption capacity (Q_m, mg/g), the affinity constant (K_L, L/mg), and pseudo-second-order rate constant (k_2, g mg^{-1} min^{-1}) parameters for adsorption of heavy metal on FA-based GP

Adsorbent	Adsorption conditions	Parameter	Cu(II)	Pb(II)	References
FA-GP	Ci: 100-250 mg/L, pH 7, Solid/liquid = 0.15 g/L	Q_m	99		[35]
		K_L	0.13		
		k_2	2.8×10^{-5}		
FA-GP	Ci: 10-140 mg/L, pH 5-6, Solid/liquid = 1.4-2.0 g/L	Q_m	96.84	134.95	[36]
		K_L	0.061	0.0607	
		k_2	0.018		
FA-GP	Ci: 100-1000 mg/L, pH 3, Solid/liquid = 4.0 g/L	Q_m		111.1	[41]
		K_L		0.6429	
		k_2		2.7×10^{-3}	
FA/iron ore tailing-GP	Ci: 100–200 mg/L, pH 6, Solid/liquid = 3.0 g/L	Q_m	113.41		[42]
		K_L	0.073		
	Ci: 100–200 mg/L, pH 5, Solid/liquid = 3.0 g/L	Q_m	100.81		
		K_L	0.069		
	Ci: 100–200 mg/L, pH 4, Solid/liquid = 3.0 g/L	Q_m	79.31		
		K_L	0.064		
FA-GP	Ci: 376 mg/L, Solid/liquid = 5.0 g/L	k_2	0.028		[38]
FA-GP	Ci: 246–2501 mg/L, Solid/liquid = 5.0 g/L	Q_m	68.9		[40]

MK—Metakaolin, *FA*—Fly ash, *BA*—Bottom ash, *BFS*—Blast furnace slag

maximum ion exchange capacities of Na^+ and K^+-GP by Pb^{2+} ranged from 2.5 to 3.0 mmol/g (517.5–621.0 mg/g). The release of Na and K from the GP was less than the adsorption of Pb^{2+}, suggesting that ion exchange is not the only operating mechanism [28].

Mužek et al. investigated removal of Cu(II) and Co(II) using a GP prepared from fly ash (FA), sodium hydroxide, and silicate (initial SiO_2/Al_2O_3 = 4.61, Na_2O/Al_2O_3 = 0.69, and H_2O/Na_2O = 11.19). The Langmuir parameters Q_m and K_L were found to be 68.9 mg/g and 7.2 L/mg for Cu(II), and 50.3 mg/g and 0.7 L/mg for Co (II). By the end of the adsorption process, significant amounts of Na, lesser amounts of Si, and nondetectable amounts of Al were found in the remaining solution, supporting ion exchange mechanism and high stability of GP [40].

The similarity between zeolites and FA-based GPs was claimed by some authors. Muzek et al. [39] noticed the similarity of the adsorption behavior of FA-based GP and zeolite Na-X toward Co(II). The following values reveal also that the adsorption parameters of Pb(II) on FA-based GP are close to those on faujasite [41]:

	FA-GP	Faujasite
Q_m (mg/g)	111.11	142.86
K_L (L/mg)	0.6429	0.2966
k_2 (g mg^{-1} min^{-1})	26.73×10^{-4}	13.5×10^{-4}

The adsorption of heavy metals was found to increase with increasing pH due to a decrease of competition between heavy metal ions and H_3O^+ [36, 41, 42]. The Q_m of Cu(II) increases from 79.31 to 113.41 mg/g with pH increase from 4 to 6 [42].

In many studies, the adsorption of heavy metals on FA-based GPs was found to be endothermic and thus entropy driven (positive values of $\Delta H°$ and positive values of $\Delta S°$). The entropy increase in adsorption process may be due to desolvation of metal ions because of their adsorption on the surface of GP [36, 37, 40, 41].

Zeolite-Based Geopolymers

Zeolites were incorporated into GP preparations for many purposes. The first was to increase the adsorption capacity of GP [43–46]. The second was that GP works as a binder for zeolites powder and consequently enables shaping of zeolites as high mechanical strength spheres, granules, or extrudates which can be used as commercial adsorbents for purification of water [44, 47]. The third was to combine the microporosity of zeolites with the mesoporosity of GPs [47]. However, many of these studies evidenced partial or complete dissolutions of crystalline zeolite in the amorphous GP matrix [43, 45, 46, 48] which indicate the participation of zeolite in the geopolymerization process as an aluminosilicate source.

Some of the parameters for adsorption heavy metals on zeolite-based GP are listed in Table 4.3 [43–45]. El-Eswed et al. studied the adsorption of Pb(II), Zn(II),

Cd(II), and Cu(II) on a GP synthesized from natural zeolite (phillipsite) and natural kaolinite using alkali sodium hydroxide. The adsorption rate constants (k_2) for adsorption of heavy metals on the GP samples were less than those obtained in the case of natural kaolinite (Table 4.3), which indicate that GP pores are less accessible for heavy metals than kaolinite sheets [45]. On the other hand, the Q_m values for adsorption of heavy metals on the zeolite/kaolinite-based GP [61.31 mg/g for Pb(II)] were higher than those obtained in the case of raw natural zeolite (40.19 mg/g) and natural kaolinite (9.61 mg/g) [44]. The following trend was obtained for the adsorption of heavy metals on zeolite/kaolinite-based GP [45]:

	Pb(II)	Zn(II)	Cd(II)	Cu(II)
Q_m (mg/g)	61.31	33.47	30.53	24.18
Q_m (mmol/g)	0.296	0.512	0.272	0.381

Andrejkovicova et al. studied adsorption of Pb(II), Cd(II), Cu(II), Zn(II), and Cr(III) onto MK/zeolite-based GP which synthesized by alkali activation (sodium hydroxide and silicate) of a solid mixture of MK, zeolite (clinoptilolite). Depending on the obtained Q_m in mg/g values, the following sequence was obtained [49]:

Pb(II) (202.72) > Cd(II) (53.99) > Cu(II) (35.71) > Zn(II) (30.79) > Cr(III) (18.02)

However, the sequences for Q_m in mmol/L are:

Pb(II) (0.978) > Cu(II) (0.561) > Cd(II) (0.480) ≈ Zn(II) (0.471) > Cr(III) (0.348)

Al-Zboon et al. used natural zeolitic tuff as a sole precursor for preparation of GP adsorbent. The GP was prepared from zeolitic tuff (phillipsite and chabazite) and 14 M NaOH solution (1:1.25 mass ratio). The maximum adsorption capacity (Q_m) of GP toward Zn(II) was 14.8 mg/g, and the K_L was 0.7 L/mg. The adsorption capacity was pH independent in the range from 5 to 7. The equilibration time was 30 min, and the adsorption process was, as usual, endothermic and entropy driven [46].

4.2.7.5 Geopolymers as Ion Exchangers/Adsorbents for Cationic Organic Dyes

The adsorption of dyes' pollutants on the GP received little attention in the literature. Li et al. investigated adsorption of cationic dyes (methylene blue and crystal violet) on FA-based GP. The adsorption capacity of the GP (31.99 mg MB/g and 40.80 mg CV/g) was much higher than that of the unreacted FA precursor (1.60 mg MB/g and 1.63 mg CV/g), and the rate constant of absorption on the GP (6.25×10^{-5} and 2.28×10^{-5} mg g^{-1} min^{-1}, respectively) was much lower than that on unreacted FA (1.01×10^{-2} and 2.25×10^{-3} mg g^{-1} min^{-1}, respectively). Thus, geopolymerization process generates more sites for adsorption/ion exchange of cationic dyes but decreases the rate of adsorption by restricting the accessibility

Table 4.3 Langmuir adsorption capacity (Q_m, mg/g), the affinity constant (K_L, L/mg), and pseudo-second-order rate constant (k_2, g mg^{-1} min^{-1}) parameters for adsorption of heavy metal on zeolite-based GP

Adsorbent	Adsorption conditions	Parameter	Cu(II)	Pb(II)	Cd(II)	Ni(II)	Zn(II)	References
Phillipsite	Ci: 10–100 mg/L, pH 4, Solid/liquid = 1.0 g/L	Q_m	8.46					[43]
		K_L	0.196					
Kaolin		Q_m	5.98					
		K_L	0.020					
Phillipsite/kaolin-GP		Q_m	12.4					
		K_L	0.413					
Phillipsite	Ci: 10–100 mg/L, pH 4, Solid/liquid = 1.0 g/L	Q_m		72.6				[44]
		K_L		0.253				
Kaolin		Q_m		21.0				
		K_L		0.253				
Phillipsite/kaolin-GP		Q_m		112				
		K_L		0.146				
Phillipsite	Ci: 10–100 mg/L, pH 4, Solid/liquid = 1.0 g/L	Q_m	16.07	40.19	12.77	13.74	8.329	[45]
		K_L	0.123	0.088	11.18		0.3015	
		k_2	1.5×10^{-4}	4.3×10^{-5}	6.8×10^{-5}	4.5×10^{-4}	1.8×10^{-4}	
Kaolin		Q_m	7.212	9.61	8.35	1.607	19.00	
		K_L	0.0783	0.276	14.96		0.0145	
		k_2	5.7×10^{-4}	2.842×10^{-4}	10.4×10^{-3}	2.5×10^{-4}	5.5×10^{-4}	
Phillipsite/kaolin-GP		Q_m	24.18	61.31	30.53	16.63	33.47	
		K_L	0.304	0.1326			0.0593	
		k_2	3.8×10^{-5}	5.05×10^{-5}	8.7×10^{-5}	2.2×10^{-4}	7.6×10^{-5}	

(continued)

Table 4.3 (continued)

Adsorbent	Adsorption conditions	Parameter	Cu(II)	Pb(II)	Cd(II)	Ni(II)	Zn(II)	References
Clinoptilolite/MK-GP	Ci: 20–3000 mg/L, pH 6–7, Solid/liquid = 1.0 g/L	Q_m	35.71	202.72	53.99		30.79	[49]
		K_L	0.337	0.038	0.125		0.483	
Phillipsite/Chabazite-GP	Ci: 10–160 mg/L, pH 7, Solid/liquid = 8.0 g/L	Q_m					14.7	[46]
		K_L					1.26	
Mordenite/MK-GP	Ci: 250 mg/L	Q_m	7.8					[48]

MK—Metakaolin, *FA*—Fly ash, *BA*—Bottom ash, *BFS*—Blast furnace slag

of these sites for large molecular size dyes [50]. The adsorption of methylene blue on zeolite/kaolinite-based GP was similar (26 mg/g) [43]. It is worth to mention that the reactions of methylene blue and crystal violet in highly basic conditions of GP predation conditions need further research since these dyes may undergo hydrolysis reactions [51].

Barbosa et al. studied the adsorption of cationic methyl violet 10B dye on a mesoporous GP which was prepared from MK, rice husk ash (96.68% SiO_2), potassium hydroxide, water, and soybean oil (initial SiO_2/Al_2O_3 molar ratio = 4, K_2O/Al_2O_3 = 2, H_2O/K_2O = 10.4). The BET surface area of the produced GP, pore volume, and pore diameter were 62 m^2/g, 0.36 cm^3/g, and 14.3 nm, respectively, which were higher than those for ordinary GP prepared without oil (27 m^2/g, 0.13 cm^3/g, and 9.1 nm, respectively). Furthermore, the adsorption parameters of the mesoporous GP (Q_m, $K_{L,}$ and k_2 values were 40.25 mg/g, 0.0171 L/mg, and 0.0122 g mg^{-1} min^{-1}, respectively) were higher than those of the ordinary GP for adsorption of methyl violet 10B (Q_m = 13.4 mg/g and k_2 = 0.021 g mg^{-1} min^{-1}, respectively) [52]. Noteworthy, as in the work Li et al. [50], the work of Barbosa et al. indicated that the rate constant k_2 of methyl violet 10B found in the case of unreacted MK (0.01342 g mg^{-1} min^{-1}) was higher than that obtained in the case of MK-based GP (0.01217 g mg^{-1} min^{-1}).

4.2.8 Comparison of Geopolymers with Zeolites

4.2.8.1 Synthesis Conditions

Hydrothermal crystallization of aluminosilicate gel has been used in zeolite synthesis processes for a long time [53]. Zeolites are usually synthesized from aqueous sodium silicate and sodium aluminate in a closed hydrothermal system at a specific temperature, autogenous pressure, and varying time (ranges from few hours to several days) [54]. The time needed to start crystallization of mordenite was reported to increase with a decrease in temperature of crystallization; 4 weeks at 100 °C and 1 h at 350 °C [55]. To be fabricated as pellets or extrudates, the zeolite powder must be mixed with clay and water followed by calcination at 300–600 °C [54]. Thus, synthesis of zeolite requires relatively high energy.

However, the synthesis of zeolite from coal fly ash (FA type F, low calcium) was attempted under mild conditions. Low-silica zeolitic materials (NaP1, A, X, KM, chabazite, and faujasite) were obtained using different conditions of the open or closed system, different NaOH or KOH solutions/fly ash ratios, atmospheric or water vapor pressures, and crystallization time ranged from 3 to 48 h at 80–200 °C [56]. Franus et al. synthesized three types of zeolites from FA by varying the reaction conditions: Na-X (20 g FA per 0.5 L of 3 M NaOH at 75 °C), Na-P1 (20 g FA per 0.5 L of 0.5 M NaOH at 95 °C), and sodalite (20 g FA per 0.8 L of 5 M NaOH and 0.4 L of 3 M NaCl at 95 °C) [57]. Thus, the type of synthetic zeolite

obtained from FA is a function of pH, the concentration of reagents, and temperature [58].

GPs are the amorphous analogues of zeolites because synthesis of both materials can be conducted under hydrothermal conditions. In GP synthesis, the temperature and the amount of water are generally kept lower than those in zeolite synthesis. The temperatures employed in GP synthesis range from 40 to 80 °C, and the water content can be expressed as H_2O/M_2O molar ratios of around 10–20 (M = Na^+ or K^+) [53]. Some of the reported water/FA mass ratios for the preparation of FA-based GP and zeolite were about 0.4 [59, 60] and 30 [57], respectively. Thus, from the economic, energy, and water saving point of views, GPs have been synthesized under better conditions than zeolites.

4.2.8.2 Crystallinity

On the contrary to crystalline zeolites which have definite peaks in their XRD patterns, the GPs are often found to be X-ray amorphous. A "hump" centered at approximately 27–29° 2θ is usually the major characteristic of the XRD pattern of GPs [8]. However, high-resolution microscopy (Fig. 4.2) showed that the GP contains nano-crystalline aluminosilicate particles [53]. In general, longer reaction times in GP synthesis generated more crystalline products embedded in the amorphous GP [53]. Furthermore, GPs prepared using CsOH (as an alkaline activator) were found to contain significant amounts of crystalline zeolites A, X, and F [21, 22].

It is worth to emphasize that activation of MK with alkaline sodium silicate, rather than sodium hydroxide solution, causes rapid nucleation of solid products surrounding the dissolving MK particles and consequently gives geopolymeric rather than highly crystalline zeolitic products [53].

4.2.8.3 Surface Area and Porosity

Franus et al. synthesized three kinds of zeolitic materials from FA: sodalite, Na-P1, and Na-X, with BET specific surface area of 33, 71, and 166 m^2/g, respectively. The textural analysis indicates that sodalite and Na-P1 are mesoporous–microporous, and the Na-X is microporous [57]. The small pore size of sodalite (2.3 Å) renders it low potential application in ion exchange. On the other hand, the larger pore size of Na-X (7.3 Å) makes this zeolite a promising ion exchanger [56].

It is well established that geopolymerization process increases the specific surface area of aluminosilicate source (MK, FA, BFA). Wang et al. reported that geopolymerization resulted in an increase of BET surface area from 8.4 m^2/g in the case of FA to 31.8 m^2/g in the corresponding GP [29]. A similar trend was observed by Li et al. where the surface area increases from 16.45 m^2/g in unreacted FA to 20.48 m^2/g in the FA-based GP [41]. Furthermore, Luukkonen et al. observed that the BET surface area increases from 2.79 and 11.5 m^2/g in case of

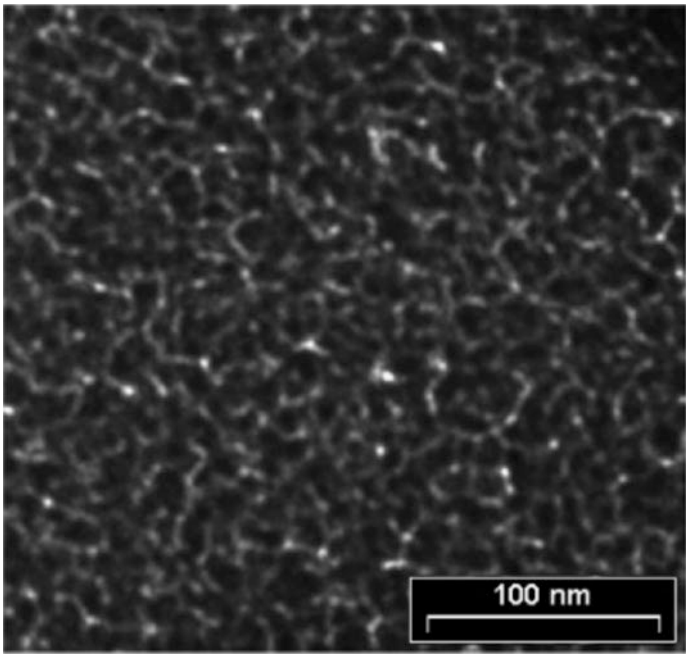

Fig. 4.2 TEM micrograph of a section of MK-based GP [53]. Reprinted with permission from (Provis J. L., Lukey G. C., van Deventer J. S. J. Do Geopolymers Actually Contain Nanocrystalline Zeolites? A Reexamination of Existing Results. Chem. Mater. 2005, 17, 3075–3085). Copyright (2005) American Chemical Society

Table 4.4 Specific surface areas, and volumes of the geopolymers and their raw materials [33]

	BFA	BFS-GP	MK	MK-GP
Specific surface area (m^2/g)	2.79	64.5	11.5	22.4
Marco-mesopore volume (cm^3/g)	0.008	0.070	0.047	0.165
Micropore volume (cm^3/g)	0.001	0.025	0.005	0.008

unreacted BFS and MK, respectively, to 64.5 and 22.4 m^2/g in case of their corresponding GPs (Table 4.4) [33]. The average BET surface area of 34 samples of MK-based GPs prepared using different initial Si/Al and Na or K/Al molar ratios were 50 ± 27 m^2/g, and the average pore size was 22 ± 6 nm (mesoporous) [26].

GPs are macroporous/mesoporous in comparison with microporous zeolites. As evident from Table 4.4, the % macro-mesoporosity values of BFS-GP and MK-GP (74 and 95.4%, respectively) are higher than the % microporosity values (26 and 4.6%, respectively). [33]. For 34 samples of MK-based GPs prepared under different experimental conditions, the % macroporosity, mesoporosity, and microporosity were 31 ± 19, 69 ± 19, and 0.52 ± 0.13, respectively [26].

Table 4.5 Comparison between geopolymers and synthetic zeolites

Aspect of comparison	Geopolymers	Synthetic zeolites
Temperature of synthesis	40–80 °C	100–600 °C
Amount of water used in the synthesis	Low water/FA mass ratio = 0.4 Low H_2O/Na_2O molar ratio = 10–20	High water/FA mass ratio = 20–40 High H_2O/Na_2O molar ratio = 30
Mechanical strength	Low temperature 40-80 °C is enough to obtain a high-strength product	Fragile powder, high temperature 500–600 °C is required to obtain granules or extrudates
Stability in aqueous solutions and thermal stability	Stable	Unstable except in the case of high Si/Al molar
Crystallinity	Amorphous	Crystalline
Porosity	Mesoporous, high pore size distribution	Microporous, low pore size distribution
Specific surface area (m^2/g)	20–70	30–170
CEC (meq/g)	0.1–4	0.5–5

According to several studies, GPs have a wider pore distribution than zeolites [19, 41]. The pore size distribution curve of FA-GP was found to be centered at around 14 nm with a wider distribution than faujasite which was sharp and centered at 4 nm [41]. Furthermore, Skorina observed that the average pore size ranged from 5.7 to 20.7 nm [19].

Many attempts have been made to increase the porosity of GP by employing H_2O_2 and sodium dodecyl sulfate as foaming agents. A porous MK-based GP was found to have a bulk density of 0.79 g/cm^3 and total porosity of 60.3%. The pores of the GP were found to center at about 15 nm, which reflected the presence of plenty of mesopores [31]. As the amount of H_2O_2 increases from 0.30 to 1.2% (w/w), the density of MK/FA-based GP decreases from 0.98 to 0.44 g/cm^3 and the porosity increases from 52.0 to 78.4% [61]. The total porosity of FA/iron ore tailing-based GP ranges from 56.9 to 74.6%. The fraction of pores with diameters larger than 50 nm (macropores) for porous GP was higher than that for reference GP. The pore diameter of the porous GP shifts to higher values with the addition of more H_2O_2 [42]. A general comparison of GPs with synthetic zeolites is presented in Table 4.5.

4.2.8.4 Cation Exchange Capacity

In zeolites, the exchangeable metal cations balance the negative charge on the surface of zeolite pores. This negative charge results from the partial replacement of Si by Al tetrahedra [58]. Thus, synthetic zeolites with low Si/Al molar ratio like

faujasite, chabazite, herschelite, NaP1, and 4A have high cation exchange capacity (CEC). For example, the CEC values of zeolite X and NaP1 are 5.0 and 2.7 meq/g, respectively (ammonium method). These values are higher than those obtained for natural clinoptilolite (1.5–2.0 meq/g) [56]. Franus et al. synthesized zeolites from coal FA, namely, Na-X, Na-P1, and sodalite with CEC 1.8, 0.72, and 0.56 meq/g, respectively (Ba^{2+} method) [57].

The CEC values of GPs are comparable to those of zeolites. Some of the reported CEC values of different GPs are: 0.13 [62], 4.15 [27], 1.1 [26], 2.02 meq/g [24] using NH_4^+ method, and 0.2–0.3 meq/g using Ba^{2+} method [28]. Thus, although GPs are cementitious materials which are characterized by compact structure, they are, like zeolites, good ion exchangers.

4.2.8.5 Selectivity for Metal Ions

In general, the selectivity of cationic exchangers typically increases with increase of charge and ionic size of the exchanging ion: $Th^{4+} > La^{3+} > Ce^{3+} > Ba^{2+} > Sr^{2+} > Ca^{2+} > Co^{2+} > Ni^{2+} > Cu^{2+} > Mg^{2+} > Be^{+2} > Ag^+ > Rb^+ > Cs^+ > K^+ > Na^+ > H^+ > Li^+$ [63]. Similarly, the zeolite ion exchange capacity increases with increasing ionic size. The selectivity sequence of clinoptilolite toward metal ions follows the sequence: $Cs^+ > K^+ > Rb^+ > Na^+ > Li^+$ and $Ba^{2+} > Sr^{2+} > Ca^{2+} > Mg^{2+}$ [64]. The selectivity of clinoptilolite for heavy metals varies somewhat in the literature: Pb (II) > Cd(II) > Cu(II) ≈ Zn(II) [65], Pb(II) > Cd(II) > Cu(II) > Zn(II) [64], and Pb(II) > Cu(II) > Cd(II) ∼ Zn(II) [66, 67].

From a collection of trends discussed in Sect. 3.1, the following sequence can be deduced in the case of ion exchange/adsorption of metal ions on GPs:

$Cs^+ > Cu^{2+} \sim Pb^{2+} > Ba^{2+} > Sr^{2+} > K^+ > NH_4^+ > Li^+ > Cd^{2+} > Mg^{2+} > Na^+$ [23, 25, 26, 28, 29]. Thus, the selectivity sequence of GPs toward metal ions is similar but not identical to those of zeolites. It is worth to mention that the selectivity order changes with the concentration of metal ions in solution and depends on whether it is based on values in mg/g (incorrect) or mmol/g.

4.2.8.6 Stability in Acidic Solutions

The disintegration of zeolites in acidic medium is related to the number of Al atoms, which appear to be the sites of acid attack. Zeolites with high Si/Al molar ratio are stable in acidic medium. Zhuou and Zhu investigated the stability of synthetic zeolites in HCl solution at pH 1 for 3 h by studying their XRD patterns. NaZSM-5 (Si/Al = 12.5–26), NaZSM-11 (Si/Al = 25), Hβ (Si/Al = 14.5), and dealuminated Na-Y (Si/Al = 7) were stable while Na-Y (Si/Al = 2.66) and Na-A (Si/Al = 1) were not and dissolved completely in acidic solutions [68].

Although these have usually Si/Al ratio of about 2, GPs have high acid resistance, and this may be one of the reasons for devoting attention to these materials [69]. Li et al. reported that after 60 days of soaking GP blocks in acetic acid buffer

(pH 3.6), the mass loss of GP was 2.5% [70]. Furthermore, the stability of the GP paste was inferred from the fact that the chemical composition (XRF), especially the % Si and Al, of GP, was not affected by ion exchange process (0.5 g GP/250 ml of 0.1 M $BaCl_2$ and $SrCl_2$) [28].

4.2.8.7 Thermal Stability

Synthetic zeolites like Na-P1, A, X, Y, and P, prepared from FA, have high thermal stability because of their high Si/Al molar ratio. Na-P1, Na-X, and sodalite maintain their crystalline structure at temperatures below 300, 700, and 900 °C, respectively [58]. Similarly, GPs are known to be of excellent thermal stability and already used in fire-resistant coatings, thermal insulation, and furnace linings [71]. After 2 h calcination at 1000 °C, the FA-based GPs can keep a compressive strength of 30 MPa [70].

4.2.8.8 Mechanical Strength

Synthetic zeolites are fragile and often obtained as a powder. These can be fabricated as pellets or extrudates by mixing with a binder like clays followed by calcination at 300–600 °C to get extrudates or granules of sufficient mechanical strength for the purpose of industrial ion exchange processes [54]. On the other hand, GPs as ion exchangers can be formulated as pellets or granules directly during synthesis at 40–80 °C. The compressive strengths of GPs, prepared from FA of different origins, ranged from 30 to 80 MPa [71].

4.2.8.9 Regeneration

Regeneration of the ion exchanger saturated with metal ions results in re-use of the ion exchanger and recovery of metal ions. Thus, the possibility of regeneration has a positive impact on the environment in eliminating the possibility of creating new toxic waste. The adsorption of heavy metals on zeolites was found to be reversible, and thus, the regeneration of zeolite is possible [64]. However, the decrease in adsorption/desorption capacity of clinoptilolite with increasing regeneration cycles was remarkable in the case of removal of Pb(II) and Zn(II) from the water. Successive regeneration cycles using 3 M KCl resulted in more than 50% reduction of adsorption efficiency after 9 and 4 cycles for Pb(II) and Zn(II), respectively [65]. This decrease may be due to the decomposition of clinoptilolite during regeneration.

GPs have been shown to be regenerable in several studies, but a limited number of cycles were investigated. Granules of MK-based GP, which were suitable for continuous column mode for adsorption of ammonium ion, are amenable for multiple regenerations with NaCl/NaOH, although two regeneration cycles

decreased the NH_4^+ removal significantly [20]. However, some studies reported that the adsorption of heavy metals on GP was not reversible. Cheng et al. found that the % desorption of Pb(II), Cd(II), Cr(III), and Cu(II) from GP loaded with maximum amounts of these heavy metals was 5.9, 2.1, 14.7, and 1.9%, respectively [29]. Thus, the possibility of regeneration of GPs, as well as zeolites, is still open to further research.

4.2.9 Stabilization/Solidification/Encapsulation of Ion Exchangers in Geopolymers

An integrated process consists of adsorption followed by solidification/stabilization has been suggested in the literature as a method for encapsulation of exhausted ion exchangers (like fly ash and red mud). For example, heavy metal-loaded fly ash and red mud have been successfully solidified by adding Portland cement producing durable concrete blocks with a compressive strength of 30 MPa [72].

Since alkali-activated aluminosilicates or GPs are alternatives for Portland cement, GPs have been used to encapsulate exhausted ion exchangers. Ipatti investigated encapsulation of exhausted granular boric acid-based ion exchange resins in alkali-activated blast furnace slag (37.7% CaO, 34.4% SiO_2, and 8.4% Al_2O_3). The alkali activation using $Ca(OH)_2$ and NaOH effectively produced GPs containing ion exchanger with compressive strengths varied between 9 and 19 MPa [73].

Kuenzel investigated encapsulation of Cs^+- and Sr^{2+}-loaded clinoptilolite in MK-based GP (initial Si/Al molar ratio of 2, Na/Al = 0.7–1.3, H_2O/Al = 9). The leached Cs^+ and Sr^{2+} concentrations were below the detection limit (5 ppm). Ion exchange of Cs^+ with the charge balancing ions (Na^+) in GP may be the main factor responsible for the immobilization of Cs^+ in the GP matrix. The uptake of Sr^{2+} and Cs^+ of GP per 1 mol of Al was estimated to be 0.4 and 0.2 mol, respectively. The SEM/EDS studies revealed that the high alkalinity of activating solution (sodium hydroxide and silicate) causes dissolution of clinoptilolite containing Cs^+ and Sr^{2+} (in addition to the MK precursor) followed by the bound of these ions to the MK-based GP aluminosilicate phase (see Fig. 4.3) [74].

The reported high compatibility observed between the organic resins and inorganic GP phases [75] is a promising property that makes GPs potential hosts for encapsulation of exhausted organic ion exchangers which may be a subject for future research.

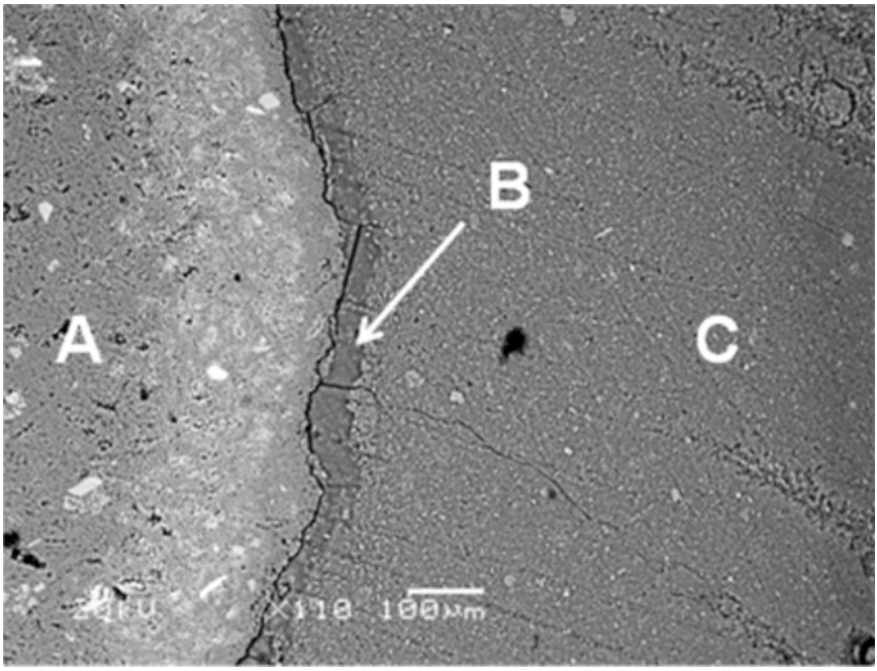

Fig. 4.3 SEM image of MK-based GP used for encapsulation of clinoptilolite containing Cs^+ (A: clinoptilolite, C: MK-based GP, and B: interfacial zone) [74]. Reprinted with permission from (Kuenzel C., Cisneros J.F., Neville T.P., Vandeperre L.J., Simons S.J.R., Bensted J., Cheeseman C.R. Encapsulation of Cs/Sr contaminated clinoptilolite in geopolymers produced from metakaolin. Journal of Nuclear Materials. 2015, 466, 94–99). Copyright (2015) Elsevier B.V

4.3 Concluding Remarks

1. GPs could be used in the treatment of wastewater. The increase in pH of wastewater due to contact with unreacted alkali in GP is expected to be limited due to the buffering capacity of real wastewater and the acidity of industrial wastewater.
2. Despite the high solubility of Cs^+ in water, it could be removed from aqueous solutions using GPs with highly variable adsorption capacity (15–40 mg/g).
3. Complete ion exchange of Na^+ in GP by NH_4^+ was achieved, so GP was applied as an effective ion exchanger for removal of NH_4^+ from real wastewater. The adsorption capacity ranged from 20 to 75 mg/g.
4. Less ion exchange efficiency was obtained in the case of Mg^{2+} and Ca^{2+}.
5. GPs have high ion exchange capacity for Sr^{2+} and Ba^{2+}, as adsorption capacities up to about 250 and 400 mg/g, respectively, were achieved.
6. The adsorption capacities of Pb(II) were 110–130, 50–150, and 60–200 mg/g in the case FA-GP, MK-GP, and zeolite-GP, respectively. On the other hand, the adsorption capacities of Cu(II) were 70–110, 30–50, and 12–36 mg/g,

respectively. These values reflected the strong ability of GPs prepared from various sources for the removal of heavy metals from water.

7. The geopolymerization process results in a remarkable increase in the BET surface area, the adsorption capacity (Q_m), and affinity constant (K_L) relative to starting aluminosilicate precursors (MK and FA). However, the adsorption rate constant (k_2) decreases upon geopolymerization which reflects the slow adsorption rate of heavy metals by GPs due to diffusion limitations in the GP.
8. Increasing the porosity of GPs does not necessarily increase the adsorption capacity and rate constant.
9. The adsorption of ingoing metal ions is associated with the release of outgoing ions. Some interesting features include efficient regeneration of GP adsorbents by NaCl solution, increasing ionic strength and decreasing pH result in a decrease of adsorption, poor adsorption of oxyanions forming metal ions like As(III) and Sb(III) on GPs, and the positive entropy and positive enthalpy of adsorption process (endothermic). Actually, there were no sufficient evidence that support specific chemical bonding of metal ions to the surface of GPs.
10. Exhausted ion exchangers and zeolites (loaded with pollutants) could be encapsulated in GP matrix to give high compressive strength products (with minimum leachability of pollutants). Synthesis of Cs bearing zeolite embedded in the GP matrix is a promising technique for immobilization of Cs^+.
11. GPs have many features that are close to those of zeolites like high cation exchange capacity, high surface area, and thermal stability.
12. The synthesis of GPs is easier because of lower energy and water demand compared to the synthesis of zeolite. The prepared GP could be fabricated directly as high compressive strength granules at low temperature (40–80 °C).
13. Since GPs are more acid resistant than zeolites, GPs are expected to be more stable in the regeneration cycle, but this issue needs further investigations.
14. Zeolites embedded in GPs may be promising materials since they have the advantages of microporous zeolites and meso-/macroporous GPs.
15. GPs are cementing materials as well as ion exchangers which make them multifunctional materials that can serve as a construction material for the removal of pollutants from the environment.
16. The regeneration of exhausted GPs (used in wastewater treatment) and the encapsulation of exhausted zeolites in GP matrix using solidification/stabilization technique are two interesting future research areas.
17. The superiority of GPs to synthetic zeolites in respect of mechanical strength, stability, and cost may be the driving force for using GPs as ionic exchangers in the future.

References

1. Davidovits J (1991) Geopolymers: inorganic polymeric new materials. J Therm Anal 37:1633–1656
2. Provis JL, Fernández-Jiménez A, Kamseu E, Leonelli C, Palom A (2014) Binder chemistry—low-calcium alkali-activated materials. In: Provis JL, van Devente JSJ (eds) Alkali activated materials: state-of-the-art report, RILEM TC 224-AAM, Springer, pp 93–123
3. Ducman V, Korat L (2016) Characterization of geopolymer fly-ash based foams obtained with the. Mater Charact 113:207–213. https://doi.org/10.1016/j.matchar.2016.01.019
4. Melar J, Renaudin G, Leroux F, Hardy-Dessources A, Nedelec J, Taviot-Gueho C, Petit E, Steins P, Poulesquen A, Frizon F (2015) The porous network and its interface inside geopolymers as a function of alkali cation and aging. J Phys Chem C 119(31):17619–17632. https://doi.org/10.1021/acs.jpcc.5b02340
5. Zhang L, Zhang F, Liu M, Hu X (2017) Novel sustainable geopolymer based syntactic foams: an eco-friendly alternative to polymer based syntactic foams. Chem Eng J 313:74–82. https://doi.org/10.1016/j.cej.2016.12.046
6. Zhang Z, Provis JL, Reid A, Wang H (2014) Geopolymer foam concrete: an emerging material for sustainable construction. Constr Build Mater 56:113–127. https://doi.org/10.1016/j.conbuildmat.2014.01.081
7. Zhang F, Zhang L, Liu M, Mu C, Liang YN, Hu X (2017) Role of alkali cation in compressive strength of metakaolin based geopolymers. Ceram Int 43(4):3811–3817. https://doi.org/10.1016/j.ceramint.2016.12.034
8. Duxson P, Fernandez-Jimenez A, Provis JL, Lukey GC, Palomo A, Van Deventer JSJ (2007) Geopolymer technology: the current state of the art. J Mater Sci 42:2917–2933
9. Vance ER, Perera DS (2009) Geopolymers for nuclear waste immobilization. In: Provis JL, Van Deventer JSJ (eds) Geopolymers: structure, processing, properties and industrial applications. CRC Press and Woodhead Publishing Limited, Oxford, pp 401–420
10. Wang Y, Han F, Mu J (2018) Solidification/stabilization mechanism of Pb(II), Cd(II), Mn(II) and Cr(III) in fly ash based geopolymers. Constr Build Mater 160:818–827. https://doi.org/10.1016/j.conbuildmat.2017.12.006
11. Waijarean N, MacKenzie KJD, Asavapisit S, Piyaphanuwat R, Jameson GNL (2017) Synthesis and properties of geopolymers based on water treatment residue and their immobilization of some heavy metals. J. Mater. Sci. 52(12):7345–7359. https://doi.org/10.1007/s10853-017-0970-4
12. El-Eswed BI, Aldagag OM, Khalili FI (2017) Efficiency and mechanism of stabilization/solidification of Pb(II), Cd(II), Cu(II), Th(IV) and U(VI) in metakaolin based geopolymers. Appl Clay Sci 140:148–156. https://doi.org/10.1016/j.clay.2017.02.003
13. El-Eswed BI (2018) Solidification versus adsorption for immobilization of pollutants in geopolymeric materials: a review, solidification. Ares A (ed) InTech. https://doi.org/10.5772/intechopen.72299. Available from: https://www.intechopen.com/books/solidification/solidification-versus-adsorption-for-immobilization-of-pollutants-in-geopolymeric-materials-a-review
14. Al-Mashqbeh A, Abuali S, El-Eswed B, Khalili FI (2018) Immobilization of toxic inorganic anions (Cr2O72-, MnO4- and Fe(CN)63-) in metakaolin based geopolymers: A preliminary study. Ceram Int 44(5):5613–5620. https://doi.org/10.1016/j.ceramint.2017.12.208
15. Davidovits J (2017) Geopolymers: ceramic-like inorganic polymers. J Ceram Sci Technol 08:335–350. https://doi.org/10.4416/JCST2017-00038
16. Foo KY, Hameed BH (2010) Insights into the modeling of adsorption isotherm systems. Chem Eng J 156(1):2–10. https://doi.org/10.1016/j.cej.2009.09.013
17. Tan KL, Hameed BH (2017) Insight into the adsorption kinetics models for the removal of contaminants from aqueous solutions. J Taiwan Inst Chem Eng 74:25–48. https://doi.org/10.1016/j.jtice.2017.01.024

18. Bortnovsky O, Dědeček J, Tvarůžková Z, Sobalík Z, Šubrt J (2008) Metal ions as probes for characterization of geopolymer materials. J Am Ceram Soc 91:3052–3057. https://doi.org/10.1111/j.1551-2916.2008.02577.x
19. Skorina T (2014) Ion exchange in amorphous alkali-activated aluminosilicates: potassium based geopolymers. Appl Clay Sci 87:205–211. https://doi.org/10.1016/j.clay.2013.11.003
20. Luukkonen T, Věžníková K, Tolonen E, Runtti H, Yliniemi J, Hu T, Kemppainen K, Lassi U (2017) Removal of ammonium from municipal wastewater with powdered and granulated metakaolin geopolymer. Environ Technol:1–10. https://doi.org/10.1080/09593330.2017.1301572
21. Yuan J, He P, Jia D, You J, Liu X, Zhang Y, Cai D, Yang Z, Duan X, Wang S, Zhou Y (2017) Effects of Na + substitution Cs + on the microstructure and thermal expansion behavior of ceramic derived from geopolymer. J Am Ceram Soc 100:4412–4424. https://doi.org/10.1111/jace.14968
22. Arbel Haddad M, Ofer-Rozovsky E, Bar-Nes G, Borojovich EJC, Nikolski A, Mogiliansky D, Katz A (2017) Formation of zeolites in metakaolin-based geopolymers and their potential application for Cs immobilization. J Nucl Mater 493:168–179. https://doi.org/10.1016/j.jnucmat.2017.05.046
23. López FJ, Sugita S, Tagaya M, Kobayashi T (2014) Metakaolin-based geopolymers for targeted adsorbents to heavy metal ion separation. J Mater Sci Chem Eng 2:16–27. https://doi.org/10.4236/msce.2014.27002
24. Lee NK, Khalid HR, Lee HK (2017) Adsorption characteristics of cesium onto mesoporous geopolymers containing nano-crystalline zeolites. Microporous Mesoporous Mater 242:238–244. https://doi.org/10.1016/j.micromeso.2017.01.030
25. O'Connor SJ, MacKenzie KJD, Smith ME, Hanna JV (2010) Ion exchange in the charge-balancing sites of aluminosilicate inorganic polymers. J Mater Chem 20:10234–10240. https://doi.org/10.1039/C0JM01254H
26. Luukkonen T, Tolonen E, Runtti H, Kemppainen K, Perämäki P, Rämö J, Lassi U (2017) Optimization of the metakaolin geopolymer preparation for maximized ammonium adsorption capacity. J Mater Sci 16. https://doi.org/10.1007/s10853-017-1156-9
27. Belchinskaya L, Novikova L, Khokhlov V, Tkhi JL (2013) Contribution of ion-exchange and non-ion-exchange reactions to sorption of ammonium ions by natural and activated aluminosilicate sorbent. J Appl Chem:1–9. http://dx.doi.org/10.1155/2013/789410
28. Uehara M, Isogaya S, Yamazaki A (2008) Ion-exchange properties of hardened geopolymers paste from fly ash. Clay Sci 14(3):127–133. https://doi.org/10.11362/jcssjclayscience.14.3_127
29. Cheng TW, Lee ML, Ko MS, Ueng TH, Yang SF (2012) The heavy metal adsorption characteristics on metakaolin-based geopolymer. Appl Clay Sci 56:90–96. https://doi.org/10.1016/j.clay.2011.11.027
30. Kara İ, Yilmazer D, Akar STI (2017) Metakaolin based geopolymer as an effective adsorbent for adsorption of zinc(II) and nickel(II) ions from aqueous solutions. Appl Clay Sci 139:54–63. https://doi.org/10.1016/j.clay.2017.01.008
31. Tang Q, Ge Y, Wang K, He Y, Cui X (2015) Preparation and characterization of porous metakaolin-based inorganic polymer spheres as an adsorbent. Mater Des 88:1244–1249. https://doi.org/10.1016/j.matdes.2015.09.126
32. Ge Y, Cui X, Kong Y, Li Z, He Y, Zhou Q (2015) Porous geopolymeric spheres for removal of Cu(II) from aqueous solution: synthesis and evaluation. J Hazard Mater 283:244–251. https://doi.org/10.1016/j.jhazmat.2014.09.038
33. Luukkonen T, Runtti H, Niskanen M, Tolonen E, Sarkkinen M, Kemppainen K, Ramo J, Lassi U (2016) Simultaneous removal of Ni(II), As(III), and Sb(III) from spiked mine effluent with metakaolin and blast-furnace-slag geopolymers. J Environ Manage 166:579–588. https://doi.org/10.1016/j.jenvman.2015.11.007
34. Medpelli D, Sandoval R, Sherrill L, Hristovski K, Seo D (2015) Iron oxide-modified nanoporous geopolymers for arsenic removal from ground water. Resour-Effi Technol 1 (1):19–27. https://doi.org/10.1016/j.reffit.2015.06.007

35. Wang S, Li L, Zhu ZH (2007) Solid-state conversion of fly ash to effective adsorbents for Cu removal from wastewater. J Hazard Mater 139(2):254–259. https://doi.org/10.1016/j.jhazmat.2006.06.018
36. Al-Zboon K, Al-Harahsheh MS, Bani Hani F (2011) Fly ash-based geopolymer for Pb removal from aqueous solution. J Hazard Mater 188:414–421. https://doi.org/10.1016/j.jhazmat.2011.01.133
37. Al-Harahsheh MS, Al Zboon K, Al-Makhadmeh L, Hararah M, Mahasneh M (2015) Fly ash based geopolymer for heavy metal removal: A case study on copper removal. J Environ Chem Eng 3(3):1669–1677. https://doi.org/10.1016/j.jece.2015.06.005
38. Mužek MN, Svilović S, Zelić J (2013) Fly ash-based geopolymeric adsorbent for copper ion. Desalin Water Treat 52:2519–2526. https://doi.org/10.1080/19443994.2013.792015
39. Mužek MN, Svilović S, Zelić J (2016) Kinetic studies of cobalt ion removal from aqueous solutions using fly ash-based geopolymer and zeolite NaX as sorbents. Sep Sci Technol 51(18):2868–2875. https://doi.org/10.1080/01496395.2016.1228675
40. Muzek MN, Svilovic S, Ugrina M, Zelic J (2016) Removal of copper and cobalt ions by fly ash-based geopolymer from. Desalin Water Treat 57:10689–10699. https://doi.org/10.1080/19443994.2015.1040077
41. Liu Y, Yan C, Zhang Z, Wang H, Zhou S, Zhou W (2016) A comparative study on fly ash, geopolymer and faujasite block for Pb removal from aqueous solution. Fuel 185:181–189. https://doi.org/10.1016/j.fuel.2016.07.116
42. Duan P, Yan C, Zhou W, Ren D (2016) Development of fly ash and iron ore tailing based porous geopolymer for removal of Cu(II) from wastewater. Ceram Int 42(12):13507–13518. https://doi.org/10.1016/j.ceramint.2016.05.143
43. Yousef RI, El-Eswed B, Alshaaer M, Khalili F, Khoury H (2009) The influence of using Jordanian natural zeolite on the adsorption, physical, and mechanical properties of geopolymers products. J Hazard Mater 165:379–387. https://doi.org/10.1016/j.jhazmat.2008.10.004
44. El-Eswed B, Yousef RI, Alshaaer M, Khalili F, Khoury H (2009) Alkali solid-state conversion of kaolin and zeolite to effective adsorbents for removal of lead from aqueous solution. Desalin Water Treat 8:124–130. https://doi.org/10.5004/dwt.2009.672
45. El-Eswed B, Alshaaer M, Yousef RI, Hamadneh I, Khalili F (2012) Adsorption of Cu(II), Ni(II), Zn(II), Cd(II) and Pb(II) onto Kaolin/Zeolite based- geopolymers. Adv Mater Phys Chem 2:119–125. https://doi.org/10.4236/ampc.2012.24B032
46. Alzboon K, Al Smadi B, Al-Khawaldh S (2016) Natural volcanic tuff-based geopolymer for Zn removal: adsorption isotherm, kinetic, and thermodynamic study. Water Air Soil Pollut:227–248. https://doi.org/10.1007/s11270-016-2937-5
47. Papa E, Medri V, Amari S, Manaud J, Benito P, Vaccari A, Landi E (2018) Zeolite-geopolymer composite materials: production and characterization. J Clean Prod 171:76–84. https://doi.org/10.1016/j.jclepro.2017.09.270
48. Alshaaer M, Zaharaki D, Komnitsas K (2014) Microstructural characteristics and adsorption potential of a zeolitic tuff–metakaolin geopolymer. Desalin Water Treat 56(2):338–345. https://doi.org/10.1080/19443994.2014.938306
49. Andrejkovičov S, Sudagar A, Rocha J, Patinha C, Hajjaji W, Ferreira da Silva E, Velosa A, Rocha F (2016) The effect of natural zeolite on microstructure, mechanical and heavy metals adsorption properties of metakaolin based geopolymers. Appl Clay Sci 126:141–152. https://doi.org/10.1016/j.clay.2016.03.009
50. Li L, Wang S, Zhu Z (2006) Geopolymeric adsorbents from fly ash for dye removal from aqueous solution. J Colloid Interface Sci 30(1):52–59. https://doi.org/10.1016/j.jcis.2006.03.062
51. Mills A, Hazafy D, Parkinson J, Tuttle T, Hutchings MG (2011) Effect of alkali on methylene blue (C.I. Basic Blue 9) and other thiazine dyes. Dyes Pigm 88(2):149–155. https://doi.org/10.1016/j.dyepig.2010.05.015
52. Barbosa TR, Foletto EL, Dotto GL, Jahn SL (2018) Preparation of mesoporous geopolymer using metakaolin and rice husk ash as synthesis precursors and its use as potential adsorbent

to remove organic dye from aqueous solutions. Ceram Int 44:416–423. https://doi.org/10.1016/j.ceramint.2017.09.193
53. Provis JL, Lukey GC, van Deventer JSJ (2005) Do geopolymers actually contain nanocrystalline zeolites? A reexamination of existing results. Chem Mater 17:3075–3085. https://doi.org/10.1021/cm050230i
54. Schmidt W (2012) Synthetic inorganic ion exchange materials. In: Inamuddin, Luqman M (eds) Ion exchange technology I. Theory and materials. Springer, pp 277–298
55. Bajpai PK (1986) Synthesis of mordenite type zeolite. Zeolites 6:2–8
56. Querol Carceller X, Moreno N, Alastuey A, Juan Mainar R, Andres Gimeno JM, Lopez-Soler Á, Ayora C, Medinaceli A, Valero A (2007) Synthesis of high ion exchange zeolites from coal fly ash. Geologica Acta 5(1):49–57. http://dx.doi.org/10.1344/105.000000309
57. Franus W, Wdowin M, Franus M (2014) Synthesis and characterization of zeolites prepared from industrial fly ash. Environ Monit Assess 186:5721–5729. https://doi.org/10.1007/s10661-014-3815-5
58. Jha B (2016) Basics of zeolites. In: Jha B, Singh DN (eds) Fly ash zeolites: innovations, applications, and directions, advanced structured materials. Springer. https://doi.org/10.1007/978-981-10-1404-8_2
59. Van Jaarsveld JGS, Van Deventer JSJ, Schwartzman A (1999) The potential use of geopolymeric materials to immobilise toxic metals: part II. Material and leaching characteristics. Mineral Eng 12(1):75–91. https://doi.org/10.1016/S0892-6875(98)00121-6
60. Van Jaarsveld JGS, Van Deventer JSJ (1999) The effect of metal contaminants on the formation and properties of waste-based geopolymers. Cem Concr Res 29:1189–1200. https://doi.org/10.1016/S0008-8846(99)00032-0
61. Novais RM, Buruberri LH, Seabra MP, Labrincha JA (2016) Novel porous fly-ash containing geopolymer monoliths for lead adsorption from wastewaters. J Hazard Mater 318:631–640. https://doi.org/10.1016/j.jhazmat.2016.07.059
62. Buic Z, Zelić B (2009) Application of clay for petrochemical wastewater pretreatment. Water Qual Res J Can 44:399–406
63. Nasef MM, Ujang Z (2012) Introduction to ion exchange processes. In: Inamuddin, Luqman M (eds) Ion exchange technology I. Theory and materials. Springer, pp 1–40
64. Margeta K, Logar NZ, Siljeg M, Farkas A (2013) Natural zeolites in water treatment—how effective is their use, water treatment. In: Dr. Elshorbagy W (ed) InTech. https://doi.org/10.5772/50738. Available from: https://www.intechopen.com/books/water-treatment/natural-zeolites-in-water-treatment-how-effective-is-their-use
65. Katsou E, Malamis S, Tzanoudaki M, Haralambous KJ, Loizidou M (2011) Regeneration of natural zeolite polluted by lead and zinc in wastewater treatment systems. J Hazard Mater 189 (3):773–786. https://doi.org/10.1016/j.jhazmat.2010.12.061
66. Cincotti A, Mameli A, Locci AM, Orrù R, Cao G (2006) Heavy metals uptake by Sardinian natural zeolites: experiment and modeling. Ind Eng Chem Res 45(3):1074–1084. https://doi.org/10.1021/ie050375z
67. Sprynskyy M, Buszewski B, Terzyk AP, Namieśnik J (2006) Study of the selection mechanism of heavy metal (Pb2 + , Cu2 + , Ni2 + , and Cd2 +) adsorption on clinoptilolite. J Colloid Interface Sci 304(1):21–28. https://doi.org/10.1016/j.jcis.2006.07.068
68. Zhou CF, Zhu JH (2005) Adsorption of nitrosamines in acidic solution by zeolites. Chemosphere 58(1):109–114. https://doi.org/10.1016/j.chemosphere.2004.08.056
69. Abora K, Beleña I, Bernal SA, Dunster A, Nixon PA, Provis JL, Tagnit-Hamou A, Winnefeld F (2014) Durability and testing—chemical matrix degradation processes. In: Provis JL, van Devente JSJ (eds) Alkali activated materials: state-of-the-art report, RILEM TC 224-AAM. Springer, pp 177–221
70. Li Q, Sun Z, Tao D, Xu Y, Li P, Cui H, Zhai J (2013) Immobilization of simulated radionuclide 133Cs + by fly ash-based geopolymer. J Hazard Mater 262:325–331. https://doi.org/10.1016/j.jhazmat.2013.08.049

71. Bernal SA, Krivenko PV, Provis JL, Puertas F, Rickard WDA, Shi C, Van Riessen A (2014) Other potential applications for alkali-activated materials. In: Provis JL, van Devente JSJ (eds) Alkali Activated materials: state-of-the-art report, RILEM TC 224-AAM. Springer, pp 339–379
72. Hizal J, Tutem E, Guclu K, Hugul M, Ayhan S, Apak R, Kilinckale F (2013) Heavy metal removal from water by red mud and coal fly ash: an integrated adsorption–solidification/stabilization process. Desalin Water Treat 51:7181–7193. https://doi.org/10.1080/19443994.2013.771289
73. Ipatti A (1992) Solidification of ion-exchange resins with alkali-activated blast-furnace slag. Cem Concr Res 22:281–286. https://doi.org/10.1016/0008-8846(92)90066-5
74. Kuenzel C, Cisneros JF, Neville TP, Vandeperre LJ, Simons SJR, Bensted J, Cheeseman CR (2015) Encapsulation of Cs/Sr contaminated clinoptilolite in geopolymers produced from metakaolin. J Nucl Mater 466:94–99. https://doi.org/10.1016/j.jnucmat.2015.07.034
75. Ferone C, Roviello G, Colangelo F, Cioffi R, Tarallo O (2013) Novel hybrid organic-geopolymer materials. Appl Clay Sci 73:42–50. https://doi.org/10.1016/j.clay.2012.11.001

Chapter 5
Microwave-Assisted Hydrothermal Synthesis of Agglomerated Spherical Zirconium Phosphate for Removal of Cs^+ and Sr^{2+} Ions from Aqueous System

Arshid Bashir, Lateef Ahmad Malik, G. N. Dar and Altaf Hussain Pandith

Abstract Crystalline and agglomerated spherical alpha zirconium phosphate nanoparticles hereafter α-ZrP were synthesized by a facile and rapid microwave-hydrothermal (MW-HT) approach within 30 min at 120 °C in the absence of any complexing or structure directing agent (SDA). The material was characterized by Fourier-transform infrared (FT-IR), powdered X-ray diffraction (PXRD), scanning electron microscopy (SEM), energy dispersive spectroscopic analysis (EDS) and surface area analysis (BET). It crystallizes in the monoclinic *P121/n1* space group with the following cell parameters: $a = 5.288$, $b = 9.174$, $c = 15.384$ Å and $\beta = 102.384$. Crystallite sizes in the range 3–4 nm evaluated using Scherer equation were obtained for α-ZrP. Ion exchange performance of α-ZrP towards removal of Cs^+ and Sr^{2+} ions was examined under noncompetitive batch conditions. Distribution studies indicate higher selectivity of α-ZrP towards Sr^{2+} uptake (K_d ca. 4.3×10^4) in comparison with Cs^+ (K_d ca. 2.4×10^3). This study suggested to agglomerated α-ZrP as potential adsorbent for the removal of radioactive Sr^{2+} from acidic wastewater.

A. Bashir · L. A. Malik · A. H. Pandith (✉)
Department of Chemistry, University of Kashmir, Hazratbal, Srinagar 190006, Jammu and Kashmir, India
e-mail: altafpandit23@gmail.com

A. Bashir
e-mail: arshidbashir7@gmail.com

G. N. Dar
Department of Physics, University of Kashmir, Hazratbal, Srinagar 190006, Jammu and Kashmir, India

Inamuddin et al. (eds.), *Applications of Ion Exchange Materials in the Environment*,
https://doi.org/10.1007/978-3-030-10430-6_5

List of abbreviations

AAS	Atomic absorption spectroscopy
BET	Surface area analysis
CP	Co-precipitation
DFT	Density functional theory
EDS	Energy dispersive spectroscopic analysis
FT-IR	Fourier transform infrared
IEC	Ion exchange capacity
K_d	Distribution coefficient
MW-HT	Microwave hydrothermal
PXRD	Powdered X-ray diffraction
PZC	Point of zero charge
SDA	Structure directing agents
SEM	Scanning electron microscopy
ZrP	Zirconium Phosphate

5.1 Introduction

Owing to fast population growth and industrialization, water contamination has become a challenging environmental issue nowadays. It is, therefore, essential to control the adverse effects of water contamination which include organic pollutants, toxic metals (Pb, Cd, Hg, Zn, Cr, Ni) and radionuclides ($^{137}Cs^{+}$, $^{90}Sr^{2+}$ and $^{234}U^{6+}$). Global energy demand necessitates the use of nuclear laboratories for meeting energy needs, which in turn constantly release radionuclide wastes into the environment. $^{90}Sr^{2+}$ is a potent, long-lived and hazardous fissionable product of ^{235}U radionuclide with detrimental health hazards [1, 2]. The presence of toxic metals at trace level is believed to be a risk to the ecological environment as well as to the human health.

A wide range of technologies have been investigated for the removal of radioactive wastes from contaminated water, namely chemical precipitation [3], biosorption [4], coagulation [5], reverse osmosis [6], membrane filtration [7], adsorption [8–10] and ion exchange [11–15]. However, some of these removal methods have limitations of reduced efficiency, high cost and production of secondary sludge. Owing to simple column operation and fast kinetics, ion exchange method has been considered most effective for the abatement of metallic ionic species. Ion exchange is the stoichiometric exchange of similarly charged ions between ion exchange material and guest ions. Ion exchange is in many ways similar to an adsorption process; however, adsorption is purely a surface phenomenon whereas ion exchange is fundamentally a bulk phenomenon involving an entire volume of the material. From a consideration of efficiency, thermal stability and robustness, layered metal (IV) phosphates with special reference to zirconium phosphate (ZrP), have attracted considerable attention as an ion exchange material owing to their high ion exchange capacity, enhanced radiolytic stability, easy preparation procedures,

abundant surface hydroxyl groups and tunable interlayer gallery to accommodate large cations and complex ions [16–18]. Nanosized ZrP being completely inorganic ion exchange material has attracted attention due to the high specific surface area, associated with improved stability towards acids, radiation and heat for better column operations. ZrP has been the adsorbent of choice for efficient detection and removal of radionuclides especially $^{137}Cs^{+}$ from acidic wastewaters [19, 20].

Various solution-based approaches such as co-precipitation [21], microemulsion [17, 22], hydrothermal methods [23], ionothermal method (wherein, the ionic liquids or deep eutectic mixtures have been used as both the solvent and the template) [24] and minimalistic liquid-assisted route [25] have been utilized as synthetic strategies for α-ZrP nanostructures. In recent years, microwave-assisted hydrothermal (MW-HT) method has gained more momentum for the synthesis of inorganic nanocrystals as it offers great control over morphology [26]. Most often precipitation of Zr (IV) involves excessive use of complexing agents (HF, NH_4F and oxalic acid) to yield a crystalline phase of α-ZrP which seriously limits the processing of ZrP-based materials [25, 27]. Therefore, in this work, for the first time, a facile, rapid and environmentally friendly MW-HT method has been developed to prepare crystalline α-ZrP in the absence of any complexing or structure directing agent with desired ion exchange properties for $^{137}Cs^{+}$ and $^{90}Sr^{2+}$ removal.

5.2 Materials and Methods

5.2.1 *Preparation of Agglomerated Spherical Zirconium Phosphate*

All chemicals were of analytical grade and used as received without further purification. $SrCl_2$ as a source of Sr^{2+} ions was used for batch studies. It is highly soluble and stable with rutile-type structure. $SrCl_2$ is very hazardous when ingested and a potent irritant whose LD_{50} is 2250 mg/kg [rat]. So care must be taken in handling this material and avoid direct skin and eye contact. In an archetypical procedure, 1 g of zirconyl chloride octahydrate ($ZrOCl_2{\cdot}8H_2O$) was mixed with 10 mL of 3.0 M phosphoric acid (H_3PO_4) under constant stirring. The resulting solutions were then introduced into a 20 mL glass vessel specified for a microwave oven (Monowave 200, Anton Parr, USA) and then irradiated by microwaves at an autogenerated pressure with a hold time of 30 min at 120 °C. The obtained white gelly type product was centrifuged, washed with deionized water and dried at 80 °C for 24 h.

5.2.2 *Characterization*

Fourier-transform infrared (FT-IR) spectra of the sample were recorded over a range of 400–4000 cm^{-1} using the Perkin Elmer Spectrum 100 FT-IR.

The crystalline nature of the prepared samples was examined by X-ray diffractometer, Ultima-IV, Rigaku Corporation, Tokyo, Japan using Cu Kα radiation. The crystallite size of α-ZrP nanocrystals was determined using classical Scherer equation from intense (002) reflection plane [28].

$$D = \frac{K\lambda}{\beta \cos\theta} \tag{5.1}$$

In which D is the average crystallite size, λ is the X-ray wavelength (in nm), $K = 0.9$ is the shape factor, θ is the angle of the intense reflection and β is the full width at half maximum (FWHM) of the intense peak (in radians). The average crystallite size of ZrP is found to be around 3–4 nm. The morphology was observed using scanning electron microscope (Hitachi, S3000H. Japan). Zeta potential over a varied pH range was obtained at 25 °C using a Zetasizer Nano ZS (Malvern Instruments Ltd., UK). The N_2 adsorption–desorption isotherms were measured with micromeritics ASAP 2020 H surface area analyser at 77 K. The specific surface areas of ZrP were measured with Brunauer–Emmett–Teller (BET) and adsorption analysis. Before the test, the powder samples were degassed at 300 °C under vacuum for 3 h.

5.2.3 Ion Exchange Properties

Ion exchange capacity (IEC) is the measure of the equilibrated concentration of cations which can be retained on the exchange material per mass of exchanger. A usual column chromatographic technique was used to calculate IEC. During this process, 250 mL selected alkali or alkaline metal ion (1.0 M) solution was slowly passed through column bed packed with 1 g exchange material at a flow rate of 0.5 mL min^{-1}. The effluent was then analysed titrimetrically for total exchanged H^+ ion concentration using a standard NaOH solution (0.01 M).

5.2.4 Elution Behaviour

The rate of the exchange of H^+ ions adhered to the exchange material was studied by the elution behaviour of the exchange material. In a typical procedure, a column packed with 1 g of the α-ZrP was eluted with 100 mL of $SrCl_2$ molar solution, maintained at a constant flow rate. Collected 10 mL fractions of the effluent were then analysed for the total H^+ ion concentration to be exchanged.

5.2.5 Distribution Studies

Distribution studies using α-ZrP were carried out by a usual batch method. In general, 40 mg of adsorbent was added to a 50 mL vial with different initial metal concentrations. After shaking for sufficient time to ensure the adsorption equilibrium of Cs^+ and Sr^{2+} ions, the supernatant containing these non-adsorbed metal ions was removed and analysed using AAS. Distribution coefficient (K_d) is a standard exchange parameter to check the effectiveness of the material. It mainly depends upon nature of exchange material, solvent and exchanging ion. The distribution coefficients of adsorbed/exchanged metal ions were calculated as [12, 13];

$$K_d = \frac{C_0 - C_e}{C_e}\frac{V}{m}\left(\text{mL g}^{-1}\right) \tag{5.2}$$

where K_d is the distribution coefficient (mL g^{-1}), C_0 is the initial metal concentration, C_e is its equilibrium concentration, V is the volume of the solution and m is the mass of the exchange material. All the batch experiments were carried out at $V/m \sim 750$ mL/g).

5.3 Results and Discussion

5.3.1 Fourier-Transform Infrared (FT-IR) Characterization

The FT-IR spectrum of ZrP was recorded in the range of 4000–400 cm^{-1} and is shown in Fig. 5.1 where all the peaks are characteristics of α-ZrP. The broadband at 3352 cm^{-1} is attributed to O–H symmetric stretching mode of intercalated water or the water absorbed. Moreover peak at 1631 cm^{-1} is assigned to HOH bending mode of water. More covalent nature of P–O bonds in phosphate tetrahedron can be affirmed by P–O symmetrical stretching vibration at 1057 cm^{-1} [29]. The peaks at 1390 and 521 cm^{-1} can be attributed to the stretching frequency of P–OH, and Zr–O, respectively [30].

5.3.2 Powder X-ray Diffraction Studies

The PXRD technique was used to investigate the crystallinity and phase of the samples. The typical PXRD pattern of α-ZrP is shown in Fig. 5.2. Peaks at 2θ of 11.77, 19.83, 24.96, 33.90, 37.60 and 48.48 were indexed to (0 0 2), (−1 1 1), (−1 1 3), (−3 1 1), (1 1 5) and (1 1 7) planes, respectively. Intense peak at 2θ = 11.77 indexed to (0 0 2) reflection of the monoclinic phase corresponding to the *P121/n1* space group serves as a fingerprint for the layered α-ZrP material. The interlayer distance of 7.6 Å corresponds to (002) plane, was estimated from Bragg's law

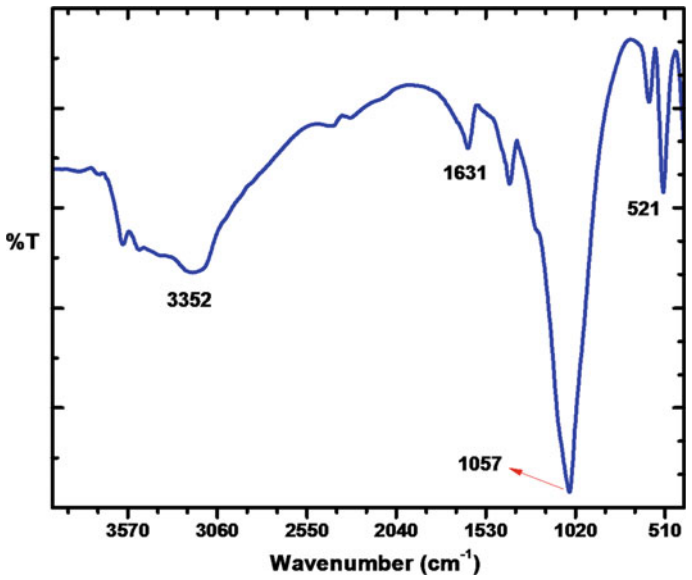

Fig. 5.1 FT-IR spectra of ZrP, all the peaks indicating the successful formation of α-ZrP

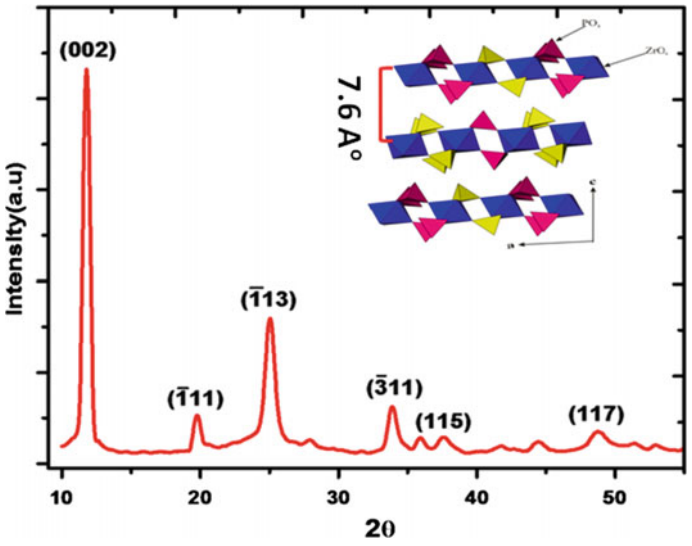

Fig. 5.2 PXRD of α-ZrP showing prominent peaks, indicative of its crystalline and layered nature. The material crystallized into monoclinic phase, space group *P121/n1* with interlayer spacing ca. 7.6 Å as shown in the inset along with crystal structure of α-ZrP

(shown as an inset in Fig. 5.2) and is in agreement with the previous reports [31]. Moreover, the average crystallite size of 3–4 nm was calculated using the classical Scherer relationship.

5.3.3 *Scanning Electron Microscopy (SEM) and Energy Dispersive (EDS) Characterization*

Figure 5.3 represents SEM images and EDS spectra of α-ZrP to elucidate its morphology and elemental composition. SEM images (Fig. 5.3a, b) recorded at different magnifications indicate agglomeration of ZrP nanoparticles within the material. For the purpose of comparison, SEM images were also recorded for Sr^{2+} adsorbed ZrP (Sr–ZrP) and the results clearly indicate that the surface of α-ZrP is fully covered with $^{90}Sr^{2+}$ ions with morphology change to a sheet-like structure (Fig. 5.3c). The EDS spectrum (Fig. 5.3d) reveals that α-ZrP is composed of oxygen, phosphorus and zirconium with the atom per cent of the elements as; 77.16, 14.21 and 8.63 respectively, suggesting the formula for typical α-ZrP, i.e. $Zr(HPO_4)_2{\cdot}H_2O$.

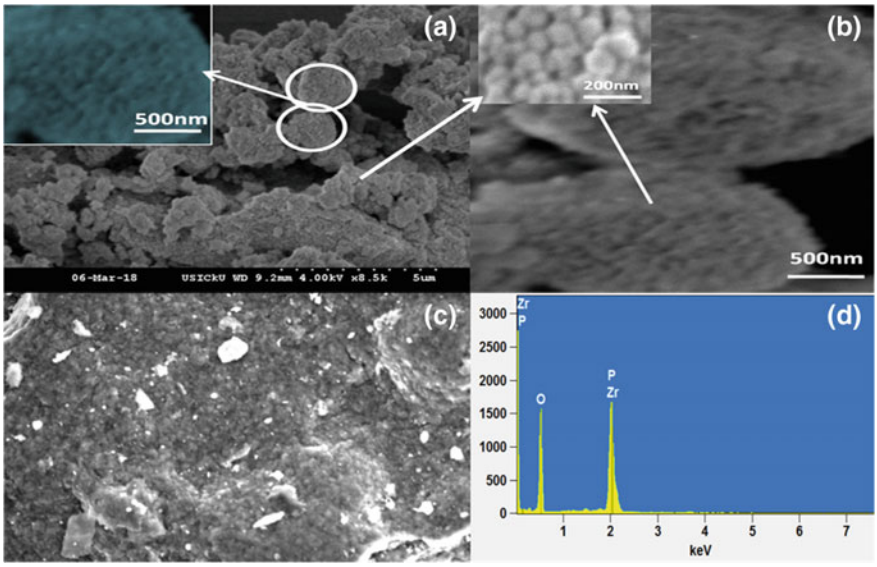

Fig. 5.3 SEM images and EDX spectra of α-ZrP. **a**, **b** SEM image of α-ZrP showing agglomerated nanoparticles. **c** SEM image of Sr^{2+} adsorbed α-ZrP (Sr–ZrP) showing sheet-like morphology and **d** EDX spectra of α-ZrP with % elemental composition of O, P and Zr as; 77.16, 14.21 and 8.63

5.3.4 Zeta and Surface Area Analysis

Higher specific surface area of the adsorbent material plays a significant role in the adsorption of toxic metals. For better performance of α-ZrP nanoparticles, the surface area by N_2 adsorption–desorption at 77 K was evaluated. As shown in Fig. 5.4a adsorption–desorption isotherm indicates hysteresis loop in the P/P^0 range of 0.43–0.85. This may be ascribed to the presence of mesopores in the α-ZrP nanocrystals. Calculated BET surface area comes out to be 484.38 $m^2\ g^{-1}$, necessary for efficient sorption of $^{137}Cs^+$ and $^{90}Sr^{2+}$. The higher specific surface area could be attributed to its nearly spherical morphology.

pH of the solution has the ability to affect the surface charge of adsorbent, the degree of ionization of functional groups associated with an adsorbent and more importantly speciation of metal ions in aqueous medium. High adsorption capacity for $^{90}Sr^{2+}$ was observed over a wide range of pH, especially pH < 7.0 which was much higher than that of other adsorbents under the same conditions. The higher adsorption capacity for $^{90}Sr^{2+}$ was due to the negatively charged surface of α-ZrP over the whole pH range [32]. From Fig. 5.4b, it is evident that more negative zeta potential of α-ZrP is favourable for the desired pre-concentration and adsorption of $^{137}Cs^+$ and $^{90}Sr^{2+}$ ions. Point of zero charges (pH $_{PZC}$) has been defined as the pH where the surface of adsorbent is having no net charge. In addition, the surface is positively charged at pH values below pH $_{PZC}$ and negatively charged at pH values above pH $_{PZC}$ [33]. As clearly seen from Fig. 5.4b, the surface is negatively charged even at pH ca. 3.0. Maximal adsorption of $^{90}Sr^{2+}$ was found at pH in the range 4.0–8.0 and hence the pH 5.0 as an optimum parameter for maximal uptake of $^{90}Sr^{2+}$ from the acidic aqueous medium was selected.

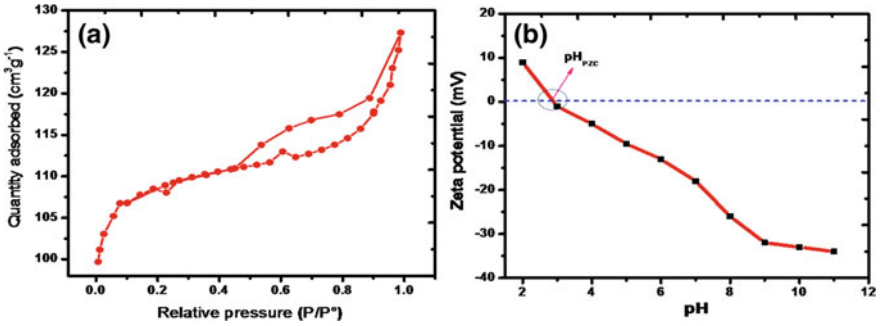

Fig. 5.4 BET and Zeta potential of α-ZrP. **a** The N_2 adsorption–desorption curve of α-ZrP with specific surface area of 484.38 $m^2\ g^{-1}$ and **b** Zeta potential of α-ZrP over varied pH, indicating higher acidity of phosphate hydrogen

5.3.5 Ion Exchange Characteristics

In order to examine the ion exchange performance of α-ZrP, the ion exchange capacities of some alkali and alkaline earth metal cations were determined; the obtained results are tabulated in Table 5.1. At neutral pH, the material shows the good exchange capacity of 3.79 meq. g^{-1} for $^{90}Sr^{2+}$ ions in aqueous medium. As evident from the IEC, size and charge of the exchanging ions influence the ion exchange capacity and the overall selectivity order based on IEC was $Na^+ < K^+ < Rb^+ < Cs^+ < Ca^{2+} < Sr^{2+}$. This order is primarily in accordance with the charge and hydrated ionic radii of the exchanging ions and partly due to entropy contributions of ion exchange process [34–36]. Ions with smaller hydrated radii and more charge readily enter the pores of the exchanger. For the purpose of comparison, ZrP was also synthesized by an ordinary sol-gel procedure represented as ZrP(CP). As shown in Fig. 5.5a, the calculated ion exchange capacity in case of MW-HT synthesized α-ZrP was found to be much higher than that of ZrP(CP).

Fast exchange kinetics were further investigated and confirmed from elution behaviour of column packed with 1 g α-ZrP. Elution results indicate fast exchange at the beginning with most of the H^+ ions eluted out in the first 50 mL fraction of the effluent (Fig. 5.5b).

Noncompetitive batch measurements were carried out to evaluate the efficiency of ZrP towards safe removal of radioactive $^{137}Cs^+$ and $^{90}Sr^{2+}$ from acidic aqueous media. Radioactive wastewaters contaminated with radioactive elements are mostly

Table 5.1 Ion exchange capacity of ZrP towards alkali and alkaline earth metals

S. No.	Cation	Ionic radii (Å)	Pauling radii (Å)	Hydrated ionic radii (Å)	IEC in meq./g
1	Na^+	0.97	0.97	2.76	1.87
2	K^+	1.33	1.33	2.32	2.13
3	Rb^+	1.52	1.53	2.28	2.68
3	Cs^+	1.74	1.76	2.26	2.98
4	Ca^{2+}	0.94	0.99	6.30	3.01
5	Sr^{2+}	1.06	1.13	6.10	3.79

Table 5.2 Sorption data of α-ZrP towards Sr^{2+} removal at different metal ion concentrations

C_0 (ppm)	C_e (ppm)	Removal (%)	K_d
5	1.5	70.0	1.75×10^3
10	0.07	98.3	4.33×10^4
15	0.26	98.2	4.25×10^4
20	3.31	83.5	3.79×10^3
30	9.0	70.0	1.75×10^3
50	15.6	68.8	1.65×10^3

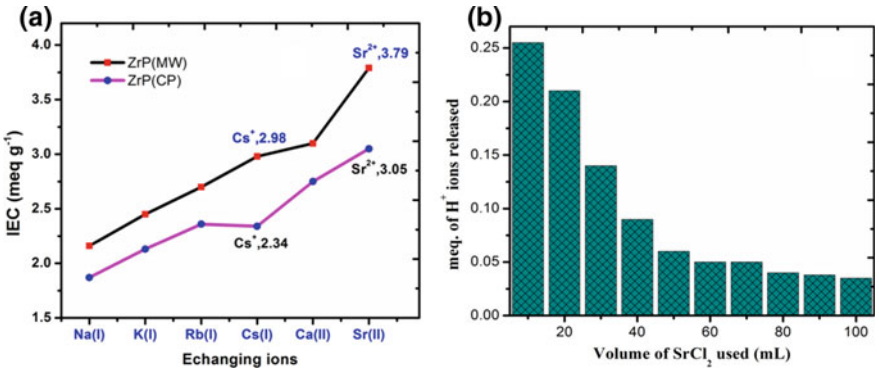

Fig. 5.5 Graphs showing IEC and Elution behaviour of α-ZrP. **a** IEC of α-ZrP for exchange of alkali and alkaline earth metals, wherein hydrated radii and charge of the exchanging ions play a dominant role therefore showing a maximum at Sr^{2+} and **b** Elution behaviour of α-ZrP indicating quick release of H^+ ions initially

acidic due to the use of HNO_3 for nuclide dissolution. It is, therefore, desirable that the exchange material should remain stable under acidic conditions without appreciable loss of adsorption performance. To examine the stability, a known amount of ZrP was immersed in aqueous solutions of different pH (ca. 3.0–6.0), the pH range, generally found in nuclear wastewater. After shaking for 6 h and centrifugation, the collected samples were further screened for IEC with respect to $^{90}Sr^{2+}$ and the results indicate no appreciable change in $^{90}Sr^{2+}$ IEC. The uptake experiments for $^{137}Cs^+$ and $^{90}Sr^{2+}$ were performed using the batch method. An initial metal ion concentration of 10 ppm was used, as this concentration is more relevant and meaningful in the context of the industrial wastewater conditions. The removal percentage of the metal ions can be estimated as [19];

$$\%\text{Removal} = \frac{C_0 - C_e}{C_0} \times 100 \tag{5.3}$$

Where these terms have their usual meanings. At an optimized pH, initial metal concentration (10 ppm) and V/m = 750 mL g^{-1}, about 98.3% of $^{90}Sr^{2+}$ was removed from the aqueous solution within 160 min of contact time. Although adsorption of Cs^+ reached equilibrium within 40 min, however, the removal % was only 76.5%. This enhanced and selective removal efficiency towards $^{90}Sr^{2+}$ ions as compared to Cs^+ ions was assigned primarily to more charge which therefore assists in more exchange of $^{90}Sr^{2+}$ ions. Effect of Sr^{2+} ion concentration on the adsorption characteristics was studied under batch mode and the results have been summarized in Table 5.2. Based on the results, per cent removal, as well as distribution coefficient, decreased with the increase in metal concentration beyond the optimum concentration (15.0 ppm). Selective adsorption towards $^{90}Sr^{2+}$ ions can also be expressed in terms of the distribution coefficient (K_d) which is a tool to check the excellency of the adsorbent material. An excellent material is the one whose K_d

value reached or is above 10^4 mL g^{-1} [37]. Based on the higher affinity of α-ZrP towards Sr^{2+} ions, the K_d value obtained is 4.3×10^4 mL g^{-1}, much higher than for Cs^+ (2.4×10^3).

5.3.6 *Mechanism of Sr^{2+} Interaction with Zirconium Phosphate*

To gain more insight about the mechanism of ion exchange (ion interaction) process, at the atomic level, density functional theory (DFT) calculations have been carried out previously by Zhang et al. on Pb(II)–ZrP interacting system [38]. In their work, a single layer of ZrP containing two types of oxygen atoms: bridging oxygen atom (linking Zr and P atom of phosphate tetrahedron) and terminal oxygen (oxygen of hydroxyl group) have been proved to be the facile interacting sites. Metal ions have been found to interact at both the oxygen atoms with more favourable interaction at bridging oxygens, which from Mulliken charge analysis have been shown to carry a more partial negative charge that terminal one. It is, therefore, justified that the bridging oxygen offers more favourable adsorption site for metal cations than terminal ones. Based on the above findings, we propose that the preferential binding site for the ion exchange and adsorption of Cs and Sr ions on this material are the bridging oxygen atoms as compared to terminal ones. At acidic pH, bridging oxygens were protonated and exchanged its H^+ ions with Cs and Sr ions from acidic contaminated water (Fig. 5.6).

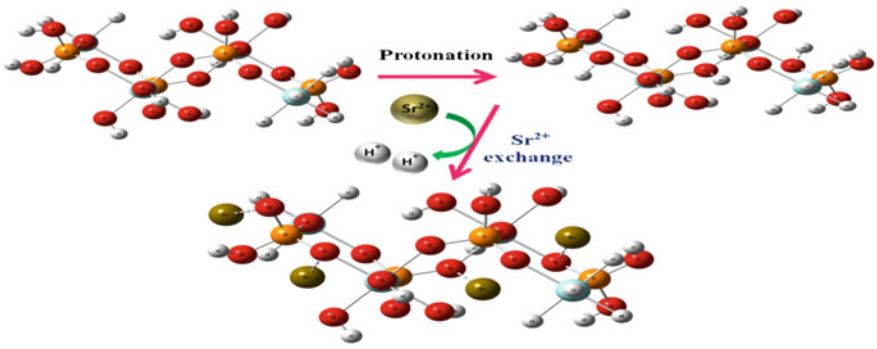

Fig. 5.6 Ball and Stick model sketch of α-ZrP layers. Based on the Mulliken charge analysis, bridging oxygen atoms were shown to be the dominating site for the exchange of Sr^{2+} ions. Red = oxygen, orange = phosphorus, cyan = Zirconium and golden brown = Strontium

5.4 Conclusion

The ZrP agglomerated nanospheres were successfully synthesized by a rapid and facile MW-HT method at an ambient temperature. The material possesses high crystallinity with a crystallite size of 3–4 nm along with high specific surface area suitable for better performance. The material exhibits better adsorption performance towards removal of Cs^+ and Sr^{2+} ions from acidic wastewater as compared to zirconium phosphate synthesized by a routine sol-gel/co-precipitation method. Removal of metal cations was observed to depend on hydrated radii and also charge on the exchanging ions wherein, Sr^{2+} exhibited twofold increase in adsorption than that with Cs^+. The material showed a good reproducibility with negligible loss of IEC and K_d over successive 5 batch cycles.

Acknowledgements We thank the Head Department of Chemistry, the University of Kashmir for providing all the necessary facilities to carry out this work. We would also like to thank Mainak Roy and S. N. Achary, Chemistry Division, BARC, Mumbai for their help with PXRD and FT-IR studies. A. B. would like to thank the Council of Scientific and Industrial Research (CSIR), GOI, for financial assistance in the form of a Junior Research Fellowship (JRF). G. N. thanks the DST, GOI, for a research grant for carrying out this work.

References

1. Rahman ROA, Ibrahium HA, Hung YT (2011) Liquid radioactive wastes treatment: a review. Water 3:551–565
2. Paulus WJ, Komarneni S, Roy R (1992) Bulk synthesis and selective exchange of strontium ions in Na_4Mg_6 Al_4 $Si_4O_{20}F_4$ mica. Nature 357:571–573
3. Sun JM, Shang C, Huang JC (2003) Co-removal of hexavalent chromium through copper precipitation in synthetic wastewater. Environ Sci Technol 37:4281–4287
4. Abdelfattah I, Ismail AA, Sayed FA et al (2016) Biosorption of heavy metals ions in real industrial wastewater using peanut husk as efficient and cost effective adsorbent. Environ Nanotech Monit Manag 6:176–183
5. Boccelli DL, Small MJ, Dzombak D (2005) Enhanced coagulation for satisfying the arsenic maximum contaminant level under variable and uncertain conditions. Environ Sci Technol 39:6501–6507
6. Vergili I, Kaya Y, Sen U et al (2012) Techno-economic analysis of textile dye bath wastewater treatment by integrated membrane processes under the zero liquid discharge approach. Resour Conserv Recycl 58:25–35
7. Jawor A, Hoek EMV (2010) Removing cadmium ions from water via nanoparticle-enhanced ultrafiltration. Environ Sci Technol 44:2570–2576
8. Abdolali A, Ngo HH, Guo W et al (2016) A breakthrough biosorbent in removing heavy metals: equilibrium, kinetic, thermodynamic and mechanism analyses in a lab-scale study. Sci Total Environ 542:603–611
9. Cheng Y, Wang XD, Jaenicke S et al (2018) Mechanochemistry-based synthesis of highly crystalline γ-zirconium phosphate for selective ion exchange. Inorg Chem 57:4370–4378
10. Wen T, Zhao Z, Shen C et al (2016) Multifunctional flexible free-standing titanate nanobelt membranes as efficient sorbents for the removal of radioactive $^{90}Sr^{2+}$and $^{137}Cs^+$ions and oils. Sci. Rep. 6, 20920. https://doi.org/10.1038/srep20920

11. Xiao X, Hayashi F, Shiiba H et al (2016) Platy $KTiNbO_5$ as a selective Sr ion adsorbent: crystal growth, adsorption experiments, and DFT calculations. J Phys Chem C 120:11984–11992
12. Mertz JL, Fard ZH Kanatzidi MG et al (2013) Selective removal of Cs^+,Sr^{2+} and Ni^{2+} by $K_{2x}Mg_xSn_{3-x}$ S_6(x = 0.5 − 1) (KMS-2) relevant to nuclear waste remediation. J Chem Mater 25:2116–2127
13. Manos MJ, Kanatzidis MG (2016) Metal sulfide ion exchangers: superior sorbents for the capture of toxic and nuclear waste-related metal ions. Chem Sci 7:4804–4824
14. Zhu Y, Shimizu T, Kitajima T (2014) Synthesis of robust hierarchically porous zirconium phosphate monolith for efficient ion adsorption. New J Chem. https://doi.org/10.1039/c4nj01749h
15. He W, Ai K, Ren X et al (2017) Inorganic layered ion-exchangers for decontamination of toxic metal ions in aquatic systems. J Mater Chem A 5:19593–19606
16. Mrad O, Abdul-Hadi A, Arsan H (2011) Preparation and characterization of three different phases of zirconium phosphate: study of the sorption of ^{234}Th,^{238}U, and^{134} Cs. J Radioanal Nucl Chem 287:177–183
17. Bashir A, Ahad S, Pandith AH (2016) Soft template assisted synthesis of zirconium resorcinol phosphate nanocomposite material for the uptake of heavy-metal ions. Ind Eng Chem Res 55:4820–4848
18. Varshney KG, Pandith AH, Gupta U (1998) Synthesis and characterization of zirconium alumino phosphate: a new cation exchanger. Langmuir 14:7353–7358
19. Mu W, Yu Q, Zhang R et al (2017) Controlled fabrication of flower-like α-zirconium phosphate for the efficient removal of radioactive strontium from acidic nuclear wastewater. J Mater Chem A 5:24388–24395
20. Mosby BM, Goloby Clearfield A et al (2014) Designable architectures on nanoparticle surfaces: zirconium phosphate nanoplatelets as a platform for tetravalent metal and phosphonic acid assemblies. Langmuir 30:2513–2521
21. Hajipour AR, Karimi H (2014) Synthesis and characterization of hexagonal zirconium phosphate nanoparticles. Mater Lett 116:356–358
22. Bellezza F, Cipiciani A, Costantino U et al (2006) Zirconium phosphate nanoparticles from water-in-oil microemulsion. Colloid Polym Sci 285:19–25
23. Shuai M, Mejia AF, Chang YW et al (2013) Hydrothermal synthesis of layered α-zirconium phosphate disks: control of aspect ratio and polydispersity for nano-architecture. Cryst Eng Comm 15:1970–1977
24. Smeets S, Liu L, Dong (2015) Ionothermal synthesis and structure of a new layered zirconium phosphate. J Inorg Chem 54:7953–7958
25. Cheng Y, Wang X, Jaenicke S et al (2017) Minimalistic liquid-assisted route to highly crystalline α-zirconium phosphate. Chem Sus Chem. https://doi.org/10.1002/cssc.201700885
26. Muraliganth T, Murugan A V and Manthiram A (2009) Facile synthesis of carbon-decorated single-crystalline Fe_3O_4 nanowires and their application as high performance anode in lithium ion batteries. Chem Commun:7360–7362
27. Pica M, Nocchetti M, Ridolfi B et al (2010) Nanosized zirconium phosphate/AgCl composite materials: a new synergy for efficient photocatalytic degradation of organic dye pollutants. J Mater Chem A 3:5525–5534
28. Culity BD (1976) Elements of X-ray diffraction. Addison-Wesly Publishing Co. Inc. (Chapter 14)
29. Zhang Q, Du Q, Jiao T et al (2013) Selective removal of phosphate in waters using a novel cation adsorbent: zirconium phosphate(ZrP) behavior and mechanism. J Chem Eng 221:315–321
30. Horsley SE, Nowell DV, Stewart DT (1974) The infrared and raman spectra of α -zirconium phosphate. Spectrochim Acta Part A Mol Spectrosc 30:535–541
31. Troup JM, Clearfield A (1977) On the mechanism of ion exchange in zirconium phosphates. 20. Refinement of the crystal structure of a-zirconium phosphate. Inorg Chem 16:12, 197

32. Kalita H, Rajput S, Kumar BNP et al (2016) Fe_3O_4@zirconium phosphate core–shell nanoparticles for pH-sensitive and magnetically guided drug delivery applications. RSC Adv 6:21285–21292
33. Gatabia MP, Moghaddam HM, Ghorbani M (2016) Point of zero charge of maghemite decorated multiwalled carbon nanotubes fabricated by chemical precipitation method. J Mol Liq 216:117–125
34. Ahad S, Islam N Pandith AH et al (2015) Adsorption studies of Malachite green on 5-sulphosalicylic acid doped tetraethoxysilane (SATEOS) composite material. RSC Adv 5:92788–92798
35. Inamuddin, Khan SA, Siddiqui WA et al (2007) Synthesis, characterization and ion-exchange properties of a new and novel 'organic–inorganic' hybrid cation exchanger: Nylon-6,6, Zr(IV) phosphate. Talanta 71:841–847
36. Ahad S, Bashir A, Pandith AH et al (2016) Exploring the ion exchange and separation capabilities of thermally stable acrylamide zirconium(IV) sulphosalicylate (AaZrSs) composite material. RSC Adv 6:35914–35927
37. Zhao J, Islam SM, Kanatzidis MG et al (2017) Homologous series of 2D chalcogenides Cs − Ag − Bi − Q (Q = S, Se) with ion-exchange properties. J Am Chem Soc 139:12601–12609
38. Wang L, Xu WH, Yang R et al (2013) Electrochemical and density functional theory investigation on high selectivity and sensitivity of exfoliated nano-zirconium phosphate toward lead(II). J Anal Chem 85:3984–3990

Chapter 6
Metal Hexacyanoferrates: Ion Insertion (or Exchange) Capabilities

Angelo Mullaliu and Marco Giorgetti

Abstract Metal hexacyanoferrates are mixed-valence compounds characterized by open 3D frameworks that confer a variety of properties and allow the applicability in several fields. In this chapter, we focused on ion exchange capabilities. In the first instance, we examined diffusion-driven processes. Secondly, we addressed to electrochemically driven processes, reviewing the main currently used methods and applications.

List of Abbreviations

AM	Active material
API	Active pharmaceutical ingredient
CuHCF	Copper hexacyanoferrate
CV	Cyclic Voltammetry
ESIX	Electrochemically switched ion exchange
GCPL	Galvanostatic cycling with potential limitation
LOD	Limit of detection
MHCF	Metal hexacyanoferrate
MHCM	Metal hexacyanometallate
NiHCF	Nickel hexacyanoferrate
PB	Prussian blue
PBA	Prussian blue analogue

A. Mullaliu · M. Giorgetti (✉)
Department of Industrial Chemistry, University of Bologna,
Viale Del Risorgimento 4, 40136 Bologna, Italy
e-mail: marco.giorgetti@unibo.it

Inamuddin et al. (eds.), *Applications of Ion Exchange Materials in the Environment*,
https://doi.org/10.1007/978-3-030-10430-6_6

6.1 Introduction

Prussian blue (PB), named also ferric ferrocyanide, iron(III) hexacyanoferrate(II), and Milori Blue, was first synthesized accidentally in 1704 by Heinrich Diesbach of Berlin, assuming originally the name of *Berliner Blau*. The involuntarily finding arose from the preparation of crimson lake color and was based on the contamination of potash (potassium carbonate) by the "animal oil" elixir of the alchemist Johann Konrad Dippel, which was the source for the cyanide building block in PB. Prussian blue is the first synthetic coordination compound which has replaced as blue pigment the much more expensive *lapis lazuli* [1]. After its discovery, it was extensively used in painting, wallpaper, flags, postage stamps, tea colorant and became the official uniform color of the Prussian Army [2]. Even Van Gogh probably used it in his masterpiece *Starry Night* (Fig. 6.1).

The crystal structure of this compound has been first investigated in 1936 through X-ray diffraction by Keggin and Miles [3]. They reported:

> […] The iron atoms are arranged, ferrous and ferric alternately, at the corners of a cubic lattice of 5.1 Å edge, and the CN groups lie in the edges of these small cubes. The alkali atoms occur at the centres of alternate small cubes. […]

Buser et al. [4] further investigated this peculiar compound which revealed a cubic elementary cell (cell length of about 10 Å) and an exceptionally low density (roughly 1.8 g cm^{-3}) compared to other iron salts (>3 g cm^{-3}). This is due to the linking together the fashion iron atoms and that the formation of cavities, tunnels and vacancies throughout the 3D-dimensional lattice.

Prussian blue can exist in two different forms, namely "soluble" and "insoluble" (Fig. 6.2), characterized by the general formula $KFeFe(CN)_6$ and $Fe_4[Fe(CN)_6]_3$,

Fig. 6.1 Van Gogh's Starry Night. Van Gogh probably used the Prussian blue pigment. Available at Wikimedia Commons free repository

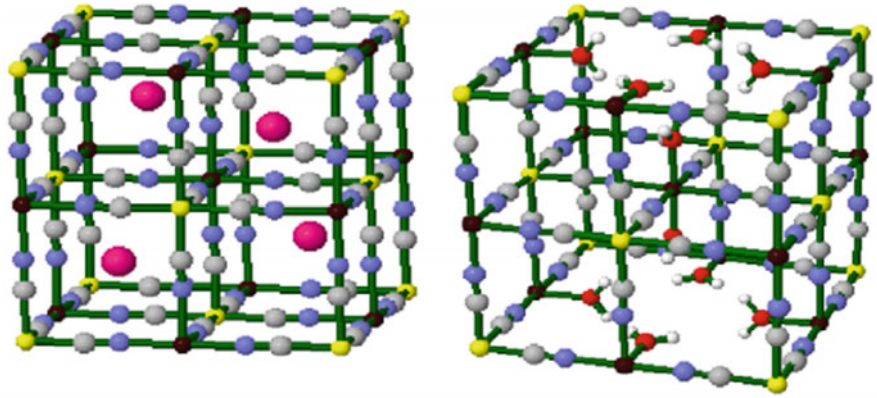

Fig. 6.2 Structures of soluble (left) and insoluble (right) Prussian blue, Fe(II) yellow, Fe(III) red violet, K magenta, C gray, N blue, O red. Reproduced with permission from [7]. Copyright Elsevier (2010)

respectively. Despite their names, both forms are insoluble in water, deriving these appellatives from the tendency to form a colloidal suspension. Structurally speaking, the soluble PB, i.e., the one originally proposed by Keggin and Miles, presents a highly ordered structure with alternating iron species in an octahedral environment connected through cyanide bridges in an ideally infinite 3D crystal lattice. Contrarily, the insoluble form is distinguished by the absence of $[Fe(CN)_6]^{4-}$ units and their replacement by water molecules and alkali cations, which explains also the dissimilarity in stoichiometry compared to the soluble form. Concerning the insoluble PB, the vacant sites can be either randomly or systematically distributed, the casual vacancies leading to a face-centered cubic crystal shape (space group 225 *Fm-3m*), while the non-random distribution to a cubic primitive or lower symmetry lattice (space group 221 *Pm-3m*) [4, 5]. In other words, the casual allocation of vacant sites increases the apparent symmetry of the lattice shape. The crystal space group has been found to be influenced by synthesis conditions and post-synthesis treatments, given that a slow crystallization led to a non-statistical arrangement of the vacancies and that this ordering can be partially destroyed by dehydrating and heating the sample [4].

The typical interatomic distances in PB are Fe^{II}–C = 2.00(4) Å, Fe^{III}–N = 1.98 (4) Å, and C–N = 1.10(5) Å [4], being the iron species distance Fe^{II}–Fe^{III} roughly 5.1 Å, as Keggin and Miles have reported. The cubic cell is, however, constituted by four of such cubes, resulting in a lattice length of about 10.2 Å, which corresponds to the distance of two consecutive Fe^{II}–Fe^{II}. The atoms arrangement guarantees enough space to accommodate water molecules and ions inside the zeolitic channels of approximately 3 Å, as well as in the cavities of about 5 Å arising from $[Fe(CN)_6]^{4-}$ vacancies.

Hence, the cubic open framework is formed by –CN–Fe^{III}–N–C–Fe^{II}– units, being the Fe^{II} in the *4a* (or *1a*) Wyckoff position, the Fe^{III} in *4b* (or *1b*), the C and N in *24e* (or *6e*), and the alkali metals at the cube center in *8c* (or *8 g*), if a *Fm-3m* (or

Pm-3m) symmetry is considered. Moreover, neutron diffraction [6] revealed the presence of two crystallographically and chemically distinct (deuterated) water molecules within the structure, where the first is part of the Fe^{III} coordination shell and fills empty nitrogen sites of the $[Fe(CN)_6]^{4-}$ vacancies, while the second kind occupies interstitial positions as alkali ions and represents uncoordinated water.

Metal hexacyanometallates (MHCMs) or Prussian blue analogues (PBAs) have general formula $A_xM_y[B(CN)_6]{\bullet}mH_2O$, where *M* and *B* are transition metals, *A* is an alkali ion, *x* and *y* are stoichiometric coefficients and depend on the presence of vacancies, while *m* is the number of water molecules in the structure. In the case of metal hexacyanoferrates (MHCFs), *B* is represented by iron. Transition metals *M* and *B* are linked through cyanides in a precise fashion, the *M* metal bound to the N-end, while the *B* metal to the C-end, constituting the repeating –CN–M–NC–B– unit. The orthogonal and almost linear –CN–M–NC–B– atomic chains, coupled to a high degeneration and short intermetallic distance, make PBAs a prototype for the study of highly ordered electron scattering contributions [8, 9]. As in the case of PB, the lattice shape is generally cubic with few exceptions [10, 11], while the lattice length is commonly around 10 Å and depends on structural metals' size, their oxidation states and moisture degree. Therefore, the –CN–M–NC–B– fragment can be finely tuned by changing, for instance, metallic species to define and modulate a series of physicochemical properties that are herein briefly introduced.

PBAs are classified as mixed-valence compounds [12] for the metal-to-metal charge transfer that occurs, which is the cause for instance of the blue color of PB. By tuning the oxidation state of the iron species in PB, Everitt's salt (white colored) or Berlin green can be obtained, in both cases, iron species are divalent or trivalent, respectively. Generally, the modulation of oxidation states can be achieved through the synthesis. Synthesis of metal hexacyanoferrates is commonly based on bulk co-precipitation methods in an aqueous medium, where $[Fe(CN)_6]^{3-/4-}$ and M^{n+} salts are simultaneously mixed under constant stirring to yield a precipitate, easily recovered by filtration [13–15]. An alternative synthetic procedure is based on electrochemical routes [16–20], whose advantage consists in the functionalization of a conductive substrate with a thin film, characterized by an extended active area per surface. The film can be further modified through polarization of either a current or potential, which will be extensively discussed in the next section.

Analogues of Prussian blue have been widely synthesized for several applications, for instance, analyte sensors [21, 22], magnetic devices [23], electrochromism [24], charge storage [25], and ion exchange sieves [26], and even antibacterial agents against *Escherichia coli* and *Staphylococcus aureus* [27]. The employment in all the cited technological applications is related to the structure of PBAs and the activity of the constituting metals.

The peculiar zeolitic structure of metal hexacyanoferrates which allows the flux of different ions into the channels of the tri-dimensional network, coupled to the redox activity of the metals, such as Cu and Fe in copper hexacyanoferrate, permits the use of MHCFs in electrocatalysis toward the oxidation of several organic analytes, and therefore, the fabrication of amperometric sensors has been proposed for instance for ascorbic acid [28], cysteine [29], and dopamine [30]. Prussian blue

films were found to be excellent catalysts for hydrogen peroxide reduction in the presence of O_2, with selectivity and activity close to those of peroxidase modified electrodes [31, 32], and a review on PB-based sensors and biosensors has been more recently reported [33]. Among the metal hexacyanoferrates, the copper analogue has been widely studied and its electrocatalytic properties have been investigated by many research groups. Malinauskas et al. [34] described a hydrogen peroxide sensor using a CuHCF-modified carbon paste electrode. Baioni et al. studied the electrocatalytic properties of CuHCF nanoparticles deposited by electrostatic layer-by-layer technique [35]. Brett et al. [36] underlined the role of the H_2O_2 determination in the development of biosensors, as it is a by-product of the reaction catalyzed by oxidase enzymes.

Photoinduced magnetization was first observed by Sato et al. [23] in cobalt hexacyanoferrate, where magnetization was controlled via photoirradiation, causing the variation in oxidation number of the transition metal ions through an internal photochemical redox reaction. The starting hexacyanoferrate was constituted by the Co^{III}–NC–Fe^{II} fragment, characterized by low spin Co(III) (t_{2g}^6, $S = 0$) and low spin Fe(II) (t_{2g}^6, $S = 0$). The irradiation through red light was responsible for the change in spin states, hence in magnetization value, inducing the system to change into Co^{II}–NC–Fe^{III}, characterized by high spin Co(II) ($t_{2g}^5 e_g^2$, $S = 3/2$) and low spin Fe (III) (t_{2g}^5, $S = 1/2$). The increase of the contribution of the paramagnetic components resulted in an enhancement of the magnetization, and it could be partly inverted by illuminating the system with an incident blue light. Besides, spin transition at the Co site can be induced not only by photoirradiation, but also by an anatase-driven stimulus, as reported by Giorgetti et al. [37].

Berrettoni et al. adopted a new notation for the Fe–Co system in cobalt hexacyanoferrates, suggesting the use of the $(FeCo)^{ox\ number}$ notation for the oxidation state, which represents the actual situation where $Co^{II/III}$ and $Fe^{II/III}$ metal ions coexist at different ratios [37, 38].

Electrochromism is the property of certain materials to change color when placed in an electric field. This is stimulated by redox reactions and is the basis for electrochromic devices, such as electrochromic displays. Neff et al. [39] studied in 1981 the electrochromic properties of a thin film of Prussian blue in the form of $KFeFe(CN)_6$ deposited on a conductive substrate. During reduction, they observed the formation of Everitt's salt ($K_2FeFe(CN)_6$), while during oxidation the shift to Berlin green ($K_xFe(Fe^{III-x}(CN)_6$; $x < 1$) by adopting KCl or K_2SO_4 aqueous solutions. Furthermore, they noticed that potassium ion migration into or out of the film was associated with the redox reactions, being the potassium inserted during reduction, and extracted in the oxidative step. Electrochromism is a common feature in PBA materials, such as ruthenium purple (iron hexacyanoruthenate) [40], vanadium hexacyanoferrate [41], copper hexacyanoferrate [42], and palladium hexacyanoferrate [43], and it is always accompanied with redox reactions of the transition metals and migration of ions to achieve charge neutrality.

The migration of ions occurring together with the change in oxidation state can have several applications, like wastewater treatment, desalination, and building

energy storage devices. PBAs are able to host monovalent, divalent, and trivalent ions (e.g., Rb^{+}, Pb^{2+}, Al^{3+}, Y^{3+}) with a good cycle stability and fast kinetics [44], thanks to the presence of vacancies and water molecules within the structure, which allow for the reversible exchange/insertion of multivalent ions. These aspects will be explored in the more detailed way in the next section.

6.2 Ion Exchange

In this section, applications of metal hexacyanoferrate materials in various technological fields driven by *host-guest* chemistry will be presented. Subsection 2.1 describes the use of metal hexacyanoferrates as potentiometric ion sensor. Indeed, by considering the metal hexacyanoferrate the *ionofore* (a term coined by Pressman [45] which indicates the *host* in a simple *host-guest* equilibrium) and the analyte being the *guest*, several potentiometric ion sensors have been proposed. Subsection 2.2 extends this concept to the recovery of metal ions, and the cases of cesium and thallium sorption are described. Subsection 2.3 introduces the concept of electrochemically switched ion exchange (ESIX) as the combination of ion exchange and electrochemistry as a friendly method for ion separation. Eventually, Subsection 2.4 summarizes the use in batteries, due to the natural predisposition for reversible ion intercalation.

6.2.1 Ion Exchange in MHCF at Work: Potentiometric Ion Sensors

The participation of cations in redox reactions of metal hexacyanoferrates provides a unique opportunity for the development of potentiometric sensors for monovalent ions such as cesium (Cs^{+}), potassium (K^{+}), and sodium (Na^{+}) but potentially also for divalent ones such as lead (Pb^{2+}), zinc (Zn^{2+}), and nickel (Ni^{2+}). For instance, by considering a copper hexacyanoferrate film deposited on a conductive substrate, the typical electrochemical response of potassium salt is the one displayed in Fig. 6.3. It indicates a main electrochemical system at about +0.65 V versus SCE related to the redox reaction involving the ferric and ferrous states of the hexacyanoferrate [42, 46], while the occurrence of a second electrochemical process at more negative potentials was postulated to involve the electro-activity of copper.[1]

[1]The occurrence of a second electrochemical process at the copper site at more negative potentials was postulated to involve the Cu^{II}/Cu^{I} redox couple by Shankaran et al. in 1999 [28] and by Makowski et al. in 2002 [99]. The process appears much less reversible respect to Fe^{III}/Fe^{II}, and the large potential difference between anodic and cathodic features can be rationalized in term of structural reorganization of the ionic site. Details are available in [100].

Such electrochemical behavior of copper hexacyanoferrate film can be explained by considering the simplified reaction (only Fe is electroactive):

$$KCuFe^{III}(CN)_6 + K^+ + e^- \overset{\text{insertion}}{\underset{\text{release}}{\rightleftarrows}} K_2CuFe^{II}(CN)_6$$

for which the Nernst equation holds:

$$E = E^0 + \left(\frac{RT}{F}\right) \ln \frac{a_{Fe^{III}} \cdot a_{K^+}}{a_{Fe^{II}}}$$

where the electrode potential E is related to the activity of the oxidized and reduced forms of the copper hexacyanoferrate film in the solid ($a_{Fe^{III}}$ and $a_{Fe^{II}}$) and the activity of the potassium ion in solution (a_{K^+}). Being constant the ratio of the activity of the solids $a_{Fe^{III}}/a_{Fe^{II}}$, a distinct potentiometric Nernstian response is expected for the potassium ions and therefore such films can be utilized for the development of a potentiometric sensor for potassium. The simple reaction cited above can be extended to other cations, and some pioneering work in this direction has been done in the late 90 s. The potentiometric responses of copper hexacyanoferrate membrane electrodes were examined for alkali, alkaline earth, heavy metals, and ammonium ions [47], also using a nickel hexacyanoferrates electrode in coated wire configuration [21] as well as composite electrodes made of graphite, paraffin, and metal hexacyanoferrates [48]. Lately, a different approach for simultaneous determination of K^+ and Na^+ at Prussian blue electrode was proposed. The sensing signal resulted from the influence of Na^+ on the cathodic peak potential of the voltammetric response of the Prussian blue (PB) [49].

The shape of the curve in Fig. 6.3 also indicates that the potassium can be reversibly inserted and released during the electrochemical process. An insertion was observed during the cathodic scan while a release took place in the opposite direction. This is a consequence of the zeolitic channels of the metal hexacyanoferrate structures which allowed the incorporation of the ions in their cavities. The size of the cavities plays a key role since ions (guests) can generally enter and leave the (host) structure with or without hindrance depending on the effective size of the hydrated cations [21]. Small cations can easily penetrate the host structure while large cations must be partially dehydrated in order to be accommodated into the host. This, in turn, leads to the observed potentiometric selectivity [50] toward different cations in metal hexacyanoferrates. As observed by Umezawa et al. [47], the selectivity coefficients of $K_2Cu_3[Fe^{II}(CN)_6]_2$ for alkali metal ions were in the order $Cs^+ > Rb^+ > K^+ > Na^+ > Li^+$. The selectivity order may reflect their dehydration energies needed for their accommodation from the solution side into the available structural site. The same selectivity order has been observed by Giorgetti et al. in the case of nickel derivatives [21].

By considering the metal hexacyanoferrate salt as the *ionofore* in potentiometric sensors (which is also the *host*) with the *guest* being the analyte, a summary (not extensive) of proposed potentiometric sensors based on metal hexacyanoferrates is presented in Table 6.1. The direct detection of the ion's activity in a sample rather

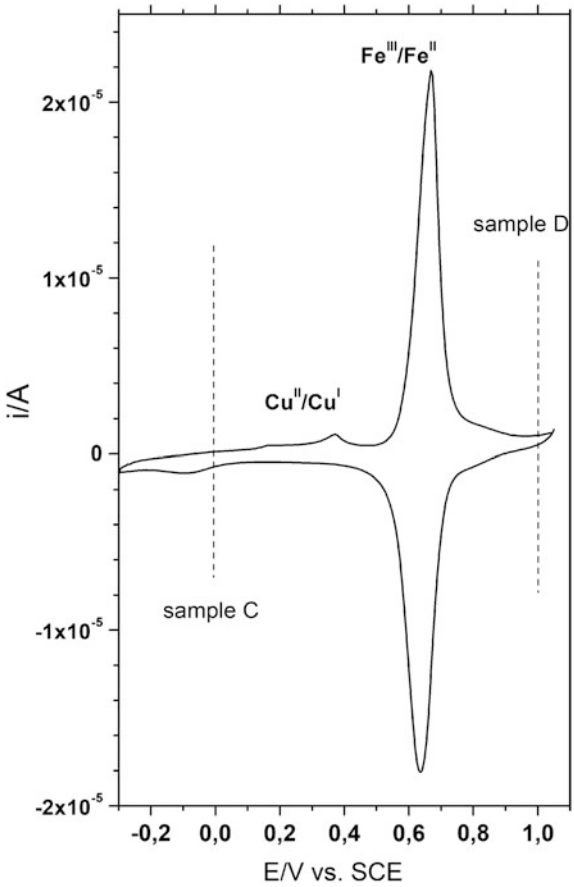

Fig. 6.3 Cyclic voltammogram of a pristine CuHCF-modified glassy carbon (GC) electrode in 0.1 M KCl + 0.1 M HCl electrolyte. Scan rate: 0.02 V s^{-1}. Reproduced with permission from [46]. Copyright Elsevier (2010)

Table 6.1 Potentiometric sensors based on metal hexacyanoferrates

Analyte	Metal in MHCF	References
K^+	Cu, Fe, Co, Ni	[51–55]
Cs^+	Cu	[56]
K^+, NH^{4+}	Cu	[57]
K^+, Rb^+, Cs^+, NH^{4+}	Cu, Ni, Fe	[58, 59]
Mono and divalent cations	Cu, Ni	[47]
Li^+, Na^+, K^+, Rb^+, Cs^+, Tl^+	Tl	[60]
Cs^+, Na^+, K^+, Na^+	Ni	[21]
As^{3+}	Fe	[61]
NH^{4+}	Cu	[62]
K^+, Cs^+	Fe, Cu, Ag, Ni, Cd	[48]

than their concentration is the unique property of these sensors. Also, the measured activity described the so-called free concentration of the analyte which can be smaller with respect to the total concentration, for instance, in the presence of a complexing agent in solution.

Additionally, Prussian blue analogues have been developed in ion-selective electrodes based on intercalation compounds for their predictable and reproducible potentials, which can be tuned by the synthesis (by properly selecting the type and oxidation state of the transition metal precursors) and/or by reducing or oxidizing a posteriori the synthesized compound. Within this context, potassium-, sodium-, and calcium-intercalated PBAs based on copper, nickel, and iron hexacyanoferrate have been studied for K^+, Na^+, and Ca^{2+} ion-selective electrodes [63], showing limits of detection (LOD) and selectivity coefficients against a range of interfering ions commensurate with available ion-selective electrodes in the market.

6.2.2 An Ion Exchange-Based Approach for the Recovery of Metal Ions: The Case of Cesium and Thallium

The structure of PB contributes to its peculiar characteristics as a *synthetic sponge*, being able to host a variety of ions and molecules in the zeolitic cavities. Two important uses feature its employment as a safe and effective drug for cesium and thallium poisoning. Given the ability of PB to work as antidote for both these toxic metals, the US Food and Drug Administration has cleared Prussian blue as a drug in October 2003, approving a label for Radiogardase® (Heyltex Corporation, Katy, TX), using PB as active pharmaceutical ingredient (API), as a medicinal agent for internal contamination from radioactive cesium or thallium [64].

Cesium-137 is a radioactive isotope of cesium produced during the nuclear fission of Uranium-235, according to the reaction:

$$^{235}_{92}\mathrm{U} + ^{1}_{0}n \rightarrow ^{137}_{55}\mathrm{Cs} + ^{96}_{37}\mathrm{Rb} + 3^{1}_{0}n$$

The health hazards of Cs-137 concern the radioactive decays. A β particle is emitted together with the formation of the metastable form of Ba-137 (denoted with *m*), that is, a high energetic isotope of barium. The decay of the latter to its fundamental state is concomitant with the release of the energy surplus via γ photons.

$$^{137}_{55}\mathrm{Cs} \rightarrow ^{137m}_{56}\mathrm{Ba} + ^{0}_{-1}\beta \rightarrow ^{137}_{56}\mathrm{Ba} + ^{0}_{0}\gamma$$

The exposure of human tissues to such energetic rays and β particles can cause illness or death, depending on the dose, and is associated with the development of the cancer for prolonged exposure times [65]. For this reason, the toxicity of Cs-137 is labeled as radiotoxicity and is a physical phenomenon.

Internal contamination of radiocesium occurs mainly via inhalation, although ingestion and percutaneous absorption are probable [66]. The cesium body uptake resembles the potassium one, being uniformly distributed in all soft tissues, e.g., muscle tissues, and eliminated through the kidneys. The spontaneous physiological release of cesium takes place predominantly through the urine (precisely, 10% in the following 48 h after contamination, remaining though in the organism for 110 days or more), while is secreted mostly through feces if PB treatment is carried out [67].

Few accidents in the past, like Chernobyl and Fukushima, released massive amounts of radioactive cesium in the environment. One among these, the tragedy happened in 1987 in Goiania, Brazil, arose from a theft and the rupture of the source of a cesium-137 teletherapy unit. The radiological accident occurred after the dispersion of cesium chloride contained in the source, provoked the irradiation and internal contamination of several persons [68]. During this calamity, PB was first tried on human beings as a potential antidote. Indeed, this radiological disaster provided the clinical case to carry out several studies and collect a variety of information and data on the interaction of PB with the human body. PB turned out to be an effective antidote against cesium, well tolerated when administered orally (the typical cure consisted in 3 grams per day), non-toxic, unreactive, and tasteless, while only minimal side effects were reported [65]. From a chemical point of view, different physicochemical processes expected to be involved due to cesium uptake. Ion trapping within cavities, physical adsorption due to electrostatic forces, and ion exchange may all be involved, the latter being likely the prevalent means [69]. Indeed, the cesium can be exchanged with the alkali ions already present in the PB structure. The cesium uptake from PB is affected by several parameters, like pH,

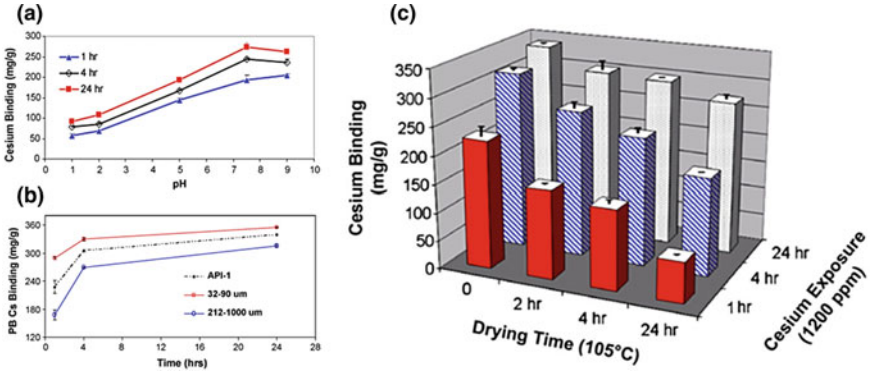

Fig. 6.4 (a) The pH-dependent cesium binding profile of API-1, incubated with 600 ppm cesium in pH solutions 1, 2, 5, 7.5, and 9 at 37 °C for 1, 4, and 24 h. (b) Comparison of cesium binding among API-1 and API-1 particle size fractions (32–90 μm and 212–1000 μm) were incubated with 1200 ppm cesium in the pH 7.5 solution at 37 °C for 0, 0.5, 1, 2, 3 4, and 24 h, respectively. (c) Effect of drying (105 °C). API-1 was dried for 0, 2, 4 and 24 h at 105 °C and then incubated with 1200 ppm cesium in the pH 7.5 solution at 37 °C for 0, 1, 2, 4, and 24 h, respectively. Reproduced with permission from [69]. Copyright Elsevier (2008)

residence time, particle sizes, and water content. To simulate an in vivo system, tests have been carried out in vitro at different values of pH, ranging from 1 to 9, and at incubation times of 1, 4, and 24 h [69] (Fig. 6.4a). As a matter of fact, the human gastrointestinal tract features a wide pH range and variable residence times. It is evident from Fig. 6.4a that the higher amount of cesium binding was detected for physiological pH 7.5 and 24 h of incubation time. Given that the cesium uptake is, in this case, a physical phenomenon involving mainly the ion exchange and diffusion into the crystal lattice, it appears to be a slow process and to reach the maximum sorption after a prolonged time, i.e., 24 h. At low pH values, the Cs-ions compete with hydronium ions (H_3O^+), whose abundancy overwhelms the Cs-concentration, so that uptake is negatively affected.

Figure 6.4b displays the cesium binding at different PB particle sizes: The uptake is favored at low particle dimensions, probably for the higher surface to volume ratio, enhancing the diffusion step. Moreover, a periodic monitoring of the moisture content plays an important role, as visible from Fig. 6.4c, evidencing as the hydration of PB might favor the interaction with Cs^+ allowing a greater uptake [69, 70].

Thallium intoxication is considered the second most frequent cause of intentional or accidental human poisoning [71]. Its popularity as human poisoning agent, in the form of thallium sulfate (Tl_2SO_4), increased during the last century, after it was banned as a depilatory and cosmetic medium. In *The Pale Horse* of Agatha Christie, thallium featured as the poisoning agent. The absence of color, taste, and odor, the sufficient solubility in water (a dose of roughly 1 g appears to be lethal), and its symptoms that could be misunderstood for an encephalitis, together with its high chemical toxicity, has made it a powerful and lethal poison [1].

Treatment with PB has been exploited as an intoxication curing agent during some clinical cases [65].

6.2.3 Electrochemically Driven Ion Exchange

The verified biological tolerance of PB paved the way for its study and use as a human drug. However, ion exchange is not a singularity of PB; it is instead a common feature of the class of PBAs. For this reason, metal hexacyanoferrates have been intensively studied for their ion exchange capabilities [72–75], in particular where there is neither biological interaction nor health hazard, for the lack of information about the interaction of PBAs with organisms. Radionuclide separation in contaminated wastewaters provides an example for this application. High stability toward γ radiation also exhibited by metal hexacyanoferrates [76].

Conventional inorganic and organic ion exchangers for radionuclide separations have been largely examined; however, their use poses several problems since they generate secondary wastes, e.g., solutions used to elute, wash, and load the exchangers, without mentioning that exchangers can be used typically only once before required disposal [77]. In this regard, the concept of electrochemically

switched ion exchange (ESIX) was introduced. ESIX is the combination of ion exchange and electrochemistry and the answer to a selective, reversible, non-expensive, and environmentally friendly method for ion separation [77]. Basically, an electrochemically active material (AM) is first deposited on a conductive substrate, which is characterized by a high surface area; second, by tuning the potential the active redox sites of AM are forced to reduce/oxidize, driving at the same time the uptake/release of ions, respectively, to maintain charge neutrality. As described in the following equation, the oxidized form of AM (denoted as AM^{ox}) can be reduced to AM^{red} if a proper cathodic potential is applied, forcing meanwhile the insertion of a general cation M^{n+}. Additionally, ESIX offers the possibility to reverse the process, by inverting the polarization and applying an anodic potential to the system: The regeneration of AM takes place in concomitance with the release of the cations.

$$AM^{ox} + xM^{n+} + xne^{-} \underset{\text{release}}{\overset{\text{uptake}}{\rightleftarrows}} M_xAM^{red}$$

In a two-step process, it is then possible to deplete a system from a certain cation, e.g., radioactive cesium depletion from cesium-rich wastewaters, and to release it in an appropriate system for disposal, regenerating the AM ion exchanger. In case of employment of a metal hexacyanoferrate (e.g., nickel hexacyanoferrate $KNi^{II}Fe^{III}(CN)_6$) as AM and Cs^+ as M^{n+} cation, the above equation can be written as:

$$KNi^{II}Fe^{III}(CN)_6 + Cs^+ + e^- \underset{\text{release}}{\overset{\text{uptake}}{\rightleftarrows}} KCsNi^{II}Fe^{II}(CN)_6$$

where the reduction/oxidation of the iron species in nickel hexacyanoferrate allows the insertion/extraction of cesium ions.

ESIX is an electrochemically driven method and represents a promising alternative to diffusion-driven processes whenever the application of a potential is feasible. This may involve either a potentiostatic or potentiodynamic approach, the former consisting in the application of a selected and fixed potential for a certain time, while the latter scans over a range of potentials with a defined scan rate. The latter technique is commonly known as cyclic voltammetry (CV).

Although the applicability of CV on a large scale remains an issue, since the film coating does not match size and thickness requirements, solutions to overcome this problem have been proposed: For instance, by dispersing metal hexacyanoferrate nanoparticles in water to form an ink, it is possible to coat different-sized arrays with low-cost printing methods [26, 78, 79]. Among PBAs, copper hexacyanoferrate (CuHCF) has been used for Cs removal from wastewaters, principally for its chemical stability under wide pH range and low radiolytic decomposition if exposed to highly energetic rays [26, 73, 76, 78, 80–82]. Figure 6.5 presents the main results of a study conducted by Chen et al. [78]: The uptake/release of cesium

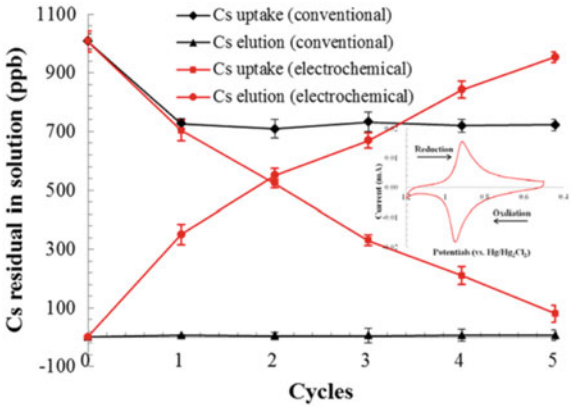

Fig. 6.5 Cesium uptake/elution using Cu-HCFIII film in the conventional and electrochemical system (insert: cyclic voltammograms response, scan rate = 20 mV/s). Reprinted with permission from [78]. Copyright (2013) American Chemical Society

was performed in both conventional (diffusion controlled) mode and electrochemically driven mode, and results were compared. The different effectiveness of the two methods regarding the decontamination of cesium in the water sample can be easily identified. The electrochemical mode is not only more efficient in depleting the system from cesium, but it results to be reversible, contrary to the conventional mode, where the cesium insertion takes place (in spite of the limiting diffusion gradient which lowers its effectiveness), but its extraction is not feasible spontaneously in the experimental time.

For this study, the electrochemical switching took place in a three-electrode cell by using SCE as the reference electrode, platinum as the counter electrode, and the $CuHCF^{III}$ film coated electrode as the working electrode (2.5×2.0 cm^2). ESIX was carried out by using the prepared $CuHCF^{III}$ film in 1 ppm $CsNO_3$/1 ppm $NaNO_3$ electrolyte for Cs uptake and 1 ppm $NaNO_3$ electrolyte for Cs elution to enhance solution conductivity. The potential has been scanned in the range $0.0 < E < 1.3$ V versus SCE, with a negative polarization (starting from 1.3 V) for Cs uptake and a positive polarization (starting from 0.0 V) for Cs release. The procedure was repeated 5 times, and the Cs concentrations were measured by ICP-MS. About 92.05% of total Cs was adsorbed, while more than 97.22% of the adsorbed Cs was reversibly eluted from the CuHCF film. Overall, the film could be successfully regenerated, whereas the uptake/release easily controlled by switching the applied potential.

The complexity of biological interactions and wastewaters might limit the selectivity of trapping and/or exchanging cesium and thallium, making it a chemically challenging task. Indeed, these metals, commonly present as monovalent

ions, can compete with alkali and alkaline earth metals, which generally present at significantly higher concentration level. Thus, it is crucial to assess the selectivity[2] and activity of metal hexacyanoferrates toward different isolated ions and their mixtures.

To this purpose, the affinity of metal hexacyanoferrates toward different ions has been widely studied. For the employment of a new ion exchanger technology, it is suggested to verify the affordability on real matrices, whose effects can deviate from the results of the analysis. Seawater represents a very complex matrix in respect to selective ion exchange, due to the presence of competing ions, complexing anions, dissolved organic matter, and suspended colloids. In a study carried out by Sangvanich et al. [81], a sample of seawater considered for the challenging metals contains precisely 4500 ppm Na, 1000 ppm Mg, 200 ppm Ca, 100 ppm K, 1 ppm Se, and 0.5 ppm (each) of Mn, Fe, Co, Cu, Zn, and Mo, with an artificial addition of 0.5 ppm of starting concentrations of Cs and Tl. Besides, distribution coefficients (K_d, mL/g), which are partition coefficients between liquid supernatant phase and solid phase, were calculated for both Cs and Tl varying the pH value of the sample (Table 6.2). The partitioning of an analyte in two media follows the *Nernst partition law*, according to which the ratio of concentrations (or better activities) in both phases is a constant, namely the partition coefficient:

$$K_d = \frac{a_{\text{phase 1}}}{a_{\text{phase 2}}}$$

In general terms, the higher the K_d value, the stronger the binding affinity, where a value of 5000 and above is considered good, and a K_d value greater than 50,000 is considered excellent. CuHCF and PB were considered as ion exchangers, and their performances compared.

According to Table 6.2, CuHCF displays high selectivity toward cesium and thallium within the wide tested pH range, despite the abundance of other metal ions. Only copper and zinc bind very well close to neutral pH, but this does not influence the binding of Cs^+ and Tl^+. Contrarily, their uptake in PB was strongly affected by the presence of both zinc and copper.

To further evaluate the possible application of these exchanger materials in industrial and nuclear waste water, Sangvanich [81] considered as matrices all three natural glasses of water, i.e., river, sea, and ground waters, as well as acidic and alkaline media (cf. Table 6.3).

The absorption affinities toward Cs^+ and Tl^+ were higher in case of river and groundwaters, presumably due to the substantially lower ionic strength compared to seawater. PB seems much more sensitive toward the presence of competing ions, especially in acidic (pH = 1.1, K_d = 5400) and alkaline (pH = 8.6, K_d = 73,000) waters. On the other side, a better performance was recorded for CuHCF, whose

[2]The selectivity of metal ions in metal hexacyanoferrates for potentiometric purposes (equilibrium condition) has been presented in Sect. 2.1, and details on the selectivity coefficient are available in references [44, 47].

Table 6.2 Distribution coefficients (K_d, mL/g) for adsorption of various cations on CuHCF (on SAMMS) and PB in seawater

Competing metal	Concentration (ppm)	Sorbent	pH 0.1	pH 2.1	pH 3.4	pH 6.3	pH 7.3
Cs(l)	0.5	SAMMS	26,000	46,050	75,000	110,000	140,000
		PB	680	770	950	17,000	53,000
Tl(l)	0.5	SAMMS	8300	12,000	14,000	14,000	14,000
		PB	450	280	550	4500	8600
Na(l)	4500	SAM MS	0	19	0	14	0
		PB	0	1	4	16	8
M_s(ll)	1000	SAMMS	0	15	0	10	5
		PB	0	0	13	11	4
Ca(II)	200	SAMMS	0	13	2	10	0
		PB	0	0	26	0	0
K(l)	100	SAMMS	0	0	0	8	0
		PB	0	0	29	18	19
Se(IV)	1	SAMMS	8	0	120	110	140
		PB	0	29	230	450	490
Mn(ll)	0.5	SAMMS	0	0	16	68	270
		PB	0	1	19	910	4100
Fe(lll)	0.5	SAMMS	26	26	3300	1400	520
		PB	0	0	0	1700	0
Cu(ll)	0.5	SAMMS	0	0	4200	14,000	6500
		PB	6800	14,000	20,000	610,000	560,000
Zn(ll)	0.5	SAMMS	0	0	4200	19,000	79,000
		PB	0	29	110	260,000	81,000
Mo(VI)	0.5	SAMMS	61	130	220	41	17
		PB	170	110	660	170	95

Reproduced with permission from [81]. Copyright Elsevier (2010)
Measured in pH-adjusted filtered sea water, S/L of 1.0 g/L

Table 6.3 Adsorption affinity (K_d in mL/g) of Cs and Tl on FC-Cu-EDA-SAMMS (CuHCF as exchanger) and Prussian blue in various matrices

Matrix	Metal (ppb)	S/L (g/LJ)	FC-Cu-EDA-SAMMS		Prussian Bice	
			Cs	Tl	Cs	Tl
Columbia River water, pH 7.3	500	1.0	1,700,000	3,100,000	250,000	1,200,000
Haitfoid groundwater, pH 7.5	500	1.0	1,400,000	2,800,000	250,000	79,0000
Sequim Bay seawater, pH 7.4	500	1.0	240,000	16,000	85,000	15,000
0.085 M HCl, pH 1.1	50	0.2	156,000	NA	5400	NA
0.2 M $NaHCO_3$. pH 8.6	50	0.2	230,000	NA	73,000	NA

Reproduced with permission from [81]. Copyright Elsevier (2010)

affinity (expressed as K_d) toward Cs^+ was above 10^5, indicating that it was not negatively affected either by water source or pH medium. Affinity toward Tl^+ also followed the similar trend, with CuHCF presenting superior sorption affinity compared to PB, although data are not available for extreme pH values.

The mentioned study and results were in agreement with earlier reported works in the literature. In particular, Zadronecki et al. [83] reported that copper hexacyanoferrate displayed an exceptionally high affinity toward thallium ions, in spite of its physical similarities to K^+ ions. As a matter of fact, Tl^+ and K^+ share the same formal oxidation state, ionic radius, and real solvation energy, which might let assume a comparable insertion mechanism and transport in the CuHCF lattice. Chemical properties of these two cations are, however, rather different, being thallium much softer than potassium [84]. Experiments conducted in an aqueous environment in the presence of both Tl^+ and K^+ revealed an affinity of 100–250 times higher for Tl^+, which may be due to a strong chemical interaction between Tl^+ and CN^- ions, which constitute the building block of the hexacyanoferrate structure, providing an irreversible ion trapping.

6.2.4 *Reversible Ion Insertion in Battery Systems*

As previously discussed and outlined in Scheme 6.1, the insertion/extraction of ions into PBAs crystal lattices can be either spontaneous, i.e., diffusion-driven, or forced through the application of a potential. Another possible way to drive the ion flow from and/or to a host material is the electrode polarization mediated by the application of a current. The galvanostatic method relies on the employment of a constant current, while the response as a function of the potential is recorded. The use

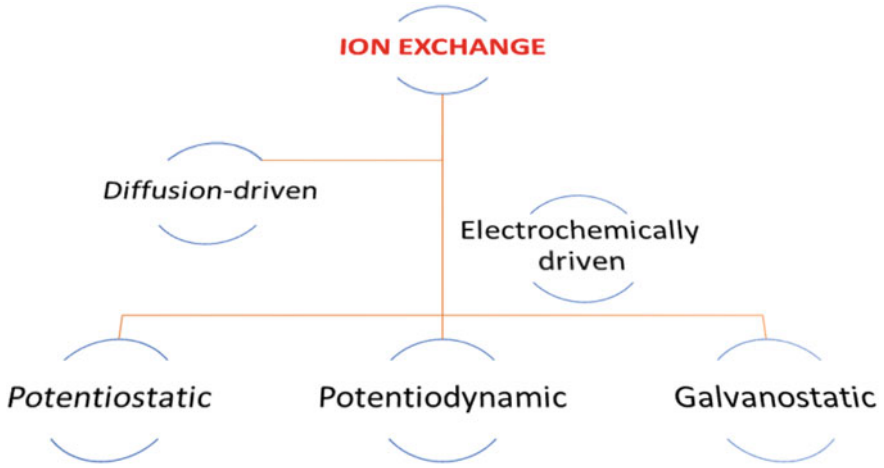

Scheme 6.1 Ion exchange pathways

of a negative current to the studied electrode forces its reduction, and therefore, the cation insertion into its lattice is expected to compensate the charge excess. On the contrary, by reversing the current polarization at a certain potential, the electrode experiences an oxidation, which the concomitant cation extraction. Multiple steps performed alternating the current polarization within a defined potential range are the basis for galvanostatic cycling with potential limitation (GCPL) technique, commonly used for rechargeable battery systems.

Briefly, a battery is a device that converts chemical energy into electrical energy and is a two-electrode system constituted by a positive and negative electrode, kept away by an electrolyte-soaked separator. Lithium-ion batteries were introduced in the market in the 90s by Sony and were based on the first investigation of Mizushima, Jones, Wiseman, and Goodenough published in 1981 [85]. The positive electrode material was a lithium rich cobalt oxide, Li_xCoO_2, while Li metal was adopted as the negative electrode, being later replaced by Li-intercalated graphite, Li_zC_6, for safety reasons, while an organic solution containing Li^+ ions served as the electrolyte. The reactions taking place at the electrodes in a battery system are listed below:

$$\text{Positive electrode: } Li_xCoO_2 + yLi^+ + ye^- \underset{\text{charge}}{\overset{\text{discharge}}{\rightleftarrows}} Li_{x+y}CoO_2$$

where $x \geq 0.067$ and $x + y \leq 1$

$$\text{Negative electrode: } Li_zC_6 \underset{\text{charge}}{\overset{\text{discharge}}{\rightleftarrows}} Li_{z-y}C_6 + yLi^+ + ye^-$$

where $z \leq 1$

During the discharge process, the intercalation of Li-ions is forced in the cobalt oxide insertion material, causing the reduction of the cobalt species, while the reverse occurs in the charging process, being the Li-ions released in the electrolyte solution and the cobalt species oxidized to the original oxidation state. At the negative electrode, the specular redox reactions take place, being the lithium de-intercalated and re-inserted in the graphite layers.

Because of the limited lithium resources and the difficulties during its extraction [86], new alternative strategies involving the replacement of lithium are currently studied and evaluated. Within this framework, other alkaline metals have been investigated for battery use as well as aqueous systems, to cut down the safety hazard regarding Li-ion batteries. PBA materials, and in particular metal hexacyanoferrates, have been intensively studied as insertion materials due to the ease of synthesis and separation and wide versatility toward several ions, ranging from monovalent ions such as lithium [87, 88], sodium [89, 90], and potassium [91, 92], to divalent ions, for instance, calcium [93] and magnesium [94], as well as trivalent ions such as aluminum [95]. This adaptability to ions of different sizes and charge is the reflection of the PBAs structural features: The presence of large tunnels and vacancies allows to accommodate a variety of ions, regardless their size and hydration shell (in the case, water is employed as solvent).

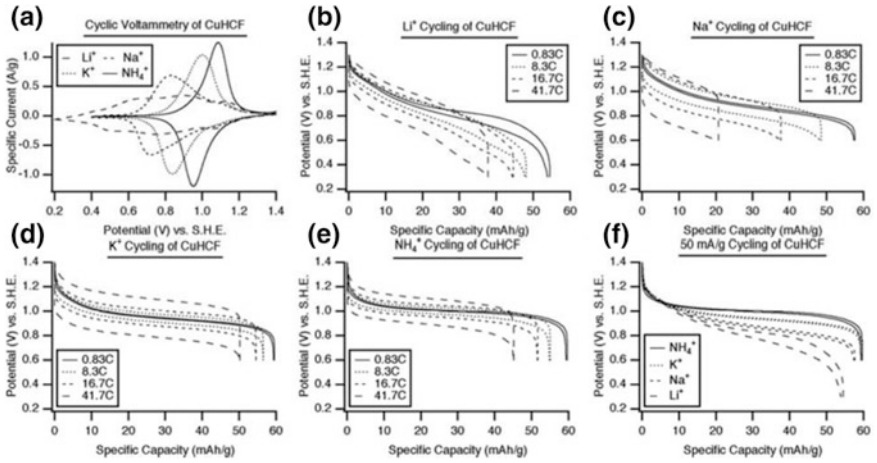

Fig. 6.6 Electrochemical performance of CuHCF. (a) Cyclic voltammetry of CuHCF with Li^+, Na^+, K^+, and NH_4^+ ions, and (b) through (e): The potential profiles of CuHCF during galvanostatic cycling of with Li^+, Na^+, K^+, and NH_4^+, respectively, at several current densities. (f) The potential profiles of CuHCF during galvanostatic cycling of Li^+, Na^+, K^+, and NH_4^+, at 50 mA/g (0.83C). Reproduced with permission from [87]. Copyright Electrochemical Society

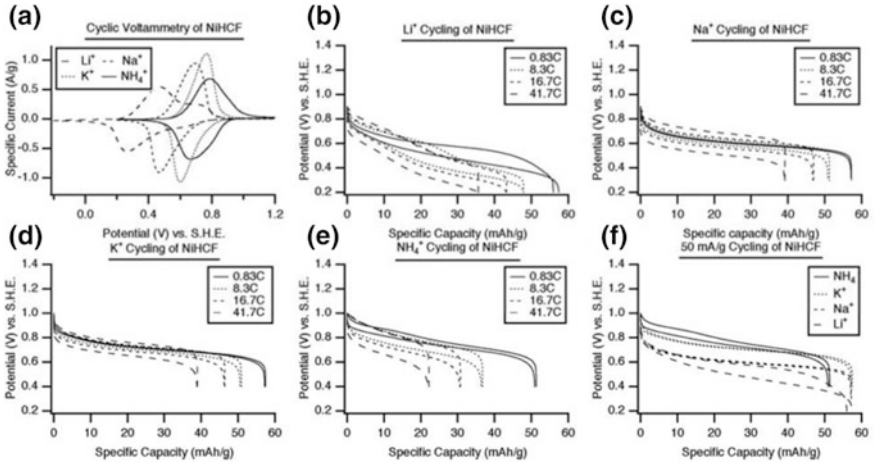

Fig. 6.7 Electrochemical performance of NiHCF. Cyclic voltammetry of NiHCF with Li^+, Na^+, K^+, and NH_4^+ ions, and (**b**) through (**e**): The potential profiles of NiHCF during galvanostatic cycling of Li^+, Na^+, K^+, and NH_4^+, respectively, at several current densities. (**f**) The potential profiles of NiHCF during galvanostatic cycling of Li^+, Na^+, K^+, and NH_4^+, at 50 mA/g (0.83C). Reproduced with permission from [87]. Copyright Electrochemical Society

The results of work on different aqueous systems of Wessells et al. [87] have been presented in Figs. 6.6 and 6.7, where CuHCF and NiHCF, respectively, have been tested in aqueous media containing Li^+, Na^+, K^+, and NH_4^+ ions. Both cyclic

voltammetry and galvanostatic cycling have been used to assess the electrochemical behavior of these two analogues, by employing several current rates, i.e., by changing the amount of the draining (cf. discharge process) and supplied (cf. charge process) current. The high-rate capability, deriving from the ability to retain most of the capacity at high current densities, might be attributed to the rigid, open framework lattices of the studied materials.

CVs displayed in Figs. 6.6 and 6.7 suggest that the ionic radius of the inserted species affects the electrochemical performance of the intercalation host. It has been proven [96] that large cations prefer to occupy the body-centered site with large space, while small cations prefer to occupy the face-centered site for short cation–anion bonding distance. Furthermore, the voltage for the insertion/de-insertion process is also highly correlated to the ionic radius, the insertion of larger cations occurring at higher voltages as a rule of thumb. The high-rate capacity retention of CuHCF was observed when it was cycled with K^+, NH_4^+, and Li^+, while poor-rate capability was noticed during reaction with Na^+. Contrarily, NiHCF showed good performance during the reaction with both Na^+ and K^+, whereas the cycling of Li^+ and NH_4^+ was not as satisfactory as in the case of CuHCF material. The difference in the behavior of Li^+ and Na^+ cannot be easily explained; however, the reason might be addressed rather to chemical than physical interactions, since lattice parameters differ by less than 1%.

Overall, CuHCF has been proven to be an excellent candidate for large-scale energy storage systems for the high efficient electrochemical performances, being able to stand even more than 40 k cycles of charge/discharge in the aqueous inexpensive medium [97]. The reason of such performance was identified as the combination of the activity of both metallic species, in this case, Cu and Fe, and the little lattice strain involved during the insertion/release processes [98].

6.3 Conclusion

Metal hexacyanoferrates feature a generally cubic open framework of repeating and orthogonal—Fe–C–N–M–N–C chains, resulting in a porous structure distinguished by large interstitial voids and vacancies. The structural skeleton together with the redox activity of the metallic centers is responsible for a wide range of properties, such as electrochromism, photoinduced magnetization, charge storage, sensing of biological analytes as well as mono-, bi-, and trivalent ions. In this chapter, we focused on ion exchange capabilities of this class of compounds, starting by introducing diffusion-driven processes, for instance, the recovery of radionuclides or toxic agents from wastewaters and human bodies after intoxication or poisoning, then proceeding with electrochemically driven approaches. These are classified as either potentiostatic, potentiodynamic, or galvanostatic and were discussed and presented with meaningful examples, ranging from ESIX-based depletion of ions to battery systems.

References

1. Ware M (2008) Prussian blue: artists' pigment and chemists' sponge. J Chem Educ 85:612. https://doi.org/10.1021/ed085p612
2. Davies H, Prussian blue: from the great wave to Starry Night, how a pigment changed the world. ABC News (2017)
3. Keggin JF, Miles FD (1936) Structures and formulae of the Prussian blues and related compounds. Nature 137:577–578. https://doi.org/10.1038/137577a0
4. Buser HJ, Schwarzenbach D, Petter W, Ludi A (1977) The crystal structure of Prussian blue: $Fe_4[Fe(CN)_6]3.xH_2O$. Inorg Chem 16:2704–2710. https://doi.org/10.1021/ic50177a008
5. Wills, AS (2005) Annual reports section "A" (inorganic chemistry). Magnetism 101:472–488. https://doi.org/10.1039/b408369p
6. Herren F, Ludi, A, Fischer, P, Halg, W (1980) Neutron diffraction study of Prussian blue, $Fe4[Fe(CN)_6]3.xH_2O$. location of water molecules and long-range magnetic order, Inorg Chem 19:956–959. https://doi.org/10.1021/ic50206a032
7. Shokouhimehr M, Soehnlen ES, Khitrin A, Basu S, Huang SD (2010) Biocompatible Prussian blue nanoparticles: preparation, stability, cytotoxicity, and potential use as an MRI contrast agent. Inorg Chem Commun 13:58–61. https://doi.org/10.1016/j.inoche.2009.10.015
8. Giorgetti M, Berrettoni M, Filipponi A, Kulesza PJ, Marassi R (1997) Evidence of four-body contributions in the EXAFS spectrum of $Na_2Co[Fe(CN)_6]$. Chem Phys Lett 275:108–112. https://doi.org/10.1016/S0009-2614(97)00724-0
9. Giorgetti M, Berrettoni M (2008) Structure of Fe/Co/Ni hexacyanoferrate as probed by multiple edge X-ray absorption spectroscopy. Inorg Chem. https://doi.org/10.1021/ic800289c
10. Rodríguez-Hernández J, Reguera E, Lima E, Balmaseda J, Martínez-García R, Yee-Madeira H (2007) An atypical coordination in hexacyanometallates: Structure and properties of hexagonal zinc phases. J Phys Chem Solids 68:1630–1642. https://doi.org/10.1016/j.jpcs.2007.03.054
11. Kareis CM, Lapidus SH, Her JH, Stephens PW, Miller JS (2012) Non-Prussian blue structures and magnetic ordering of Na $2Mn^{II}[Mn^{II}(CN)_6]$ and Na $2Mn^{II}[Mn^{II}(CN)_6]2H_2O$. J Am Chem Soc 134:2246–2254. https://doi.org/10.1021/ja209799y
12. Martínez-García R, Knobel M, Balmaseda J, Yee-Madeira H, Reguera E (2007) Mixed valence states in cobalt iron cyanide. J Phys Chem Solids 68:290–298. https://doi.org/10.1016/j.jpcs.2006.11.008
13. Wang RY, Wessells CD, Huggins RA, Cui Y (2013) Highly reversible open framework nanoscale electrodes for divalent ion batteries. Nano Lett 13:5748–5752. https://doi.org/10.1021/nl403669a
14. Omarova M, Koishybay A, Yesibolati N, Mentbayeva A, Umirov N, Ismailov K, Adair D, Babaa M-R, Kurmanbayeva I, Bakenov Z (2015) Nickel hexacyanoferrate nanoparticles as a low cost cathode material for lithium-ion batteries. Electrochim Acta 184:58–63. https://doi.org/10.1016/j.electacta.2015.10.031
15. Wessells CD, McDowell MT, Peddada SV, Pasta M, Huggins RA, Cui Y (2012) Tunable reaction potentials in open framework nanoparticle battery electrodes for grid-scale energy storage. ACS Nano 6:1688–1694. https://doi.org/10.1021/nn204666v
16. Mortimer RJ, Rosseinsky DR (1983) Electrochemical polychromicity in iron hexacyanoferrate films, and a new film form of ferric ferricyanide. J Electroanal Chem Interfacial Electrochem 151:133–147. https://doi.org/10.1016/S0022-0728(83)80429-X
17. Guadagnini L, Maljusch A, Chen X, Neugebauer S, Tonelli D, Schuhmann W (2009) Visualization of electrocatalytic activity of microstructured metal hexacyanoferrates by means of redox competition mode of scanning electrochemical microscopy (RC-SECM). Electrochim Acta 54:3753–3758. https://doi.org/10.1016/j.electacta.2009.01.076

18. Shan Y, Yang G, Gong J, Zhang X, Zhu L, Qu L (2008) Prussian blue nanoparticles potentiostatically electrodeposited on indium tin oxide/chitosan nanofibers electrode and their electrocatalysis towards hydrogen peroxide. Electrochim Acta 53:7751–7755. https://doi.org/10.1016/J.ELECTACTA.2008.05.035
19. Mortimer RJ, Rosseinsky DR, Glidle A (1992) Polyelectrochromic Prussian blue: a chronoamperometric study of the electrodeposition. Sol Energy Mater Sol Cells 25:211–223. https://doi.org/10.1016/0927-0248(92)90069-2
20. Zadronecki M (1999) Study of growth and the electrochemical behavior of Prussian blue films using electrochemical quartz crystal microbalance. J Electrochem Soc 146:620. https://doi.org/10.1149/1.1391653
21. Giorgetti M, Scavetta E, Berrettoni M, Tonelli D (2001) Nickel hexacyanoferrate membrane as a coated wire cation-selective electrode. Analyst 126:2168–2171. https://doi.org/10.1039/b107034g
22. Giorgetti M, Tonelli D, Berrettoni M, Aquilanti G, Minicucci M (2014) Copper hexacyanoferrate modified electrodes for hydrogen peroxide detection as studied by X-ray absorption spectroscopy. J Solid State Electrochem 18:965–973. https://doi.org/10.1007/s10008-013-2343-5
23. Sato O, Iyoda T, Fujishima A, Hashimoto K (1996) Photoinduced magnetization of a cobalt-iron cyanide. Science (80-.). 272:704–705. https://doi.org/10.1126/science.272.5262.704
24. Bueno PR, Giménez-Romero D, Ferreira FF, Setti GO, Garcia-Jareño JJ, Agrisuelas J, Vicente F (2009) Electrochromic switching mechanism of iron hexacyanoferrates molecular compounds: the role of fe2 + (cn)6 vacancies. J Phys Chem C 113:9916–9920. https://doi.org/10.1021/jp901146w
25. Neff VD (1985) Some performance characteristics of a Prussian blue battery. J Electrochem Soc 132:1382. https://doi.org/10.1149/1.2114121
26. Chen R, Tanaka H, Kawamoto T, Asai M, Fukushima C, Kurihara M, Watanabe M, Arisaka M, Nankawa T (2012) Preparation of a film of copper hexacyanoferrate nanoparticles for electrochemical removal of cesium from radioactive wastewater. Electrochem Commun 25:23–25. https://doi.org/10.1016/j.elecom.2012.09.012
27. Ciabocco, M, Cancemi, P, Saladino, ML, Caponetti E, Alduina R, Berrettoni M (2018) Synthesis and antibacterial activity of iron-hexacyanocobaltate nanoparticles. J Biol Inorg Chem 1–14. https://doi.org/10.1007/s00775-018-1544-x
28. Ravi Shankaran, D, Sriman Narayanan S (1999) Characterization and application of an electrode modified by mechanically immobilized copper hexacyanoferrate. Fresenius J Anal Chem 364:686–689. https://doi.org/10.1007/s002160051414
29. Chen SM, Chan CM (2003) Preparation, characterization, and electrocatalytic properties of copper hexacyanoferrate film and bilayer film modified electrodes. J Electroanal Chem 543:161–173. https://doi.org/10.1016/S0022-0728(03)00017-2
30. Zhou D-M, Ju H-X, Chen H-Y (1996) Catalytic oxidation of dopamine at a microdisk platinum electrode modified by electrodeposition of nickel hexacyanoferrate and Nafion®. J Electroanal Chem 408:219–223. https://doi.org/10.1016/0022-0728(95)04522-8
31. de Lara González, GL, Kahlert, H, Scholz, F (2007) Catalytic reduction of hydrogen peroxide at metal hexacyanoferrate composite electrodes and applications in enzymatic analysis. Electrochim Acta 52:1968–1974. https://doi.org/10.1016/j.electacta.2006.08.006
32. Karyakin AA (2001) Prussian blue and its analogues: electrochemistry and analytical applications. Electroanalysis 13:813–819. https://doi.org/10.1002/1521-4109(200106)13:10%3c813:AID-ELAN813%3e3.0.CO;2-Z
33. Ricci F, Palleschi G (2005) Sensor and biosensor preparation, optimisation and applications of Prussian blue modified electrodes. Biosens Bioelectron 21:389–407. https://doi.org/10.1016/j.bios.2004.12.001
34. De Mattos IL, Gorton L, Laurell T, Malinauskas A, Karyakin AA (2000) Development of biosensors based on hexacyanoferrates. Talanta 52:791–799. https://doi.org/10.1016/S0039-9140(00)00409-4

35. Baioni AP, Vidotti M, Fiorito PA, Ponzio EA, De Torresi SIC (2007) Synthesis and characterization of copper hexacyanoferrate nanoparticles for building up long-term stability electrochromic electrodes. Langmuir 23:6796–6800. https://doi.org/10.1021/la070161h
36. Pauliukaite R, Florescu M, Brett CMA (2005) Characterization of cobalt- and copper hexacyanoferrate-modified carbon film electrodes for redox-mediated biosensors. J Solid State Electrochem 9:354–362. https://doi.org/10.1007/s10008-004-0632-8
37. Giorgetti M, Aquilanti G, Ciabocco M, Berrettoni M (2015) Anatase-driven charge transfer involving a spin transition in cobalt iron cyanide nanostructures. Phys Chem Chem Phys 17:22519–22522. https://doi.org/10.1039/C5CP03580E
38. Berrettoni M, Giorgetti M, Zamponi S, Conti P, Ranganathan D, Zanotto A, Saladino ML, Caponetti E (2010) Synthesis and characterization of nanostructured cobalt hexacyanoferrate. J Phys Chem C 114:6401–6407. https://doi.org/10.1021/jp100367p
39. Ellis D, Eckhoff M, Neff VD (1981)Electrochromism in the mixed-valence hexacyanides. 1. Voltammetric and spectral studies of the oxidation and reduction of thin films of Prussian blue. J Phys Chem 85:1225–1231. https://doi.org/10.1021/j150609a026
40. Rajan KP, Neff VD (1982) Electrochromism in the mixed-valence hexacyanides. 2. Kinetics of the reduction of ruthenium purple and Prussian blue. J Phys Chem 86:4361–4368. https://doi.org/10.1021/j100219a017
41. Carpenter MK, Conell RS, Simko SJ (1990) Electrochemistry and electrochromism of vanadium hexacyanoferrate. Inorg Chem 29:845–850. https://doi.org/10.1021/ic00329a054
42. Siperko LM, Kuwana T (1983) Electrochemical and spectroscopic studies of metal hexacyanometalate films. J Electrochem Soc 130:396. https://doi.org/10.1149/1.2119718
43. Jiang M, Zhao Z (1990) A novel stable electrochromic thin film: a Prussian blue analogue based on palladium hexacyanoferrate. J Electroanal Chem Interfacial Electrochem 292:281–287. https://doi.org/10.1016/0022-0728(90)87343-I
44. Wang RY, Shyam B, Stone KH, Weker JN, Pasta M, Lee H-W, Toney, MF, Cui Y (2015) Reversible multivalent (monovalent, divalent, trivalent) ion insertion in open framework materials. Adv Energy Mater n/a-n/a. https://doi.org/10.1002/aenm.201401869
45. Pressman BC, Harris EJ, Jagger WS, Johnson JH (1967) Antibiotic-mediated transport of alkali ions across lipid barriers. Proc Natl Acad Sci USA 58:1949–1956. https://doi.org/10.1073/PNAS.58.5.1949
46. Guadagnini L, Tonelli D, Giorgetti M (2010) Improved performances of electrodes based on Cu^{2+}-loaded copper hexacyanoferrate for hydrogen peroxide detection. Electrochim Acta 55:5036–5039. https://doi.org/10.1016/j.electacta.2010.04.019
47. Tani Y, Eun H, Umezawa Y (1998) A cation selective electrode based on copper(II) and nickel(II) hexacyanoferrates: Dual response mechanisms, selective uptake or adsorption of analyte cations. Electrochim Acta 43:3431–3441. https://doi.org/10.1016/S0013-4686(98)00089-9
48. Düssel H, Dostal A, Scholz F (1996) Hexacyanoferrate-based composite ion-sensitive electrodes for voltammetry. Fresenius J Anal Chem 355:21–28. https://doi.org/10.1007/s0021663550021
49. Ang JQ, Li SFY (2012) Novel sensor for simultaneous determination of K^+ and Na^+ using Prussian blue pencil graphite electrode. Sens Actuators, B Chem 173:914–918. https://doi.org/10.1016/j.snb.2012.07.119
50. Bakker E, Pretsch E, Bühlmann P (2000) Selectivity of potentiometric ion sensors, Anal Chem 72:1127–1133. https://doi.org/10.1021/ac991146n
51. Engel D, Grabner EW (1985) Copper hexacyanoferrate-modified glassy carbon: a novel type of potassium-selective electrode, Berichte Der Bunsengesellschaft Für Phys. Chemie 89:982–986. https://doi.org/10.1002/bbpc.19850890911
52. Cox JA, Das BK (1985) Voltammetric determination of nonelectroactive ions at a modified electrode. Anal Chem 57:2739–2740. https://doi.org/10.1021/ac00290a068
53. Krishnan V, Xidis AL, Neff VD (1990) Prussian blue solid-state films and membranes as potassium ion-selective electrodes. Anal Chim Acta 239:7–12. https://doi.org/10.1016/S0003-2670(00)83828-3

54. Ho K-C, Lin C-L (2001) A novel potassium ion sensing based on Prussian blue thin films. Sens Actuators B Chem 76:512–518. https://doi.org/10.1016/S0925-4005(01)00605-0
55. Zhiqiang G, Xingyao Z, Guangqing W, Peibiao L, Zaofan Z (1991) Potassium ion-selective electrode based on a cobalt(II)-hexacyanoferrate film-modified electrode. Anal Chim Acta 244:39–48. https://doi.org/10.1016/S0003-2670(00)82476-9
56. Huang C-Y, Lee J-D, Tseng C-L, Lo J-M (1994) A rapid method for the determination of 137Cs in environmental water samples. Anal Chim Acta 294:221–226. https://doi.org/10.1016/0003-2670(94)80198-3
57. Thomsen KN, Baldwin RP (1989) Amperometric detection of nonelectroactive cations in flow systems at a cupric hexacyanoferrate electrode. Anal Chem 61:2594–2598. https://doi.org/10.1021/ac00198a002
58. Thomsen KN, Baldwin RP (1990) Evaluation of electrodes coated with metal hexacyanoferrate as amperometric sensors for nonelectroactive cations in flow systems. Electroanalysis 2:263–271. https://doi.org/10.1002/elan.1140020402
59. Hartmann M, Grabner EW, Bergveld P (1991) Alkali ion sensor based on Prussian blue-covered interdigitated array electrodes. Sens Actuators B Chem 4:333–336. https://doi.org/10.1016/0925-4005(91)80132-4
60. Chen SM, Peng KT, Lin KC (2005) Preparation of thallium hexacyanoferrate film and mixed-film modified electrodes with cobalt(II) hexacyanoferrate. Electroanalysis 17:319–326. https://doi.org/10.1002/elan.200403065
61. Zen JM, Chen PY, Kumar AS (2003) Flow injection analysis of an ultratrace amount of arsenite using a prussian blue-modified screen-printed electrode. Anal Chem 75:6017–6022. https://doi.org/10.1021/ac0301649
62. Liu R, Sun B, Liu D, Sun A (1996) Flow injection gas-diffusion amperometric determination of trace amounts of ammonium ions with a cupric hexacyanoferrate. Talanta 43:1049–1054. https://doi.org/10.1016/0039-9140(96)01858-9
63. Klink S, Ishige Y, Schuhmann W (2017) Prussian blue analogues: a versatile framework for solid-contact ion-selective electrodes with tunable potentials. ChemElectroChem 4:490–494. https://doi.org/10.1002/celc.201700091
64. US Department of Health and Human Services, Radiogardase® (2012). http://www.remm.nlm.gov
65. Altagracia-Martinez M, Kravzov-Jinich J, Martínez-Núñez J, Ríos-Castañeda C, López-Naranjo F (2012) Prussian blue as an antidote for radioactive thallium and cesium poisoning. Orphan Drugs Res Rev 13. https://doi.org/10.2147/odrr.s31881
66. Richmond CR (1968) Accelerating the turnover of internally deposited radiocesium, Diagnosis Treat Depos Radionuclides
67. Thompson DF, Church CO (2001) Prussian blue for treatment of radiocesium poisoning. Pharmacotherapy 21:1364–1367. https://doi.org/10.1592/phco.21.17.1364.34426
68. International Atomic Energy Agency (1988) The radiological accident in Goiânia, Vienna. doi:92-0-129088-8
69. Faustino PJ, Yang Y, Progar JJ, Brownell CR, Sadrieh N, May JC, Leutzinger E, Place DA, Duffy EP, Houn F, Loewke SA, Mecozzi VJ, Ellison CD, Khan MA, Hussain AS, Lyon RC (2008) Quantitative determination of cesium binding to ferric hexacyanoferrate: Prussian blue. J Pharm Biomed Anal 47:114–125. https://doi.org/10.1016/j.jpba.2007.11.049
70. Catalan R, Agrisuelas J, Cuenca A, Garcia-Jareno JJ, Roig AF, Vicente, F, Garc JJ (2015) Interfacial role of cesium in Prussian blue films. J Electrochem Soc 162 H727–H733. https://doi.org/10.1149/2.1061509jes
71. Kravzov J, Rios C, Altagracia M, Monroy-Noyola A, López F (1993) Relationship between physicochemical properties of prussian blue and its efficacy as antidote against thallium poisoning. J Appl Toxicol 13:213–216. https://doi.org/10.1002/jat.2550130313
72. Zhang H, Zhao X, Wei J, Li F (2015) Removal of cesium from low-level radioactive wastewaters using magnetic potassium titanium hexacyanoferrate. Chem Eng J 275:262–270. https://doi.org/10.1016/j.cej.2015.04.052

73. Loos-Neskovic C, Ayrault S, Badillo V, Jimenez B, Garnier E, Fedoroff M, Jones DJ, Merinov B (2004) Structure of copper-potassium hexacyanoferrate (II) and sorption mechanisms of cesium. J Solid State Chem 177:1817–1828. https://doi.org/10.1016/j.jssc.2004.01.018
74. Michel C, Barré Y, de Dieuleveult C, Grandjean A, De Windt L (2015) Cs ion exchange by a potassium nickel hexacyanoferrate loaded on a granular support. Chem Eng Sci 137:904–913. https://doi.org/10.1016/j.ces.2015.07.043
75. Yousefi T, Torab-Mostaedi M, Moosavian MA, Mobtaker HG (2015) Potential application of a nanocomposite: HCNFe@polymer for effective removal of Cs (I) from nuclear waste. Prog Nucl Energy 85:631–639. https://doi.org/10.1016/j.pnucene.2015.08.006
76. Arisaka M, Watanabe M, Ishizaki M, Kurihara M, Chen R, Tanaka H (2015) Cesium adsorption ability and stability of metal hexacyanoferrates irradiated with gamma rays. J Radioanal Nucl Chem 303:1543–1547. https://doi.org/10.1007/s10967-014-3710-0
77. Lilga MA, Orth RJ, Sukamto JPH, Rassat SD, Genders JD, Gopal R (2001) Cesium separation using electrically switched ion exchange. Sep Purif Technol. https://doi.org/10.1016/s1383-5866(01)00145-9
78. Chen R, Tanaka H, Kawamoto T, Asai M, Fukushima C, Kurihara M, Ishizaki M, Watanabe M, Arisaka M, Nankawa T (2013) Thermodynamics and mechanism studies on electrochemical removal of cesium ions from aqueous solution using a nanoparticle film of copper hexacyanoferrate. ACS Appl Mater Interfaces 5:12984–12990. https://doi.org/10.1021/am403748b
79. Chen R, Asai M, Fukushima C, Ishizaki M, Kurihara M, Arisaka M, Nankawa T, Watanabe M, Kawamoto T, Tanaka H (2015) Column study on electrochemical separation of cesium ions from wastewater using copper hexacyanoferrate film. J Radioanal Nucl Chem 303:1491–1495. https://doi.org/10.1007/s10967-014-3588-x
80. Ayrault S, Jimenez B, Garnier E, Fedoroff M, Jones DJ, Loos-Neskovic C (1998) Sorption mechanisms of cesium on $Cu^{II2}Fe^{II}(CN)_6$ and $Cu^{II3}[Fe^{III}(CN)_6]2$ hexacyanoferrates and their relation to the crystalline structure. J Solid State Chem 141:475–485. https://doi.org/10.1006/jssc.1998.7997
81. Sangvanich T, Sukwarotwat V, Wiacek RJ, Grudzien RM, Fryxell GE, Addleman RS, Timchalk C, Yantasee W (2010) Selective capture of cesium and thallium from natural waters and simulated wastes with copper ferrocyanide functionalized mesoporous silica. J Hazard Mater 182:225–231. https://doi.org/10.1016/j.jhazmat.2010.06.019
82. Parajuli D, Takahashi A, Noguchi H, Kitajima A, Tanaka H, Takasaki M, Yoshino K, Kawamoto T (2016) Comparative study of the factors associated with the application of metal hexacyanoferrates for environmental Cs decontamination. Chem Eng J 283:1322–1328. https://doi.org/10.1016/j.cej.2015.08.076
83. Zadronecki M, Linek IA, Stroka J, Wrona PK, Galus Z (2001) High affinity of thallium ions to copper hexacyanoferrate films. J Electrochem Soc 148:E348. https://doi.org/10.1149/1.1381074
84. Greenwood NN, Earnshaw A (1989) Chemistry of the elements. Pergamon Press, Oxford
85. Mizushima K, Jones P, Wiseman P, Goodenough JB (1981) Li_xCoO2 ($0 < x \leq 1$): a new cathode material for batteries of high energy density. Solid State Ionics 3–4:171–174. https://doi.org/10.1016/0167-2738(81)90077-1
86. Rongguo C, Juan G, Liwen Y, Huy D, Liedtke M (2016) Supply and demand of lithium and gallium
87. Wessells CD, Peddada SV, McDowell MT, Huggins RA, Cui Y (2012) The effect of insertion species on nanostructured open framework hexacyanoferrate battery electrodes. J Electrochem Soc 159:A98. https://doi.org/10.1149/2.060202jes
88. Mullaliu A, Sougrati M-T, Louvain N, Aquilanti G, Doublet M-L, Stievano L, Giorgetti M (2017) The electrochemical activity of the nitrosyl ligand in copper nitroprusside: a new possible redox mechanism for lithium battery electrode materials? Electrochim Acta 257. https://doi.org/10.1016/j.electacta.2017.10.107

89. Moritomo Y, Urase S, Shibata T (2016) Enhanced battery performance in manganese hexacyanoferrate by partial substitution. Electrochim Acta 210:963–969. https://doi.org/10.1016/j.electacta.2016.05.205
90. Song J, Wang L, Lu Y, Liu J, Guo B, Xiao P, Lee J-J, Yang X-Q, Henkelman G, Goodenough JB (2015) Removal of interstitial H_2O in hexacyanometallates for a superior cathode of a sodium-ion battery. J Am Chem Soc 137:150213162944002. https://doi.org/10.1021/ja512383b
91. Wessells CD, Peddada SV, Huggins RA, Cui Y (2011) Nickel hexacyanoferrate nanoparticle electrodes for aqueous sodium and potassium ion batteries. Nano Lett 11:5421–5425. https://doi.org/10.1021/nl203193q
92. Eftekhari A (2004) Potassium secondary cell based on Prussian blue cathode. J Power Sources 126:221–228. https://doi.org/10.1016/j.jpowsour.2003.08.007
93. Shiga T, Kondo H, Kato Y, Inoue M (2015) Insertion of calcium ion into Prussian blue analogue in nonaqueous solutions and its application to a rechargeable battery with dual carriers. J Phys Chem C 119:27946–27953. https://doi.org/10.1021/acs.jpcc.5b10245
94. Chae MS, Hyoung J, Jang M, Lee H, Hong S-T (2017) Potassium nickel hexacyanoferrate as a high-voltage cathode material for nonaqueous magnesium-ion batteries. J Power Sources 363:269–276. https://doi.org/10.1016/j.jpowsour.2017.07.094
95. Liu S, Pan GL, Li GR, Gao XP (2014) Copper hexacyanoferrate nanoparticles as cathode material for aqueous Al-ion batteries. J Mater Chem A 3:959–962. https://doi.org/10.1039/C4TA04644G
96. Ling C, Chen J, Mizuno F (2013) First-principles study of alkali and alkaline earth ion intercalation in iron hexacyanoferrate: the important role of ionic radius. J Phys Chem C 117:21158–21165. https://doi.org/10.1021/jp4078689
97. Wessells CD, Huggins RA, Cui Y (2011) Copper hexacyanoferrate battery electrodes with long cycle life and high power. Nat Commun 2:550. https://doi.org/10.1038/ncomms1563
98. Mullaliu A, Aquilanti G, Conti P, Plaisier JR, Fehse M, Stievano L, Giorgetti M (2018) Copper electroactivity in Prussian blue based cathode disclosed by Operando XAS. J Phys Chem C 122(2018):15868–15877. https://doi.org/10.1021/acs.jpcc.8b03429
99. Makowski O, Stroka J, Kulesza PJ, Malik MA, Galus Z (2002) Electrochemical identity of copper hexacyanoferrate in the solid-state: evidence for the presence and redox activity of both iron and copper ionic sites. J Electroanal Chem 532:157–164. https://doi.org/10.1016/S0022-0728(02)00965-8
100. Giorgetti M, Guadagnini L, Tonelli D, Minicucci M, Aquilanti G (2012) Structural characterization of electrodeposited copper hexacyanoferrate films by using a spectroscopic multi-technique approach. Phys Chem Chem Phys 14:5527. https://doi.org/10.1039/c2cp24109a

Chapter 7
Biosorbents and Composite Cation Exchanger for the Treatment of Heavy Metals

Muhammad Shahid Nazir, Zaman Tahir, Majid Niaz Akhtar and Mohd Azmuddin Abdullah

Abstract Heavy metals have seriously affected the quality of water, soil, and marine ecosystems. More economical, efficient and effective water purification and desalination methods need to be developed to remove persistent heavy metal ion contamination, especially in drinking water. Among low-cost methods with different degree of effectiveness for heavy metal ion removal highlighted in this chapter are the agro-based biosorbents and biopolymers based on cellulose, chitosan, and alginate. Factors influencing the efficiency of nanofiber membranes and packed-bed adsorbers have been addressed. Different types of composite ion exchangers are discussed.

7.1 Introduction

Environmental pollution is a major global concern today due to rapid industrialization and increases in population [1, 2]. Heavy metal ions such as mercury, plumbum, and cadmium may come from chemical industries, textile, mining, agriculture, cosmetics, paper, and leather, or from natural weathering of the earth's crust and soil erosion [3, 4]. Pollution from heavy metal ions and dyes has seriously

M. S. Nazir
Department of Chemistry, COMSATS University Islamabad, Lahore Campus (CUI), Islamabad 54000, Pakistan

Z. Tahir
Department of Chemical Engineering, COMSATS University Islamabad, Lahore Campus (CUI), Islamabad 54000, Pakistan

M. N. Akhtar
Department of Physics, Muhammad Nawaz Sharif University of Engineering and Technology (MNSUET), Multan 60000, Pakistan

M. A. Abdullah (✉)
Institute of Marine Biotechnology, Universiti Malaysia Terengganu, 21030, Kuala Nerus, Terengganu, Malaysia
e-mail: azmuddin@umt.edu.my

Inamuddin et al. (eds.), *Applications of Ion Exchange Materials in the Environment*,
https://doi.org/10.1007/978-3-030-10430-6_7

affected the environment with deleterious effects especially on water, soil, and marine ecosystems [5]. Though a number of heavy metals within permissible limit are good for health, they are highly toxic beyond limits and becoming indigestible in the body and accumulate in the soft tissue. Persistent accumulation destroys the nervous system, leading to skin allergies, kidney dysfunction, and increase in the risk of cancer. Arsenic, for example, is carcinogenic even at extremely low levels of exposure and therefore needs to be regulated and controlled [6]. Lead–acid batteries, wire or pipes, metal recycling and foundries release lead in large quantities to the environment and could cause lead poisoning and severe damages to the human body, organs, and tissues, especially children [7–9]. Mercury inhaled in the body gets oxidized and converted into inorganic ions (Hg^{2+}), entering the brain cells causing harmful diseases such as acrodynia, Hunter–Russell syndrome, and Minamata disease [10, 11].

Nutritionally essential metals for the body in specific quantities include iron, cobalt, copper, chromium (III), molybdenum, selenium, manganese, and zinc [12]. Below or beyond the permissible limit for the optimal nourishment of these metals will have dire consequences on health [13]. Some metal elements such as silicon, nickel, boron, and vanadium, though not identified as essential to human health and may supposedly have beneficial effects at low exposure levels, are still toxic at higher levels [14, 15]. It becomes imperative therefore to remove the heavy metal ions from the polluted system and contaminated water sources. Adsorption is potentially the most suitable technique for heavy metal separation due to its effectiveness, regeneration easiness, and inexpensive nature [16, 17]. Extensive research has been done to explore new adsorbents for the removal of heavy metal ions such as the waste material from forestry, fishery, and agricultural by-products [18]. This chapter is aimed to highlight the different types of agro-based biosorbents, biopolymers, packed-bed adsorbers, ionic membrane, and the cation exchanger materials for the removal of heavy metals.

7.2 Agro-Based Biosorbents for Heavy Metal Removal

Plant biomass is the most abundant resource in the world which mainly comprises of wood and agricultural waste such as seed, leaf, root, bark, peel, guava seeds, neem leaves, and eucalyptus bark. The agro-biomass, mainly consisting of cellulose, hemicelluloses, lignin, protein, sugar, water, starch, and diverse functional groups including amine, aldehyde, hydrocarbons, ketonic groups, is also suitable to be developed into biosorbents and will be efficient as agro-based products and by-products for wastewater treatment. These are mostly naturally abundant materials which are eco-friendly, easily accessible, economical in nature and have all been demonstrated to be the promising materials for the extraction of heavy metals from the aqueous phase. With the wide variety and flexibility for physical and chemical modification, biosorbents can be made more efficient and readily

Table 7.1 Different types of agro-based biosorbent for heavy metal ion removal

Cheap sorbent	Target metal	pH	Uptake of metal (approx. mg/g)
(1) *Seed part*			
Caesalpinia bonducella	Ni(II)	5	189
Guava	Cr(VI)	1	10.5
Papaya	Cu(II)	6	213
Prosopis juliflora	Pb(II)	6	40
Polyalthia longifolia	Cd(II)	6	21
Strychnos potatorum	Pb(II)	5	16
(2) *Leaf part*			
Pine	As(V)	4	3.3
Japanese plum	Cd(II)	6	29
Japanese plum ash	Cd(II)	6	21.3
Drumstick	Cd(II)	5	171
	Cu(II)	6	168
	Ni(II)	6	164
Azadirachta indica	Cr(V)	2	63
Helianthus annuus	Cu(II)	5–6	89
(3) *Root part*			
Water hyacinth	Cu(II)	5–6	32.5
	Cr(III)		34
Palm oil	Cu(II)	7	200
	Pb(II)		150
(4) *Bark part*			
White popinac	Cu(II)	6	147
	Cd(II)	5	168
	Pb(ii)	5	185
Eucalyptus globulus	Cr(VI)	2	45
Cryptomeria	Cr(VI)	3	72
Drumstick tree	Ni(II)	6	30.4
(5) *Peel part*			
Manioc	Pb(II)	8	5.8
	Cu(II)		8
	Cd(II)		293
Modified orange	Ni(II)	5.5	163
	Pb(II)		476
Citrus limetta	Cr(VI)	2	250
Punica granatum	Fe(II)	6	18.5
Cucumis melo	Pb(II)	4–5	168
Khamara	Cr(VI)	1–2	294

Adapted from [110]

applicable for large-scale removal of toxic heavy metal ions [19]. Table 7.1 lists the different types of agro-based biosorbents used for heavy metal ion removal.

Seeds, leaves, roots, barks, and peels are the different plant parts that have been reported as promising materials to be used as biosorbents for metal ion removal. Omri et al. prepared chemically activated carbon powder (with KOH) from *Ziziphus spina-christi* seeds (ZSAC) to remove Mn(II) from aqueous solutions [20]. The maximum adsorption capacity for Mn(II) was 172 mg/g. The use of *Nauclea diderrichii* seeds however achieved Cd(II) ion adsorption as 6.3 mg/g and Hg(II) ion sorption as 6.15 mg/g from aqueous solutions at 333 K [21]. Similarly, the pristine bamboo leave powder attained low Hg(II) sorption as 27.11 mg/g but comparable to Triton X-100 and SDS-modified materials [22]. The *Moringa oleifera* leaves were more promising for Ni(II), Cu(II), and Cd(II) ion removal with sorption capacities of 163.88, 167.9, and 171.37 mg/g, respectively [23]. Low sorption capacities of 32.51 and 33.98 mg/g, respectively, have also been reported for the removal of Cu(II) and Cr (III) from the wastewater by the *Eichhornia crassipes* roots [24]. The barks have exhibited different efficiencies. While the *acacia leucocephala* bark powder results have exhibited high adsorption capacities of 147.1, 167.7, and 185.2 mg/g for the removal of Cu(II), Cd(II), and Pb(II), respectively [25], the *M. oleifera* bark only achieved 30.38 mg/g for the removal of Ni(II) [26], and the *Eucalyptus* bark attained the sorption capacity up to 45 mg/g for the removal of Cr(VI) [27]. High adsorption capacities have been reported with chemically modified orange peel with 476.1, 293.3, and 162.6 mg/g sorption capacities for the removal of Pb(II), Cd(II), and Ni(II) ions, respectively [28]. The use of mosambi peel and *Trewia nudiflora* fruit peel to remove Cr(VI) ions also resulted in high sorption capacity of around 250 and 294.12 mg/g, respectively [29, 30]. The mango peel waste (MPW) on the other hand only obtained the adsorption capacities of 46.09, 39.75, and 28.21 mg/g for the removal of Cu(II), Ni(II), and Zn (II), respectively from aqueous solutions and real electroplating industry wastewaters. FTIR characterization studies suggested that carboxyl and hydroxyl functional groups played prominent roles in the adsorption of metallic ions [31].

Heavy metal ions have also been separated from aqueous solutions by using various types of a stalk of sunflower, *Zea maize,* and corn with different extent of adsorption capacities. The cornstalks modified via graft copolymerization for the sequestration of Cd (II) from aqueous solution has exhibited the important effects of adsorbent dosage and pH range of 3–7 to achieve more than 90% metal removal, following the Langmuir and Freundlich isotherm models [32, 33]. Husk is another form of agricultural residues which may come in the form of rice husk, Bengal husk, hazelnut husk, and coffee husk that can be processed into biosorbents. Modification of rice husk through tartaric acid and carboxylic acid and used to remove Cu(II) and Pb(II) ions has resulted in sorption capacities of 29 and 108 mg/g, respectively, at room temperature, and the kinetics data were well fitted to the Langmuir isotherm [34]. High sorption of Cr (III) from aqueous solutions at 91.64 mg/g has also been reported for Bengal gram husk [35], but the coffee husk as an adsorbent for Zn(II), Cu(II), Cd(II), and Cr(VI) removal achieved far lower sorption capacities of 5.6, 7.5, 6.9, and 7 mg/g, respectively [36]. Plant fiber is

mainly composed of cellulose, hemicellulose, lignin, and pectin, and the metal adsorption takes place in the fibers due to the presence of functional groups such as carboxylic, phenolic, hydroxylic, and carbonyl groups. Bagasse, an agricultural solid waste from the sugar industry, is composed of lignin, pentose, and cellulose as major constituents, and hence, the presence of carboxylic, carbonyl, amine, and hydroxyl groups helps in the binding of metal ions through cation exchange on adsorptive sites. Sugarcane bagasse as a biosorbent for Ni(II) ion uptake has shown the maximum nickel ion uptake of 2 mg/g at STP, following the Langmuir, Freundlich, and Sips isotherm models [37]. Low sequestration of Pb(II), Cd(II), and Zn(II) from aqueous solutions as 36,14 and 8 mg/g, respectively, have also been reported using raw agave bagasse adsorbent [38]. Pb(II) ion removal at 6.366 and 7.297 mg/g adsorption capacity using both the pristine and modified bagasse with sulfuric acid, respectively [39], and 35.71 mg/g mercury sorption on sugarcane bagasse [40], have been reported. The lignocellulose from *Citrus* reticulate modified with H_2SO_4 and EDTA attained sorption capacities of 87.14 and 86.4 mg/g, respectively, for Cu(II) and Zn(II), and kinetics were well fitted to the Langmuir isotherm [41]. The raw oil palm empty fruit bunch fibers (EFB) developed as biosorbent without any chemical modification exhibited more than 92% adsorption efficiency with the highest Pb(II) sorption as 47.98 mg/g after 90 min at pH 7.5 [42] and reached to 94% efficiency at 0.005–0.02 mm powder size with 47.49 mg/g Pb (II) ion removal at pH 7.5, in 60 min [43]. The Pb(II), Zn(II), and Ni(II) sorption remained around 48.4, 43.51, and 31.77 mg/g, respectively, at pH 7 utilizing magnetic (empty fruit bunches) EFB biosorbent [19]. The EFB cellulosic fibers modified with EDTA showed the highest Pb(II) adsorption as 236.7 mg/g sorbents [44]. The EFB cellulose and hydroxyapatite when developed into chemically modified carbon electrode (Cellulose-HAp-CME) composite have successfully detected trace Pb(II) ions in the complex medium such as blood serum, in the physiologically relevant range of 10–60 ppb, resulting in the limit of detection (LOD) of 0.11 ppb and limit of quantification (LOQ) of 0.36 ppb. The enhanced sensor sensitivity has been attributed to the hydroxyapatite being successful in capturing the Pb from aqueous media, and its composite with cellulose further provided a large number of ligands to allow metal ion sorption via surface complexation or ionic exchange reaction [45].

7.3 Biopolymers

7.3.1 Functional Groups

Biomaterials extracted from organisms such as plant, bacteria, fungi, and algae have been comprehensively studied as substitute adsorbent for heavy metal ion removal (Table 7.2) [44, 46, 47]. Adsorbents based on biomaterials and biopolymers have been more popular than the conventional synthetic adsorbents due to their abundance, low cost, biodegradability, non-toxic nature, and the intrinsic functional

moieties on the surfaces facilitating their use without the need for elaborate functionalization procedures [48]. Biosorption can be explained by mechanisms such as physicosorption, chemisorption, microprecipitation, ion exchange, and chelation. Metal ion bonding relies on adsorbent constituents, effective sites in different functional groups, and the interaction of biosorbents and the liquid solvent with the dissolved materials [46]. The cellulose, hemicelluloses, lignin, and pectin with a small amount of protein in some biomaterials provide affinity toward metal ions, and the functional groups such as phenolic groups, aromatic amines, ethers, ketones, aldehydes, and carboxylic group significantly increase metal ion affinity to make weak or strong bonds. In aqueous media, polysaccharides and proteins also provide active sites to bind metal ions. Among several groups, the sulfur group is more significant in adsorption with high affinity toward heavy metals [44, 49]. The xanthate group, one of the sulfur-containing groups used to adsorb heavy metals efficiently, is highly stable in the basic medium due to the presence of sulfur and has high adsorption capacity. Modified sugarcane bagasse with xanthate group has been developed where the presence of polysaccharides necessitates no refractory post-treatment like the ion-exchange chelating resins of plastic. The two types of novel bioadsorbents, the charred xanthate sugarcane bagasse (CXSB) and charred aminated sugarcane bagasse (CASB), are efficient cation exchangers for the removal of cadmium, lead, copper, nickel, and zinc ions from the aqueous solution [49]. Surface-modified cellulose sorbents from EFB have been suggested to play dual functions in environmental remediation: firstly for heavy metal removal from the wastewater, and secondly for the use of metal-loaded sorbent in the desulfurization of diesel. The developed sorbent materials with high S removal and low C content reduction characteristics have been very efficient [44]. The two most abundant biopolymers—cellulose and chitosan—and the ionic membranes and packed-bed adsorber will be elaborated further in the following sections.

7.3.2 Cellulose

Cellulose and hemicelluloses are the most abundant biopolymers, already processed in refining industries such as pulp mills, with no ecological footprints as compared to starch which can be used as a food source [50]. One promising water-soluble hemicellulose is *O*-acetyl galactoglucomannan (GGM), produced from softwood by pressurized hot water extraction (PHWE) or by the thermomechanical pulping process by ultrafiltration of wastewater. A by-product of the pulping industry, GGM, therefore, exists in huge quantities with tremendous prospects as a renewable raw material for novel functional products. GGM has a linear backbone of randomly distributed (1 → 4)-linked β–d-mannopyranosyl (Manp) and (1 → 4)-linked β–d-glucopyranosyl (Glcp) monomers, with β–d-galactopyranosyl (Galp) units as single side units [51]. Partially acetylated and the *O*-acetyl groups of GGM

Table 7.2 Different types of adsorber and the corresponding functional groups for heavy metal ion removal

Name	Functional groups	Ions removed	Type	Organic polymer	Inorganic matrix
Ascophyllumnodosum (brown marine macro-algae)	Carboxylic and sulfonic groups	Na^+, K^+, Mg^{2+}, Ca^{2+}, or Cu^{2+} removal	Biomass		
Poly-*o*-anisidine Sn(IV) tungstate		Hg^{2+}	Organic–inorganic type composite cation exchanger		
Polyaniline zirconium(IV) arsenate		Ba^{2+}–Pb^{2+}, Pb^{2+}–Ni^{2+}, Cd^{2+}–Hg^{2+}, Ni^{2+}–Hg^{2+}, Zn^{2+}–Pb^{2+}, Ca^{2+}–Bi^{3+}, Al^{3+}-Hg^{2+}, Ca^{2+}–Pb^{2+}			
Cladophora sp. (chitosan/algal)		Cd^{2+}, Zn^{2+}	Biomass		
Polypyrrole Sn(IV) phosphate		K^+, Na^+, Ca^{2+}, Cd^{2+}, Cu^{2+}, Hg^{2+}, Ni^{2+}, Mn^{2+}, Zn^{2+}	Organic–inorganic type composite cation exchanger		
Polymethacrylic acid-grafted chitosan/bentonite (PMAA-g-CS/B)	–OH and $–NH_2$ backbones	Pb^{2+}	Biomass		
Polyvinyl alcohol Sn(IV) tungstate		Aniline			
Poly-*o*-toluidine Zr(IV) phosphate		Hg^{2+}	Organic–inorganic type composite cation exchanger		
Polypyrrole zirconium titanium phosphate (PPZTP)		Na^+, K^+, Mg^{2+}, Ca^{2+}, Sr^{2+}, Ba^{2+}		Polypyrrole	ZTP
Polyaniline Sn(IV) silicate		Cd^{2+}			
ISME based on graphene Th(IV) phosphate		Pb^{2+}	Ion-selective membrane		
Polyaniline-Zr(IV) selenoiodate		Li^+, Na^+, K^+			
Polyaniline-Zr(IV) selenomolybdate		Li^+, Na^+, K^+			
Polythiophene/tinphosphate		Hg^{2+}			
(PEDOT:PSS) Zr(IV) phosphate		Cd^{2+}			
Polyethylenimine-modified fungal biomass		Cr^{4+}	Biomass		

(continued)

Table 7.2 (continued)

Name	Functional groups	Ions removed	Type	Organic polymer	Inorganic matrix
Poly-*o*-toluidine zirconium (IV) iodosulfosalicylate		Cr^{3+}	Organic–inorganic type composite cation exchanger		
Single-walled carbon nanotube cerium(IV) phosphate		Cd^{2+}			
Poly-*o*-toluidine zirconium (IV) iodosulfosalicylate		Cr^{3+}			
Sodium dodecyl sulfate-ironsilicophosphate (SDS-FeSP)		Zn^{2+} and Mg^{2+}			
Tin(IV) tungstoselenate		Ba(II)			
Antimonic acid		Na(I)			
Chromium ferrocyanide		K(I)			
Niobium antimonate		Mg(II)			
Stannic selenite		Li(I)			
Stannic boratomolybdate		Zr(IV)			
Aluminum antimonate		Ag(I)			
Bismuth tungstate		Pb(II)			
Cerium antimonate		Hg(II)			
Cobalt antimonate		Bi(III)			
Thorium phosphate		Sr(II)			
Ammonium molybdophosphate loaded on silica matrix (SM-AMP20, 20 wt% AMP)		Cs^{+}			
Polypyrrole Sn(IV) arsenotungstate (PPy-SnAT)					
Phosphorylated fullerene/ sulfonated polyvinyl alcohol (PFSP)		Cu^{2+}	Membrane		
Graphene Th(IV) phosphate		Pb^{2+}			

Adapted from [110]

are positioned arbitrarily at C2 and C3 positions of the mannose monomers in the main chain. For ion removal use, GGM derivatives can be synthesized with either charged or neutral groups, by substituting the hydroxyl groups or the charged polymers attached to the reducing end of GGM. The GGM-based hydrogels have been synthesized where the GGM fractions react with glycidyl methacrylate in transesterification reaction, followed by GGM macro-monomers applied as

biobased cross-linkers in the preparation of numerous hydrogels via methacrylic monomer bearing a quaternary ammonium group. These have been tested as a bioadsorbent for the removal of toxic As and Cr ions from aqueous solutions [51].

Hydrogels are three-dimensional cross-linked polymer network structures consisting of hydrophilic copolymers prepared from biopolymers such as cellulose, chitosan, starch, and alginate, which are effective for metallic ion removal and biocompatible, low cost, easily available, and biodegradable. Novel hydrogel beads via blending and dissolving cellulose and collagen in ionic liquid (IL), 1-butyl, 3-methylimidazolium chloride [C4mim]Cl have been synthesized and characterized. The mechanical properties of the hydrogel beads are enhanced due to the presence of cellulose. Among important factors influencing sorption efficiency onto the collagen/cellulose hydrogel beads (CCHBs) are the collagen/cellulose mass ratio, contact time, pH, and initial Cu(II) solution concentration [52]. Lignocellulosic materials have different types of functionalities for metal ions uptake, but the sorption capacity may not be that significant. The sorption capacity of cellulosic materials can be enhanced to a greater extent through chemical modification such as introducing highly efficient and selective polysaccharide-based super-sorbents having single kind of functional groups such as in hydroxyethyl cellulose (HEC) for metal ion adsorption. The HEC-Suc-Na sorbents have been applied for Pb(II), Cr(VI), Co(II), Cu(II), and Ni(II) sorption in aqueous solution and regenerated [53, 54]. Succinylated cornstarch, polysaccharides, and chitosan are also attaining significance in metallic ion removal due to high sorption capacity, cheap, commercial accessibility, eco-friendly nature, and strong affinity toward Pb, Cd, and Cu ions and dyes [54–58].

7.3.3 Chitosan

Chitosan is a linear polysaccharide-type natural polymer consisting of β-[1–4]-2-acetamido-2-deoxy-d-glucose units with unique features for heavy metal ion removal, biological, chemical, and pharmaceutical applications. Originated from the chitin component of the shells of a crustacean such as crab, shrimp, and cuttle fish, chitosan is the second largest organic compound after cellulose and it is easily available in nature, biocompatible, biodegradable, non-toxic, and suitable for metal ion chelation [59–64]. However, chitosan has limited applications due to its specific solubility in few dilute acid solutions and hence physical and chemical modifications are required to overcome the drawbacks such as the graft copolymerization of vinyl monomers. Chitosan can be grafted with different types of functionalities, i.e., the free amino groups on deacetylated units and hydroxyl groups on the C3 and C6 carbons on acetylated or deacetylated units (Fig. 7.1). Grafted chitosan is responsible for the covalent binding of other molecules in the chitosan backbone [65]. Zeta potential and functionality of polymers can be enhanced by grafting up to two monomers which impart two different side chain connections to the backbone for

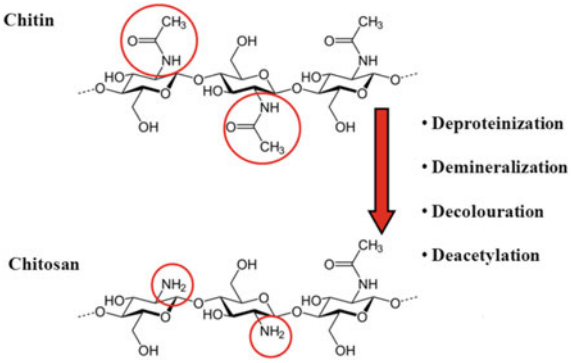

Fig. 7.1 Representative structure of chitosan, showing monomer identities, and linkage types [111]

cross-linking. Double-grafted copolymers using styrene and isoprene have centipede-like copolymers resembled structure with promising characteristics including water insolubility and enhanced active sites for the removal of heavy metals from aqueous solutions [66]. Chitosan-g-maleic anhydride-g (methacrylic acid) has been synthesized via copolymerization of chitosan, maleic anhydride, and methacrylic acid (ceric ammonium nitrate used as initiator) and applied for the removal of Cu(II) and Pb(II) from aqueous solutions [67].

The adsorption capacity of chitosan can be enhanced by blending with nanosized particles of zinc oxide, nano-zero-valent iron, or titanium oxide. Nanosized titanium oxide (TiO_2) has specific characteristics such as high physical and chemical stabilities, good mechanical strength, adequate chemical resistivity, and a higher surface area to improve the adsorption capacity of chitosan. Chitosan/TiO_2 nanofibrous adsorbents have been synthesized by two methods involving TiO_2 nanoparticle-coated chitosan nanofibers, followed by electrospinning of chitosan/TiO_2 solutions. The results for the removal of Pb(II) and Cu(II) ions in a batch-mode binary system showed that the chitosan/TiO_2 composite nanofibrous adsorbent was superior to TiO_2-coated chitosan nanofibers [68]. A metal becomes positively charged species by losing electrons present in the outermost orbit. When positive charge character on the metal increases, it behaves as Lewis acid and can readily combine with the negatively charged species like phosphate which is a strong Lewis base. Metal ions anchored composites like Zr^{4+}, Fe^{3+}, and Ca^{2+} loaded onto chitosan-supported bentonite (CSBent) (Fig. 7.2) achieving 40.86, 22.15, and 13.44 mg/g phosphate removal, better than individual CSBent [69]. Chitosan/algal (*Cladophora* sp.) composite microbeads have been produced and used for the removal of heavy metal ions. Bleached algal biomass was incorporated into the chitosan matrix through cross-linking with glutaraldehyde. The sorption capacity of the microbeads was high for Cr(III) and Cu(II), but the microbeads with bleached algal biomass exhibited higher sorption capacity for Cd(II) and Zn(II) ions compared to the plain glutaraldehyde cross-linked chitosan microbeads, suggesting the contribution of the algal biomass to the sorption [70].

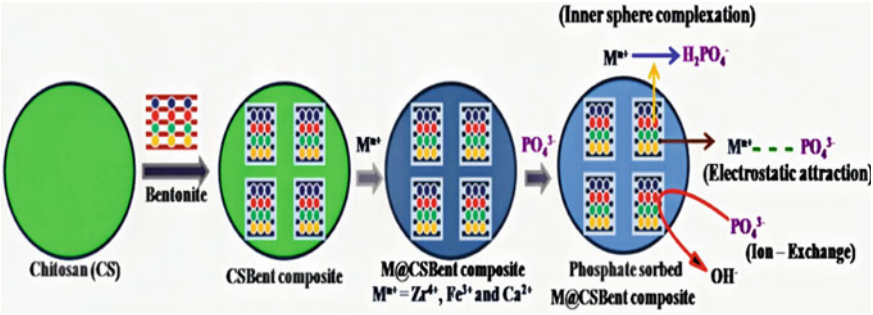

Fig. 7.2 Metal ions anchored composites loaded onto chitosan-supported bentonite (CSBent) and the phosphate removal [69]

7.3.4 Nanofiber Membranes and Packed-Bed Adsorbers

Nanofibrous membrane adsorbents or electrospun fibers (Fig. 7.3) have attained prominence for adsorption of metal ions due to specific characteristics including high specific surface area and porous structure [71]. Sodium alginate (SA), a linear natural polysaccharide consisting of 1,4-linked-b-D-mannuronic acid and a-L-guluronic acid residues, has received considerable attention as adsorbent for the removal of heavy metals, not only because of its biodegradability, hydrophilicity, and abundance in nature, but more due to the presence of carboxylate groups (COOH) which could form complex with variety of multivalent ions [72–74]. However, sodium alginate as hydrogel or adsorbent has the poor mechanical strength and the mechanical strength can be enhanced by physical or chemical modification through the addition of functional groups, incorporation of organic or inorganic filler, hydrophilic vinyl monomers grafting, or chemical blending with other polymers [72]. Marine algae are the major source of SA [75] where the polymers may be dissolved for blending in a common solvent for subsequent cross-linking reaction, melt mixing, or forming interpenetrating networks (IPN) of the polymers [76]. Sodium alginate-polyaniline (SAP) nanofibers have been evaluated as an adsorbent for the removal of Cr(VI) ion from aqueous solution by batch mode. The existence of the electrostatic interaction between the Cr(VI) ions and SAP nanofibers has been proposed where the Langmuir maximum sorption capacity of SAP nanofibers for Cr(VI) ion at 303 K was calculated to be 73.34 mg/g, and the desorption and regeneration experiment further showed that the SAP nanofibers can be reused for more than three successive cycles [72].

Chitosan nanofibers consist of complex chemical structure, involving strong inter- and intramolecular interactions, and thus are difficult to synthesize by electrospinning [77]. Electrospinnability can be enhanced by blending chitosan with polymers such as poly(vinyl alcohol), poly(ethylene oxide), polyacrylamide, and silk [78, 79]. Specific surface area and porous structure of membrane strongly influence the adsorption capacity of electrospun membrane [80]. Chitosan has −OH

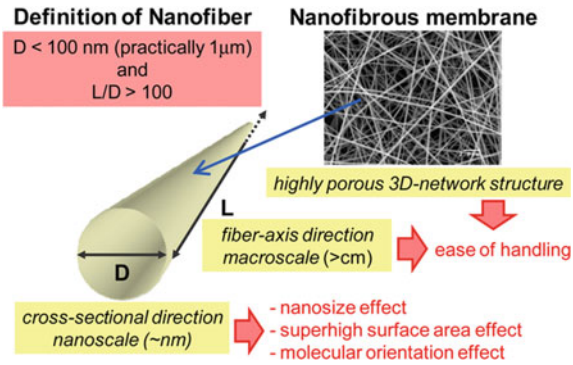

Fig. 7.3 Nanofiber membrane [112]

and $-NH_2$ groups for interacting with heavy metal ions and can be readily cross-linked to make it an efficient matrix for composite material fabrication [81]. Chitosan is promising material with significant characteristics such as cross-linking nature toward glutaraldehyde, epichlorohydrin, and β-cyclodextrin polyaldehyde and has shown high affinity for heavy metal ions [48]. Chitosan/poly(ethylene oxide) (PEO) membranes at different chitosan loadings have been fabricated. The chitosan/PEO membrane does not contain beads mesopores and high specific surface area due to the hydrogen bonding among chitosan and PEO molecules; this membrane showed high adsorption of Cu(II), Zn(II), and Pb(II) ions at 120, 117, and 108 mg g^{-1}, respectively [82]. Chitosan/polyvinyl alcohol (PVA)/zeolite nanofibrous composite electrospun membranes have been developed by incorporating zeolite as filler. Zeolite has been extensively used as an adsorbent with inherent ideal structure for heavy metal ion sorption. It mainly consists of three components: aluminosilicate framework, exchangeable cations, and water within the pores. Heavy metal ions are retained by zeolite due to its porous surface and also due to exchange of cations. The composite nanofibrous membranes, due to incorporation of zeolite, have the swelling during operation reduced with fast removal of Cr(VI), Fe(III), and Ni(II) [83]. Cross-linked hydrogels synthesized from *N*,*N*,*N*-trimethyl chitosan chloride (*N*-quaternized chitosan) (NQC) and poly (acrylic acid) (PAA) in variable weight ratios (3:1), (1:1), and (1:3) have been characterized for biodegradation in simulated body fluid (SBF) and cytotoxicity against HepG-2 liver cancer cells. The hydrogels formed via electrostatic and H-bonding interactions are more crystalline compared to both NQC and PAA matrices. These are more easily biodegradable exhibiting better adsorption capacities to Fe(III) and Cd(II) ions compared to chitosan, but lesser adsorption capacities toward Cr(III), Ni(II), and Cu(II) ions than the chitosan. The synthesized hydrogels exhibited better antibacterial activities against gram-positive and gram-negative bacteria as compared to NQC alone. Additionally, upon increasing the hydrogel concentration in the culture medium, the inhibition rate was also enhanced [84].

Packed-bed adsorbers have been extensively used for water sanitation and pollution control and have considered advantageous for groundwater, wastewater, and industrial waste treatment [85]. Packed-bed columns such as the cellulose

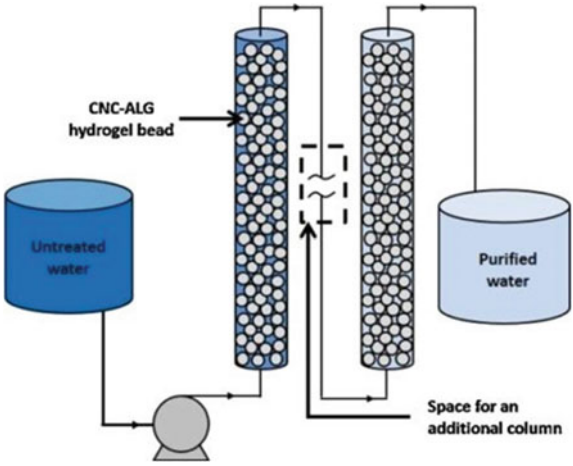

Fig. 7.4 Cellulose nanocrystal-alginate (CNC-ALG) hydrogel bead column [90]

nanocrystal-alginate (CNC-ALG) hydrogel bead column (Fig. 7.4) provide information on the operating conditions such as breakthrough and saturation conditions, mass transfer parameters, process feasibility, and costs and are capable to treat the specific amount of wastewater in short time periods. The performance is influenced by factors such as feed flow, the concentration of pollutant, properties of fluid, bed configuration, and multicomponent systems due to competitive adsorption, i.e., organic and inorganic material mixtures (heavy metals, dyes, pharmaceuticals, and others) [86–88]. Competitive adsorption causes a decrease in performance of adsorbent in both batch reactors and packed-bed column. Several researchers have reported that the instantaneous exclusion of different heavy metal ions implies competitive adsorption via a diverse range of adsorbents including activated carbons, zeolites, and other materials. The efficiency of these multimetallic systems mainly depends upon the nature and number of the co-ions, pH, concentration, and temperature. Competitive adsorption is thought to be the best in packed-bed columns instead of batch reactors, for the removal of heavy metal ions, due to the lower residence time than the adsorption equilibrium time. Moreover, mass transfer resistances are considerable in this operating setup. Consequently, continuous adsorption systems should be intensified to enhance their performance for the removal of heavy metal ions and to make the whole process economical for water treatment [89, 90].

7.4 Composite Ion Exchangers

Composite ion-exchange materials are promising materials among ion exchangers to address environmental and industrial problems. The organic and inorganic ion-exchange materials have some limitations when used individually. The organic

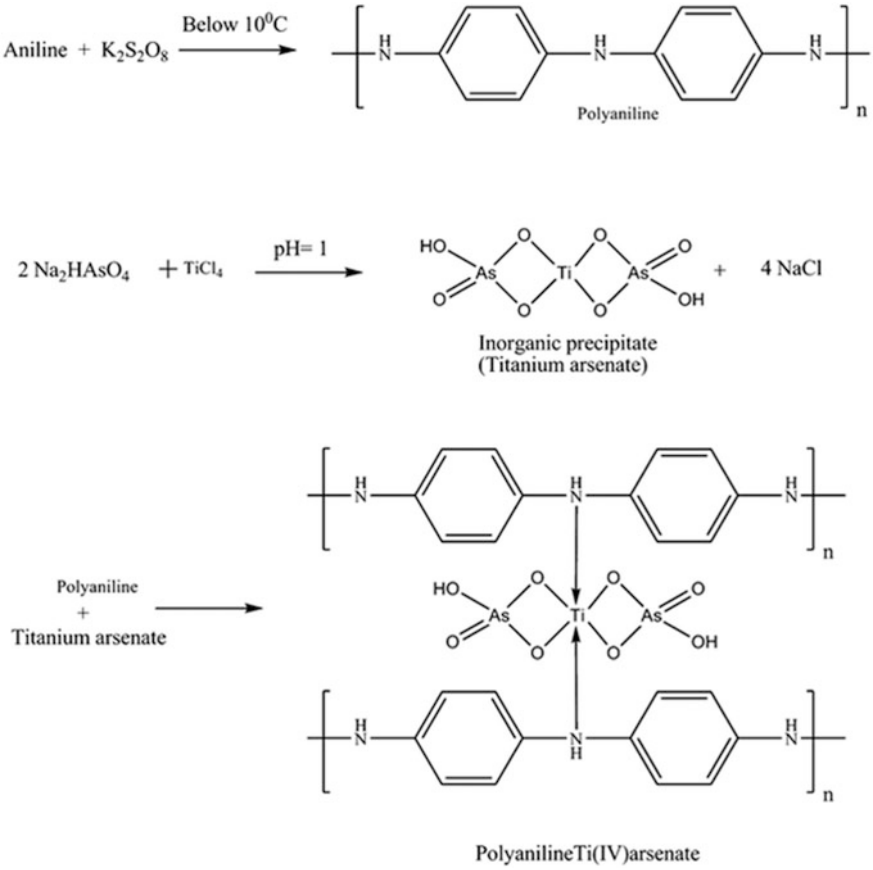

Fig. 7.5 Polyaniline-Ti(IV) As cation exchanger (proposed structure) [95]

ion exchangers have low mechanical strength and degrade at high temperatures or when exposed to the radiated environment, while the inorganic ion exchangers are difficult to acquire in granular form. The hybrid ion exchangers have, therefore, addressed the individual drawbacks with dual advantages of the promising characteristics of a polymer and the fundamental properties of an inorganic exchanger. Ion-exchange composite fabrication with controlled functionality and hydrophobicity has opened up a new path for the synthesis of new organometallic materials with superior ion exchange capacity, granulometric properties, reproducibility, high chemical and thermal stabilities, and also good selectivity for heavy metals. Composites, due to their intercalation properties, have been preferred for ion-exchanging processes, ion-selective electrodes, catalysts, sorbents, and in the host–guest chemistry to separate radioactive isotopes as well as in pollution control and waste water treatment [91–94]. Polyaniline (PANI)-based composite materials have been used globally with commercially existing conducting polymers due to

their promising characteristics including proton doping ability, cost-effectiveness, easy synthesis, exceptional redox recyclability, variable electrical conductivity, and thermal and chemical stabilities. These intrinsic characteristics have made PANI composites suitable as an ion exchanger, catalyst, and ion-selective electrode and applicable to economical pollution control and water treatment. The PANI-Ti(IV) composite (Fig. 7.5) achieves enhanced thermal stability up to 78% (400 °C) and chemical stability, improved capability to remove heavy metals and photochemical degradation of dyes, and considerable ion exchange capacity (1.37 meq g^{-1}) [95].

Ion-exchange hybrid membranes (IEMs) are promising as active separators in various electrically driven techniques such as demineralization of sugarcane juice, production of basic chemical and industrial products as well as biological waste treatment. Membrane processes are more reliable as compared to other traditional techniques due to low energy requirements, economical viability, and low ecological footprints [96–98]. The IEMs have been fabricated by the cross-linking of multisilicon copolymers. Maleic anhydride (MA), sodium styrene sulfonate (SSS), and ©-methacryloxypropyltrimethoxy silane (©-MPS) were copolymerized to form ternary multisilicon copolymer, followed by cross-linking with polyvinyl alcohol (PVA) to obtain cation-exchange hybrid membranes. The as-synthesized hybrid membranes are made up of multifunctional groups –SO_3Na, –COOH, and –Si–OH from the multisilicon copolymer, and –C–OH from PVA and cross-linked together via –Si–O–Si–, –Si–O–C– and –(C=O)–O–C– bonding (Fig. 7.6). The fabricated hybrid membranes consisting of poly(MA-CO-SSS-CO-©-MPS) polymer achieved tensile strength (*TS*) of 25.6–32.1 MPa and elongation at break (E_b) of 68–161%. The enhanced filler concentration improves the swelling resistance at room temperature or 65 °C. Another example of the use of a hybrid membrane is in diffusion dialysis (DD) (Fig. 7.7). The –SO_3Na groups, present in the chain, can act as strong ion-exchange sites to facilitate counterion (Na^+) transport. Hydrogen bonding can take place among –OH groups and the co-ions (OH^-). Further, –COOH groups are known as weak acidic groups and can behave as a weak ion-exchange or hydrogen-bonding provider. The membranes have exhibited high dialysis coefficient of OH^- ions (0.011–0.019 m/h and 0.021–0.031 m/h at 20 and 40°C, respectively). The higher numbers of hydrophilic –OH and Si–OH groups in the membrane matrix control the structure of PVA-based hybrid membranes [99].

Polyvinyl chloride (PVC)-based heterogenous strong acidic cation-exchange membranes have been synthesized (Fig. 7.8) via solution casting method using ionic liquid (IL) tetradecyl(trihexyl)phosphonium decanoate and dioctyl phthalate (DOP) as plasticizers and the suspension polymerized polyvinylchloride (S-PVC) as well as the emulsion polymerized polyvinylchloride (E-PVC) as binders [100]. The DOP-fabricated membranes exhibited transport number around 0.5, while the IL-contained membranes—1.0. The Na^+ ion diffusivity values through the membrane were of magnitude 5 as measured by the Donnan dialysis method [100]. Another novel IL-based nanocomposite heterogeneous cation-exchange membranes have been developed via solution casting method and phase inversion technique by incorporating inorganic ion-exchanger tin(IV) antimonophosphate and 1-dodecyl-3-methylimidazolium bromide, [C_{12}mim][Br]. The concentration of IL

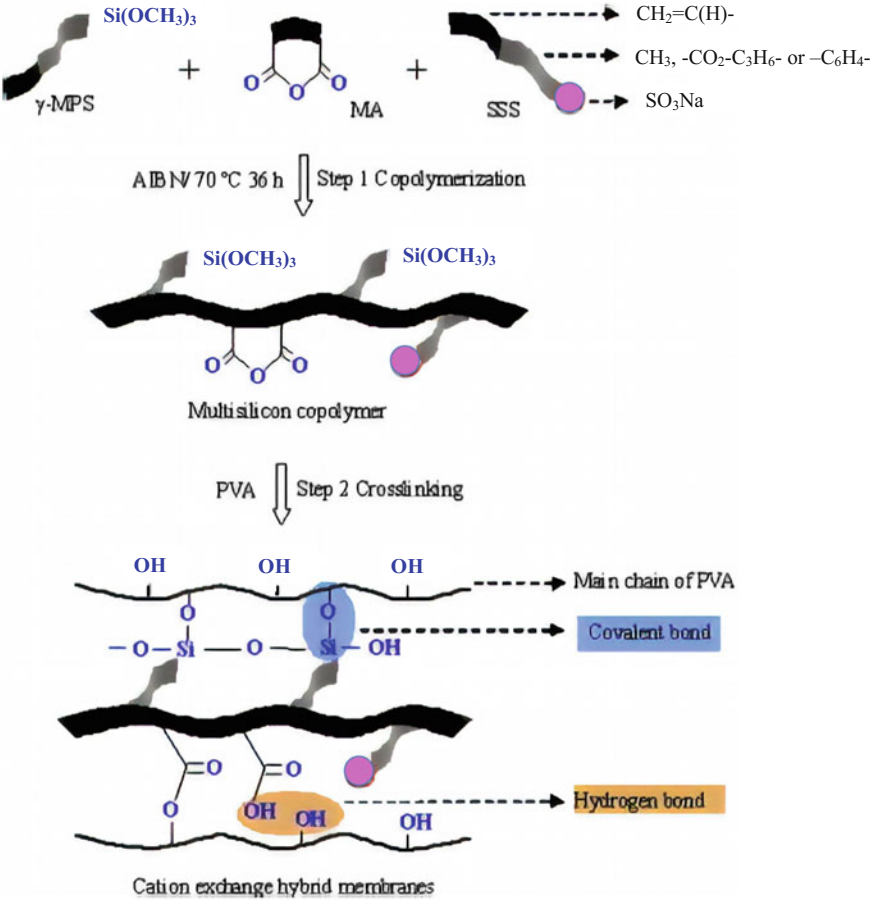

Fig. 7.6 Cation-exchange hybrid membrane based on multifunctional groups $–SO_3Na$, –COOH, and –Si–OH from the multisilicon copolymer, and –C–OH from PVA. Modified from [99]

was varied in the synthesized membranes to investigate its influence on the physical, chemical, morphological, and electrochemical properties. The PVC and tetrahydrofuran (THF) were used as the film-forming binder and the solvent, respectively. The long-chain IL with weaker interactions toward the ion exchanger could enhance the membrane performance without leaching out. IL imparts specific properties to the membrane matrix such as low IL concentration resulting in weak interactions, while higher IL concentration increases the hydrophobic interactions among alkyl chains of its own [101].

Nanocomposites with polymer/layered silicate have attracted immense interest due to their exceptional performances as compared to the conventional composites. Incorporation of inorganic particle-filled composites enhances physical and mechanical properties, thermal and chemical resistance, and gas barrier, resulting in

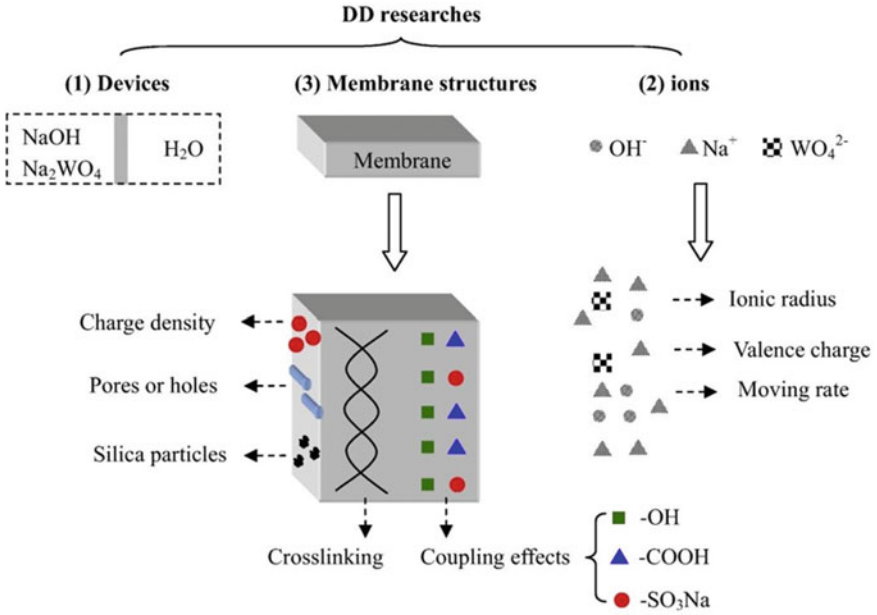

Fig. 7.7 Diffusion dialysis depicting $–SO_3Na$ groups, present in the chain, that act as strong ion-exchange sites to facilitate counterions (Na^+) transport [99]

high-performance materials at an affordable cost. The polymer–clay nanocomposites have been fabricated via solution intercalation, melt intercalation, and in situ polymerization. The allocation and distribution of the layered silicate in the polymer matrix impart favorable properties to the nanocomposites to fulfill the main aim of fabrication procedures by attaining the best distribution of the clays in the polymer matrix with a strong polymer–clay interaction. The major drawbacks with the solution and melt intercalation techniques are the requirement of huge quantities of solvent and the polymer penetration into the interlayer space at the low speed. The in situ polymerization technique and the clay/polymer nanocomposites with high homogeneity, on the other hand, allow the swelling of the organoclay, leading to external stimulation of reactive groups attached to the surface, followed by the polymer forming among the intercalated sheets. In situ polymerization allows homogeneous distribution and plays a vital role in the exfoliation process [102, 103]. Photopolymerization has been rarely used to fabricate polymer/montmorillonite clay nanocomposites. In nanocomposite formation, the initiation step is of significant importance and the photoinitiated cationic polymerization has become promising with the discovery of iodonium and sulfonium salts, in which on high irradiation, the absorption decays to yield protons [104, 105].

The diphenyliodonium-loaded clay as an initiator as well as inorganic filler has been used to synthesize Poly(cyclohexene oxide)-Montmorillonite (PCHO/clay) nanocomposite through in situ photoinitiated polymerizations (Fig. 7.9). The actual

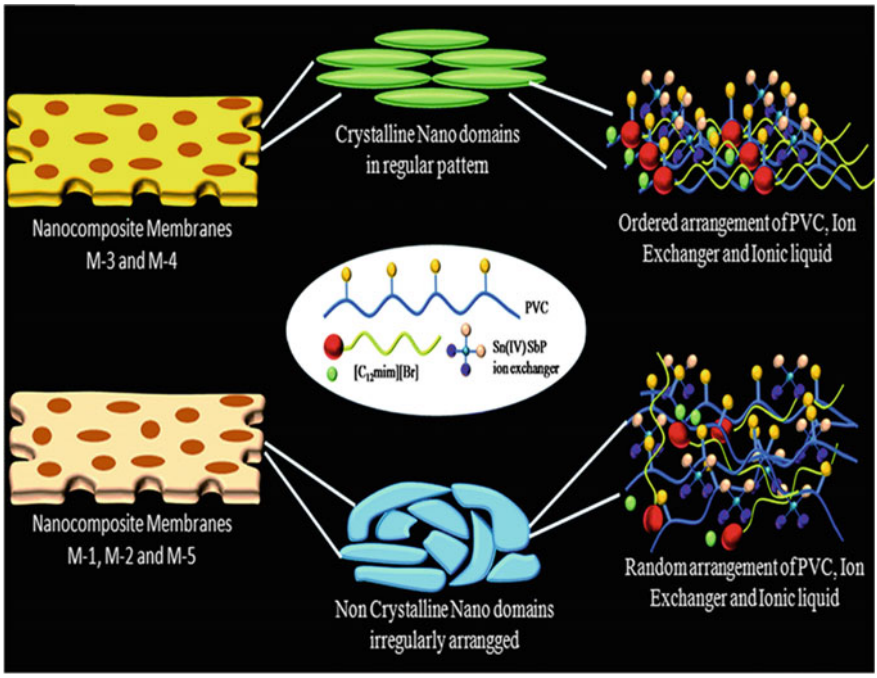

Fig. 7.8 Polyvinyl chloride (PVC)-based heterogenous strong acidic cation-exchange membranes [101]

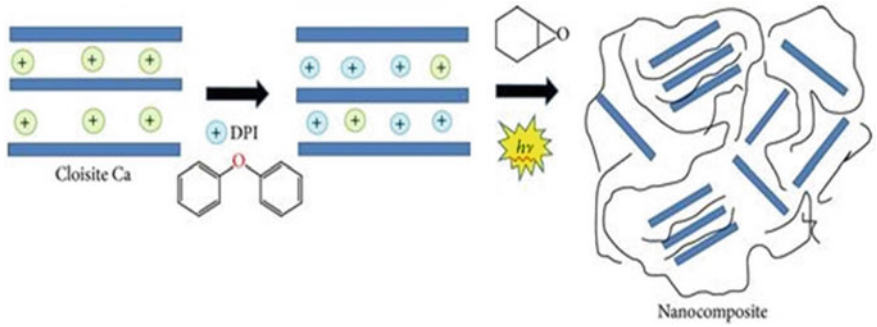

Fig. 7.9 Cation exchange and nanocomposite preparation. Cloisite-Ca: cloisite calcium, DPI: diphenyliodonium, UV light, nanocomposite: poly(cyclohexene oxide)-montmorillonite nanocomposite structure [106]

propagation starts in the interlayer space of the clay platelets so that the clay particles can precisely spread in the polymer matrix resulting in the exfoliated (PCHO)/clay nanocomposites. The catalyst was loaded by means of cation-exchange process of diphenyliodonium, and the second step was the in situ

photopolymerizations of CHO in catalyst loaded clay [106]. Sodium gordaite (NaG − $NaZn_4(OH)_6(SO_4)Cl \cdot 6H_2O$) is naturally available but can also be manufactured easily under the presence of air as well as under inert atmosphere. Sodium gordaite-based composite cation exchangers have been synthesized and used to remove Na^+ with Ca^{2+}, K^+, and Li^+. The composite material has extraordinary potential to be used as cation exchanger [107]. Novel carboxylic bioresin from raw areca nut husk has been developed via mercerization and ethylenediamine tetraacetic dianhydride (EDTAD) carboxylation. Mercerized lignin was obtained from the vesicles of the husk, and the EDTAD was grooved in via acylation reaction in dimethylformamide media. The carboxylic groups were introduced for functionalization of mercerized husk (FMH) in order to achieve high adsorption capacity of 0.735 mM/g and a cation exchange capacity of 2.01 meq/g. The FMH exhibited up to 99% efficiency for the sequestration of Pb(II) from synthetic wastewater and successfully and efficiently eliminated Pb(II) and Cd(II) simultaneously along with Fe, Mg, Ni, and Co from wastewater of real Pb–acid battery [108]. Another novel biocomposite adsorbent has been synthesized by incorporating 2-hydroxyethyl methacrylate (HEMA), acrylamide (AM) and cross-linker *N*, *N*′-methylene bis

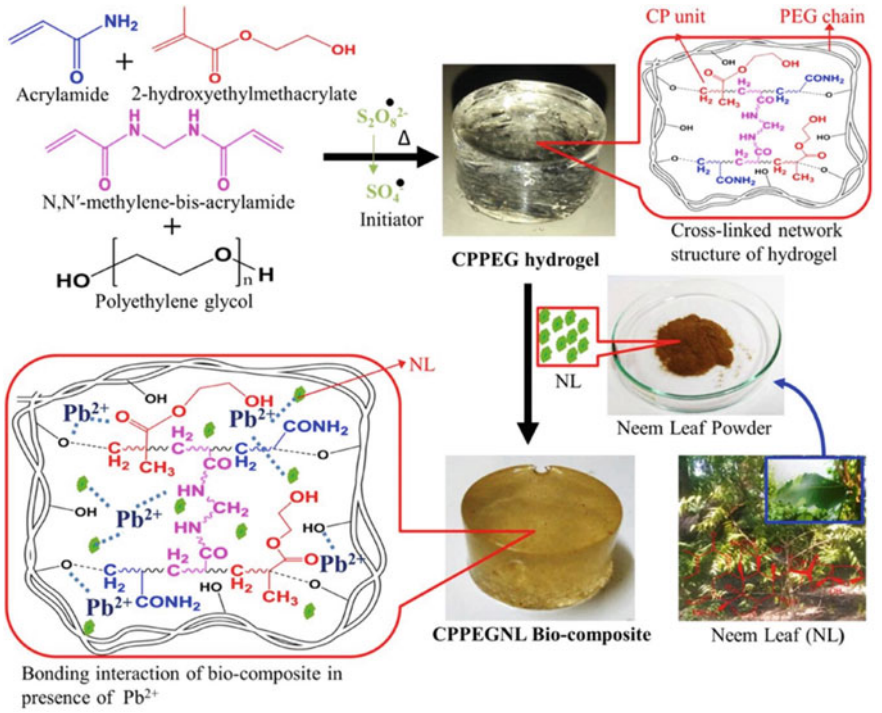

Fig. 7.10 Novel biocomposite adsorbent by incorporation of 2-hydroxyethyl methacrylate (HEMA), acrylamide (AM) and cross-linker *N*,*N*′-methylene bis acrylamide (MBA), polyethylene glycol (PEG), and neem leaf [109]

acrylamide (MBA), polyethylene glycol (PEG), or neem leaf (NL) (Fig. 7.10). The high sorption capacity of around 182.85 mg/g (92.5%) for Pb(II) has been achieved, and the functionalized biocomposite has been proposed for removing the polar molecules and the metal ions from water [109].

7.5 Conclusion and Future Outlook

Increasing industrialization has led to contamination and pollution of the soil with toxic chemicals which eventually reach the drinking water and the food cycle. Groundwater includes diverse toxic materials such as heavy metals, organic contaminants, and pathogens. Several waterborne diseases caused due to the increased concentration of fluoride, heavy metals, different pathogens, arsenic, and natural organic matters. The most hazardous heavy metals are lead (Pb), chromium (Cr), arsenic (As), zinc (Zn), cadmium(Cd), copper (Cu), mercury (Hg), chromium (Cr), and nickel (Ni). There is an urgent need for developing promising materials and purifying technologies to eliminate these chemicals from drinking water sources. Natural and modified adsorbents are the best options for beneficial and successful purification of water. Several types of natural and agro-based adsorbents have been used for contaminated water purification, and the chitosan, cellulose, and clay and their tailored composites are among the most effective in comparison with other low-cost adsorbents. Of increasing interest is the use of ion-exchange hybrid membranes as promising active separators especially industrial and biological waste treatment. It is more reliable due to low energy requirements, economical viability, and low ecological footprints. The nanocomposites with polymer/layered silicate also need to explore more suitable, eco-friendly, inorganic particle-filled composites.

References

1. Inglehart R, Norris, P (2003) Rising tide: gender equality and cultural change around the world. Cambridge University Press
2. Grimm NB et al (2008) Global change and the ecology of cities. Science 319(5864):756–760
3. Organization WH (1992) WHO commission on health and environment: report of the panel on industry
4. Flower SRL (2015) Environmental pollution-especially air pollution-and public health
5. Förstner U, Wittmann GT (2012) Metal pollution in the aquatic environment. Springer Science & Business Media
6. Mushak P (2007) Hormesis and its place in nonmonotonic dose–response relationships: some scientific reality checks. Environ Health Perspect 115(4):500
7. Mishra MK (2013) A study of intermetallics in Cu–Sn system and development of Sn–Zn based lead free solders
8. Matte TD, Landrigan PJ, Baker EL (1992) Occupational lead exposure. Hum Lead Exposure 155–168

9. Choudhary R et al (2016) Equipment-free, single-step, rapid, "on-site" kit for visual detection of lead ions in soil, water, bacteria, live cells, and solid fruits using fluorescent cube-shaped nitrogen-doped carbon dots. ACS Sustain Chem Eng 4(10):5606–5617
10. Mudgal V et al (2010) Effect of toxic metals on human health. Open Nutr J 3(1):94–99
11. Harikumar P et al (2011) Study on the leaching of mercury from compact fluorescent lamps using stripping voltammetry. J Toxicol Environ Health Sci 3(1):008–013
12. Lokeshappa B et al (2012) Assessment of toxic metals in agricultural produce. Food Public Health 2(1):24–29
13. Pais I, Jones JB Jr (1997) The handbook of trace elements. CRC Press
14. Soetan K, Olaiya C, Oyewole O (2010) The importance of mineral elements for humans, domestic animals and plants—a review. Afr J Food Sci 4(5):200–222
15. Underwood E (2012) Trace elements in human and animal nutrition: Elsevier
16. Fu F, Wang Q (2011) Removal of heavy metal ions from wastewaters: a review. J Environ Manage 92(3):407–418
17. Ngah WW, Hanafiah M (2008) Removal of heavy metal ions from wastewater by chemically modified plant wastes as adsorbents: a review. Biores Technol 99(10):3935–3948
18. Barakat M (2011) New trends in removing heavy metals from industrial wastewater. Arab J Chem 4(4):361–377
19. Daneshfozoun S, Abdullah M, Abdullah B (2017) Preparation and characterization of magnetic biosorbent based on oil palm empty fruit bunch fibers, cellulose and Ceiba pentandra for heavy metal ions removal. Ind Crops Prod 105:93–103
20. Omri A, Benzina M (2012) Removal of manganese (II) ions from aqueous solutions by adsorption on activated carbon derived a new precursor: ziziphus spina-christi seeds. Alexandria Eng J 51(4):343–350
21. Omorogie M (2014) Adsorption of some toxic metal ions onto west african boxwood (naucleadiderrichii, merrill) seed epicarp doped with nanoparticles
22. Mondal DK, Nandi BK, Purkait M (2013) Removal of mercury (II) from aqueous solution using bamboo leaf powder: equilibrium, thermodynamic and kinetic studies. J Environ Chem Eng 1(4):891–898
23. Reddy DHK et al (2012) Optimization of Cd(II), Cu(II) and Ni(II) biosorption by chemically modified *Moringa oleifera* leaves powder. Carbohyd Polym 88(3):1077–1086
24. Li X et al (2013) Adsorption, concentration, and recovery of aqueous heavy metal ions with the root powder of *Eichhornia crassipes*. Ecol Eng 60:160–166
25. Munagapati VS et al (2010) Biosorption of Cu(II), Cd(II) and Pb(II) by acacia leucocephala bark powder: kinetics, equilibrium and thermodynamics. Chem Eng J 157(2–3):357–365
26. Reddy DHK et al (2011) Biosorption of Ni(II) from aqueous phase by *Moringa oleifera* bark, a low cost biosorbent. Desalination 268(1–3):150–157
27. Sarin V, Pant KK (2006) Removal of chromium from industrial waste by using eucalyptus bark. Biores Technol 97(1):15–20
28. Feng N et al (2011) Biosorption of heavy metals from aqueous solutions by chemically modified orange peel. J Hazard Mater 185(1):49–54
29. Saha R et al (2013) Removal of hexavalent chromium from water by adsorption on mosambi (*Citrus limetta*) peel. Res Chem Intermed 39(5):2245–2257
30. Bhattacharya P et al (2013) Potential of biosorbent developed from fruit peel of *Trewia nudiflora* for removal of hexavalent chromium from synthetic and industrial effluent: Analyzing phytotoxicity in germinating Vigna seeds. J Environ Sci Health Part A 48(7): 706–719
31. Iqbal M, Saeed A, Kalim I (2009) Characterization of adsorptive capacity and investigation of mechanism of Cu^{2+}, Ni^{2+} and Zn^{2+} adsorption on mango peel waste from constituted metal solution and genuine electroplating effluent. Sep Sci Technol 44(15):3770–3791
32. Zheng L et al (2010) Equilibrium and kinetic studies of adsorption of Cd(II) from aqueous solution using modified corn stalk. J Hazard Mater 176(1–3):650–656
33. Zheng L et al (2010) Removal of cadmium (II) from aqueous solution by corn stalk graft copolymers. Biores Technol 101(15):5820–5826

34. Wong K et al (2003) Removal of Cu and Pb by tartaric acid modified rice husk from aqueous solutions. Chemosphere 50(1):23–28
35. Ahalya N, Kanamadi R, Ramachandra T (2005) Biosorption of chromium (VI) from aqueous solutions by the husk of Bengal gram (*Cicer arientinum*). Electron J Biotechnol **8**(3):0–0
36. Oliveira WE et al (2008) Untreated coffee husks as biosorbents for the removal of heavy metals from aqueous solutions. J Hazard Mater 152(3):1073–1081
37. Alomá I et al (2012) Removal of nickel (II) ions from aqueous solutions by biosorption on sugarcane bagasse. J Taiwan Inst Chem Eng 43(2):275–281
38. Velazquez-Jimenez LH, Pavlick A, Rangel-Mendez JR (2013) Chemical characterization of raw and treated agave bagasse and its potential as adsorbent of metal cations from water. Ind Crops Prod 43:200–206
39. Martín-Lara MÁ et al (2010) Modification of the sorptive characteristics of sugarcane bagasse for removing lead from aqueous solutions. Desalination 256(1–3):58–63
40. Khoramzadeh E, Nasernejad B, Halladj R (2013) Mercury biosorption from aqueous solutions by sugarcane bagasse. J Taiwan Inst Chem Eng 44(2):266–269
41. Boota R, Bhatti HN, Hanif MA (2009) Removal of Cu(II) and Zn(II) using lignocellulosic fiber derived from Citrus reticulata (Kinnow) waste biomass. Sep Sci Technol 44(16):4000–4022
42. Daneshfozoun S, Abdullah B, Abdullah MA (2014) Heavy metal removal by oil palm empty fruit bunches (OPEFB) biosorbent. In: Applied mechanics and materials. Trans Tech Publications
43. Daneshfozoun S, Abdullah B, Abdullah MA (2016) The effects of oil palm empty fruit bunch sorbent sizes on plumbum (II) ion sorption. In: Advanced materials research. Trans Tech Publications
44. Nazir MS, Ajab H, Raza MR, Abdullah MA (2018) Surface modification of cellulose fibers from oil palm empty fruit bunches for heavy metal ion sorption and diesel desulphurization. Desalin Water Treat 107: 241–256
45. Ajab H, Dennis JO, Abdullah MA (2018) Synthesis and characterization of cellulose and hydroxyapatite-carbon electrode composite for trace plumbum ions detection and its validation in blood serum. Int J Biol Macromol 113:376–385
46. Kaur R et al (2012) Biosorption the possible alternative to existing conventional technologies for sequestering heavy metal ions from aqueous streams: a review. Univ J Environ Res Technol 2(4)
47. Wei W et al (2016) Biosorption of Pb(II) from aqueous solution by extracellular polymeric substances extracted from *Klebsiella* sp. J1: adsorption behavior and mechanism assessment. Sci Rep 6:31575
48. Sargın İ (2015) Preparation of chitosan microcapsules and investigation of its metal adsorption properties. Selçuk Üniversitesi Fen Bilimleri Enstitüsü
49. Homagai PL (2018) Studies on the development of natural cation exchanger for heavy metals removal
50. Zhang YHP (2013) Next generation biorefineries will solve the food, biofuels, and environmental trilemma in the energy–food–water nexus. Energy Sci Eng 1(1):27–41
51. Dax D et al (2013) Amphiphilic spruce galactoglucomannan derivatives based on naturally-occurring fatty acids. BioResources 8(3):3771–3790
52. Wang J et al (2013) Collagen/cellulose hydrogel beads reconstituted from ionic liquid solution for Cu(II) adsorption. Carbohyd Polym 98(1):736–743
53. Abbas A et al (2017) Design, characterization and evaluation of hydroxyethylcellulose based novel regenerable supersorbent for heavy metal ions uptake and competitive adsorption. Int J Biol Macromol 102:170–180
54. Abbas A et al (2017) Modified hydroxyethylcellulose: a regenerable super-sorbent for Cd^{2+} uptake from spiked high-hardness groundwater. Cellul Chem Technol 51(1–2):167–174
55. Kweon D-K et al (2001) Adsorption of divalent metal ions by succinylated and oxidized corn starches. Carbohyd Polym 46(2):171–177

56. Song X et al (2006) Preparation and properties of octenyl succinic anhydride modified early indica rice starch. Starch-Stärke 58(2):109–117
57. Marcazzan M et al (1999) An ESR assay for α-amylase activity toward succinylated starch, amylose and amylopectin. J Biochem Biophys Methods 38(3):191–202
58. Yamaguchi R et al (1981) Preparation of partially *N*-succinylated chitosans and their cross-linked gels. Carbohyd Res 88(1):172–175
59. Rinaudo M (2006) Chitin and chitosan: properties and applications. Prog Polym Sci 31(7): 603–632
60. Kumar MNR (2000) A review of chitin and chitosan applications. React Funct Polym 46 (1):1–27
61. Shukla SK et al (2013) Chitosan-based nanomaterials: a state-of-the-art review. Int J Biol Macromol 59:46–58
62. Sorlier P et al (2001) Relation between the degree of acetylation and the electrostatic properties of chitin and chitosan. Biomacromol 2(3):765–772
63. Miretzky P, Cirelli AF (2009) Hg(II) removal from water by chitosan and chitosan derivatives: a review. J Hazard Mater 167(1–3):10–23
64. Dash M et al (2011) Chitosan—a versatile semi-synthetic polymer in biomedical applications. Prog Polym Sci 36(8):981–1014
65. Jayakumar R et al (2005) Graft copolymerized chitosan—present status and applications. Carbohyd Polym 62(2):142–158
66. Ryu SW et al (2004) Synthesis of well-defined high-density branched polymers carrying two branch chains in each repeating unit by coupling reaction of benzyl bromide-functionalized polystyrenes with polymer anions comprised of two polymer segments. Macromolecules 37(17):6291–6298
67. Lavanya R et al (2017) Adsorptive removal of copper (II) and lead (II) using chitosan-g-maleic anhydride-g-methacrylic acid copolymer. Int J Biol Macromol 104:1495–1508
68. Razzaz A et al (2015) J Taiwan Inst Chem Eng
69. Kumar I, Natrayasamy V (2017) Development of multivalent metal ion imprinted chitosan biocomposites for phosphate sorption
70. Sargın İ, Arslan G, Kaya M (2016) Efficiency of chitosan–algal biomass composite microbeads at heavy metal removal. React Funct Polym 98:38–47
71. Pereao O et al (2017) Electrospinning: polymer nanofibre adsorbent applications for metal ion removal. J Polym Environ 25(4):1175–1189
72. Karthik R, Meenakshi S (2015) Removal of Cr(VI) ions by adsorption onto sodium alginate-polyaniline nanofibers. Int J Biol Macromol 72:711–717
73. Lim S-F et al (2009) Removal of copper by calcium alginate encapsulated magnetic sorbent. Chem Eng J 152(2–3):509–513
74. Dogan H (2012) Preparation and characterization of calcium alginate-based composite adsorbents for the removal of Cd, Hg, and Pb ions from aqueous solution. Toxicol Environ Chem 94(3):482–499
75. Davis TA, Volesky B, Mucci A (2003) A review of the biochemistry of heavy metal biosorption by brown algae. Water Res 37(18):4311–4330
76. Chang C, Zhang L (2011) Cellulose-based hydrogels: present status and application prospects. Carbohyd Polym 84(1):40–53
77. Lee KY et al (2009) Electrospinning of polysaccharides for regenerative medicine. Adv Drug Deliv Rev 61(12):1020–1032
78. Huang Z-M et al (2003) A review on polymer nanofibers by electrospinning and their applications in nanocomposites. Compos Sci Technol 63(15):2223–2253
79. Elsabee MZ, Naguib HF, Morsi RE (2012) Chitosan based nanofibers, review. Mater Sci Eng C 32(7):1711–1726
80. Ramakrishna S et al (2006) Electrospun nanofibers: solving global issues. Mater Today 9(3): 40–50
81. Ahmed S, Ikram S (2015) Chitosan & its derivatives: a review in recent innovations. Int J Pharm Sci Res 6(1):14

82. Shariful MI et al (2017) Adsorption of divalent heavy metal ion by mesoporous-high surface area chitosan/poly (ethylene oxide) nanofibrous membrane. Carbohyd Polym 157:57–64
83. Habiba U et al (2017) Chitosan/(polyvinyl alcohol)/zeolite electrospun composite nanofibrous membrane for adsorption of Cr^{6+}, Fe^{3+} and Ni^{2+}. J Hazard Mater 322:182–194
84. Mohamed RR, Elella MHA, Sabaa MW (2017) Cytotoxicity and metal ions removal using antibacterial biodegradable hydrogels based on *N*-quaternized chitosan/poly (acrylic acid). Int J Biol Macromol 98:302–313
85. Gupta V et al (2009) Low-cost adsorbents: growing approach to wastewater treatment—a review. Crit Rev Environ Sci Technol 39(10):783–842
86. Goel J et al (2005) Removal of lead (II) by adsorption using treated granular activated carbon: batch and column studies. J Hazard Mater 125(1–3):211–220
87. Han R et al (2009) Characterization and properties of iron oxide-coated zeolite as adsorbent for removal of copper (II) from solution in fixed bed column. Chem Eng J 149(1–3):123–131
88. Taty-Costodes VC et al (2005) Removal of lead (II) ions from synthetic and real effluents using immobilized Pinus sylvestris sawdust: adsorption on a fixed-bed column. J Hazard Mater 123(1–3):135–144
89. Chen JP, Wang X (2000) Removing copper, zinc, and lead ion by granular activated carbon in pretreated fixed-bed columns. Sep Purif Technol 19(3):157–167
90. Mohammed N et al (2016) Continuous flow adsorption of methylene blue by cellulose nanocrystal-alginate hydrogel beads in fixed bed columns. Carbohyd Polym 136:1194–1202
91. Mojumdar S, Varshney K, Agrawal A (2006) Hybrid fibrous ion exchange materials: past, present and future. Res J Chem Environ 10(1):89–97
92. Mojumdar S et al (2006) Synthetic and ion-exchange studies on a lead selective acrylamide thorium (IV) phosphate hybrid fibrous ion exchanger. Res J Chem Environ 10:85–89
93. Varshney K, Agrawal A, Mojumdar S (2007) Pyridine based cerium (IV) phosphate hybrid fibrous ion exchanger: synthesis, characterization and thermal behaviour. J Therm Anal Calorim 90(3):731–734
94. Varshney K, Agrawal A, Mojumdar S (2007) Pyridine based thorium (IV) phosphate hybrid fibrous ion exchanger: synthesis, characterization and thermal behaviour. J Therm Anal Calorim 90(3):721–724
95. Shahadat M et al (2012) Synthesis, characterization, photolytic degradation, electrical conductivity and applications of a nanocomposite adsorbent for the treatment of pollutants. RSC Adv 2(18):7207–7220
96. Pouliot Y, Conway V, Leclerc P-L (2014) Separation and concentration technologies in food processing. In: Food processing: principles and applications, pp. 33–60
97. Camacho LM et al (2013) Advances in membrane distillation for water desalination and purification applications. Water 5(1):94–196
98. Drioli E, Macedonio EF (2010) Membrane research, membrane production and membrane application in China
99. Wu Y et al (2015) The effects of multi-functional groups from PVA and ternary multisilicon copolymer on diffusion dialysis. Sep Purif Technol 141:124–131
100. Gizli N, Çınarlı S, Demircioğlu M (2012) Characterization of poly (vinylchloride) (PVC) based cation exchange membranes prepared with ionic liquid. Sep Purif Technol 97:96–107
101. Kaushal S et al (2017) Synthesis and characterization of a tin (IV) antimonophosphate nano-composite membrane incorporating 1-dodecyl-3-methylimidazolium bromide ionic liquid. RSC Adv 7(21):12561–12569
102. Ray SS, Okamoto M (2003) Polymer/layered silicate nanocomposites: a review from preparation to processing. Prog Polym Sci 28(11):1539–1641
103. Pavlidou S, Papaspyrides C (2008) A review on polymer–layered silicate nanocomposites. Prog Polym Sci 33(12):1119–1198
104. Kaur M, Srivastava A (2002) Photopolymerization: a review. J Macromol Sci Part C Polym Rev 42(4):481–512

105. Fuchs Y, Soppera O, Haupt K (2012) Photopolymerization and photostructuring of molecularly imprinted polymers for sensor applications—a review. Anal Chim Acta 717:7–20
106. Bayram I, Oral A, Şirin K (2013) Synthesis of poly(cyclohexene oxide)-montmorillonite nanocomposite via in situ photoinitiated cationic polymerization with bifunctional clay. J Chem 2013
107. Maruyama SA et al (2017) Synthesis, cation exchange and dehydration/rehydration of sodium gordaite: $NaZn_4(OH)_6(SO_4)Cl \cdot 6H_2O$. Appl Clay Sci 146:100–105
108. Kulkarni VV, Golder AK, Ghosh PK (2018) Synthesis and characterization of carboxylic cation exchange bio-resin for heavy metal remediation. J Hazard Mater 341:207–217
109. Maity J, Ray SK (2018) Removal of Pb(II) from water using a bio-composite adsorbent-A systematic approach of optimizing synthesis and process parameters by response surface methodology. J Environ Manage 209:112–125
110. Jain CK, Malik DS, Yadav AK (2016) Applicability of plant based biosorbents in the removal of heavy metals: a review. Environ Process 3(2):495–523
111. Raftery R, O'Brien FJ, Cryan S-A (2013) Chitosan for gene delivery and orthopedic tissue engineering applications. Molecules 18(5):5611–5647
112. Matsumoto H, Tanioka A (2011) Functionality in electrospun nanofibrous membranes based on fiber's size. Surface Area, and Molecular Orientation. 1:249–264

Chapter 8
Rare Earth Elements—Separation Methods Yesterday and Today

Dorota Kołodyńska, Dominika Fila, Bernadeta Gajda, Jerzy Gęga and Zbigniew Hubicki

Abstract Rare earth elements (REEs) belong to the group of strategic elements. Their separation together with the spectral, magnetic and coordinative properties of REEs is essential for their further applications. However, separation of individual REEs on an industrial scale is very complex. Obtaining REEs of high purity requires purification of their concentrates. This is usually achieved by precipitation of REEs such as double sulphates $NaLn(SO_4)_2$ or oxalates $Ln_2(C_2O_4)_3$ as well as extraction and/or ion exchange method application. Currently, the recovery of rare earth metals from secondary sources is also very important. The details connected with the rare earth element recovery from nickel–metal hydride batteries and permanent magnets as well as their separation will be described in the paper.

8.1 Introduction

Due to their unique electrical, optical and magnetic properties, rare earth elements are very popular and used in many different areas of life. Although these elements have long been used in the production of glass, lighting and catalysts are also sought after by developing markets such as battery alloys and permanent magnets. The constantly growing demand for elements requires searching for alternative sources of their recovery. Although rare earth elements quite often occur in nature,

D. Kołodyńska (✉) · D. Fila · Z. Hubicki
Department of Inorganic Chemistry, Faculty of Chemistry, Maria Curie-Sklodowska University, M. Curie Sklodowska Sq. 2, 20-031 Lublin, Poland
e-mail: d.kolodynska@poczta.umcs.lublin.pl

B. Gajda
Department of Metals Extraction and Recycling, Faculty of Production Engineering and Materials Technology, Czestochowa University of Technology, J.H. Dąbrowskiego 69, 42-201 Częstochowa, Poland

J. Gęga
Department of Chemistry, Faculty of Production Engineering and Materials Technology, Czestochowa University of Technology, J.H. Dąbrowskiego 69, 42-201 Częstochowa, Poland

Inamuddin et al. (eds.), *Applications of Ion Exchange Materials in the Environment*,
https://doi.org/10.1007/978-3-030-10430-6_8

their extraction and separation have been big problems, mainly due to their high chemical similarities. The difficulty is also due to the fact that they occur very often together in the natural environment. Because of their similar physicochemical properties, their separation is problematic [1, 2].

Rare earth elements belong to the group of strategic elements. Their production is unequally distributed around the world. Their largest deposits are located in China, which is the main exporter of these materials. China is responsible for more than 80% of current global mining production and controls over 50% of the global mineral resources of these elements. China has become an industry leader, owing to which it has gained an advantage in every segment of production: ore mining, separation of elements, refining metals, creating alloys and processing them into production components. By introducing dumped prices, the Chinese degraded competing suppliers and dominated the world market for rare earth metals. Ultimately, China drastically raised commodity prices and almost completely limited their exports, thereby blocking the activities of global electronics companies. With the declining availability of rare earth elements in the global market, there is a need to search for and develop effective and economical methods of recovering these elements from secondary sources [2–4].

Currently, the recovery of rare earth metals from secondary sources, such as electronic and electrical equipment, is carried out using traditional pyrometallurgical or hydrometallurgical methods. In these technologies, many indirect operations can be distinguished to obtain the pure metal. These operations can be divided into four basic stages: homogenization, concentration, dissolution and separation of metals and their purification. The chemical similarities of rare earth metals and their ability to create isomorphic mixtures have resulted in difficulty of their separation. Therefore, physicochemical methods of their recovery from secondary sources are of great importance. Common methods of concentration, recovery and separation of rare earth ions include precipitation and coprecipitation, ion exchange, solvent extraction, electrochemical and membrane processes, adsorption as well as oxidation and reduction methods. Among the mentioned methods, ion exchange has played a significant role in the chemical technology of recovery and separation of rare earth ions from solutions with different concentrations for a long time. Application of ion exchange in the sorption and separation processes of rare earth ions is an important aspect towards separation of pure metals from wastewaters as well as from the solutions obtained after the leaching process of raw materials containing these elements [5–8].

8.2 Rare Earth Elements

8.2.1 General Characteristics

Rare earth elements (REEs), also known as rare earths (REs) or rare earth metals (REMs), according to the classification by the International Union of Pure and

Applied Chemistry (IUPAC) are a group of 17 elements including scandium (Sc), yttrium (Y) and 15 lanthanides (Ln): lanthanum (La), cerium (Ce), praseodymium (Pr), neodymium (Nd), promethium (Pm), samarium (Sm), europium (Eu), gadolinium (Gd), terbium (Tb), dysprosium (Dy), holmium (Ho), erbium (Er), thulium (Tm), ytterbium (Yb) and lutetium (Lu). The discovery of lanthanides dates back to 1794 when a mixture of lanthanides was first extracted from iterbite mineral by the Finnish chemist Johan Gadolin [9–13]. These elements can be divided into light rare earth elements (LREE): from La to Eu and heavy rare earth elements (HREE): from Ga to Lu. The basis for this division is the significant difference in atomic masses between Eu (151.964) and Gd (157.250) [10, 14–16].

The amount of these elements is not as small as results from their name. They occur in the Earth's crust in larger quantities than, for example, silver which content is about 6×10^{-6} % or platinum. The average distribution of yttrium is 3.3×10^{-3} %, lanthanum 3×10^{-3} % and the other lanthanides from 6×10^{-3} to 5×10^{-5} %. However, despite their relatively common occurrence, they are rarely found in a concentrated form that would be favourable for their extraction [17].

The amount of lanthanides depends on the atomic number of a given element. The increase in the atomic number causes a decrease their occurrence. In addition, elements with an odd atomic number are less common than those with even atomic numbers [18, 19].

8.2.2 The Occurrence of Rare Earth Elements

Rare earth elements belong to the group of lithophile elements. They do not occur in the Earth's crust in a free state but in the form of mixtures, usually isomorphous which makes their extraction and separation problematic. All lanthanides generally occur together except for promethium which nucleus is unstable. These are found in nature as abundant but rare minerals present in igneous or sedimentary rocks which include argillaceous. In the acidic igneous rocks, contents of rare earth are higher than in the basic ones. Relative abundance of lanthanides is presented in Fig. 8.1. The sedimentary rocks are characterized by a lower content of REE than the igneous ones [20]. Table 8.1 presents the average contents of rare earth elements in the igneous and sedimentary rocks.

There have been about 250 identified minerals containing rare earth elements. These can be divided into minerals containing light lanthanides, i.e. from La to Sm and those containing Y as well as heavy lanthanides, i.e. from Gd to Lu. Lanthanides occur in the form of silicates, phosphates, carbonates and fluorocarbons. Among the richest sources of rare earth elements are minerals such as monazite $(Ce,La)PO_4$, bastnasite $(La,Ce)CO_3F$, allanite $(Ce,Ca,Y,La)_2(Al,Fe)_3(SiO_4)_3(OH)$ and xenotime $(Y)PO_4$ [13, 16, 20–24].

Monazite, bastnasite and allanite are minerals that are the main source of light rare earth metals. They are primarily characterized by high contents of lanthanum and cerium. Xenotime is the main source of heavy rare earth elements which

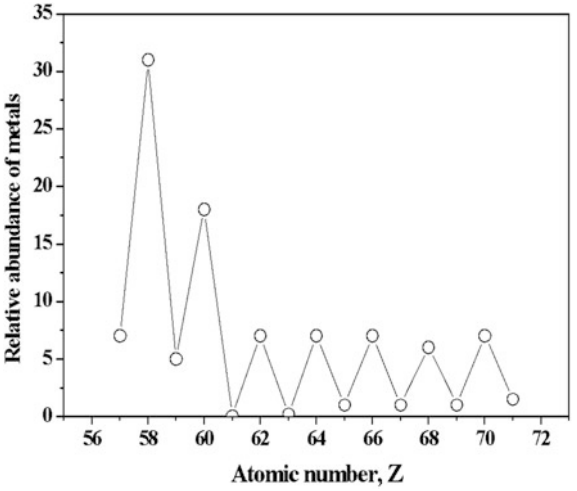

Fig. 8.1 Relative abundance of lanthanides (own elaboration based on [19])

Table 8.1 Average REE contents in rocks (mg/kg) (own elaboration based on [20])

REE	Igneous rocks		Sedimentary rocks
	Acid	Basic	Argillaceous
La	30–150	2–70	30–90
Ce	80–250	4–60	3–90
Pr	6–30	1–15	6–10
Nd	18–80	2–30	18–35
Sm	6–11	0.1–1.7	5–7
Eu	1–2	0.01–4	1–2
Gd	4–10	0.1–8	5–7.5
Tb	1–1.25	0.1–1.2	0.9–1.1
Dy	5–8	0.05–7	4–6
Ho	1.3–2	0.1–1.5	1–1.8
Er	3.4–0.7	0.1–1	2.5–4
Tm	0.3–0.7	0.1–0.6	0.2–0.6
Yb	3–4.5	0.1–3.5	2.2–4
Lu	0.5–1.2	0.1–0.6	0.5–1.2

contains a high concentration of yttrium; hence, its general formula is $(Y)PO_4$. Monazite and bastnasite deposits account for approximately 99% of the total production of rare earth. These minerals contain about 60–75% of rare earth metal oxides and other elements [24]. Monazite and xenotime contain thorium and uranium which create problems related to the safe operation, processing and economical utilization. The bastnasite deposits are very valuable because these do not contain radioactive elements [9, 13, 16, 17].

The composition of individual minerals depends on the place of their occurrence. Although mineral deposits are scattered all over the world, their main mining is

currently taking place in China [12]. Bastnasite deposits constitute the two largest sites of rare earth elements. These are the Bayan-Obo in Inner Mongolia in North China and the Mountain Pass in Southern California [15, 22, 25]. Abundant monazite deposits are found on the beaches in India and coastal sands in Brazil, Australia and Malaysia [2, 9, 10, 22, 26].

Promethium is the only element that does not occur in nature. It was obtained as a result of artificial nuclear transformations and detected in uranium fission products. Lanthanides can be also found in small amounts in marine waters, biosphere as well as in plants and animals as secondary components. Their occurrence was registered on the Sun, Moon and stars as components of meteorites [9, 20].

8.2.3 Physicochemical Properties of Rare Earth Elements

REEs are an unusual group of metallic elements with unique properties: chemical, catalytic, magnetic, metallurgical and phosphorescent which consists of seventeen elements belonging to lanthanides [27, 28]. Lanthanides in the free state are silvery white, soft and malleable metals. About 25% of produced RE metals are used in the metallic form as the so-called mischmetal including [29]: 45–50% cerium, 22–25% lanthanum, 18% neodymium, 5% praseodymium and 1% samarium with deoxidizing and desulphurizing properties. Lanthanides are characterized by very similar chemical and physical properties. This is due to the fact that they have similar atomic and ionic radii and the same electronic structure of valence shells. As the f-electron elements, these have the electronic configuration of $4f^{1-14}5d^{0.1}6s^2$ (Table 8.2).

All lanthanides are very reactive metals and strongly electropositive, and in contact with the air gets tarnished. Their oxides and hydroxides have evidently basic properties. Lanthanide hydroxides do not dissolve in excess of bases. The basic properties of lanthanides decrease with the decreasing ionic radius (from La to Lu). Some elements additionally form ions on the second or fourth oxidation state which is associated with obtaining the more stable electronic configuration $4f^0$, $4f^7$lub $4f^{14}$, for example, Ce(IV), Tb(IV), Yb(II), Eu(II). II and IV oxidation states are unstable in aqueous solutions except for cerium(IV) salts. Europium forms the most durable compounds on the second oxidation state. Lanthanides are characterized by low electronegativity and high boiling or melting points. Lanthanide ions except for La(III) and Lu(III) exhibit strong paramagnetism which is associated with the presence of the unpaired electrons subshell 4f. La(III) and Lu(III) ions are diamagnetic. At low temperatures, Gd(III), Dy(III), Eu(III), Er(III) and Ho(III) ions become ferromagnetic. The colour of lanthanide ions is associated with f-f electronic transitions. All ions absorb light in the visible and near ultraviolet ranges. Many of them show a characteristic colour in both the solid state and in the solution. The orbitals f located deep inside the atom are largely shielded from external influences which indicate that they do not participate in the bond formation, and as a result, sharp absorption bands are observed [30, 31].

Table 8.2 Physicochemical properties of rare earth elements (own elaboration based on [11])

Element	Symbol	Atomic number	Atomic weight	Electron configuration
Scandium	Sc	21	44.9559	$3d^1 4\ s^2$
Yttrium	Y	39	88.9059	$4d^1 5\ s^2$
Lanthanum	La	57	138.9055	$5d^1 6\ s^2$
Cerium	Ce	58	140.12	$4f^2 6\ s^2$
Praseodymium	Pr	59	140.9077	$4f^3 6\ s^2$
Neodymium	Nd	60	144.24	$4f^4 6\ s^2$
Promethium	Pm	61	145.0	$4f^5 6\ s^2$
Samarium	Sm	62	150.36	$4f^6 6\ s^2$
Europium	Eu	63	151.96	$4f^7 6\ s^2$
Gadolinium	Gd	64	157.25	$4f^7 5d^1 6\ s^2$
Terbium	Tb	65	158.9254	$4f^9 6\ s^2$
Dysprosium	Dy	66	162.50	$4f^{10} 6\ s^2$
Holmium	Ho	67	164.9304	$4f^{11} 6\ s^2$
Erbium	Er	68	167.26	$4f^{12} 6\ s^2$
Thulium	Tm	69	168.93	$4f^{13} 6\ s^2$
Ytterbium	Yb	70	173.04	$4f^{14} 6\ s^2$
Lutetium	Lu	71	174.967	$4f^{14} 5d^1 6\ s^2$

A characteristic phenomenon found in a series of lanthanides is the so-called lanthanide contraction. As the charge of the nucleus increases, the atomic and ionic radii of lanthanides decrease with the increasing atomic number. Passing from La (III) to Lu(III), the ionic radius decreases from 0.106 to 0.085 nm. The contraction comes from the interactions of the increasing nuclear charge on a slightly changing electron shell in which the subshell 4f got extended. When it is filled up with electrons, the nucleus is less and less affected by the electrons of external subshells. This phenomenon is characteristic of lanthanides on various oxidation states; however, it is the most visible for ions on the third oxidation state (Fig. 8.2) [30, 32].

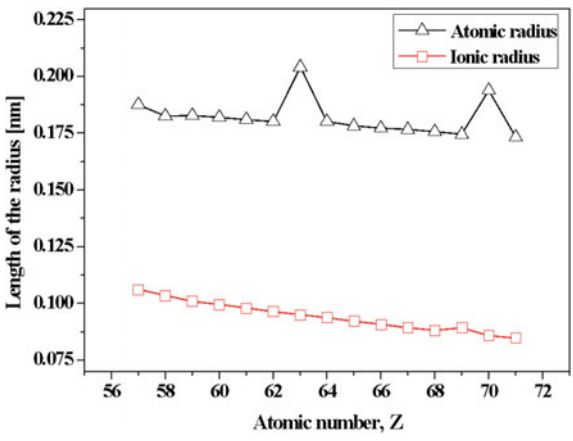

Fig. 8.2 Lanthanide contraction (own elaboration based on [30, 32])

8.2.4 Application of Rare Earth Metals

Consumption of REEs in individual countries around the world is a measure of their technological level and modernity which is associated with the production of new and multifunctional materials for medical diagnostics, optics, nuclear technologies, laser production, telecommunications, metal alloys, aviation and cosmonautics as well as petrochemistry. Progress in the above fields is possible due to the development of technologies for separation and purification of REEs. According to the data of the US Geological Survey published in 2015, approximately 97% of REEs production came from China. From the point of view of the use of secondary sources—apatite phosphogypes from the Kola Peninsula (containing about 1% of rare earth oxides (REO)) stored at the former Chemical Plant "Wizów"/Bolesławiec (Poland) seems to be an attractive source [19, 33].

REEs are essential in everyday life all over the world in both developed and developing countries in the use of the greener technologies. They have many desirable properties, such as clear optical properties including fluorescence and coherent light emission which is necessary for laser devices, the ability to create with other metals very durable and light magnetic materials as well as unique nuclear, metallurgical, chemical, catalytic, electrical, magnetic and optical properties. These properties contributed to their increasing variety of applications. They are primarily used in many high-tech sectors, in metallurgy, glass and ceramics, electronics, petrochemical industry, nuclear energy production, agriculture, medicine, in the production of military and defence systems as well as renewable energy sources. Due to the continuous development of modern and advanced technologies, lanthanides are constantly gaining importance. Rare earth elements are also used in high-performance magnets ($Nd_2Fe_{14}B$ and $SmCo_5$, Sm_2Co_{17}), rechargeable nickel–metal hydride batteries (NiMH), TV sets, computer hard drives, plasma and LCD screens, laptop computers, cell phones, DVD players, cameras, electric motors and generators of hybrid cars. Figure 8.3 shows the use of rare earth elements in various

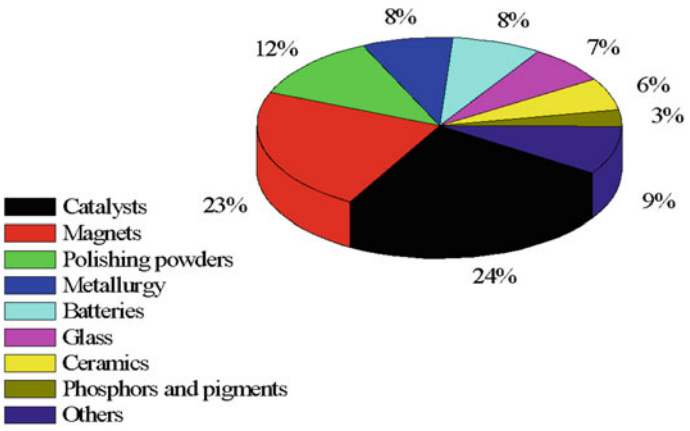

Fig. 8.3 Main applications of rare earth elements (own elaboration based on [36, 37])

areas of life. Due to their characteristic magnetic, spectroscopic and optical properties, REEs are widely used not only in various branches of industry such as electronics, nucleonics, optoelectronics, powder metallurgy or the nuclear industry but also in many fields of science (physics, biochemistry, medicine and pharmacy). For example, REE compounds are used as catalysts for cracking heavy hydrocarbons in oil refineries, exhaust catalysts as well as methane conversions, in the computer industry, mobile telephony, lasers and medicine. The mischmetal alloy, i.e. a mixture of rare earth elements such as Ce, La, Nd, Pr and smaller amounts of Sm, Tb and Y, is used as a deoxidizer and a desulphurizing agent of steel [12, 34, 35]. Table 8.3 presents the most important applications of individual rare earth elements.

Table 8.3 Most important industrial applications of rare earth elements (own elaboration based on [12, 15, 34, 35, 38])

Symbol of element	Application
La	Catalyst in the oil refining, production of hybrid car engines, batteries, lenses, projectors, X-ray films, polishing powders
Ce	Additive to steel, production of polishing powders, lenses, cathode-ray tubes, as a yellow dye in dyeing glass and ceramics, catalyst
Pr	Anticorrosive component, signal amplifier in fibre optics, additive to protective glasses, as a green dye
Nd	Production of lasers, batteries, supermagnets, wind turbines, engines for hybrid cars, wind generators in wind power plants, loudspeakers
Pm	As a source of beta radiation, production of nuclear batteries, portable X-ray equipment, paints
Sm	Production of supermagnets, reactor rods, lasers
Eu	Production of LCD televisions, fluorescent lighting, lasers, mercury lamps, construction of control rods in atomic reactors
Gd	Production of lasers, magnets, hard discs, contrast agent in magnetic resonance, production of control rods in nuclear reactors, alloy additive
Tb	Production of magnets, lasers, fluorescent lamps, phosphors for lamps and displays, as radiological screens and fuel cells
Dy	Production of strong magnets, lasers, hybrid engines, hard disc drives
Ho	Production of magnets, lasers, dyeing glass and zirconia, used in nuclear reactors
Er	Production of lasers used in medicine, phosphors, photographic filters, control rods in nuclear reactors, used in the dyeing glass
Tm	Production of ceramic magnetic materials, surgical lasers, reactors, portable X-ray devices
Yb	Manufacture of optical fibres, solar cells, lasers, oxidizer in the alloys
Lu	Lutetium isotope is used in radioactive dating
Sc	High-strength Al–Sc alloys, metal alloys for the aerospace industry, dentistry
Y	Production of capacitors, phosphors, oxygen sensors, radars, lasers, superconductors, radioactive yttrium isotopes in radiotherapy

8.2.5 Production and Consumption of Rare Earth Elements in the World

REEs have been designated as strategic metals due to the risk of supply limitation, environmental hazard related to the limitation of production possibilities conditioned by the need to maintain environmental quality standards as well as economic effects of supply limitation. In 2014, the total global production of REEs was estimated to be 110,000 tons [24, 39]. The value of production has been growing year by year. In 2016, the value of REEs production was estimated to be 126,000 tons which were 85% in China, 10% in Australia and the rest in Malaysia, Brazil, India, Russia and Vietnam [40, 41]. According to the estimates by Curtin University and IMCOA, the demand for REEs by 2020 may increase by more than 50% compared to the level from 2014, reaching around 200,000–250,000 tons (Fig. 8.4) [41].

However, according to the US Geological Survey (USGS) based on REEs production data from 2015, the top six rare-earth-producing countries include (1) China with the mine production of 105,000 tons. China dominates rare earth mineral production to such a degree that its export practices were recently challenged by the USA, European Union and Japan, resulting in the World Trade Organization (WTO) ruling against the country's rare earth export quotas in 2014 (in the past China exported only 31,000 tons of its rare earth production); (2) Australia with the mine production of 10,000 tons is the world's third-largest known rare-earth-producing country; (3) the USA with the mine production 4,100 tons. The Molycorp's Mountain Pass mine is the only one producing rare earth minerals in the USA. Overall, the US rare earth production drops from 5,400 tons in 2014 to 4,100 tons in 2015; (4) Russia with the mine production of 2,500 tons is expected to be able to meet Russian rare earth demand and increase

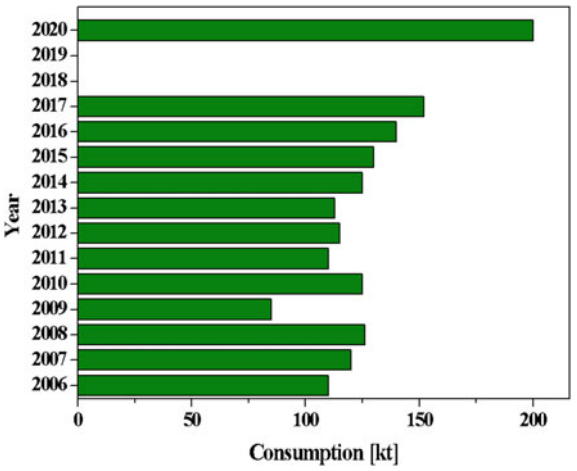

Fig. 8.4 Consumption of rare earths in 2006–2020 (own elaboration based on [41])

production. However, Russian rare earth production stayed flat in 2015 at 2,500 tons; 5) Thailand with the mine production of 1,100 tons. Thailand has raised production of rare earth minerals by 300 tons in 2014 to 1,100 tons in 2015; and (6) Malaysia with the mine production of 200 tons. Malaysia is home to the world's largest rare earth refinery, Lynas Corporation's Lynas Advanced Materials Plant (LAMP). The LAMP facility handles refining duties for Lynas's mines in Australia.

It should be mentioned that China is the only country in the world that can provide rare earth products of all grades and specifications such as not only metals, alloys or carbonates but also most of the final products, e.g. phosphors, LEDs, catalysts, NiMH batteries, magnets etc. The main process steps of REEs production are connected in mining (open-pit mining and underground mining) and processing. In open-pit mining, the first step is soil, waste rock and vegetation removal. The second step is milling. The ore is crushed, ground to fine powder in the mill in order to obtain the high surface needed for the further separation. The third step is the separation of valuable REEs from the rest of the ore by physical separation methods. The most commonly used methods have been magnetic separation and flotation with consumption of water, chemicals as well as a high amount of energy.

RE minerals have different magnetic susceptibilities. Some of these are paramagnetic which is connected with the Fe and Mn contents or contribution of REEs themselves. In magnetic separation, no chemicals are used. The method can be wet or dry depending on grain size, water availability and dust issues. It is characterized by the low operating cost but on the other hand by significant power requirements. However, with a good release, recovery can be very high.

As for flotation, its product is enriched to obtain the concentrates (30–70%). Finally, the concentrates are further extracted and separated; however, the MREEs and HREEs such as Sm, Eu, Tb and Dy are obtained by metallothermic reduction in a vacuum. In this case, the reaction proceeds at 1723–2023 K and needs the inert gas presence.

Separation of individual REEs is difficult due to their chemical similarity. Monotonic evolution from La(III) to Lu(III) makes the separation between two ions very difficult and only possible by the complexation process.

The Bayan-Obo Mines in Inner Mongolia and Sichuan in China are the largest rare earth mines in the world. The main product is iron ore with LRE as a side product. The surface mining extracts a bastnasite–monazite mix containing LREE and also thorium. Monazites are processed by acid and alkaline methods. In the acid method, ground (100–150 mesh) concentrate is subjected to the reaction with acid at 473 K. The ore decomposition takes place in the steel or cast iron apparatus operated periodically or continuously. The principal processes run according to the following reactions:

$$2\mathrm{REPO_4} + 3\mathrm{H_2SO_4} \rightleftarrows \mathrm{RE_2(SO_4)_3} + 2\mathrm{H_3PO_4} \tag{8.1}$$

$$\mathrm{Th_3(PO_4)_4} + 6\mathrm{H_2SO_4} \rightleftarrows 3\mathrm{Th(SO_4)_2} + 4\mathrm{H_3PO_4} \tag{8.2}$$

$$\mathrm{ThSiO_4 + 2H_2SO_4 \rightleftarrows Th(SO_4)_2 + \ SiO_2 + 2H_2O} \tag{8.3}$$

$$\mathrm{SiO_2 \times H_2O + H_2SO_4 \rightleftarrows SiO_2 + H_2SO_4 \times H_2O} \tag{8.4}$$

At low temperature, acid excess and longer reaction time are needed. Additionally, at temperatures, 573–623 K, water-insoluble thorium pyrophosphate is formed. However, in the presence of an appropriate excess of acid, the decomposition process itself is not selective. Further possibilities for thorium separation from rare earth are by the leaching process.

In the alkaline method, the ground rare earth is melted with sodium hydroxide or sodium carbonate or treated with the aqueous solution of sodium hydroxide. As a result, phosphates become hydroxides:

$$\mathrm{2REPO_4 + 6NaOH \rightleftarrows 2RE(OH)_3 + 2Na_3PO_4} \tag{8.5}$$

$$\mathrm{Th_3(PO_4)_4 + 12NaOH \rightleftarrows 3Th(OH)_4 + 4Na_3PO_4} \tag{8.6}$$

To prevent the formation of Ce(IV) which impedes the dissolving of the precipitate, the addition of some reductants, e.g. glucose, is recommended [42].

Since 1970s, the solvent extraction (SX) is the only industrial technology for REE separation. However, the families of thorium and uranium are responsible for the radioactivity of REE-based products. The most popular isotopes are as follows: ^{232}Th family (^{232}Th, ^{228}Ra, ^{228}Th), ^{238}U family (^{238}U, ^{234}U, ^{230}Th, ^{226}Ra, ^{210}Pb) and ^{235}U family (^{235}U and ^{227}Ac).

As for the solvent extraction process, there should be taken into account the following extractants:

(1) strongly acidic (alkylphosphoric derivatives) such as HDEHP, D2EHPA, P204, bis(2-ethylhexyl) hydrogen phosphate, phosphoric acid bis(2-ethylhexyl)ester; HEHEHP, HEHEHPA, PC88A, P507, Ionquest 801, 2-ethylhexyl hydrogen-2-ethylhexyl phosphonate, phosphonic acid (2-ethylhexyl)-mono(2-ethylhexyl) ester or cyanex 272, LIX 272, P229, di-isooctylphosphinic acid and Ionquest 290, bis (2,4,4-trimethylpentyl)phosphinic acid. These extractants extract REE in the acidic medium systems, and the extraction increases with the atomic number of REE (Y(III) occurs between Ho(III) and Er(III)). Additionally, anions and diluents have a very limited impact on selectivity. The effectiveness of the process is dependent largely on acidity of the aqueous phase (in the case of less acidic extractants, saponification is required to extract REE). Moreover, alkyl-phosphorics are stronger extractants but more difficult to back-extract (increasing reactant costs in processes).

(2) weakly acidic extractants (carboxylic acids) such as versatic acids (versatic 10, versatic 911), naphthenic acids (NOR180), CA-100 (sec-nonylphenoxyacetic acid). These are much less acidic than phosphorous acidic extractants and can be applied in neutral aqueous solutions. For example, versatic acids extract REE in the pH 4–6 range, naphthenic acids have been widely used but the

composition of the extractant is often not stable and CA-100 extracts at lower pH value than versatic ones.

(3) neutral extractants/molecular extractants—in this group, the most popular are TBP (tri n-butyl phosphate), DBBP (dibutyl butyl phosphonate), TOPO, cyanex 921 (trioctylphosphine oxide), cyanex 923, cyanex 925—the liquid mixture of four trialkylphosphine oxides. These extractants only extract REE nitrates with no or limited extraction of REE chlorides or sulphates. In the case of the neutral extractants, the efficiency of the process can be increased by a salting out effect with non-extracted salts (i.e. sodium or ammonium nitrate). It should be noticed that TBP selectivity is relatively low and highly influenced by REE concentration in the aqueous phase.

(4) basic extractants/anion exchangers—primary amines (Primene™ JM-T (t-alkyl primary amine) or N1923 (sec C-alkyl amine)), quaternary ammonium salts (Aliquat 336, Adogen 464—tricaprylmethylammonium chloride). The primary amines extract REE sulphates, and quaternary ammonium salts extract REE nitrates or REE thiocyanates. However, no extraction occurs in the chloride medium. This system offers possibilities for separation of non-REEs by amine extractants. Additionally, primary amines are efficient extractants to separate Th from U and REEs (after sulphuric acid leaching from the monazite). The selectivity between adjacent REEs is rather low (F = 1.2–1.9) and not really large enough for separation [43].

While carrying out the liquid–liquid extraction process, the low mutual solubility of both extracted and extractant phases and the difference in phase density (the greater the difference in density between the solvent and the sample, the faster and more accurate the separation of layers) should be taken into account. Unfortunately, in practice, emulsions at the interface are often formed. These are readily created when the alkaline solution is extracted. Another factor is the polarity of solvents and extracted compound (organic compounds that are composed of main hydrocarbons have a hydrophobic character; i.e., they dissolve better in nonpolar solvents). Therefore, in the extraction process, modifiers are often added—mainly to improve certain properties, such as solubility, viscosity, hydrodynamics, kinetics and an anti- or synergic agent that affect the change of partition coefficients and/or selectivity. The most popular are both aliphatic (kerosene) and aromatic (i.e. solvesso) hydrocarbons. As synergistic agents, TBP and TOPO are used; however, as modifiers alcohols C8-C12 or phenols C9 can be applied.

The main environmental threats associated with the extraction and processing of rare earth are related to the contamination of radioactive water containing radionuclides such as thorium and uranium as well as heavy metals, acids and fluorides. The air pollution is associated with the presence of the above-mentioned radionuclides, heavy metal ions and HF, HCl, SO_2, etc. There are estimates that around 20,000 tons of rare earth oxides have been illegally extracted and smuggled out of China. Most of these mines probably did not meet any emission standards [44]. In this case both acidic method REO are roasted at 673 and 723 K in concentrated sulphuric acid to remove fluoride and CO_2, after filtration, REEs were

leached using $(NH_4)HCO_3$ and HCl (to obtain the REE chlorides concentrate) and the alkaline method affect the environment.

For separation and refining of REO, extraction mainly based on 2-ethylhexyl hydrogen-2-ethylhexylphosphonate and HCl has been adopted followed by precipitation using $(NH_4)HCO_3$ or oxalic acid forming ($RE_2(C_2O_4)_3$ or $RE_2(CO_2)_3$). In the next step, these were heated and REOs formed by oxidation. LREEs have been extracted by molten salt electrolysis based on chloride or oxide. In the case of bastnasite, the ore was crushed and separated by both gravity and magnetic ways as well as the gravity one for the next step of flotation separation where 70% mixture of REO was obtained. In Sichuan, bastnasite is treated win the oxidating roasting-hydrochloric leaching process. The roast is carried out at 873 K to remove CO_2. The REE concentrates are leached in hydrochloric acid, precipitated by sodium hydroxide solution and leached in hydrochloric acid.

Besides the REE mining, the most important sources of REEs in soils are phosphate fertilizers produced from the natural phosphates. Therefore, the attempts to find solutions for the more efficient use, end-of-life recycling or reusing of rare earth, as well as potential substitutes, need to be intensified. Rare earth recycling is still in early stage and is connected with recycling of phosphors, permanent NdFeB magnets, industrial residues, nickel–metal hydride batteries and various other rare-earth-containing products. However, only phosphors and batteries can be recycled on an industrial scale. Therefore, taking the above into account there is the need to develop a new hydrometallurgical technology for the recovery of these valuable elements or their compounds from spent electronic equipment such as nickel–metal hydride batteries (NiMH), computer hard drives or electric motors and generators of hybrid cars. On the global level, the Waste of Electrical and Electronic Equipment (WEEE) is estimated to be around 50 mln tons per year. In Europe, the amount of generated WEEE is about 12 mln tons per year. Therefore, the recycling market for rare earth in Europe has great potential as the EU is a significant consumer of rare-earth-containing products. Among firms which initiated the projects for recycling of electronic devices such as phones and laptops, the Umicore in Belgium and the Saubermacher in Austria should be mentioned [45, 46].

8.3 Rare Earth Element Recovery from Nickel–Metal Hydride Batteries

The use of REE alloys in the nickel–metal hydride (NiMH) batteries is based, among others, on their hydrogen storage properties as hydrogen storage alloys. For example, $LaNi_5$ used as the negative electrode material in NiMH when transforming into $LaNi_5H_6$ is able to absorb large amounts of hydrogen; the density of hydrogen is higher than in liquid hydrogen (1 m^3 contains 88 kg of hydrogen). Hydrogen uptake takes place at room temperature whereas dehydrogenation at temperatures up to 100 °C.

Hydrogen storage alloys based on $LaNi_5$ are expensive because of the requirement of high-purity lanthanum and nickel. Therefore, lanthanum has been partly replaced by mischmetal (a mixture of rare earth elements such as Ce, La, Nd, Pr and in smaller quantities of Sm, Tb and Y). It has been used as a deoxidizing and desulphurizing agent of steel.

The recycling of NiMH accumulators has been based on their conversion into a stainless steel (as a cheap source of nickel) [47]. Due to limited supplies from China, a method for recovery of nickel, cobalt and rare earth metals from NiMH batteries has been developed. Acids such as HCl, H_2SO_4 or HNO_3 were used for this purpose. The most favourable results were obtained with a 4 M HCl solution [48]. From the REE leaching solutions, they were precipitated in the form of phosphates. The technology for the precipitation of double sulphates with the use of Na_2SO_4 has also been developed [49]. Zhang et al. reported a hydrometallurgical process for the separation and recovery of nickel, cobalt and rare earth metals from NiMH batteries [50, 51].

Li et al. [52] formulated a flow sheet for a hydrometallurgical procedure including leaching in 3 M H_2SO_4, solvent extraction, evaporation and crystallization to recover nickel, cobalt and rare earth from NiMH batteries. The recovery of rare earth elements such as La(III) and Nd(III) from spent nickel–metal hydride (NiMH) batteries by a novel synthetic adsorbent was described in a paper by Gasser and Aly [53]. The layered double hydroxides (LDHs), also known as hydrotalcite (HT)-like materials, were used. They belong to a class of synthetic two-dimensional nanostructured anionic clays. The batch-type experiments were conducted to investigate capacity and uptake of REEs by Mg–Fe-LDH- cyanex-272 using separate nucleation and ageing steps. The effects of some parameters, such as contact time, system pH and adsorbent weight, were investigated.

This process has been tested to separate La(III) and Nd(III) from the NiMH battery using H_2SO_4 as the leaching agent. The stripping of pure La(III) from the solid phase was performed using 0.01 M HCl at 298 K. La(III) and Nd(III) were removed from the filtrate in the form of oxalates, which were calcined at 773 K. After analysing the resulting mixture, it was shown that the neodymium precipitation percentage was higher than 97% and that of lanthanum was lower than 0.8%. The rare earth was obtained as a chloride solution with an overall recovery of 97.8%. Several other studies described the dissolution of rare earth from NiMH batteries by leaching with H_2SO_4 or HCl.

As leaching and precipitating agents used were 2 M HCl and 2 M NaOH solutions, respectively, at room temperature. After calcination at 1273 K, crystalline phases such as NiO, CeO_2 and $LaCoO_3$ were obtained [54]. The nickel was extracted with a solution of ammonia. After heating, nickel hydroxide was obtained which was converted into an oxide during calcination process. The precipitate containing the remaining CeO_2 and $LaCoO_3$ was digested in HCl at room temperature. At this stage, $LaCoO_3$ passed into the solution and CeO_2 remained in the sludge. Provazi et al. [55] studied the recycling of various metals, including cerium and lanthanum, from a mixture obtained from different types of batteries. After grinding to remove volatile metals such as cadmium, zinc and mercury,

the whole matter was heated at 1273 K for 4 h in an inert atmosphere. At this stage, manganese oxides were reduced to MnO and the whole material was leached with sulphuric acid. An attempt was made to separate metals in the leaching solution by selective precipitation and solvent extraction. The extraction with cyanex 272 proved to be the most effective method. Larsson et al. [56] used a similar methodology.

The industrial-scale pilot plant has been operating in Hoboken near Antwerp (Belgium) since 2011. The assumed capacity of the installation is 7,000 tons which are approximately 150 tons of hybrid batteries for electric vehicles or 250 mln batteries for mobile phones. Nickel–metal hydride and lithium-ion batteries have also been recycled. The batteries were placed in a vertical shaft furnace, along with a small amount of coke and slag. From the bottom of the shaft furnace, air enriched with oxygen was supplied. This process required a relatively small amount of energy as the significant energy released during organic electrolyte combustion. Valuable metals from a Ni–Co–Cu–Fe alloy such as Ca, Al, Si and Fe as well as Li and REEs were found in the slag in the form of oxides. These oxide slags can be processed to recover lithium and to manufacture rare earth metal concentrates which can then be used as raw materials in the Solvay REE separation plant (formally Rhodia) in La Rochelle (France).

The recycling process combines the capabilities of Umicore's proprietary ultra-high temperature (UHT) battery recycling process in Antwerp (Hoboken) with the Solvay rare earth refining competences. Rhodia is an international chemical company and a major player in the automotive, electronics, flavours and fragrances, health, personal and home care markets, consumer goods and industrial markets. Umicore is a global material technology group that focuses on application areas where its expertise in materials science, chemistry and metallurgy makes areal difference. Its activities are centred on catalysis, energy materials, performance materials and recycling. After the separation of the nickel and iron from the rare earth, Umicore processed the rare earth into a high-grade concentrate that can be refined and formulated into rare earth materials. The recycling process can be applied to different kinds of NiMH batteries, ranging from portable applications of rechargeable AA (double-A) and AAA (triple-A) batteries used in cordless phones, toys and games to those used in hybrid electric vehicles. Recently, Honda Motor Co., Ltd. and the Japan Metals & Chemicals Co., Ltd. announced to set up a recycling plant to extract REEs from used nickel–metal hydride batteries collected from the Honda hybrid vehicles at Honda dealers inside and outside of Japan. However, the recycling technology and process have not been disclosed. In 2016, Becker et al. [57] developed a hydrometallurgical process for recovery of components from electrode fractions separated from spent NiMH and Li-ion batteries. As a result, collective concentrates of Ni–Co oxides, as well as lanthanide oxides, were obtained. This technology was run in a pilot scale in waste treatment plant at Gorzow Wielkopolski (Poland). Most of the presented above technologies produce a mixture of lanthanides in the metallic form (as a mischmetal) or in the form of their oxides.

8.4 Rare Earth Element Recovery from Permanent Magnets

According to Molycorp in the case of the permanent magnets during their production, the following steps were distinguished: RE mining and concentration, separation of ores into oxides, refining of oxides to metals, forming metals into magnet alloy powders (75–80% in China and 20–25% in Japan) and NdFeB magnet manufacturing (75–80% in China, 17–25% in Japan and 3–5% in Europe). Main rare earth magnet applications are presented in Fig. 8.5.

Bulk permanent magnets are indispensable components of numerous consumer and industrial products for energy conversion. The escalation of rare earth costs presents an opportunity for new magnets with an energy product of 100–200 kJ/m^3, intermediate between ferrite (<38 kJ/m^3) and NdFeB (>200 kJ/m^3), provided that the costs of raw materials and manufacturing kept low [58]. NdFeB magnets are comprised of a $Nd_2Fe_{14}B$ matrix phase, surrounded by a neodymium-rich boundary phase, with small admixtures of Pr, Ga, Tb, Dy and others such as Co, V, Ti, Zr, Mo, Nb. However, the boundary phase contains Cu, Al or Ga. Dy is added to magnets to increase their thermal stability against demagnetization. Sintered NdFeB magnets (also known as Neo magnets, neodymium magnets or NIB) are the most powerful and advanced permanent magnets. These are characterized by high remanence, improved coercive force and better energy. The NdFeB magnets have some limitations due to their poor corrosion resistance. However, they can be easily formed into various sizes and different shapes like discs, rings, blocks and segments. The second type of magnets is based upon samarium–cobalt alloys ($SmCo_5$ or Sm_2Co_{17}) which contain admixtures of different transition metals, such as Fe, Zr and Cu (even though they are without protective coatings) [6]. Therefore, the recovery is only relevant for large magnets which can be directly reused after cutting by applying hydrometallurgical and pyrometallurgical processes. Demand

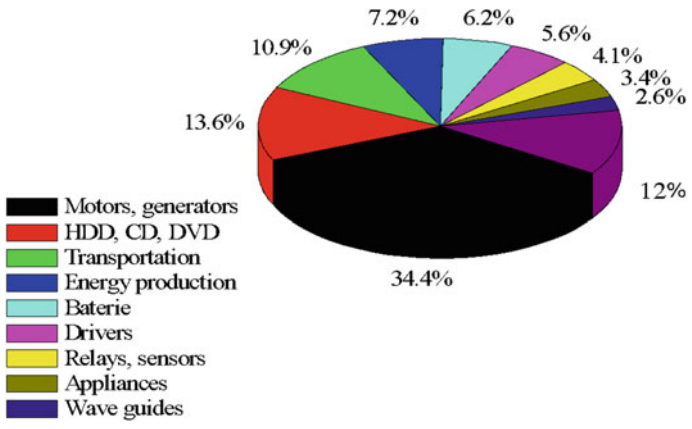

Fig. 8.5 Main rare earth magnet applications (own elaboration based on [58])

for REEs in magnets is predicted to grow by 6–8%. Much of this growth will be related to continuing demand for the use in consumer electronic equipment, wind turbines, motors in electric vehicles, the growth of neo magnets to perform at elevated temperatures. Firms like Hitachi, Showa Denko and Mitsubishi Materials are all searching ways of recycling REEs from discarded hard disc drives and other appliances [34]. The Hitachi approach to recover NdFeB magnets from HDDs and compressors of air conditioners is based on a combination of vibration, demagnetization and manual collection. Another recently developed technology by the University of Birmingham uses hydrogen at atmospheric pressure to separate the sintered REE magnets from the computer HDDs, leading to hydrogenated NdFeB powder.

8.5 Separation of High-Purity Rare Earth Elements

Lanthanide separation and preconcentration of high-purity compounds are the most difficult problems in inorganic chemistry and technology. For separation of lanthanide ions, it is possible to use chemical separation, fractional crystallization, solvent extraction or ion exchange processes. The rare earth elements can be successfully separated and recovered from the sulphurous acid solution using the organophosphorus compounds as extraction agents, e.g. di-2-ethylhexyl phosphoric acid or 2-ethylhexyl phosphonic acid monoethylhexyl ester of 99.9% purity. In the case of recovery and separation of thorium and rare earth elements from acidic aqueous solutions (together with a large concentration of ferric iron), the process comprises a mixture of dialkyl substituted orthophosphoric acid and the second component containing a phosphonyl group, thereby extracting thorium and other rare earth metal elements preferentially. Rare earth elements can also be successfully separated and recovered from sulphuric acid solutions.

As radioactive lanthanide isotopes are important products of the fission of ^{235}U, historically the ion exchange development of the technique followed the Manhattan project. Ion exchange separation of rare earth elements was initiated by Spedding and Powell. In the separation process of rare earth elements (III), the polystyrenesulphonic cation exchangers have been the most often used and rare earth cations exchanged with H^+, NH_4^+ or other cations derived from the ion exchange phase. Charge, size and degree of hydration of the exchanged ions are the most important factors affecting their affinity for the cation exchanger. In the case of ions with the same charge, the affinity depends on their size and degree of hydration. In the lanthanide(III) group with the increasing atomic number, there is a decrease of the ionic radius but no significant differences in their affinity for the polystyrene cation exchangers were found. For this reason, the results obtained for individual rare earth elements using HCl, HBr, HNO_3 and H_2SO_4 were not promising. Only HCl and HNO_3 can be used to separate Ln(III) from the ions that occur in higher oxidation states. Similarly, it creates the possibility of separating Ce(IV) from other rare earth elements using HNO_3. Some removal improvement of REEs can be

obtained using mineral acid solutions containing organic solvents such as methanol, ethanol, 1-propanol or acetone which significantly affects the process efficiency. Ion exchange methods involve three techniques: leaching, elution and frontal analysis. The elution technique with the use of complexing agents is usually used on an industrial scale. In this process, the order of elution of individual REEs depends on the values of stability constants of complex formation. These stability constants generally increase from light to heavy REEs. In the case of cation complexation of cations by anionic ligands, the cation exchanger prefers the cation forming the composite anion with the lowest average number of ligands and a number of analogous complexes that create the weakest complexes [33].

8.5.1 Separations of Rare Earth Elements of High Purity Using Cation Exchangers

In the case of REE separation with cation exchangers, the complexing agents used as eluents include aminopolycarboxylic acids (EDTA, NTA, HEDTA, DTPA, CDTA), carboxylic acids (acetic acid, malonic acid, maleic acid, phthalic acid), hyroxylic acids (α-hydroxyisobutyric acid, citric acid, lactic acid), keto acids (pyruvic acid), aldehyde acids (glyoxilic acid), thioacids (thiodiglycolic acid), phosphonic (1-hydroxyethane-1,1-diphosphonic) and aminophosphonic acids. However, there is a lack of the universal eluent. Therefore, the position of yttrium in the elution sequence of rare earth elements in the cation exchange systems with organic eluents is of interest; for example, yttrium(III) elutes between Dy(III)-Tb(III) with EDTA, near Nd(III) with DTPA, near Pr(III) with HEDTA, near Eu(III) with citrate at 283–293 K and Dy(III)-Ho(III) with citrate at 360–373 K, near Ho(III)-Dy(III) with lactate, near Dy(III)-Ho(III) with thiocyanate and between Sm(III)-Nd(III) with acetate. Therefore, it can be stated that the affinity for the cation exchanger and the kind of the complexing agent affected the separation process. However, the elution process depends on the stability constants (they increase from LREEs to HREEs). Among the eluents used in the process of cation exchange separation of rare earth elements, EDTA and NTA were most useful for industrial application [8, 59, 60].

8.5.2 Separations of Rare Earth Elements of High Purity Using Anion Exchangers

The ion exchange of rare earth elements on anion exchangers with organic chelating ligands has been fully investigated. However, the papers on this subject appearing in recent years indicate the particular application of anion exchangers in this field, giving new, previously unknown possibilities of their application. Anion

exchangers previously used to separate thorium(IV) and uranium(IV,VI) from lanthanides(III) solutions of mineral acids and studies of the chromatographic separation of rare earth elements (III) using anion exchangers were mainly related to isotopes of these elements and were mostly analytical, or physicochemical. In the separation process of rare earth complexes(III), the most practical importance among polystyrene-based anion exchangers was found in strongly basic, gel anion exchangers with quaternary ammonium groups. It was proved that affinity series of rare earth element(III) complexes with the aminopolycarboxylic acids for anion exchangers of various types were atypical and nonmonotonic. Application of the frontal analysis technique allowed to separate Y(III) from Ho(III);Dy(III),Er(III) and Yb(III) from Ho(III)-Er(III) using IDA (iminodiacetic acid) as well as Sm(III) from Ho(III)-Y(III); Nd(III) from Y(III); Y(III) from Ho(III)-Er(III)-Dy(III) and Yb(III) from Ho(III)-Er(III) using HEDTA ((2-hydroxyethyl) ethylenediaminetriacetic acid). In addition, based on the known affinity series of rare earth elements(III) complexes with DCTA (trans-1,2-cyclohexanodiaminotetraacetic acid) for the anion exchanger Dowex 1 × 4 the applicability of anion exchangers of polyacrylic skeleton for separation of the pairs Y(III)-Nd(III) and Y(III)-Sm(III) was shown. Also the studies to determine the effect of the addition of the polar organic solvent (methanol, ethanol, 1-propanol, 2-propanol and acetone) on separation of rare earth element(III) complexes with EDTA particularly of Y(III) from Nd(III) and Y(III) from Sm(III) were carried out [61–64]. The affinity of complexes of these elements for anion exchangers is associated with the differences in the structure of complexes being formed and physicochemical properties of anion exchangers. Moreover, it does not depend on the value of their stability constants as in the case of cation exchange of rare earth elements(III). This creates unique possibilities of separating this group of elements.

8.5.3 Separations of Rare Earth Elements of High Purity Using Chelating Ion Exchangers

Contrary to the cation and anion exchangers, chelating ion exchangers have varying degrees of affinity and selectivity with respect to rare earth elements(III). Their properties depend mainly on the nature of the functional group and less on the bead size and other physicochemical properties. The sorption selectivity particularly affects the relative position of functional groups, their spatial configuration, etc., while the less important are the properties of the matrix. Ion exchange capacity of ion exchange resins depends on the content of these groups and the pH of the solution. A negative feature is their low rate of sorption. For the separation of rare earth elements(III) and their purification from U(IV,VI), Th(IV), Fe(III), Cr(III), Cu(II), Ni(II), Co(II), Mn(II), the chelating ion exchangers with the following functional groups: phosphinic—PO(OH), phosphonic $–PO(OH)_2$, phosphate—OPO

$(OH)_2$, iminodiacetate—$CH_2N(CH_2COOH)_2$, iminodiacetate and aminoacetate—N-CH_2COOH, aminophosphonic—$CH_2NHCH_2PO(OH)_2$, carboxylic—COOH, etc. were used [33, 59, 60, 65, 66].

The chelating and selective ion exchangers were examined by Hubicki et al. [67] to separate microquantities of Sc(III) from Y(III), La(III) or lanthanides(III) by frontal analysis. The phosphonic, aminophosphonic and cellulose-phosphate ion exchangers proved to be the most effective. These ion exchangers can be used for selective separation of Sc(III) from Y(III), La(III) and Ln(III) from their salt solutions of concentrations up to 500 g/dm^3 and acidity to 6 M HC1 due to great stability of the complexes of scandium(III) with phosphonic and aminophosphonic acids. The phenol phosphonic acid precipitates Sc(III) in the presence of such complexing agents as citric and tartaric acids as opposed to other rare earth elements. The phosphonic ion exchanger can be used not only for selective separation of Sc(III) but also for its purification from many cations (6 M HC1 solution does not elute Sc(III) by gradient elution with 0.5–6 M acid). In contrast to the phosphonic, aminophosphonic and cellulose phosphate ion exchangers the significant effect of concentration of the purified rare earth element salt on their separation from Sc(III) can be seen in the case of zirconium phosphate Bio-Rad ZPH.

Good results were also obtained using chelating ion exchangers of amino acid type in the purification of rare earth element salts from Sc(III) due to the differences in stability constants of Sc(III), Y(III), La(III) and RE(III) complexes with iminodiacetic acid. The iminodiacetic chelating ions proved to be particularly useful for the separation of Y(III) concentrates from HREE especially Yb(III) as well as preparation of La(III) of high purity. Similarly, it was used with advantage in the separation of samarium from europium by the redox chromatographic method and for the separation of Y(III) from Nd(III) using the chelating ion exchangers of amino acid type and the dilute HNO_3 solution as an eluent [68]. It was stated that the sequence of elution of Nd(III) and Y(III) for all the examined ion exchangers was not in agreement with the stability constant values of the complexes of Nd(III) and Y(III) with iminodiacetate as well as *N*-benzyl-iminodiacetate acids.

8.6 Current Technologies

There are many descriptions in the literature regarding the processing of rare earth metal raw materials, but over the last three decades, the state of knowledge has not increased significantly, which would modify the chemical technology of their separation. In previous years and at present, the development of extraction methods for separation of REE proceeded simultaneously to the ion exchange method which is the most successful to obtain these elements with a high degree of purity, as the final product of the concentrates obtained in the extraction process.

In 2005, Grirem Advanced Materials Co., Ltd. developed an environmentally friendly hydrometallurgical separation process. A non-saponification solvent extraction process based on hydrochloric acid and sulphuric acid was developed to

separate Nd(III) and Sm(III). In 2008, the separation method of quadrivalent cerium, thorium and fluorine as well as to a small extent trivalent cerium from sulphate solution was introduced with the synergistic extraction stage based on P507 (2-ethylhexyl 2-ethylhexyl phosphate) or P204 (di(2-ethylhexyl)phosphoric acid). Cerium, thorium, fluorine and iron were extracted into an organic phase.

In the literature, descriptions of new extractants are available. For example, sec-nonylphenoxy acetic acid (CA-100) was developed by the Shanghai Institute of Organic Chemistry, Chinese Academy of Sciences. The studies indicated that this extractant employed on a commercial scale has several advantages including stable composition, easy preparation, stronger acidity and low solubility in the aqueous phase [69]. The only disadvantages were: limitation of the extraction system for separation of yttrium over other HREE (low separation factors), two steps for yttrium separation from the impurities after removing the light and middle lanthanides. These can be overcome in heavy lanthanides in the CA-100-EDTA systems. The separation factors of yttrium with respect to Yb, Tm or Er increased with an increase of pH, and the maximum separation was at [CA-100] > 0.04 mol/l and [EDTA]:[HRE] = 1:2. Because of both EDTA and other complexing agents (DTPA, e.g. diethylenetriaminepentaacetic acid and HEDTA, e.g. *N*-hydroxyethylethylenediaminetriacetic acid) form 1:1 complex with rare earth elements, only free (not complexed) rare earth ions take part in the extraction.

A new approach is the molecular recognition technology (MRT) using SuperLig$^{\rightarrow}$. This is an excellent method for improving metal recovery, recycling and end product fabrication processes during metal life cycles with significant operating advantages and environmental gains over traditional procedures. The SuperLig® system consists of a solid support particle, silica gel, to which a metal-selective ligand 18-crown-6 is attached. Therefore, the MRT system is based on green chemistry principles. In this case, minimal waste is generated (chemicals are used only for washing and elution of columns). No organic solvents are used. Moreover, energy requirements are minimal. First of all high selectivity of the SuperLig® products makes separation and recovery of REE possible from the leach solutions at >99% purity level, and subsequent separation of individual REE at >99% levels [70].

To develop sustainable and efficient separation technology for HREEs, the extraction of Lu(III) and neighbouring HREEs using EHEHP type acid-base coupling bifunctional ionic liquid (ABC-BIL) was presented by Dong et al. [71]. Due to low volatility and combustibility, wide liquid range, thermal stability, adjustable functional group and high conductivity, ILs have been found suitable for solvent extraction of REEs [72, 73]. Among bifunctional ILs such as tricaprylmethylammonium sec-octylphenoxy acetates ([A366][CA-12]), tricaprylmethylammonium sec-nonylphenoxy acetates ([A336][CA-100]) in chloride medium were studied [74]. The results indicated that the bifunctional ILs exhibited by the higher efficiencies than the conventional CA-12, CA-100, TBP or P350 extractants. It was also proved that ILs with bis(2-ethylhexyl)phosphate anion can also be applied [75].

Current and future approach to the separation of REEs should include economic aspects for their recovery: low carbon footprint, closed loop for most critical elements, possibility to close the loop for other strategic elements. It is obvious that the

new solvents can help with better separation of REEs to obtain good selectivity. The introduction of more friendly solvents (limitation of the use of petroleum derivative solvents), as well as new synergistic formulations and reduction of salt effluent generation, is also a great challenge. Perhaps applying ionic liquids on the commercial scale and development of new technologies others than solvent extraction will be new approaches in the near future.

Equally important are more environmentally friendly mining and processing operations for new mines and collaboration with China to improve mining operations, extended producer responsibility, more efficient use of REEs in applications or substitution as well as the development of recycling processes for rare-earth-containing products. For example, recycling of NdFeB magnets to recover Nd and Dy means that less primary ores have to be mined to ensure supply of Nd and Dy. Less mining means less overproduction of cerium and samarium. Moreover, recycling of Eu, Tb and Y from lamp phosphors helps to maintain the balance of HREEs.

8.7 Conclusions

Separation of individual REEs on an industrial scale is very complex. Obtaining REEs of high purity requires purification of their concentrates. This is usually achieved by precipitation of REEs as double sulphates $NaLn(SO_4)_2$ or oxalates $Ln_2(C_2O_4)_3$ as well as extraction and/or ion exchange method application. The details connected with the general characteristics, occurrence, physicochemical properties, application and production of REEs in the world as well as their separations by the solvent extraction and ion exchange processes were described in the paper. It should be also mentioned that their separation together with the spectral, magnetic and coordinative properties of REEs is essential for their further applications.

References

1. Gueroult R, Rax JM, Fisch NJ (2018) Opportunities for plasma separation techniques in rare earth elements recycling. J Clean Prod 182:1060–1069
2. Klinger JM (2018) Rare earth elements: Development, sustainability and policy issues. Extr Ind Soc 5:1–7
3. Chakhmouradian AR, Wall F (2012) Rare earth elements: Minerals, mines, magnets (and more). Elements 8:333–340
4. Brown TJ, Shaw RA, Bide T, Petavratzi E, Raycraft ER, Walters AS (2013) World mineral production 2007–2011, British Geological Survey
5. Anielak AM (2000) Chemiczne i fizykochemiczne oczyszczanie ścieków. Wydawnictwo Naukowe PWN Warszawa (in Polish)
6. Binnemans K, Jones PT, Blanpain B, Van Gerven T, Yang Y, Walton A, Buchert M (2013) Recycling of rare earths: A critical review. J Clean Prod 51:1–22

7. Innocenzi V, De Michelis I, Ferella F, Veglio F (2016) Rare earths from secondary sources: profitability study. Adv Environ Res 5:125–140
8. Jha MK, Kumari A, Panda R, Rajesh Kumar J, Yoo K, Lee JY (2016) Review on hydrometallurgical recovery of rare earth metals. Hydrometallurgy 165:2–26
9. Kanazawa Y, Kamitani M (2006) Rare earth minerals and resources in the world. J Alloys Compd 408–412:1339–1343
10. Castor SB, Hedrick JB (2006) Rare Earth Elements. Soc Mining, Metall Explor 769–792
11. Aide MT, Aide C (2012) Rare earth elements: their importance in understanding Soil Genesis. ISRN Soil Sci 12:1–11
12. Charalampides G, Vatalis KI, Apostoplos B, Ploutarch-Nikolas B (2015) Rare Earth Elements: Industrial Applications and Economic Dependency of Europe. Procedia Econ Financ 24:126–135
13. Porowski A, Kaczor-Kurzawa D (2016) Pierwiastki ziem rzadkich (REE) w wodach termalnych: występowanie, pochodzenie, znaczenie i perspektywy badań w Polsce. Tech Poszuk Geol Geoterm Zrównoważony Rozw 1:89–102 (in Polish)
14. Dutta T, Kim KH, Uchimiya M, Eilhann EK, Jeon BH, Deep A, Yun ST (2016) Global demand for rare earth resources and strategies for green mining. Environ Res 150:182–190
15. Humphries M (2013) Rare Earth Elements: The Global Supply Chain. Congr Res Serv 27
16. Rydel P, Nowak M (2015) Review of the major minerals of rare earth elements—gold of the 21st century. Przegląd Geol 63:348–362
17. Jeżowska-Trzebiatowska B, Kopacz S, Mikulski T (1976) Pierwiastki rzadkie część I Występowanie i technologia. Państwowe Wydawnictwo Naukowe, Warszawa
18. Haxel GB, Hedrick JB, Orris GJ (2002) Rare earth elements—critical resources for high technology. United States Geol Surv Fact Sheet 87:4
19. Charewicz W (1990) Pierwiastki ziem rzadkich: surowce, technologie, zastosowania: opracowanie zbiorowe. Wydawnictwa Naukowo-Techniczne, Warszawa (in Polish)
20. Kabata-Pendias A, Mukherjee AB (2007) Trace elements from Soil to Human. Springer, Berlin
21. Henderson P (1984) General geochemical properties and abundances of the rare earth elements. Rare Earth Element Geochemistry. Elsevier, London, pp 1–32
22. Goering PL, Fisher BR, Fowler BA (1991) The Lanthanides. In: Metals and their compounds in the environment: occurrence, analysis, and biological relevance. pp 959–970
23. Jarosinski A (2016) Możliwości pozyskiwania metali ziem rzadkich w Polsce. Zesz Nauk Inst Gospod Surowcami Miner i Energią Pol Akad Nauk 75–88
24. Davris P, Balomenos E, Taxiarchou M, Panias D, Paspaliaris I (2017) Current and Alternative Routes in the Production of Rare Earth Elements. BHM Bergund Hüttenmännische Monatshefte 162:245–251
25. Deng M, Xu C, Song W, Tang H, Liu Y, Zhang Q, Zhou Y, Feng M, Wei C (2017) REE mineralization in the Bayan Obo deposit, China: Evidence from mineral paragenesis. Ore Geol Rev 91:100–109
26. Alonso W, Sherman E, Wallington AM, Everson TJ, Field MP, Roth FF, Kirchain RE (2012) Evaluating Rare Earth Element Availability: A Case with Revolutionary Demand from Clean Technologies. Environ Sci Technol 46:3406–3414
27. Alonso E, Sherman AM, Wallington TJ, Everson MP, Field FR, Roth R, Kirchain RE (2012) Evaluating rare earth element availability: A case with revolutionary demand from clean technologies. Environ Sci Technol 46:3406–3414
28. Klinger JM (2015) A historical geography of rare earth elements: From discovery to the atomic age. Extr Ind Soc 2:572–580
29. Bielański A (2002) Podstawy chemii nieorganicznej. Wydawnictwo Naukowe PWN, Warszawa (in Polish)
30. Cotton S (2006) Lanthanide and Actinide Chemistry. Chichester
31. Huang C (2010) Rare Earth Coordination Chemistry Fundamentals and Applications. John Wiley & Sons, Asia
32. Cotton SA, Raithby PR (2017) Systematics and surprises in lanthanide coordination chemistry. Coord Chem Rev 340:220–231

33. Kołodyńska D, Hubicki Z (2012) Investigation of sorption and separation of the lanthanides on the ion exchangers of various types. In: Ion Exchange Technologies A. Kilislioglu (ed) ISBN 980-953-307-139-3, str. 101-154, http://dx.doi.org/10.5772/50857
34. Massari S, Ruberti M (2013) Rare earth elements as critical raw materials: Focus on international markets and future strategies. Resour Policy 38:36–43
35. Akah A (2017) Application of rare earths in fluid catalytic cracking: A review. J Rare Earths 35:941–956
36. Gschneidner KA (2009) The rare earth crisis -the supply demand. Situation for 2010–2015. Mater Matters 6
37. Zhou B, Li Z, Chen C (2017) Global potential of rare earth resources and rare earth demand from clean technologies. Minerals 7:1–14
38. Gonzalez V, Vignati DAL, Leyval C, Giamberini L (2014) Environmental fate and ecotoxicity of lanthanides: Are they a uniform group beyond chemistry? Environ Int 71:148–157
39. Gambogi J (2015) U.S. Geological Survey, Mineral Commodity Summaries
40. Gambogi J (2017) U.S. Geological Survey, Mineral Commodity Summaries
41. Bütikofer R (2015) Erecon: Strengthening the European rare earth supply-chain, Challenges and policy options
42. Sozański A (1981) Industrial methods for separation of thorium from rare earth elements. Prace Naukowe Instytutu Chemii Nieorganicznej i Pierwiastków Rzadkich Politechniki Wrocławskiej, Wrocław
43. Leveque A (2014) Extraction and separation of Rare Earths, EREAN Summer School Leuven University, 19 August 2014
44. Schüler D, Buchert M, Liu R, Dittrichn S, Merz C (2011), Study on Rare Earths and Their Recycling, Final Report for The Greens/EFA Group in the European Parliament
45. Umicore (2014) Rechargeable Batteries (storing energy). Retrieved from http://www.umicore.com/en/cleanTechnologies/batteries/. Accessed 20 Apr 2018
46. Saubermacher (2014) Leistungen: Entsorgungslösungen. Retrieved from http://www.saubermacher.at/de/leistungen/#elektroaltgeraeteentsorgung. Accessed 24 Apr 2018
47. Müller T, Friedrich B (2006) Development of a recycling process for nickel-metal hydride batteries. J Power Sources 158:1498–1509
48. Lyman JW, Palmer GR (1995) Hydrometallurgical treatment of nickel-metal hydride battery electrodes. In: In Third International Symposium on Recycling of Metals and Engineered Materials. November 12–15. Point Clear, Alabama (USA) 131–144
49. Yoshida T, Ono H, Shirai R (1995) Recycling of used Ni-MH rechargeable batteries. Miner Met Mater Soc 145–152
50. Zhang P, Yokoyama T, Itabashi O, Wakui Y, Suzuki TM, Inoue K (1998) Hydrometallurgical process for recovery of metal values from spent nickel-metal hydride secondary batteries. J Power Sources 50:61–75
51. Zhang P, Yokoyama T, Itabashi O, Wakui Y, Suzuki TM, Inoue K (1999) Recovery of metal values from spent nickel-metal hydride rechargeable batteries. J Power Sources 77:116–122
52. Li L, Xu S, Ju Z, Wu F (2009) Recovery of Ni, Co and rare earths from spent Ni-metal hydride batteries and preparation of spherical $Ni(OH)_2$. Hydrometallurgy 100:41–46
53. Gasser MS, Aly MI (2013) Separation and recovery of rare earth elements from spent nickel-metal-hydride batteries using synthetic adsorbent. Int J Miner Process 121:31–38
54. Kanamori T, Matsuda M, Miyake M (2009) Recovery of rare metal compounds from nickel-metal hydride battery waste and their application to CH_4 dry reforming catalyst. J Hazard Mater 169:240–245
55. Provazi K, Campos BA, Espinosa DCR, Tenório JAS (2011) Metal separation from mixed types of batteries using selective precipitation and liquid-liquid extraction techniques. Waste Manag 31:59–64
56. Larsson K, Ekberg C, Odegaard-Jensen A (2011) Metal separation after selective dissolution of nickel metal hydride batteries. 19th International Solvent Extraction Conference (ISEC2011), 3-7 October 2011. Santiago, Chili, pp 38–45

57. Becker K, Chmielarz A, Szołomicki Z, Gotfryd L, Piwowońska J, Pietek G, Pokora M (2016) Hydrometalurgiczny recykling akumulatorów Ni-MH i Li-ion. Rudy i Met Nieżelazne Recykling 61(6):235–243 (in Polish)
58. Coey JMD (2012) Permanent magnets: Plugging the gap. Scr Mater 67:524–529. https://doi.org/10.1016/j.scriptamat.2012.04.036
59. Hubicka H, Drobek D (2000) Studies on separation of intermediate and heavy lanthanide complexes with iminodiacetic acid on anion-exchangers. Chem Environ Res 9:245–257
60. Hubicka H, Kołodyńska D (2000) Study on separation of lanthanum from praseodymium complexes with IMDA by gel and macroporous anion-exchangers. J Rare Earths 18:90–96
61. Hubicka H, Kołodyńska D (2004) Separation of rare earth element complexes with trans-1,2-diaminocyclohexane-N, N, N', N'-tetraacetic acid on the polyacrylate anion-exchangers. Hydrometallurgy 71:343–350
62. Hubicka H, Kołodyńska D (2005) Effects of polar organic solvent on the separation of the Y(edta)$^-$/Nd(edta)$^-$ complexes on polyacrylic anion exchangers. J Rare Earths 23:124–128
63. Hubicka H, Kołodyńska D (2008) Application of monodisperse anion exchangers in sorption and separation of Y^{3+} from Nd^{3+} complexes with DCTA. J Rare Earths 26:619–625
64. Kołodyńska D, Hubicka H, Hubicki Z (2008) Sorption of heavy metal ions from aqueous solutions in the presence of EDTA on monodisperse anion exchangers. Desalination 227: 150–166
65. Hubicka H, Kołodyńska D (2004) Studies of applicability of strongly and weakly basic polystyrene and polyacrylate anion exchangers for separation of Y(edta)$^-$ from Sm(edta)$^-$ complexes. Chem Environ Res 13:73–85
66. Hubicka H, Kołodyńska D (2004) Separation of rare-earth element complexes with trans-1,2-diaminocyclohexane-N, N, N′, N′-tetraacetic acid on polyacrylate anion exchangers. Hydrometallurgy 71:343–350
67. Hubicki Z (1990) Studies on selective separation of Sc(III) from rare earth elements on selective ion exchangers. Hydrometallurgy 23:319–331
68. Hubicka H, Hubicki Z (1992) Studies on separation of pair Y(III)-Nd(III) on chelating ion exchangers of aminoacid type using aminopolyacetic acids as eluents. Hung J Ind Chem 20:249–254
69. Wang YG, Xiong Y, Meng SL, Li DQ (2004) Separation of yttrium from heavy lanthanide by CA-100 using the complexing agent. Talanta 63:239–243
70. Izatt SR, McKenzie JS, Izatt NE, Bruening RL, Krakowiak KE, Izatt RM (2016) Molecular recognition technology: a green chemistry. Process for separation of individual rare earth metals, White Pap Sep Rare Earth Elem
71. Dong Y, Sun X, Wang Y, Chai Y (2015) The development of an extraction strategy based on EHEHP-type functional ionic liquid for heavy rare earth element separation. Hydrometallurgy 157:256–260
72. Quinn JE, Soldenhoff KH, Stevens GW (2017) Solvent extraction of rare earths using a bifunctional ionic liquid. Part 1: Interaction with acidic solutions. Hydrometallurgy 169:306–313
73. Quinna JE, Soldenhoff KH, Stevens GW (2017) Solvent extraction of rare earth elements using a bifunctional ionic liquid. Part 2: Separation of rare earth elements. Hydroamtealrgy 169:621–629
74. Wang W, Yang HL, Cui HM, Zhang DL, Liu Y, Chen J (2011) Application of bifunctionalionic liquid extractants [A336][CA-12] and [A336][CA-100] to the lanthanum extraction and separation from rare earths in the chloride medium. Ind Eng Chem Res 50:7534–7541
75. Rout A, Kotlarska J, Dehaen W, Binnemans K (2013) Liquid–liquid extraction of neodymium (III) by dialkylphosphate ionic liquids from acidic medium: the importance of the ionic liquid cation. Phys Chem Chem Phys 15:16533–16541

Chapter 9
Sequestration of Heavy Metals from Industrial Wastewater Using Composite Ion Exchangers

Ravichandran Rathna, Sunita Varjani and Ekambaram Nakkeeran

Abstract The transition from agrarian to an industrial society has witnessed several environmental concerns globally. In recent years, contamination of water bodies with refractory contaminants discharged from industrial wastewater significantly interrupted the ecosystems. The most important pollutants in surface and groundwater are arsenic, cadmium, chromium, copper, lead, mercury, nickel and zinc; the recalcitrant pollutant and bioaccumulate in the ecosystems as metal–organic complexes. The conventional techniques used for the removal of heavy metals are chemical precipitation, chemical oxidation, coagulation, evaporation, ion exchange, membrane separation, reverse osmosis, electrolytic and adsorption. However, composite ion exchangers have proven to be versatile and efficient for removing heavy metals from contaminated water. This chapter focuses on various materials (inorganic to nanocomposite) recently developed for the removal of heavy metals from wastewater, mechanisms and treatment performance.

9.1 Introduction

Industrial and service societies play an inevitable role in the rapid development of the global economy which eventually increased the pressure on the environment [1–4]. The transition from agrarian to industrialization has witnessed several environmental concerns that were further aggravated by service industries [5]. Especially, the discharge of pollutants either organic or inorganic including heavy

R. Rathna · E. Nakkeeran (✉)
Department of Biotechnology, Sri Venkateswara College of Engineering (Autonomous), Sriperumbudur Tk 602117, Tamil Nadu, India
e-mail: nakkeeran@svce.ac.in

R. Rathna
e-mail: rathnaravi.v@gmail.com

S. Varjani (✉)
Gujarat Pollution Control Board, Sector-10A, Gandhinagar 382010, Gujarat, India
e-mail: drsvs18@gmail.com

Inamuddin et al. (eds.), *Applications of Ion Exchange Materials in the Environment*,
https://doi.org/10.1007/978-3-030-10430-6_9

metals from industries into the water bodies is a major concern to ecological and global health [6]. Heavy metals are metallic elements with relatively higher atomic masses and densities equal to or greater than 5.0 g/cm^3 [7]. The major sources of release of heavy metals into the environment are industrial discharge, mining operations, agriculture activities, faculty transportation, damming, tanneries and e-waste disposal. These sources dispose different types of organic and inorganic contaminants which get deposited in the natural biota. The most prominent perilous heavy metals of concern are arsenic (As), cadmium (Cd), chromium (Cr), copper (Cu), lead (Pb), mercury (Hg), nickel (Ni) and zinc (Zn), which are toxic even at trace concentrations. These heavy metals, in nature, are not biodegradable and tend to accumulate in living creatures leading to adverse effects beyond a certain limit.

According to central pollution control board of India (CPCBI), 80% of hazardous wastes are released from Gujarat, Maharashtra and Andhra Pradesh [8]. Pandey and Singh [9] reported an average concentration of 31,988.6 μg/g of iron (Fe), 67.8 μg/g of zinc, 26.7 μg/g of lead, 26.7 μg/g of nickel, 372.0 μg/g of manganese (Mn), 29.8 μg/g of copper, 1.7 μg/g of cadmium and 69.9 μg/g of chromium in the sediment of Ganga River. Similarly, Raju et al. [10] investigated the sediment of River Cauvery, Karnataka and found average concentrations of 11144 μg/g (iron), 1763.3 μg/g (manganese), 93.1 μg/g (zinc), 389 μg/g (chromium), 27.7 μg/g (nickel), 11.2 μg/g (copper), 4.3 μg/g (lead), 1.9 μg/g (cobalt) and 1.3 μg/g (cadmium). In the case of the Godavari River and its tributaries basin [11], iron was at higher concentration, whereas cadmium concentration was lower. The arsenic, cadmium, chromium, iron and zinc metals were under the prescribed limit of Bureau of Indian Standards (BIS). These contaminations emanated from rapid industrialization and population growth resulted in poor environmental quality.

Arsenic is a metalloid of great toxicological concern to human health. In groundwater, arsenic exists in oxy-anions as trivalent arsenite and pentavalent arsenate [12] and is a well-known carcinogen [13]. Smelting industries, thermal power plants, fuel-burning and geogenic processes are important sources of arsenic pollution. In India, West Bengal and Uttar Pradesh (Ballia and other districts) are the main regions where the groundwater is contaminated with 10–3200 ppm range of arsenic [12]. The American Conference of Governmental Industrial Hygienists (ACGIH) categorized arsenic as 'Classified A1' carcinogen and the median lethal dose of arsenic acute oral toxicity as 145 mg/kg for the mouse. Ravenscroft et al. [14] documented 0.5–5000 ppb of arsenic in groundwater in more than 70 countries. Prolonged and excess human intake of arsenic damages skin, lung, kidneys, nervous system and mucous membranes. The minimum fatal and lethal dose was estimated at 70–180 and 1–3 mg/kg arsenic trioxide for humans [15].

Cadmium is a toxic metal categorized as classified A2 carcinogen for human by ACGIH, National Toxicology Program (NTP), whereas International Agency for Research on Cancer (IARC) classified cadmium as a known human carcinogen (Group 1) while Environmental Protection Agency (EPA), United States classified Cd as Group B1 probable human carcinogen [16]. The sources of Cd contamination are refining zinc ores, smelting process, e-waste, battery waste, paint sludge, nuclear reactors, incineration and fuel. Pandey and Singh [9] reported that Cd

concentration ranged between 0.94 and 2.86 µg/g in sediments of Ganga River in Varanasi. Recently, Mohan Kumar et al. [17] reported the contamination of Hg, As and Cd in borewell water in the Kurichi industrial cluster of Coimbatore, Tamil Nadu. Chronic exposure to Cd leads to dysfunction in the respiratory, cardiovascular and renal systems. Excessive exposure of Cd in Japanese women led to 'Itai-Itai' disease. As per EPA, the reference dose for human exposure is 5×10^{-4} mg/kg/day.

Chromium is an important resource material in steel and tannery industries. Cr, in nature, exists in two main forms, namely trivalent chromium (Cr III) and hexavalent chromium (Cr VI). Cr (III) is an essential dietary element for the metabolism of sugar, protein and fat, with a recommended intake of 50–200 µg/day for adults. The human body to an extent can detoxify Cr (VI) to Cr (III). The sources of chromium pollution are mining activities, paint and pigments, industrial coolants, leather tanning, metal processing and steel fabrication. ACGIH has classified Cr as A4 (Not classifiable for human or animal) and IARC categorized as group 3 carcinogen (Not classifiable for human). Toxicological studies reported that chronic exposure of Cr (VI) is much more toxic than Cr (III); further, the uptake of Cr (VI) by the cell is higher than Cr (III). According to Occupational Safety and Health Administration (OSHA), the permissible exposure limit of Cr (III) and Cr (VI) is 8-h time-weighted average of 500 and 5 µg Cr/m^3, respectively. The present EPA regulation for the maximum level of Cr in drinking water is 100 µg/L. Cr acute poisoning occurs through ingestion while chronic poisoning occurs from inhalation and dermal contact. The average oral lethal dose of Cr (VI) in human is 1–3 g and long-term exposure led to lung cancer. Prolonged exposure of Cr led to respiratory, gastrointestinal, immunological, haematological, reproductive and developmental effects. In India, the major heavy metals' contaminated sites are Ranipet in Tamil Nadu, Kanpur in Uttar Pradesh, Vadodara in Gujarat and Talcher in Orissa. Maximum acceptable limit of Cr in water is 0.05 mg/L as per Indian Standard for Drinking Water, BIS specifications IS 10500:2012.

Copper is an essential trace element for human and plants metabolism. Copper contamination is mainly due to the industrial waste from the mining site, electroplating and smelting operations. Gotteland et al. [18] demonstrated gastric problems like nausea and vomiting due to the acute exposure of copper. Indian standard drinking water as per BIS specifications IS 10500:2012, the maximum permissible limit of Cu in drinking water is 1.5 mg/L and the highest desirable limit is 0.05 mg/L.

Lead is a naturally occurring soft, dense and pliable metal mostly used in paint and gasoline. The industrial wastes such as paint, batteries, e-waste, power plant, ceramics, cosmetic industries and bangle industries have been the major sources of lead contamination. The major lead-contaminated sites in India are Ratlam in Madhya Pradesh, Bandalamottu mines in Andhra Pradesh, Vadodara in Gujarat and Korba in Chattisgarh. Indian standard drinking water as per BIS specifications IS 10500:2012, highest desirable limit of Pb in drinking water is 0.01 mg/L and no permissible limit. Centres for Disease Control and Prevention defined reference level as 5 µg/dL of lead for adverse health effects in children and adults. Over exposure of Pb leads to neurological disorder, reproductive problems and

hypertension. The Food and Drug Administration (FDA), USA, recommends 5 ppb of Pb as an accepted value for bottled water. According to EPA, the action level of Pb in drinking water is 15 ppb.

Mercury is an environmental toxin that has adverse effects on pregnant women and children [19]. In general, Hg occurs in three forms, namely elemental, organic and inorganic forms. Elemental form of Hg volatiles readily and enters the living system through the body while inorganic form Hg is caustic to humans and enters the body through skin, whereas the organic form of Hg is lipid soluble and well absorbed via the gastrointestinal tract, lungs and skin, further have the ability to cross the placenta and contaminate breast milk. Hg is mainly released into the environment through medical instrumental waste (thermometers, barometers and sphygmomanometers), electrical appliances, lambs, thermal power plant and chlor-alkali plants. Long-term exposure of Hg leads to damage to the cardiovascular system, reproductive organs and affects the developmental metabolism. Hg at lower concentration can be nephrotoxic, neurotoxic and carcinogenic to humans. Kodaikanal in Tamil Nadu, Ganjam in Orissa and Singrauli in Madhya Pradesh are the major mercury-contaminated sites in India. Indian standard drinking water as per BIS specifications IS 10500:2012, highest acceptable limit of Hg in drinking water is 0.001 mg/L and no permissible limit.

Nickel is an essential trace metal at low concentration, especially for plants, whereas toxic at higher concentration. Ni is generally discharged into the environment from various anthropogenic activities such as thermal power plant, smelting operations and battery industries. Acute exposure to nickel in the human leads to death within 60 min at a lowest observed adverse effect level 382 M (death of one man) mg/m^3. Ni-contaminated sites in India are Joy Nagar in Chennai, industrial area of Mysore city and industrial area in Madhya Pradesh [20]. Indian standard drinking water as per BIS specifications IS 10500:2012, highest acceptable limit of Ni in drinking water is 0.02 mg/L and no permissible limit since Ni is a carcinogen.

Zinc is an essential metal ion involved in most of the biological and physiological roles in the human system. The biological half-life of Zn is about 280 days, and the human body has the ability to control the Zn level metabolically and set to a threshold [21]. However, acute exposure to Zn can lead to death. The lethal concentration to kill 50% of mice is 11,800 $mg/min/m^3$. The main sources of discharge of Zn in the environment are smelting and electroplating. Eloor-Edayar, Cochin, Kerala and Rajasthan are the main Zn-contaminated sites in India. Indian standard drinking water as per BIS specifications IS 10500:2012, the maximum permissible limit of Zn in drinking water is 15 mg/L and the highest desirable limit is 5 mg/L.

Government and regulatory bodies are more stringent for the release of pollutants including heavy metals into the environment from industrial wastewater [22]. These pollutants are removed from the wastewater to prevent and protect the ecosystem and environment. The conventional methods used for the treatment of heavy metal ions from industrial wastewater include precipitation, oxidation, coagulation, evaporation, membrane process, electrolytic method, adsorption and ion exchange [4, 23]. Chemical precipitation is the simplest and widely used

method by the industries for the treatment of inorganic effluents. The most commonly employed chemical precipitants are calcium and sodium hydroxides, metal sulphates and sulphate reducing bacteria [24, 25]. Though this method is inexpensive, simple and safe, the amount of precipitants required for the process is high and sludge disposal is cumbersome [24, 26].

Coagulation is always followed by chemical precipitation. The coagulant used for the treatment is negatively charged which reduces the positively charged heavy metals and settles at the bottom. Coagulation is not effective for treating acidic wastewater and the disposal of the generated sludge has been the problem. Chemical oxidation method is used as a pre-treatment process for industrial organic effluents. In this method, the oxidizing agent helps in structural changes in heavy metals to make it less toxic. However, this method does not completely remove the heavy metals and also generates toxic by-products. Jakob et al. [27] demonstrated thermal treatment or evaporation to treat heavy metals in municipal solid waste incinerator fly ash. However, evaporation meant to concentrate heavy metal in wastewater, the treatment is not effective and sludge treatment is an issue.

The electrochemical method is an effective method for the treatment of heavy metals, however, not widely used since the installation cost and energy requirement are high. Recently, industrialists and researchers are gaining interest towards the use of membrane process and adsorption process for heavy metals removal because these methods do not involve harsh chemicals, expensive installation and energy requirements. The literature reported that the efficiency of the adsorption process depends on the type of adsorbent used; however, the use of low-cost bioadsorbent is effective for effluents with a low concentration of heavy metals. Membrane filtration process is effective in removing heavy metals, but its use is limited due to low-permeate flux, process complexity and membrane fouling. In addition, the sludge disposal and membrane cleaning are still problematic [26, 28].

Ion-exchange process has been widely used for the removal of heavy metals from industrial effluents. The major companies that play a key role in the manufacture of ion-exchange resins for various applications are depicted in Table 9.1. The main advantage of this method is a larger treatment capacity with better kinetics and improved removal efficiency [29]. Ion-exchange resins play an important role in heavy metals treatment; the exchange of ions takes place between the resin matrix and heavy metals in the water. The resins could be regenerated and reused. This book chapter mainly deals with ion-exchange materials used for the treatment of heavy metals.

9.2 Ion-Exchange Materials

Ion-exchange process is the most common and versatile method used for removing heavy metals from industrial effluents. Table 9.2 illustrates the various commercial ion exchangers and their functional groups. The mechanism behind the process is highly selective and reversible which makes it an outstanding method. Based on the

Table 9.1 List of major companies involved in the ion-exchange resin market

Company	Country	Established year	Products
Aldex Chemical Company Limited	Canada	1927	Low sodium resin
Anhui Sanxing Resin Technology Co. Ltd.	China	2004	Ion-exchange resin and macropore resin
Auchtel Products Ltd.	India	1997	Cation and anion ion exchange for wastewater treatment
Bengbu Dongli Chemical Co. Ltd.	China	2016	Ion-exchange resin
Bio-Rad Laboratories, Inc.	USA	1952	Ion-exchange resins for purification process
DowDuPont	USA	1897	The polymeric ion-exchange resin
Eichrom Technologies Inc.	USA	1990	Analytical grade cation- and anion-exchange resins
Evoqua Water Technologies LLC	USA	2013	Ion-exchange resin for industrial, high purity, and speciality applications
Finex Oy	Finland	1990	Polymers and ion-exchange resins
Hebi Juxing Resin Co. Ltd.	China	1995	Ion-exchange resin for water treatment
Ion Exchange Ltd.	India	1964	Ion-exchange resins for water treatment, liquid waste treatment, recycle and solid waste management.
Jacobi Carbons Ab	Sweden	1916	Resinex for demineralization
Jiangsu Linhai Resin Science and Technology Co. Ltd.	China	1972	Ion-exchange resins
Jiangsu Suqing Water Treatment Engineering Group Company Ltd.	China	1970	Developing and producing ion-exchange resin for wide application
Lanxess	Germany	2004	Lewatit ion-exchange resins for industrial water treatment
Mitsubishi Chemical Corporation	Japan	1934	Ion-exchange resin for wide application
Ningbo Zhengguang Resin Co. Ltd.	China	1969	ion-exchange resin manufacture and application company
Novasep Holding	France	1995	Ion-exchange technology for bioindustrial applications
Ovivo	Canada	1975	Ion exchange for demineralization
Purolite	USA	1981	Development and production of advanced resin technologies
Resintech	Malaysia	1977	Manufactures a broad range of ion-exchange resins for water and wastewater treatment

(continued)

Table 9.1 (continued)

Company	Country	Established year	Products
Samyang Corporation	South Korea	1924	Domestic maker and seller of ion-exchange resins
Sunresin New Materials Co. Ltd.	China	2001	Chelating resin for metal ions removal and polymeric resin for herbal extracts
Thermax	India	1980	Resins for demineralization plant
Tianjin Nankai Hecheng Science & Technology Co. Ltd.	China	2004	Ion-exchange resins

resin charge, ion-exchange resins are categorized as cation exchangers and anion exchangers. The materials used for the synthesis of ion-exchange resins include organic, inorganic or organic–inorganic composite.

9.2.1 Organic Materials

Figure 9.1 depicts the various categories of organic ion-exchange resins. The organic ion-exchange resins are highly stable, uniform and reusable. Zeolites (tectosilicates) are volcanic minerals that help in detoxifying heavy metals. The most common zeolites are analcime (cubic/tetrahedral), chabazite (rhombohedral), clinoptilolite (monoclinic/orthogonal), heulandite (monoclinic/orthogonal), natrolite (orthogonal/tetrahedral), phillipsite (monoclinic) and stilbite (monoclinic). These zeolites are a three-dimensional framework that contains channels and interconnecting cages comprising aluminium, silicon and oxygen atoms [30]. Clinoptilolite is the most popularly used zeolite for the removal of heavy metals from industrial effluents. Stylianou et al. [31] demonstrated the mechanism and effective removal of Pb, Cu and Zn in fixed bed column containing natural clinoptilolite. Pb was effectively removed by the ion-exchange mechanism. Zn was removed easily than Cu by both ion-exchange and sorption mechanisms. The metal-removing capacities of bentonite, zeolite and vermiculite were highly influenced by the composition of the liquid medium, solubility of metal, pH, temperature and suspended solids [32]. Recently, Higgins Loop technology with coal as an ion-exchange resin has been proved as the effective method for the removal of heavy metals [33]. Cellulose-based ion-exchange resins are gaining attention for the removal of heavy metals. Sungur and Babaoğlu [34] have reported the selectivity of cellulose ion exchangers synthesized by esterification of hydroxyethylcellulose for the removal of Pb, Cd, Co, Cu, Fe, Ni, Zn and Cr from aqueous solutions.

Table 9.2 Various commercial ion exchangers available in the market

Ion exchanger	Manufacturers	Type	Functional group	Total exchange capacity (meq/mL)	Ion species removed
Amberlite IRC-718	Dow Chemical	The chelating cation-exchange resin	Iminodiacetic acid	1.1	Heavy metal cations (divalent/ bivalent metal ions)
Bio-Rex 5	Bio-Rad	Weak anion exchangers	The tertiary amine functional groups	1.1	I, Br and Cl
C-800 LT UPS	Aldex	Gel-type cation resin	Sulfonated styrene/ divinylbenzene copolymer	1.9	Fe and Cl
DiaIon	Mitsubishi Chemical Corporation	Gel/porous/highly porous strongly acidic cation-exchange resin/strongly basic anion-exchange resin/weakly acidic cation-exchange resin/weakly basic anion-exchange resin	Sulphonic acid/ acrylic acid/ methacrylic acid/ quaternary ammonium/tertiary amine/polyamine	–	–
Dowex 50 W-X8	Lenntech	The strongly acidic cation-exchange resin	Sulphonic acid	1.7	Cu, Cd, Zn, Ni and Pb
Duolite GT-73	Dow Chemical Company	Chelating resin	Thiol	1.4	Hg, Ag, Pb, Cu and Cd
Lewatit MonoPlus TP 214	Lanxess	Microporous chelating resin	Thiourea	1.0	Hg, Cd, Co and precious metal recovery
MB101	Bengbu Dongli Chemical Co. Ltd.	Mixed bed ion-exchange resin	Sulphonic acid/ quaternary ammonium	2.0	Used for water treatment chemicals
ASM-10-HP	ResinTech	Gel-type chlorine form hybrid anion-exchange resin	Hybrid	–	As
S 930	Purolite	Chelation resins	Iminodiacetic	–	Cu

(continued)

Table 9.2 (continued)

Ion exchanger	Manufacturers	Type	Functional group	Total exchange capacity (meq/mL)	Ion species removed
SIR-500	ResinTech	Microporous chelating weak acid cation resin	Aminophosphonic	1.4	Cu and Ni
Tulsion CXO-12	Thermax	Weak acid cation resin	Carboxylic	4.2	Selective removal of heavy metals

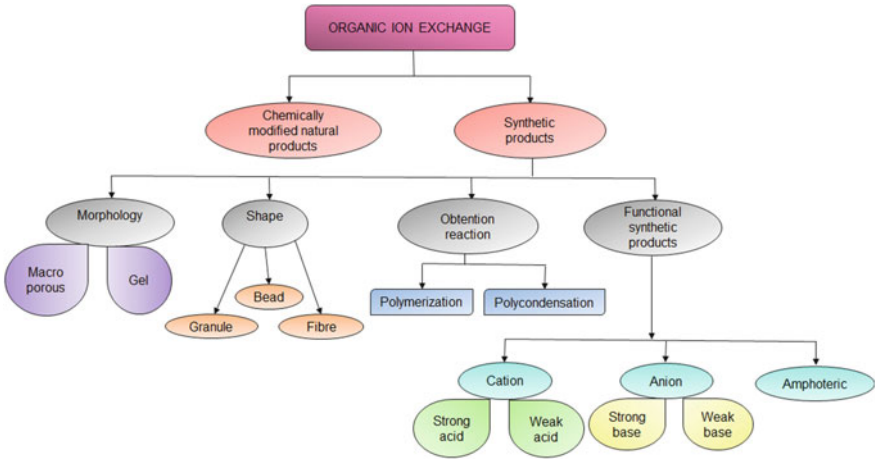

Fig. 9.1 Organic ion-exchange resin categories

9.2.2 *Inorganic Materials*

Inorganic ion-exchange resins with higher thermal and radiation stability are synthetic materials mainly developed for the selective removal of heavy metal ions. Figure 9.2 illustrates the different classification of inorganic ion-exchange resins. The first synthetic inorganic ion-exchange material was zeolite used for the treatment of industrial effluents. The synthetic zeolites are better than natural zeolites in terms of physicochemical properties like pore size, thermal stability and chemical characteristics. The main limitations of synthetic zeolites are cost and ion specificity. Chutia et al. [35] demonstrated the effective removal of arsenic at high and low initial concentration levels employing synthetic H24 (arsenic concentration: 10 mg/L, % removal: >76, capacity: 35.80 mg/g) and H90 (arsenic concentration: 10 mg/L, % removal: >80, capacity: 34.80 mg/g) zeolites.

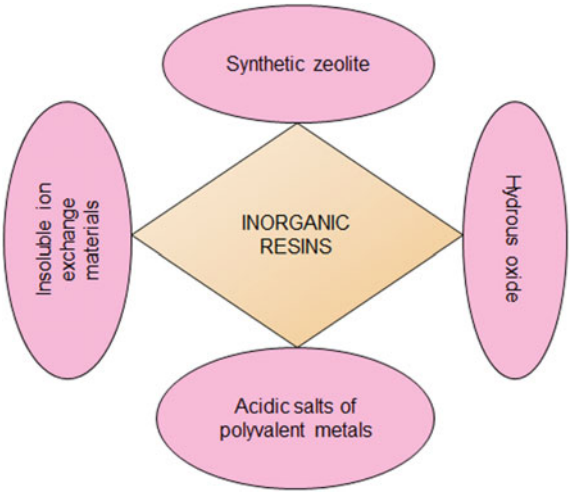

Fig. 9.2 Inorganic ion-exchange resin categories

Hydrous oxides are well-established ion-exchange materials that adsorb ions through an ion-exchange mechanism. Hydrous oxides are categorized into particle hydrates (surface phenomenon) and framework hydrates (cavities or tunnels present in the framework). Particle hydrates are formed from groups 3 and 4 of d-transitions elements and groups 13 and 14 p-representative elements. The particle hydrate interior structure is similar to calcined oxides with a hydroxyl group and water molecules on the surface. This structural resemblance is responsible for ion-exchange behaviour and amphiprotic in nature, i.e. can function as both cationic and anionic exchangers. Amphiprotic nature is controlled by pH, under basic conditions; cations are exchanged, whereas under acidic condition anions are exchanged [36]. The most common examples of particle hydrates are ZrO_2 and SnO_2. Framework hydrates are developed from oxidation states of metals present in groups 5 and 15. The most common example of framework hydrates is hydrous oxides of antimony and manganese. In general, framework hydrates are poorly crystalline which could be improved by refluxing in acid media or treatment with hydrothermal technology [36].

Acidic salts of polyvalent metals are amorphous in nature and known for their resistance to temperature and ion-exchange properties. These materials have been developed by combining acidic oxides of metals of groups 4, 5 and 6 d-transitions elements in periodic table. The structural composition depends on the environment in which the material was precipitated and these are non-stoichiometric compounds.

Insoluble ion-exchange materials are formed by the precipitation of metal salts with sodium sulphide or hydrogen sulphide. Researchers are focussed on investigating the exchange properties of insoluble sulphides such as Ag_2S, SnS, CuS, PbS, FeS, NiS with the insoluble ion-exchange materials. The materials' composition is highly responsible for its metal selectivity and ion-exchange capacity.

9.2.3 Composite Materials

Composite ion-exchange materials are advanced chemically engineered resins generated by combining organic and inorganic ion-exchange materials to overcome the individual limitations of the materials. Composite ion-exchange materials are superior in terms of versatility, mechanical stability, cost and ion-exchange capacity. Table 9.3 summarizes the work carried out on the composite ion exchanger for the removal of heavy metals. In the past two decades, sol–gel-based composite ion exchangers had a wide range of applicability in biochemical engineering and material science fields. The sol–gel method generates a hybrid composite material with properties unique from its raw material.

9.2.3.1 Hybrid Materials

The poor thermal stability of organic resins and non-reproducible nature of inorganic ion exchangers have drawn significant attention towards organic–inorganic hybrid exchangers with ameliorated characteristics. Acrylamide aluminium tungstate, a hybrid cation exchanger, can withstand temperatures up to 600 °C while retaining feasible ion-exchange capacity of 76% compared to other ion-exchange materials such as tin (IV) iodophosphate, zirconium (IV) iodomolybdate and zirconium (IV) selenophosphate. The influence of size and charge of the exchanging ion is reflected in the ion-exchange capacity of the hybrid [37, 38]. Amongst the alkali and alkaline earth metal ions, decreasing hydrated ionic radii facilitates easy entry into the pores of the exchanger resulting in higher adsorption, with an ion-exchange capacity of 1.25 meq/g for Na^+ ions [39]. The separating potential of the material has been demonstrated by achieving separations of two-component mixtures of metal ions (Pb^{2+} and Hg^{2+}) with 90% recovery for Pb^{2+} and 92% recovery for Hg^{2+}. Thus, recovery of zinc from galvanizing waste can facilitate through separation of zinc from the lead. Moreover, these heavy metals can be selectively removed from industrial and wastewater effluents to reduce their pervasive presence in the environment.

Acetonitrile stannic (IV) selenite, prepared by incorporating the organic polymer into the matrix of inorganic material, has high thermal stability with the ability to withstand temperatures up to 500 °C with retention of 60% ion-exchange capacity. The multiplication of ion-exchange capacity in comparison with stannic selenite (inorganic counterpart) is attributed to the addition of acetonitrile (organic polymer). The composite cation exchanger has an affinity sequence of $K^+ > Na^+ > Li^+$ for alkali metal ions and $Ba^+ > Sr^{2+} > Ca^{2+} > Mg^{2+}$ for alkaline earth metal ions and an ion-exchange capacity of 1.83 meq/g for Na^+ ions. This affinity sequence is in accordance with the change in hydrated radii of the exchanging ion species, that is, smaller the hydrated ionic radii greater the adsorption [40]. High adsorption of the cation exchanger towards Th^{4+} (radioactive element) makes it a potent candidate for the removal of radioactive toxicity from nuclear and industrial wastes.

Table 9.3 Composite ion exchanger for the removal of heavy metals

Composite ion exchanger	Type	Selectivity of metal ions	Operational mode	Ion-exchange capacity	Removal efficiency (%)	References
Acetonitrile stannic (IV) selenite	Hybrid cation exchanger	Th(IV)	Batch experiment	0.75–1.83 meq/g	97–98	[40]
Acrylamide aluminium tungstate	Hybrid cation exchanger	Hg(II)	Batch experiment	1.25 meq/g	97.2–99.7	[38]
Carboxymethyl cellulose Sn (IV) phosphate	Composite nano-rod-like cation exchanger	Cu(II), Ni(II), Zn(II), Mn(II)	Batch experiment	2.13 meq/g	–	[41]
Cellulose acetate-tin (IV) phosphate	Nanocomposite ion exchanger	Cd(II)	Batch experiment	1.48 meq/g	–	[48]
Chitosan-supported zirconium (IV) tungstophosphate	Biopolymeric matrix	F	Batch experiment	2025 mgF^{-}/kg	–	[42]
EDTA-zirconium iodate	Hybrid cation exchanger	Mg(II), Al(III)	Batch experiment	2.0 meq/g	88–99.3	[39]
Nylon-6,6 Sn (IV) phosphate	Fibrous type composite cation exchanger	Hg(II)	Batch experiment	2.1 meq/g	–	[43]
Polyacrylamide thorium (IV) phosphate	The hybrid fibrous ion exchanger	Pb(II)	Batch experiment	3.89 meq/g	99	[44]
Poly-o-anisidine tin (IV) arsenophoshate	Nanocomposite ion exchanger	Pb(II)	Batch experiment	1.82 meq/g	–	[50]
Sodium bis(2-ethylhexyl) sulfosuccinate-cerium (IV) phosphate	Cationic exchange	Cu(II), Pb(II), Cd(II), Zn(II), Hg(II)	Batch experiment	3.02 meq/g	–	[45]
Triton X-100 based Ce (IV) phosphate	Fibrous ion exchange	Cr(III)	Batch experiment	2.1 meq/g	–	[46]
Triton X-100-based Tin (IV) phosphate	Hybrid ion exchanger	Pb(II), Hg(II), Fe(III)	Batch experiment	2.75 meq/g	–	[47]

In addition, the practicality of the composite ion exchanger has been demonstrated by the recovery of 92% of Cu and Zn from commercially available brass alloy sample [40]. Thus, acetonitrile stannic (IV) selenite possesses characteristics of a good ion-exchange material to alleviate the detrimental effects of heavy metal toxicity on the environment.

Carboxymethyl cellulose Sn (IV) phosphate composite ion exchanger has been developed by integrating the organic polymer carboxymethyl cellulose into the matrices of inorganic ion exchanger Sn (IV) phosphate. This is known for its enhanced mechanical strength, thermal properties, chemical stability, granulometric characteristics and ion-exchange capacity. Mohammad et al. [41] have studied the forward kinetics and ion-exchange mechanism of heavy metal ions on the surface of carboxymethyl cellulose Sn (IV) phosphate composite nano-rod-like cation exchanger.

Chitosan-supported zirconium (IV) tungstophosphate ion exchanger is a novel biocomposite formed by incorporating zirconium (IV) tungstophosphate inorganic ions into the polymeric matrix of chitosan. Viswanathan and Meenakshi [42] investigated the removal of fluoride employing chitosan-supported zirconium (IV) tungstophosphate ion exchanger. The material exhibited 2025 mg/kg of defluoridation capacity, and the equilibrium sorption fitted Freundlich and Langmuir isotherms. The sorption was spontaneous and endothermic in nature and followed pseudo-second-order and intraparticle diffusion models of kinetics.

EDTA-zirconium iodate is an amorphous organic–inorganic hybrid cationic ion exchanger exhibiting high ion-exchange selectivity and capacity to Pb. Nabi et al. [39] have demonstrated the ion-exchange selectivity of EDTA-zirconium iodate towards various heavy metals. This material showed greater selectivity to Pb than other heavy metals and possessed enhanced thermal, chemical, mechanical and granular properties. Its ion-exchange capacity with good reproducibility was 2 meq Na^+/g dry exchanger.

Nylon-6,6 Sn (IV) phosphate is a cation exchanger highly selective for Hg(II). The maximum ion-exchange capacity of the composite was 2.1 meq/g for Na^+ ions [43]. Islam and Patel [44] synthesized hybrid fibrous polyacrylamide thorium (IV) phosphate ion exchanger employing co-precipitation method for effective removal of Pb (II). It was reported that pH played an important role in the removal of Pb, with an increase in pH, removal efficiency was increased from 60 to 99%. The adsorption followed first-order kinetics. This ion exchanger was not able to reduce the concentration of Pb to permissible limit. Further, studies on coupling this material with another absorbent could improve the performance.

Sodium bis(2-ethylhexyl) sulfosuccinate-cerium (IV) phosphate cation exchanger has exhibited effectiveness for the removal of Cu^{2+}, Pb^{2+}, Cd^{2+}, Zn^{2+} and Hg^{2+} in the presence of acid, alkali and other transition metal ions [45]. This material could be categorized as a green chemistry ion exchanger. Triton X-100-based Ce (IV) phosphate ion exchanger was developed by El-Azony et al. [46] for the separation of Cr (III)/Cr (VI) through surface-active phenomenon. Further, the ion-exchange capacity was 2.1 meq/g (36 mg Cr (III)/dry g) which was similar to the ion-exchange capacity of organic cation exchanger Amberlite IR-120 for Cr

(III) (35 mg/g). Varshney et al. [47] have synthesized Triton X-100-based Tin (IV) phosphate ion exchanger for the selective removal of Pb (II), Hg (II) and Fe (III). The ion-exchange capacity of this material (2.75 meq/g) was superior to that of acrylamide Ce (IV) phosphate (2.60 meq/g) and the thermal stability of this material ranged between 150 and 305°C.

9.2.3.2 Nanocomposite

Compared to inorganic ion exchangers, cellulose acetate-tin (IV) phosphate nanocomposite ion exchanger has exhibited better ion-exchange capacity and thermal properties. This material showed higher selectivity to Cd^{2+} with an ion-exchange capacity of up to 31.75 meq/g at 400 °C [48]. Further, the biostatic nature of nanocomposite ion exchanger inhibited the growth of bacteria, *Escherichia coli*. Khan and Akhtar [49] have demonstrated the separation of heavy metals by poly-o-toluidine Ce (IV) phosphate cation exchanger and studied the electrical borderline semi-conducting nature of the material. Further, the material exhibited good ion-exchange capacity, thermal property and chemical resistivity.

Khan et al. [50] synthesized poly-o-anisidine tin (IV) arsenophoshate nanocomposite cation exchanger which has selectivity for Pb (II). The material showed an ion-exchange capacity of 1.82 meq/g in the blackish granular sample. This material could be used as a membrane electrode [50] and humidity sensor [51].

Pectin thorium (IV) tungsto molybdate nanocomposite ion exchanger was prepared using sol–gel method with high ion-exchange capacity and thermal stability [52]. Pectin thorium (IV) tungsto molybdate nanocomposite showed an ion-exchange capacity of 1.10 meq/g. It is thermally stable up to 400 °C. This composite has strong selective binding to Cr and Pb.

9.3 Mechanism of Ion-Exchange Process

Ion-exchange process depends on chemical reaction and diffusion process. However, the chemical reaction is not directly involved in the ion-exchange process. Diffusion process depends solely on the material used for the development of the ion exchanger [53]. The mechanism of ion-exchange process (Fig. 9.3) is similar to oxygen transfer mechanism in the bioreactor. The ion-exchange process is heterogeneous since ions are transferred to and fro inter-phase boundaries formed by the aqueous solution and the ion exchanger. If the ion exchanger is considered as a quasi-liquid model, the inter-phase does not extend beyond a limit for its crystalline structure or matrix [53]. The first step involved in the ion exchanger is a chemical reaction where dissociation of complexes presents in the solution and diffuses towards the inter-phase film (second step) to reach the exchanger. The ions diffuse in the ion exchanger (third step) and associate reversibly with functional groups (fourth step). In this process, a concentration gradient is used as a driving

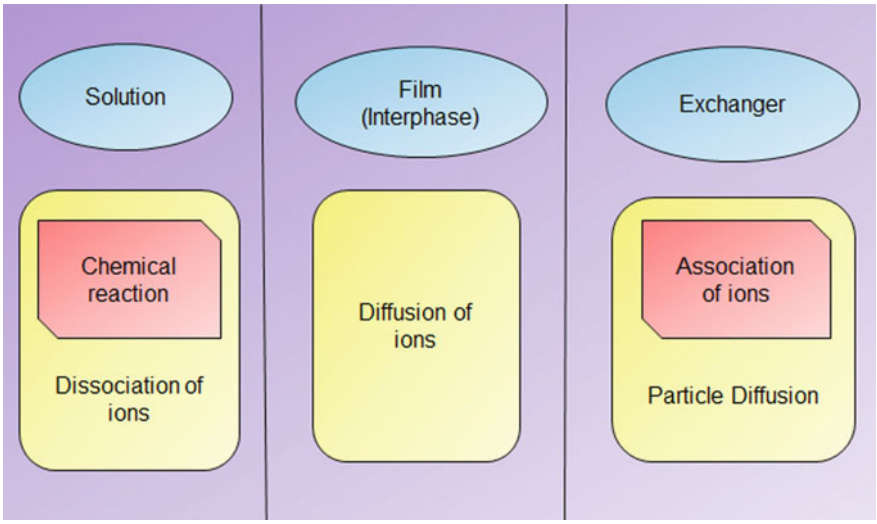

Fig. 9.3 Mechanism of ion-exchange process

force. After this step, the aqueous solution is removed from the exchanger and the ions associated with the exchanger are dissociated (fifth step) and gets associated with the liquid phase (sixth step). After this, the exchanger is regenerated for further use [54].

In this process, there are two main rate-limiting steps, (1) the mass transfer of ions diffused in the solution to film phase (depends on diffusion coefficient-film diffusion) and (2) the mass transfer of ions from film to an exchanger (physico-chemical properties of exchanger-particle diffusion).

9.4 Conclusion

Rapid discharge of heavy metals from industries to environment and stringent regulations by the regulatory bodies has led to the development of wide treatment technologies for the removal of heavy metals. Ion-exchange process is the widely used technology for the effective removal of heavy metals from the industrial wastes. In this case, ion-exchange material plays a vital role in the process performance. Composite ion exchangers have exhibited better efficiency than organic and inorganic ion exchangers. Recent advancement in nanotechnology has filled the gap between the organic and inorganic chemistry. Nano-based composite ion exchangers are still in laboratory trials and further research has to be carried out for their commercialization.

Acknowledgements Authors thank Prof. M. Sivanandham, Secretary, SVEHT and SVCE for their support and encouragement.

References

1. Williams E (2011) Environmental effects of information and communications technologies. Nature 479(7373):354–358
2. Shankar BS, Usha HS (2007) Environmental degradation due to industrialization—a case study of Whitefield Industrial Area, Bangalore, India. Environ Eng Sci 24(9):1338–1342
3. Varjani SJ, Rana DP, Jain AK, Bateja S, Upasani VN (2015) Synergistic ex-situ biodegradation of crude oil by halotolerant bacterial consortium of indigenous strains isolated from on shore sites of Gujarat, India. Int Biodeterior Biodegradation 103:116–124
4. Varjani SJ (2017) Microbial degradation of petroleum hydrocarbons. Bioresour Technol 223:277–286
5. Varjani SJ, Upasani VN (2017) A new look on factors affecting microbial degradation of petroleum hydrocarbon pollutants. Int Biodeterior Biodegradation 120:71–83
6. Varjani SJ, Gnansounou E, Pandey A (2017) Comprehensive review on toxicity of persistent organic pollutants from petroleum refinery waste and their degradation by microorganisms. Chemosphere 188:280–291
7. Tchounwou PB, Yedjou CG, Patlolla AK, Sutton DJ (2012) Heavy metal toxicity and the environment. In: Luch A (ed) Molecular, clinical and environmental toxicology, experientia supplementum, vol 101. Springer, Basel, pp 133–164
8. Marg BZ (2011) Hazardous metals and minerals pollution in India: sources, toxicity and management. A position paper. Indian National Science Academy, New Delhi, 2011. Last Accessed: 27 April 2017
9. Pandey J, Singh R (2017) Heavy metals in sediments of Ganga River: up-and downstream urban influences. Appl Water Sci 7(4):1669–1678
10. Raju KV, Somashekar RK, Prakash KL (2012) Heavy metal status of sediment in river Cauvery, Karnataka. Environ Monit Assess 184(1):361–373
11. Hussain J, Husain I, Arif M, Gupta N (2017) Studies on heavy metal contamination in Godavari river basin. Appl Water Sci. 7(8):4539–4548
12. Shankar S, Shanker U, Shikha (2014) Arsenic contamination of groundwater: a review of sources, prevalence, health risks, and strategies for mitigation. Sci World J 2014:304524. https://doi.org/10.1155/2014/304524
13. EPA, US (2001) National primary drinking water regulations: arsenic and clarifications to compliance and new source contaminants monitoring. Federal Register 66(14):69–76. Available at https://www.federalregister.gov/documents/2001/01/22/01-1668/national-primary-drinking-water-regulations-arsenic-and-clarifications-to-compliance-and-new-source. Last Accessed 27 April 2017
14. Ravenscroft P, Brammer H, Richards K (2009) Arsenic pollution: a global synthesis, vol 28. Wiley, New York
15. ATSDR (Agency for Toxic Substances and Disease Registry) (2013) Arsenic toxicity. U.S. Department of Health and Human Services, Atlanta, GA, USA. Available at https://www.atsdr.cdc.gov/csem/arsenic/docs/arsenic.pdf. Last Accessed 27 April 2017
16. ATSDR (Agency for Toxic Substances and Disease Registry) (2011) Case studies in environmental medicine (CSEM), cadmium toxicity. U.S. Department of Health and Human Services, Atlanta, GA, USA. Available at https://www.atsdr.cdc.gov/csem/cadmium/docs/cadmium.pdf. Last Accessed 27 April 2017
17. Mohan Kumar K, Hariharan V, Rao NP (2016) Heavy metal contamination in groundwater around industrial estate vs. residential areas in Coimbatore, India. J Clin Diagn Res 10(4): BC05–BC07

18. Gotteland M, Araya M, Pizarro F, Olivares M (2001) Effect of acute copper exposure on gastrointestinal permeability in healthy volunteers. Dig Dis Sci 46(9):1909–1914
19. Ye BJ, Kim BG, Jeon MJ, Kim SY, Kim HC, Jang TW, Chae HJ, Choi WJ, Ha MN, Hong YS (2016) Evaluation of mercury exposure level, clinical diagnosis and treatment for mercury intoxication. Ann Occup Environ Med 28:5. https://doi.org/10.1186/s40557-015-0086-8
20. Rathor G, Chopra N, Adhikari T (2017) Remediation of nickel ion from soil and water using nano particles of zero-valent iron (nZVI). Orient J Chem 33(2):1025–1029
21. Nriagu J (2017) Zinc toxicity in humans. School of Public Health, University of Michigan
22. Varjani S, Agarwal AK, Gnansounou E, Gurunathan B (eds) (2018) Bioremediation: applications for environmental protection and management. Springer Nature, Singapore
23. Abdel-Raouf MS, Abdul-Raheim ARM (2017) Removal of heavy metals from industrial waste water by biomass-based materials: a review. J Pollut Eff Contr 5:180. https://doi.org/10.4172/2375-4397.1000180
24. Kurniawan TA, Chan GY, Lo WH, Babel S (2006) Physico-chemical treatment techniques for wastewater laden with heavy metals. Chem Eng J 118(1–2):83–98
25. Varjani SJ, Gnansounou E (2017) Microbial dynamics in petroleum oilfields and their relationship with physiological properties of petroleum oil reservoirs. Bioresour Technol 245:1258–1265
26. Varjani SJ (2017) Remediation processes for petroleum oil polluted soil. Indian J Biotechnol 16:157–163
27. Jakob A, Stucki S, Kuhn P (1995) Evaporation of heavy metals during the heat treatment of municipal solid waste incinerator fly ash. Environ Sci Technol 29(9):2429–2436
28. Barakat MA (2011) New trends in removing heavy metals from industrial wastewater. Arab J Chem 4(4):361–377
29. Kang SY, Lee JU, Moon SH, Kim KW (2004) Competitive adsorption characteristics of Co^{2+}, Ni^{2+}, and Cr^{3+} by IRN-77 cation exchange resin in synthesized wastewater. Chemosphere 56 (2):141–147
30. Jha B, Singh DN (2016) Basics of zeolites. In: Fly ash zeolites. Springer, Singapore, pp 5–31
31. Stylianou MA, Hadjiconstantinou MP, Inglezakis VJ, Moustakas KG, Loizidou MD (2007) Use of natural clinoptilolite for the removal of lead, copper and zinc in fixed bed column. J Hazard Mater 143(1–2):575–581
32. Malamis S, Katsou E (2013) A review on zinc and nickel adsorption on natural and modified zeolite, bentonite and vermiculite: examination of process parameters, kinetics and isotherms. J Hazard Mater 252–253:428–461
33. Dennis R (2006) Coal industry turns to ion exchange technology for wastewater minimization. Industrial WaterWorld. PennWell Corporation, Tulsa, OK. Available at http://www.waterworld.com/articles/iww/print/volume-6/issue-5/columns/product-focus/coal-industry-turns-to-ion-exchange-technology-for-wastewater-minimization.html. Last Accessed: 27 April 2017
34. Sungur S, Babaoğlu S (2005) Synthesis of a new cellulose ion exchanger and use for the separation of heavy metals in aqueous solutions. Sep Sci Technol 40(10):2067–2078
35. Chutia P, Kato S, Kojima T, Satokawa S (2009) Arsenic adsorption from aqueous solution on synthetic zeolites. J Hazard Mater 162(1):440–447
36. Clearfield A (2000) Inorganic ion exchangers, past, present, and future. Solvent Extr Ion Exch 18(4):655–678
37. Nabi SA, Ganai SA, Shalla AH (2008) New organic-inorganic type acrylamide aluminum-tungstate: preparation, characterization and analytical applications as a cation exchange material. Sep Sci Technol 43(14):3695–3711
38. Nabi SA, Ganai SA, Khan AM (2008) Effect of surfactants and temperature on adsorption behavior of metal ions on organic–inorganic hybrid exchanger, acrylamide aluminum tungstate. J Surfactants Deterg 11(3):207–213

39. Nabi SA, Ganai SA, Naushad M (2008) A New Pb^{2+} ion-selective hybrid cation-exchanger-EDTA-zirconium iodate: Synthesis, characterization and analytical applications. Adsorpt Sci Technol 26(6):463–478
40. Nabi SA, Bushra R, Al-Othman ZA, Naushad M (2011) Synthesis, characterization, and analytical applications of a new composite cation exchange material acetonitrile stannic (IV) selenite: adsorption behavior of toxic metal ions in nonionic surfactant medium. Sep Sci Technol 46(5):847–857
41. Mohammad A, Amin A, Naushad M, Eldesoky GE (2012) Forward ion-exchange kinetics of heavy metal ions on the surface of carboxymethyl cellulose Sn (IV) phosphate composite nano-rod-like cation exchanger. J Therm Anal Calorim 110(2):715–723
42. Viswanathan N, Meenakshi S (2010) Development of chitosan supported zirconium (IV) tungstophosphate composite for fluoride removal. J Hazard Mater 176(1–3):459–465
43. Khan AA, Akhtar T (2009) Synthesis, characterization and ion-exchange properties of a fibrous type 'polymeric-inorganic'composite cation-exchanger Nylon-6, 6 Sn (IV) phosphate: its application in making Hg (II) selective membrane electrode. Electrochim Acta 54 (12):3320–3329
44. Islam M, Patel R (2008) Polyacrylamide thorium (IV) phosphate as an important lead selective fibrous ion exchanger: synthesis, characterization and removal study. J Hazard Mater 156(1–3):509–520
45. Iqbal N, Mobin M, Rafiquee MZA, Al-Lohedan HA (2012) Characterization and adsorption behavior of newly synthesized sodium bis (2-ethylhexyl) sulfosuccinate–cerium (IV) phosphate (AOT–CeP) cation exchanger. Chem Eng Res Des 90(12):2364–2371
46. El-Azony KM, Aydia MI, El-Mohty AA (2011) Separation of Cr (III) from Cr (VI) by Triton X-100 cerium (IV) phosphate as a surface active ion exchanger. J Radioanal Nucl Chem 289(2):381–388
47. Varshney KG, Rafiquee MZA, Somya A (2007) Synthesis, characterization and adsorption behaviour of TX-100 based Sn (IV) phosphate, a new hybrid ion exchanger. J Therm Anal Calorim 90(3):663–667
48. Rathore BS, Sharma G, Pathania D, Gupta VK (2014) Synthesis, characterization and antibacterial activity of cellulose acetate–tin (IV) phosphate nanocomposite. Carbohydr Polym 103:221–227
49. Khan AA, Akhtar T (2012) Cation-exchange kinetic studies on poly-o-toluidine Ce (IV) phosphate: a nano-composite and electrical conducting material. J Mater Sci 47(7): 3241–3247
50. Khan AA, Habiba U, Khan A (2009) Synthesis and characterization of organic-inorganic nanocomposite poly-o-anisidine Sn (IV) arsenophosphate: its analytical applications as Pb (II) ion-selective membrane electrode. Int J Anal Chem 2009:1–10
51. Khan AA, Habiba U, Shaheen S, Khalid M (2013) Ion-exchange and humidity sensing properties of poly-o-anisidine sn (IV) arsenophosphate nano-composite cation-exchanger. J Environ Chem Eng 1(3):310–319
52. Gupta VK, Agarwal S, Pathania D, Kothiyal NC, Sharma G (2013) Use of pectin-thorium (IV) tungstomolybdate nanocomposite for photocatalytic degradation of methylene blue. Carbohydr Polym 96(1):277–283
53. Zagorodni AA (2006) Ion exchange materials: properties and applications. Elsevier, London
54. Xu T (2015) Regeneration of the ion-exchange resin. Encycl Membranes 1–3

Chapter 10
Applications of Organic Ion Exchange Resins in Water Treatment

Jiafei Lyu and Xianghai Guo

Abstract Ion exchange resins are widely used in water treatment for the removal of various contaminants including natural organic matter (NOM), heavy metal ions, anions, boron, surfactants, pharmaceuticals and dyes, due to their specific advantages such as easy implementation, low cost, reversible regeneration and stability of organic polymers. Although wide applications of organic ion exchange resins have been achieved in industries, many research groups are devoted to the development of novel organic ion exchange resins for further improvement of the water treatment process. During past ten years, more attention was paid to the performance of magnetic ion exchange resins and coupling of various water treatment techniques for more efficient and low-cost separation. Through this chapter, the development of organic ion exchange resins over the past ten years will be reviewed in detail.

List of abbreviations

AMD	Acid mine drainage
BV	Bed volume
CFC	Coating copper ferrocyanide
CFIE	Chemical-free ion exchange
DF	Decontamination factor
DOM	Dissolved organic matter
DBP	Disinfection by-product
DOC	Dissolved organic carbon
DC	Diclofenac
ERD	Effective resin dose
HMO	Hydrous manganese oxide
IBU	Ibuprofen

J. Lyu · X. Guo (✉)
Department of Pharmaceutical Engineering, School of Chemical Engineering and Technology, Tianjin University, Tianjin 300350, People's Republic of China
e-mail: guoxh@tju.edu.cn

X. Guo
Key Laboratory of Systems Bioengineering (Ministry of Education), Tianjin University, Tianjin 300072, People's Republic of China

Inamuddin et al. (eds.), *Applications of Ion Exchange Materials in the Environment*,
https://doi.org/10.1007/978-3-030-10430-6_10

MIEX	Magnetic ion exchange resin
MO	Methyl orange
NOM	Natural organic matter
NDSX	Non-dispersive solvent extraction
NDMA	*N*-nitrosodimethylamine
PU	Polyurethane
PAC	Powdered activated carbon
POE	Point-of-entry
RO	Reverse osmosis
SE	Secondary effluent
SDZ	Sulfadiazine
SAC	Strong acid cation
SWRO	Seawater reverse osmosis
SBA	Strong-base anion
SMZ	Sulfamethazine
THM	Trihalomethane
THMFP	Trihalomethane formation potential
UF	Ultrafiltration
WHO	World Health Organization

10.1 Introduction

Water, where the original organisms come from on the earth, is the essential constituent of lives, sustaining every being in the world. The global water supply is at risk currently due to the worldwide population boom, regional drought and overwhelming discharge of contaminants into the natural water. Increasing risk of water supply is making a terrible influence on public health and environmental concerns. According to the reports [1], 1.2 billion people lack access to safe drinking water, 2.6 billion have little or no sanitation, and millions of people die annually—3900 children a day—from diseases transmitted through unsafe water or human excreta.

In both developing and industrialized nations, several contaminants are entering into water supplies from human activity including traditional natural organic matter (NOM), heavy metal ions from the mining industry, anions from fertilizer industry, boron, surfactants, pharmaceuticals, dyes and so on.

With the continuous prosperity of industry and population, more problems with water supply may occur in the coming decades; even global water scarcity is expected [2]. In view to addressing these problems, various research groups are involved currently to identify robust new methods of purifying water, including water disinfection, decontamination and seawater desalination, which intend to yield more viable water resources at lower cost and with less energy. Among all the

techniques examined, ion exchange resin, a polymer support fabricated with either anions or cations, meets the demands such as high capacity, low cost and less energy. It has been developed since the 1940s and commercially applied for water treatment in the worldwide.

Typically, the trapping of anion contaminants (e.g., nitrate) in ion exchange process will release a chloride ion to the solution, and the trapping of cation contaminants (e.g., calcium ion) will release a sodium ion from the cationic exchange resin [3]. The reversible ion exchange process makes it possible to reuse the resin when adsorbed contaminants are eluted off from the resin. In recent years, on one hand, researches were focused on the application of new ion exchange resins with a specific function or easy operation property like magnetic ion exchange resin (MIEX) [4, 5], which allows for faster resin agglomeration and recovery due to magnetic properties. On the other hand, the coupling of ion exchange resins with other water treatment techniques also attracted much attention for higher operation capacity, longer equipment life and lower cost. In this chapter, we plan to summarize the promising researches about the treatment of water performed with organic ion exchange resins during the last ten years.

10.2 Removal of Heavy Metals

Heavy metals exist as natural constituents on the earth and cannot be degraded or destroyed. Once ingested by a human being, heavy metals can be accumulated over a long period. The poisoning effects of heavy metals are due to their hazardous interference with the vital matrices such as proteins and nucleic acids in the normal metabolic processes of the human body. Excess intake of heavy metals leads to problems of body function including gastrointestinal disorders, diarrhea, stomatitis, tremor, ataxia, paralysis, vomiting, convulsion and depression. The contamination of surface and underground water by heavy metals can be attributed to the considerable soil pollution from mining industries. To control the heavy metal level in the water, different regulatory organizations have formulated strict guidelines for the content of heavy metals in drinking water. Detailed limits of different metals have been listed in Table 10.1 [6].

In order to remove heavy metal contaminants from water, ion exchange resins have been widely used due to good ion exchange property, low cost and high operation capacity for decades [7–14]. The chromatographic performance of organic ion exchange resins toward heavy metal removal from water reported in literature during the last ten years is summarized in Table 10.2.

In 2007, Galan et al. [15] integrated non-dispersive solvent extraction (NDSX) and ion exchange for the removal of Cr(VI) from ground waters. The final hybrid process overcomes the individual shortcomings of each technology and leads to an optimum process configuration. The groundwater was first concentrated by NDSX process, then purified with cationic ion exchange resin (Lewatit MP-64) down to

Table 10.1 The heavy metal limits permitted by the World Health Organization, European Union, United States Environmental Protective Agency and Regulation for drinking and natural waters (mg/L)

	WHO 2006 (drinking water)	EPA 2009 (drinking water)	EU 98/83/EC (drinking water)	TS 266 and RG25730 (spring water)
Al^{3+}	0.1	0.2	0.2	0.2
Fe^{2+}	0.3	0.3	0.2	0.2
As^{3+}	0.01	0.01	0.01	0.01
Ag^{3+}	0.005	0.1	–	–
Hg^{2+}	0.001	0.002	0.001	0.001
Cd^{2+}	0.003	0.005	0.005	0.005
Cr^{3+}	0.05	0.1	0.05	0.05
Pb^{2+}	0.01	0.015	0.01	0.01
Ni^{2+}	0.02	–	0.02	0.02
Ti^{4+}	–	0.002	–	–
Ba^{2+}	0.7	2.0	–	–
Mn^{2+}	0.5	0.05	0.05	0.05
Zn^{2+}	0.01	5	–	–
Cu^{2+}	2.0	1.3	2.0	2.0
Se^{4+}	0.01	0.05	0.01	0.01
Sb^{3+}	0.005	0.006	0.005	0.005
U^{3+}	0.015	0.03	–	–

0.5 mg/L Cr(VI) concentration. The employed Lewatit MP-64 resin in this study was easily regenerated by using NaOH solution.

In 2010, Rafati et al. [16] studied the removal of chromium(VI) ion from aqueous solutions with the Lewatit FO36 ion exchange resin under different experimental conditions including adsorbent dose, initial metal concentration, contact time and pH. Batch ion exchange process reached equilibrium in about 90 min and followed first-order reversible kinetics. Langmuir isotherm model was employed for the calculation of maximum ion exchange capacity which was 0.29 mmol of chromium(VI)/g at optimum pH of 6.0.

Kabir and Ogbeide [17] investigated the removal of chromate ions at trace concentration level from tannery wastewater effluent using commercially available weak-base ion exchange resin, Rohm and Haas Amberlite IR-45. The uptake of chromate reached constant equilibrium at average 9.8 mg/L for initial chromate concentration of 10 mg/L regardless of the high concentrations of chloride and sulfate ions in the wastewater. The removal efficiency of chromate was as high as 98% in column experiments, which also demonstrated that Amberlite IR-45 resin was very promising for the removal of trace concentration of chromate from tannery wastewater in the presence of high concentrations of chloride and sulfate co-ions.

Table 10.2 Heavy metals removal performance of different ion exchange resins

Resins	Heavy metal species	Treatment effluent	Removal performance[a]	References
Lewatit MP-64	Cr(VI)	Ground water (434–440 mg/L)	1.80 mol/L	[15]
Lewatit FO36	Cr(VI)	Prepared Cr(VI) aqueous solutions	15 mg/g	[16]
Armberlite IR-45	Chromate ion	Tannery wastewater effluent	9.8 mg/L	[17]
Purolite S 985	Zn(II)	Prepared Zn(II) aqueous solutions	80%	[18]
Purolite A 500	Zn(II)	Prepared Zn(II) aqueous solutions	83%	[18]
AM-2B	Zn(II)	Prepared Zn(II) aqueous solutions	75%	[18]
AV-17-8	Zn(II)	Prepared Zn(II) aqueous solutions	74%	[18]
Dowex 50WX8	Cu(II), Cd(II), Zn (II), Ni(II) and Pb(II)	Industrial wastewater	45, 50, 50, 40 and 60 mg/g	[19]
magnetic ion exchange resin (MIEX)	As(V)	Prepared As(V) aqueous solutions	3.16 μg/mg	[20]
D851	Cu(II)	Prepared Cu(II) aqueous solutions	25 mg/g	[21]
HMO-PU	Sr	Prepared Sr aqueous solutions	96.6%	[22]
CFC-PU	Cs	Prepared Cs aqueous solutions	73%	[22]

[a]Removal performance is described by uptake capacity or removal percentage according to different researches

Kocaoba [23] developed a method for the removal of Co^{2+} and Ni^{2+} using some strongly acidic cation exchange resins such as Amberlite IR 120, Amberjet 1200, Amberlite 200 and Amberlite 252 ZU. Experimental results revealed the stronger uptake of metal ions by Amberjet 1200 than the other ion exchange resins and Ni^{2+} ions were more efficiently adsorbed than Co^{2+} ions by the strongly acidic ion exchange resins.

To recover zinc(II) ions from chloride and chloride–sulfate solutions, Kononova et al. [18] tested some commercial anion exchangers with different physical and chemical structures including Purolite S 985, Purolite A 500 AM-2B and AV-17-8. Among them, Purolite S 985, Purolite A 500 and AM-2B showed good zinc recovery performance from industrial solutions and wastewater. After ion exchange recovery, zinc can be effectively eluted off by 2 M HCl.

To remove heavy metal contaminants in wastewaters in several industrial areas of Kerman, Iran, the Dowex 50WX8 (H^+) resin [19] was employed and exhibited that adsorption capacities on Cu(II), Cd(II), Zn(II), Ni(II) and Pb(II) were 45, 50, 50, 40 and 60 mg/g, respectively.

Sinha et al. [20] investigated arsenic adsorption properties from synthetic and natural water on magnetic ion exchange resins (MIEX). The results showed that adsorption equilibriums can be achieved within a contact period of 20 min. The observed optimal operating conditions for a given equilibrium concentration of C_{eq} = 10 μg/L were in pH 5.5, a dose of 520–1300 mg/L and contact time of 60 min, which gave adsorption capacity of 3.16 μg/mg and rate constants of 1.9 h^{-1}.

He et al. [21] investigated Cu(II) ion removal with D851 ion exchange resin and determined the optimum contact time, temperature and pH in the static process were 60 min, 35 °C and 5.5, respectively. In the dynamic process, wastewater containing 10 mg/L Cu(II) (pH ≈ 5.5) was treated to meet the primary standard (<0.5 mg/L) of the National Integrated Wastewater Discharge Standard (GB8978-1996). In addition, the ion exchange resin can be regenerated with 4% HCl solution.

Besides the ordinary heavy metals mentioned above, another kind of heavy metal contaminants deserves more attention, which is the radioactive heavy metals discharged from the nuclear power station, mainly including cesium-137 and strontium-90. To remove these dangerous heavy metals, Rao et al. [22] fabricated two novel ion exchange resins for removal of strontium and cesium by coating copper ferrocyanide (CFC) or hydrous manganese oxide (HMO) powders on polyurethane (PU) foam with polyvinyl acetate/acetone as a binder. Under similar conditions, in two minutes the CFC-PU foam removed about 73% of cesium from 10^{-3} M solution whereas the HMO-PU foam removed about 96.6% of strontium. Average decontamination factor (DF) of 20 was observed in pilot plant scale level. The radioactive strontium in the waste could be reduced to < 1 Bq/mL from initial activity 22 Bq/mL.

10.3 Removal of Organics

The existence of organics in water can be attributed to many different sources such as remain of organisms, chemical disinfectant process and discharged wastewater from industry. Various studies have demonstrated that a relatively large part of organic matters could not be removed by conventional processes such as coagulation and filtration. Hence, many alternative technologies for organics removal

were considered, among those anion exchange technologies have been found more effective for the removal of organic matters since the 1980s. In the ranges of natural pH [24], dissolved organic matter (DOM) is negatively charged due to the carboxylic and alcoholic functional groups, suggesting the possibility of employing anion exchange resin for removal of DOM from the water. Ion exchange process can be employed in the water treatment either alone or coupling with other techniques. Recently, much progress has been made in this area including the application of magnetic ion exchange (MIEX®) which simplified the following solid–liquid separation process and innovative cooperation with other different processes. This section is devoted to the application of ion exchange resins for removal of

Table 10.3 Organic matters removal from water with ion exchange resins

Organic matter	Resins	Treatment effluent	Removal performance[a] (%)	Dose (mL/L)	References
NOM	MIEX	Raw water	80	8	[25]
	IRA938	Raw water	80	8	[26]
	IRA-958	Raw water	82	8	
	DOWEX-11	Raw water	90	8	
	DOWEX-MSA	Raw water	85	8	
	AMBERSORB	Raw water	76	8	
	MIEX	Raw water	70	1	
	MIEX	Synthetic wastewater	60	10	[27]
	MIEX® TMP-TMA	Synthetic wastewater	64	10	[29]
	MIEX® DOC	Synthetic wastewater	77	10	
	Amberlite IRA-401	SE from sewage treatment	COD (43), BOD5 (46), DOC (45), UV254 (72)	90 L/h	[30]
DMPs	Plus	Surface water	NDMA (50), THM (no removal)	5	[34]
		Wastewater	NDMA (90), THM (no removal)		
	MIEX®	Surface water	NDMA (little), THM (60–70)	5	
		Wastewater	NDMA (little), THM (45)		
	Combination of Plus and MIEX®	Surface water	NDMA (60), THM (65)	5	
		Wastewater	NDMA (83), THM (33–50)		

(continued)

Table 10.3 (continued)

Organic matter	Resins	Treatment effluent	Removal performance[a] (%)	Dose (mL/L)	References
DOM and hardness	MIEX-Cl and MIEX-Na	Groundwater	Hardness (>55), DOC (70)	16	[31]
	Cationic Plus and anionic MIEX	Groundwater	Hardness (65), DOC (1.25 mg/L)	1.67	[33]
	Combination of pre-chlorination process, MIEX and coagulation	Lake water	THMFP (77)	8	[35]
Surfactant	MIEX	Synthetic wastewater	83	20	[36]
Methyl orange	Amberlite IRA-400	Synthetic wastewater	74.4 mg/g[b]	–	[40]
SMZ	Lewatit MP-500	Synthetic wastewater	80.7 mg/mL	1	[38]
IBU	MIER1 and MIER2 (higher surface area)	Synthetic wastewater	0.49 mmol/g, 0.52 mmol/g	0.5 g/L	[39]
DC			1.17 mmol/g, 2.65 mmol/g		
SDZ			0.85 mmol/g, 1.84 mmol/g		

[a]Removal performance is described by uptake capacity or removal percentage according to different researches
[b]Maximum monolayer adsorption capacity

various organic matters from water including natural organic matter (NOM), disinfection by-products (DBPs), pharmaceuticals, surfactants, dyes and other small organic matter. The important results are listed in Table 10.3.

10.3.1 Natural Organic Matter (NOM)

Natural organic matter (NOM) can lead to microbial re-growth in the distribution network and formation of DBPs by reacting with a chemical disinfectant. To remove the NOM contaminants in water, Humbert et al. [25] demonstrated that six anion exchange resins including MIEX and IRA938 s can remove dissolved organic carbon (DOC) by more than 75% from surface water with a dose of 8 mL/L resin after a contact time of 2 h.

Singer et al. [26] examined MIEX process performance on the natural organic matter (NOM) in batch, pilot scale and full-scale tests. Results indicated that DOC removals ranged from 28 to 88% with different doses of resin in the batch

experiments. Various pilot plant and full-scale studies showed that effective resin dose (ERD) of the order 1 mL/L was sufficient to achieve up to 70% DOC removal. Additionally, this resin can be typically regenerated with sodium chloride.

Zhang et al. [27] observed that magnetic ion exchange (MIEX®) resin can remove 60% DOC (hydrophilic and hydrophobic) rapidly in 20 min. from secondary effluent after biological treatment, and the removal ratio could be improved to 80% by adding powdered activated carbon (PAC). Following up this research, the author designed a fluidized bed MIEX® reactor [28] as the pretreatment for a submerged membrane reactor, resulting in a very high organic removal (80%) while significantly reducing the membrane fouling. In 2011, this team observed that other two magnetic ion exchange resins including MIEX® TMP-TMA and MIEX® DOC were successful for removing organic carbon from biologically treated wastewater [29]. Removal of 64% on MIEX® TMP-TMA resin and 77% on MIEX® DOC resin of dissolved organic carbon from synthetic wastewater was realized when operated in batch mode using a resin concentration of 10 mL/L. A fluidized bed MIEX® contactor was designed to effectively remove organic matter from the synthetic effluent of biologically treated sewage with more than 60% DOC removal even after 172-bed volumes. The regenerated MIEX® resin did not display any significant reduction in its ability to remove organic matter.

Based on a pilot-scale operation, Sun et al. [30] employed Amberlite IRA-401 resin for DOM removal from actual secondary effluent (SE) in a sewage treatment plant. The removal percentages for the COD, BOD_5, DOC and UV_{254} were $43 \pm 12\%$, $46 \pm 15\%$, $45 \pm 9\%$ and $72 \pm 4\%$, respectively.

To reduce hardness to moderate levels and at the same time maximize the removal of DOC, applying both anionic and cationic resins for water purification would be a promising treatment process since most of DOM is able to be removed by anion exchange resin while hardness contaminants can be removed with cation exchange resin. Apell and Boyer [31] combined magnetic anion (MIEX-Cl) and cation (MIEX-Na) exchange treatments for removal of DOM and hardness. The experimental data revealed that combined ion exchange treatment can achieve >55% total hardness removal and 70% DOC removal. This method also allowed the most efficient use of the brine regeneration solution because both sodium and chloride were used as mobile counterions. To follow up this research [32], the authors further completely mixed magnetic anion exchange resin and conventional cation exchange resin together for simultaneous removal of DOC and hardness. Both the exchange resins can be regenerated using sodium chloride. Mixed ion exchange resin can achieve 76% DOC removal and 97% total hardness removal.

Besides Boyer's studies, Arias-Paic et al. [33] simultaneously employed cationic (Plus) and anionic (MIEX) ion exchange resins in a single vessel for hardness and DOC removal at pilot and bench scales. Mixed resin treatment process showed 65% hardness removal at 600BV and enhanced DOC removal from 0.5 to 1.25 mg/L, which makes it possible to remove both DOC and hardness by single treatment process.

10.3.2 Disinfection by-Products (DBPs)

Beita-Sandí and Karanfi [34] employed a cation exchange resin (Plus) and an anion exchange resin (MIEX) individually and in combination for the removal of two main DBPs, *N*-nitrosodimethylamine (NDMA) and trihalomethanes (THMs) precursors for the purification of surface water and wastewater. Both resins in combination can simultaneously remove NDMA (43–85%) and THMs (39–65%) precursors. Plus resin showed good performance of NDMA precursor's removal. MIEX resin can reduce the concentration of THMs precursors ranging from 39 to 69%. In the combined process, both NDMA and THMs precursors can be effectively removed. In naturally attenuated wastewater effluents, the precursor's removal performances of both the Plus alone and combined resins were similar for the wastewater effluent samples.

Han et al. [35] combined pre-chlorination process, magnetic ion exchange resin (MIEX) and coagulation for the treatment of Hongze Lake water in China. MIEX can remove organics to a greater extent than coagulation with lower coagulant demand when combining with coagulation. Chlorination experimental results showed that MIEX can remove 57% chlorine demand and 77% trihalomethane formation potential (THMFP) for raw water. Pre-chlorination followed by MIEX and coagulation can afford additional organic and THMFP removals.

10.3.3 Surfactants

The use and disposal of detergents are serious concerns because of the high toxicity of their main ingredient (surfactants) on the aquatic creature. To remove diverse surfactants from wastewater, many techniques have been tried including biodegradation, coagulation, foaming, oxidation, adsorption, ion exchange and membrane processes. In 2008, Kowalska [36] carried out the comparative study on the removal efficiencies of anionic surfactant from water by means of ultrafiltration and ion exchange resin (MIEX). The MIEX resin was found better to remove surfactants over a wide range of concentrations. The increasing resin dose ranging from 2.5 to 20 mL/L improved the removal percentage from 18 to 83% in 5 min and from 61 to 92% in 40 min, respectively. Following this research, the authors integrated ultrafiltration treatment with ion exchange resin as an additional secondary treatment process to remove surfactant contaminants from aqueous solutions. The integrated purification system allowed to enhance the removal efficiency by 75% compared to individual purification processes. The presence of the ion exchange resin was also found to allow a significant reduction in membrane fouling and retention of high hydraulic efficiency [37].

10.3.4 Pharmaceuticals

Pharmaceuticals cannot disappear after their excretion but end up in the natural water. It has been reported that several pharmaceuticals can be detected in aqueous environments including sulfonamides, diclofenac and ibuprofen. In addition, numerous antibiotics like sulfonamides have been found in effluents from drug manufacturing plants. Continuous accumulation of those compounds can lead to toxicity to aquatic organisms and a threat to safe drinking water. Many pharmaceuticals possess toxicities similar to industrial chemicals and exhibit the potential to induce adverse effects on humans even below 1 ng/L. Removal of pharmaceuticals by adsorption and ion exchange was thought as the most promising techniques due to their low cost, easy regeneration and selective removal of pollutants.

Fernández et al. explored the removal of sulfamethazine (SMZ) with an anionic ion exchange resin, Lewatit MP-500 (Lanxess Chemical) [38]. Batch experiments were conducted using synthetic solutions of 30–250 mg/L SMZ with resin dose of 1 g/L. The results showed high SMZ removal capacities. According to the Langmuir model, the maximum calculated adsorption capacity was 110 mg/g wet resin. Kinetic studies demonstrated that the mass transfer coefficient and the diffusivity values were 3.2×10^{-6} to 5.4×10^{-6} cm/s and 2.1×10^{-10} to 3.8×10^{-10} cm^2/s, respectively. The adsorption rate of SMZ onto the Lewatit MP500 resin was controlled by particle diffusion. The SMZ can be eluted completely using 0.5 M NaOH in all cycles and concentrated to more than twelve times of the initial concentration.

Two magnetic ion exchange resins were used by Jiang et al. [39] for the removal of three widely detected pharmaceuticals, ibuprofen (IBU), diclofenac (DC) and sulfadiazine (SDZ). The adsorption kinetics was relatively fast and followed pseudo-second-order kinetics. Despite the different pore structures of the two resins, similar adsorption patterns of DC and SDZ were observed, implying the existence of an ion exchange mechanism. These interactions between IBU and resins were dependent on the specific surface area and functional groups of the resin including electrostatic interaction, H-bonding, van der Waals interactions and π–π interactions. The fitting of adsorption isotherms also verified the different adsorptive behavior of the three pharmaceuticals on the two magnetic ion exchange resins. The presence of $Cl^-$and SO_4^{2-} decreased the adsorption amount, but with different inhibition levels for different adsorbates. This work facilitated the understanding of the adsorption behavior and mechanism of pharmaceuticals on MIER and expanded the application of MIER to the removal of pharmaceuticals in water.

10.3.5 Dyes

Behera et al. [40] studied the removal of anionic dye methyl orange (MO) from aqueous solutions using ion exchange resin (Amberlite IRA-400) by batch

adsorption process. MO adsorption was increased with the increase of contact time, agitation speed, temperature, initial dye concentration and adsorbent dose. The optimal pH was 6.5. The maximum monolayer adsorption capacity of Amberlite IRA-400 was calculated as 74.4 mg/g at 303 K. The value of separation factor from the Langmuir equation and Freundlich constant (n) indicated favorability of adsorption. Thermodynamic parameters such as $\Delta G°$, $\Delta H°$ and $\Delta S°$ were calculated and the positive value of $\Delta H°$ (4.13, 3.63 and 7.09 kJ mol^{-1}) for corresponding initial MO dye concentrations in the solution: 50, 100 and 200 ppm, respectively, indicated that the adsorption was endothermic in nature. Kinetic results revealed that the adsorption of MO belonged to pseudo-second-order kinetic model and chemisorption type.

10.3.6 Small Organic Matter

Besides traditional dissolved organic compounds mentioned above, there are some small organic substances broadly existing in the distillery condensate, such as formic, acetic, propanoic, butanoic acids and 2-phenethyl alcohol. To reuse the distillery condensates as fermentation water, small organic substances have to be brought below their detection or quantification limit because of their inhibition to the alcoholic fermentation. Lameloise et al. [41] designed a pretreatment process using anion exchange (weak Amberlite FPA 51 resin, Dow) ahead of reverse osmosis. By integration of ion exchange and reverse osmosis, the water recovery reached 85%. In the practical alcoholic fermentation, using such treated condensate exhibited yeast viability and ethanol production performances equivalent to the blank for a final ethanol concentration of 80 g/L^{-1} close to practical value encountered in distilleries.

10.4 Desalination

An important method for the challenge of providing sample and safe drinking water under current pressures, including population growth, industrialization, contamination and drought, is seawater desalination [42]. It can offer a seemingly unlimited, steady supply of high-quality water, without impairing natural freshwater ecosystems. In recent years, numerous large-scale seawater desalination plants have been built up in water-stressed countries to augment available water resources. Ion exchange resin also plays an important role in it. Some recent progress on desalination with ion exchange resins is summarized in Table 10.4.

Hilal et al. [43] explored seven different types of ion exchange resins for the removal of chloride ions from saline water both on laboratory and pilot scales. These resins were Purolite A500TLSO_4, Purolite A400TLSO_4, Purolite A850, Purolite A109, Purolite A149S, Purolite A111 and Ambersep 900SO_4, which

Table 10.4 Desalination with ion exchange resins

Resins	Treatment effluent	Removal performance[a]	Dose	References
Ambersep 900SO4	Sodium solution 32.0 g/L	25%	1.62 L/h	[43]
CFIE	Sodium solution conductivity 20–70 μS/cm	Conductivity 0.8–1.5 μS/cm[b]	560 L BV	[45]
Monoplus S108H	Sodium solution 1970 mg/L	71.1 g Na/kg	70 L/h	[46]
	coal seam water	53.5 g Na/kg		
Lanxess S108H	Sodium solution 1259 mg/L	62.9 g Na/kg	6.9 L/h	[47]
Electrochemical ion exchange system	Simulated wastewater	83%	7.5 L/h	[48]

[a]Removal performance is described by uptake capacity or removal percentage according to different researches

[b]Conductivity of outlet after treatment with ion exchange resins

contain quaternary, tertiary, secondary and primary amino groups in the polymer matrix. It was found that sulfate–chloride exchange was very fast and Ambersep $900SO_4$ showed better removal efficiency than others, which can be attributed to the lesser hydrogen atoms density in the amine functional group of this resin. Additionally, exhausted resins can be successfully regenerated using 0.2 M Na_2SO_4 solution, and multiple regeneration/saturation cycles did not affect the performance on chloride ion removal. It was shown that the osmotic pressure of seawater was significantly reduced after SO_4^{2-}/Cl^- ion exchange. Due to this, nanofiltration membranes with lower energy consumption can be used for rejection of sulfate ions. The author has also carried out pilot-scale studies by coupling Purolite $A500TLSO_4$ resin and NF [44]. In the hybrid process, the Purolite $A500TLSO_4$ resin was able to covert >95% of chloride ions to sulfate ions and the NF process provided >99% rejection of sulfate ions.

Besides the researches on the performance of different commercially available ion exchange resins, Hu et al. [45] proposed a new chemical-free ion exchanger (CFIE) to replace the conventional two-bed (cation-anion) ion exchanger for the desalination of seawater. In this process, regeneration of resin was achieved mainly by electrically enhancing water split. After treatment, the conductivities of the synthetic desalinated seawater were reduced from the original 20–70 μS/cm to 0.8–1.5 μS/cm. The energy consumption and water recovery were 0.29–1.04 kWh/m^3 water and 81.8–94.7%, respectively. Repetitive experimental results showed that the CFIE system could run steadily, and no performance decay was detected after long-term frequent regenerations.

Pember et al. [46] studied desalination of coal seam water by ion exchange resins. The ion exchange capacity of resin for sodium removal from prepared sodium solution was calculated to be 71.1 g Na/kg resin. The resin can be regenerated by using HCl solution with 86% recovery of capacity. The capacity of ion

exchange resin for coal seam water sample was found to be only 53.5 g Na/kg resin, which can be attributed to the presence of other interfering ions and the inefficient regeneration of the resin before the test.

During the study by Millar et al. [47] on desalination from water with ion exchange resin, the performance of a strong acid cation (SAC) resin (Lanxess S108H) was examined for sodium ion removal from NaCl aqueous solutions as well as from the coal seam gas water sample. The adsorption results were described with four different adsorption models, and a maximum sodium adsorption capacity was 62.9 g Na/kg resin.

Li et al. [48] designed a novel electrochemical ion exchange system with porous cylinder electrodes for desalination without the use of costly ion exchange membrane and extra chemical reagents. The strong-base ion exchange resin grains in the anode and cathode were used as supporting electrolyte, which is capable for the treatment of wastewater with low conductivity. By this system, the removal percentage of total dissolved salts and COD can reach 83 and 92%, respectively, without consumption of extra chemical reagents.

10.5 Boron Removal

Boron is widely distributed in seawater (5 ppm) [49] and some groundwater of active volcanic and geothermal activities (119 ppm) [50]. Boron is utilized in numerous applications including glass production, detergents manufacturing, fertilizers, insecticides and nuclear engineering [51]. The widespread applications of boron compounds give rise to the enrichment of boron in the wastewater. Boron is a necessary element as a micronutrient for plants, animals and human beings, but excess boron ingestion is detrimental to some plants. Excess boron uptake can reduce fruit yields and results in premature ripening and massive leaf damage [52]. For human beings, the maximum boron concentration in drinking water was limited below 2.4 ppm in 2011 by WHO, which can be much lower in some countries [53]. Effective boron removal techniques have been always in high demand for desalination of seawater, geothermal water and industrial wastewater to meet the requirement for freshwater [54]. Among all the boron removal techniques [54–58], boron-selective ion exchange resins which possess *N*-methyl glucamine groups for the affinity to boron have been the most widely commercially employed in the practical treatment of wastewater.

Kabay et al. [59] explored two kinds of boron-selective ion exchange resins (Diaion CRB 02 and Dowex-XUS 43594.00) for the boron removal from seawater reverse osmosis (SWRO) permeate in batch and column-mode test. The halftime for boron removal was between 30 and 45 min for Dowex and 20–30 min for Diaion resins with an optimum dose of 1 g/L. For adsorption kinetics study, these resins fitted pseudo-second-order kinetics model. In addition, adsorbed boron on the resins was effectively eluted with 5% H_2SO_4 solution. These workers further explored

boron removal from geothermal water using both the resins [60] by batch and column methods. In a batch process, the parameters including adsorbent dose were optimized to be 2 g resin/1L geothermal water. Then both resins were applied in the column for dynamic boron removal. The breakthrough capacities were calculated as 2.13 and 2.02 mg B/mL resin for Diaion CRB 02 and Dowex (XUS 43594.00) resins, respectively. Boron loaded resins were eluted with 5% H_2SO_4 at SV 10 h^{-1}. Following the obtained results, this group designed a hybrid process together by integrating the RO desalination process with Dowex (XUS 43594.00) ion exchange resin together [61]. They claimed that the obtained treated water with this hybrid process can meet the requirements for irrigation. Besides this hybrid process, they also established another hybrid system by coupling Dowex (XUS 43594.00) ion exchange resin with the UF process [60]. By optimizing process parameters, they concluded that it was possible to decrease the boron concentration of the geothermal water below 1.0 mg B/L by coupling ion exchange with UF.

Based on boron adsorption mechanism, Guo et al. first time synthesized two novel boron-selective resin, CL-RESIN and NCL-RESIN, which were functionalized with pyrocatechol (CL) and nitropyrocatechol (NCL) for effective boron removal [62, 63]. The adsorption process reached to equilibrium after 12 h. The optimized pH values for adsorption [55] were pH = 9.06 for CL-RESIN and 6.70 for NCL-RESIN. The maximum adsorption capacity of 0.7886 mmol g^{-1} for CL-RESIN and 0.7931 mmol g^{-1} for NCL-RESIN was comparable to commercial IRA 743. The adsorption process is well fitted by pseudo-second-order kinetic model. For adsorption isotherms, Freundlich model fitted well at low boron concentration while Langmuir model fitted better at high concentration, indicating the involvement of a two-step adsorption process. In addition, these two resins can be easily regenerated with a weaker acid of 10% acetic acid, which avoided the treatment of much waste acid.

10.6 Removal of Anions

A wide range of anions has been continuously introduced into the drinking water cycle from fertilizers, industrial wastewater and disposal of daily used necessary. According to the World Health Organization (WHO), the permissible concentration for nitrate, sulfate and fluorine in drinking water should not exceed 10, 250, 1.5 mg/L. Excess uptake of these anions can lead to much physical disorder including methaemoglobinaemia, diarrhea and mild dental fluorosis. Anion exchange resins have been employed for the removal of excess anions from wastewater. Several ion exchange resins have been employed for the removal of anions as discussed below.

Dziubek and Maćkiewicz [64] reported the nitrate removal capacity of IONAC SR-7 resin (Bayer), a strong-base nitrate-selective ion exchange resin. The calculated total ion exchange capacity depending on the initial concentration of nitrate in water varied from 0.36 to 0.49 val/dm^3.

To improve the sustainability of tributylamine strong-base anion (SBA) exchange resin for nitrate removal from contaminated drinking water, a bioregeneration process [65] was performed on exhausted resins using a salt-tolerant, nitrate-perchlorate-reducing culture for 48 h after each cycle. The nitrate loaded on the resin was efficiently transferred into the medium in first 0.5–1 h and completely degraded by microorganisms after 10 h. Resins can be used for 4 cycles without a loss of capacity.

Another important anion contaminant in water is sulfate, which is generated mostly from acid mine drainage (AMD) when sulfide minerals are oxidized in the presence of water and oxygen, leading to natural waters unsafe for use. In order to remove sulfate from water, Guimarães and Leao [66] have investigated sulfate adsorption performance of ion exchange resin Amberlyst A21. The experimental results revealed that the acidic environment favoured sulfate sorption by Amberlyst A21, and the removal process can rapidly reach equilibrium after 45 min. Adsorption kinetics were explained by two models, the pseudo-first-order model ($k_1 = 3.05 \times 10^{-5}/s^{-1}$) and pseudo-second-order model ($k_2 = 1.67 \times 10^{-4}/s^{-1}$). Both the Freundlich and Langmuir models are well fitted the experimental data at equilibrium. This adsorption process was demonstrated to be a physisorption process ($\Delta H = -25.06$ kJ/mol) with decreasing entropy ($\Delta S = -0.042$ kJ mol^{-1} K^{-1}). Regeneration experiments showed that sulfate can be easily eluted ($\sim 100\%$) by sodium hydroxide solutions at pH 10 or 12. In fixed-bed experiments, the maximum sulfate loadings of resin varied between 8 and 40 mg (SO_4^{2-})/mL (resin).

Shahbazi et al. [67] used MP500WS resin for removing nitrate and sulfate, and the removal rate was very high. In this research, MP500WS resin was integrated into a point-of-entry (POE) treatment device. The nitrate removal of underground waters by specific resin (MP500WS macroporous resin) was significantly bringing the nitrate concentrations to a much lower level than the permissible maximum concentration assigned for drinking water.

Samadi et al. [68] investigated the adsorptive removal of fluoride by using strong-base anion resins from the water. The removal of fluoride was maximum at natural pH that can be further improved by increasing contact time and adsorbent dosage. The maximum sorption capacity of the resin was calculated to be 13.7 mg/g according to the Langmuir model, which is higher than the reports in the previous literature. Freundlich model was the most appropriate one to describe fluoride adsorption ($R^2 > 0.99$), and the pseudo-first-order model is well fitted the experimental kinetic data. It was found that the rate-limiting step was the film diffusion rather than the intraparticle diffusion. It was observed that the presence of sulfate had no significant influence on fluoride removal. However, hardness-causing species and chloride ions showed a slightly reverse effect while the highest reverse effect was observed from nitrate.

For the development of point-of-use/point-of-entry water treatment systems for anions removal from water, Markovski et al. [69] embedded aluminum (hydr)oxide material inside the pores of commercially available nitrate-selective strong-base ion exchange resin (Purolite A520E) to fabricate a novel class of hybrid media capable

of simultaneously removing nitrate and fluoride from contaminated groundwater. Future modifications and optimizations of this relatively simple and inexpensive fabrication process have the potential to yield an entirely new class of hybrid media suitable for point-of-use/point-of-entry water treatment systems.

10.7 Removal of Cations

10.7.1 Hardness

Permanent water hardness is caused by the calcium and magnesium salts that do not precipitate during boiling. The existence of hardness in water can lead to some bad influence including a metallic taste of drinking water, pipe scale and interaction with household soaps. Water softening process is designed to remove hardness-causing ions. Lazar et al. [70] presented a comparative study on the performances and behavior of the Purolite C100E and Pure Resin PC002 ion exchange resins for calcium cations removal from aqueous solutions. The retention degree of calcium cations was 92% for Purolite C100E and 89% for Pure Resin PC002.

10.7.2 Ammonium

Ammonium, mainly derived from fertilizers, the industrial effluents and animal dung, is another cationic contaminant in the wastewater. Sica et al. [71] studied ammonium removal from synthetic aqueous solutions by ion exchange resin PUROLITE C150H. The process parameters were calculated by using the Langmuir model for thermodynamic study and the shrinking core model for a kinetic study. The data were correlated with the surface properties of the substrate, and the adsorption mechanism was outlined. For initial ammonium concentrations of 25–150 mg NH_4^+/L, removal efficiencies of 80–90% were obtained.

10.8 Conclusions

Although more and more novel materials and techniques have been developed for water treatment, ion exchange resins have been important due to specific advantages including easy implementation, low cost, reversible regeneration and stability of organic polymers. In recent years, the research trend in this area has directed the wide applications of magnetic ion exchange resins (MIEX) for the removal of various contaminants and the coupling of ion exchange resins with other water treatment techniques for higher operation capacity, longer equipment life and lower

cost. To further improve the application of ion exchange resins in water treatment, designing of new material with higher exchange capacity and more selective separation performance, as well as optimal coordination between ion exchange process with other techniques, are highly desirable.

References

1. Shannon MA, Bohn PW, Elimelech M, Georgiadis JG, Mariñas BJ, Mayes AM (2008) Science and technology for water purification in the coming decades. Nature 452:301
2. Wintgens T, Salehi F, Hochstrat R, Melin T (2008) Emerging contaminants and treatment options in water recycling for indirect potable use. Water Sci Technol 57:99–107
3. Gregory J, Dhond RV (1972) Wastewater treatment by ion-exchange. Water Res 6:681
4. Allpike BP, Heitz A, Joll CA, Kagi RI, Abbt-Braun G, Frimmel FH, Brinkmann T, Her N, Amy G (2005) Size exclusion chromatography to characterize DOC removal in drinking water treatment. Environ Sci Technol 39:2334–2342
5. Boyer TH, Singer PC (2005) Bench-scale testing of a magnetic ion exchange resin for removal of disinfection by-product precursors. Water Res 39:1265–1276
6. Pehlivan R, Emre H, Key D (2012) Effect of talus deposit excavations on hydrogeochemical characteristics of kuvars spring water, Maltepe, Istanbul, Turkey. J Water Resour Protect 04:294–306
7. Kim JS, Zhang L, Keane MA (2001) Removal of iron from aqueous solutions by ion exchange with Na–Y zeolite. Sep Sci Technol 36:1509–1525
8. Kim JS, Keane MA (2000) Ion exchange of divalent cobalt and iron with Na–Y zeolite: binary and ternary exchange equilibria. J Colloid Interface Sci 232:126–132
9. Chiarle S, Ratto M, Rovatti M (2000) Mercury removal from water by ion exchange resins adsorption. Water Res 34:2971–2978
10. Al-Enezi G, Hamoda MF, Fawzi N (2004) Ion exchange extraction of heavy metals from wastewater sludges. J Environ Sci Health Part A Toxic Hazard Subst Environ Eng 39:455–464
11. Rengaraj S, Joo CK, Kim Y, Yi J (2003) Kinetics of removal of chromium from water and electronic process wastewater by ion exchange resins: 1200H, 1500H and IRN97H. J Hazard Mater 102:257–275
12. Juang RS, Lin SH, Wang TY (2003) Removal of metal ions from the complexed solutions in fixed bed using a strong-acid ion exchange resin. Chemosphere 53:1221–1228
13. Ahmed S, Chughtai S, Keane MA (1998) The removal of cadmium and lead from aqueous solution by ion exchange with Na–Y zeolite. Sep Purif Technol 13:57–64
14. Pak VN, Obukhova NG (1995) Sorption and ion-exchange processes—sorption of Sr^{2+} and Cu^{2+} from aqueous solutions with iron-containing slime. Russ J Appl Chem 68:181–184
15. Galan B, Castaneda D, Ortiz I (2008) Integration of ion exchange and non-dispersive solvent extraction processes for the separation and concentration of Cr(VI) from ground waters. J Hazard Mater 152:795–804
16. Rafati L, Mahvi AH, Asgari AR, Hosseini SS (2010) Removal of chromium (VI) from aqueous solutions using Lewatit FO36 nano ion exchange resin. Int J Environ Sci Technol 7:147–156
17. Kabir G, Ogbeide SE (2008) Removal of chromate in trace concentration using ion exchange from tannery wastewater. Int J Environ Res 2:377–384
18. Kononova ON, Mikhaylova NV, Melnikov AM, Kononov YS (2011) Ion exchange recovery of zinc from chloride and chloride-sulfate solutions. Desalination 274:150–155

19. Moosavirad SM, Sarikhani R, Shahsavani E, Mohammadi SZ (2015) Removal of some heavy metals from inorganic industrial wastewaters by ion exchange method. J Water Chem Technol 37:191–199
20. Sinha S, Amy GL, Yoon YM, Her NG (2011) Arsenic removal from water using various adsorbents: magnetic ion exchange resins, hydrous ion oxide particles, granular ferric hydroxide, activated alumina, sulfur modified iron, and iron oxide-Coated microsand. Environ Eng Res 16:165–173
21. He X, Fang Z, Jia J, Ma L, Li Y, Chai Z, Chen X (2016) Study on the treatment of wastewater containing Cu(II) by D851 ion exchange resin. Desalin Water Treat 57:3597–3605
22. Rao SVS, Lekshmi R, Mani AGS, Sinha PK (2010) Treatment of low level radioactive liquid wastes using composite ion-exchange resins based on polyurethane foam. J Radioanal Nucl Chem 283:379–384
23. Kocaoba S (2008) Adsorption of nickel(II) and cobalt(II) ions and application of surface complex formation model to ion exchange equilibria. Environ Eng Sci 25:697–702
24. Perdue E, Ritchie J (2003) Dissolved organic matter in freshwaters. Treatise Geochem 5:605
25. Humbert H, Gallard H, Suty H, Croue J-P (2008) Natural organic matter (NOM) and pesticides removal using a combination of ion exchange resin and powdered activated carbon (PAC). Water Res 42:1635–1643
26. Singer PC, Boyer T, Holmquist A, Morran J, Bourke M (2009) Integrated analysis of NOM removal by magnetic ion exchange. J Am Water Works Assoc 101:65–73
27. Zhang R, Vigneswaran S, Ngo HH, Nguyen H (2006) Magnetic ion exchange (MIEX®) resin as a pre-treatment to a submerged membrane system in the treatment of biologically treated wastewater. Desalination 192:296–302
28. Zhang R, Vigneswaran S, Ngo H, Nguyen H (2008) Fluidized bed magnetic ion exchange (MIEX®) as pre-treatment process for a submerged membrane reactor in wastewater treatment and reuse. Desalination 227:85–93
29. Tien Vinh N, Zhang R, Vigneswaran S, Huu Hao N, Kandasamy J, Mathes P (2011) Removal of organic matter from effluents by magnetic ion exchange (MIEX®). Desalination 276: 96–102
30. Sun J, Li X, Quan Y, Yin Y, Zheng S (2015) Effect of long-term organic removal on ion exchange properties and performance during sewage tertiary treatment by conventional anion exchange resins. Chemosphere 136:181–189
31. Apell JN, Boyer TH (2010) Combined ion exchange treatment for removal of dissolved organic matter and hardness. Water Res 44:2419–2430
32. Comstock SEH, Boyer TH (2014) Combined magnetic ion exchange and cation exchange for removal of DOC and hardness. Chem Eng J 241:366–375
33. Arias-Paic M, Cawley KM, Byg S, Rosario-Ortiz FL (2016) Enhanced DOC removal using anion and cation ion exchange resins. Water Res 88:981–989
34. Beita-Sandi W, Karanfil T (2017) Removal of both *N*-nitrosodimethylamine and trihalomethanes precursors in a single treatment using ion exchange resins. Water Res 124:20–28
35. Han Z-G, Chen W, Li L, Cao Z (2010) Combination of chlorine and magnetic ion exchange resin for drinking water treatment of algae. J Central South Univ Technol 17:979–984
36. Kowalska I (2008) Surfactant removal from water solutions by means of ultrafiltration and ion-exchange. Desalination 221:351–357
37. Kowalska I (2014) Nanofiltration—ion exchange system for effective surfactant removal from water solutions. Braz J Chem Eng 31:887–894
38. Fernandez AML, Rendueles M, Diaz M (2014) Sulfamethazine retention from water solutions by ion exchange with a strong anionic resin in fixed bed. Sep Sci Technol 49:1366–1378
39. Jiang M, Yang W, Zhang Z, Yang Z, Wang Y (2015) Adsorption of three pharmaceuticals on two magnetic ion-exchange resins. J Environ Sci 31:226–234
40. Behera SS, Das S, Parhi PK, Tripathy SK, Mohapatra RK, Debata M (2017) Kinetics, thermodynamics and isotherm studies on adsorption of methyl orange from aqueous solution using ion exchange resin Amberlite IRA-400. Desalin Water Treat 60:249–260

41. Lameloise M-L, Gavach M, Bouix M, Fargues C (2015) Combining reverse osmosis and ion-exchange allows beet distillery condensates to be recycled as fermentable dilution water. Desalination 363:75–81
42. Elimelech M, Phillip WA (2011) The future of seawater desalination: energy. Technol Environ Sci 333:712–717
43. Hilal N, Kochkodan V, Al Abdulgader H, Mandale S, Al-Jlil SA (2015) A combined ion exchange-nanofiltration process for water desalination: I. Sulphate-chloride ion-exchange in saline solutions. Desalination 363:44–50
44. Hilal N, Kochkodan V, Al Abdulgader H, Mandale S, Al-Jlil SA (2015) A combined ion exchange-nanofiltration process for water desalination: III. Pilot scale studies. Desalination 363:58–63
45. Hu J, Chen Y, Guo L, Chen X (2015) Chemical-free ion exchange and its application for desalination. Desalination 365:144–150
46. Pember N, Millar GJ, Couperthwaite SJ, de Bruyn M, Nuttall K (2016) BDST modelling of sodium ion exchange column behaviour with strong acid cation resin in relation to coal seam water treatment. J Environ Chem Eng 4:2216–2224
47. Millar GJ, Couperthwaite SJ, de Bruyn M, Leung CW (2015) Ion exchange treatment of saline solutions using Lanxess S108H strong acid cation resin. Chem Eng J 280:525–535
48. Li Y, Li Y, Liu Z, Wu T, Tian Y (2011) A novel electrochemical ion exchange system and its application in water treatment. J Environ Sci China 23(Suppl):S14–S17
49. Demey-Cedeno H, Ruiz M, Barron-Zambrano JA, Sastre AM (2014) Boron removal from aqueous solutions using alginate gel beads in fixed-bed systems. J Chem Technol Biotechnol 89:934–940
50. Guo Q, Zhang Y, Cao Y, Wang Y, Yan W (2013) Boron sorption from aqueous solution by hydrotalcite and its preliminary application in geothermal water deboronation. Environ Sci Pollut Res Int 20:8210–8219
51. Zelmanov G, Semiat R (2014) Boron removal from water and its recovery using iron (Fe^{+3}) oxide/hydroxide-based nanoparticles (NanoFe) and NanoFe-impregnated granular activated carbon as adsorbent. Desalination 333:107–117
52. Geffen N, Semiat R, Eisen MS, Balazs Y, Katz I, Dosoretz CG (2006) Boron removal from water by complexation to polyol compounds. J Membr Sci 286:45–51
53. Güler E, Kaya C, Kabay N, Arda M (2015) Boron removal from seawater: state-of-the-art review. Desalination 356:85–93
54. Guan Z, Lv J, Bai P, Guo X (2016) Boron removal from aqueous solutions by adsorption—a review. Desalination 383:29–37
55. Lyu J, Zeng Z, Zhang N, Liu H, Bai P, Guo X (2017) Pyrocatechol-modified resins for boron recovery from water: synthesis, adsorption and isotopic separation studies. React Funct Polym 112:1–8
56. Lyu J, Liu H, Zhang J, Zeng Z, Bai P, Guo X (2017) Metal–organic frameworks (MOFs) as highly efficient agents for boron removal and boron isotope separation. RSC Adv 7:16022–16026
57. Lyu J, Zhang N, Liu H, Zeng Z, Zhang J, Bai P, Guo X (2017) Adsorptive removal of boron by zeolitic imidazolate framework: kinetics, isotherms, thermodynamics, mechanism and recycling. Sep Purif Technol 187:67–75
58. Lyu J, Liu H, Zeng Z, Zhang J, Xiao Z, Bai P, Guo X (2017) Metal-organic framework UiO-66 as an efficient adsorbent for boron removal from aqueous solution. Ind Eng Chem Res 56:2565–2572
59. Kabay N, Sarp S, Yuksel M, Kitis M, Koseoglu H, Arar O, Bryjak M, Semiat R (2008) Removal of boron from SWRO permeate by boron selective ion exchange resins containing *N*-methyl glucamine groups. Desalination 223:49–56
60. Kabay N, Koseoglu P, Yapici D, Yuksel U, Yuksel M (2013) Coupling ion exchange with ultrafiltration for boron removal from geothermal water-investigation of process parameters and recycle tests. Desalination 316:17–22

61. Kabay N, Koseoglu P, Yavuz E, Yuksel U, Yuksel M (2013) An innovative integrated system for boron removal from geothermal water using RO process and ion exchange-ultrafiltration hybrid method. Desalination 316:1–7
62. Wang B, Guo X, Bai P (2014) Removal technology of boron dissolved in aqueous solutions —a review. Colloid Surf A 444:338–344
63. Wang B, Lin H, Guo X, Bai P (2014) Boron removal using chelating resins with pyrocatechol functional groups. Desalination 347:138–143
64. Dziubek AM, Maćkiewicz J (2009) Removal of nitrates from water by selective ion exchange. Environ Prot Eng 35:171–177
65. Ebrahimi S, Roberts DJ (2013) Sustainable nitrate-contaminated water treatment using multi cycle ion-exchange/bioregeneration of nitrate selective resin. J Hazard Mater 262:539–544
66. Guimarães D, Leao VA (2014) Batch and fixed-bed assessment of sulphate removal by the weak base ion exchange resin Amberlyst A21. J Hazard Mater 280:209–215
67. Shahbazi P, Vaezi F, Mahvi AH, Naddaffi K, Rahmani AR (2010) Nitrate removal from drinking water by point of use ion exchange. J Res Health Sci 10:91–97
68. Samadi MT, Zarrabi M, Sepehr MN, Ramhormozi SM, Azizian S, Amrane A (2014) Removal of fluoride ions by ion exchange resin: kinetic and equilibrium studies. Environ Eng Manag J 13:205–214
69. Markovski J, Garcia J, Hristovski KD, Westerhoff P (2017) Nano-enabling of strong-base ion-exchange media via a room-temperature aluminum (hydr)oxide synthesis method to simultaneously remove nitrate and fluoride. Sci Total Environ 599:1848–1855
70. Lazar L, Bandrabur B, Tataru-Farmus R-E, Drobota M, Bulgariu L, Gutt G (2014) FTIR analysis of ion exchange resins with application in permanent hard water softening. Environ Eng Manag J 13:2145–2152
71. Sica M, Duta A, Teodosiu C, Draghici C (2014) Thermodynamic and kinetic study on ammonium removal from a synthetic water solution using ion exchange resin. Clean Technol Environ Policy 16:351–359